frontiers | Research Topics

The pivotal role of oral microbiota dysbiosis and microbiota-host interactions in diseases - volume II

Edited by
Yulong Niu, Xin Xu and Jin Xiao

Published in
Frontiers in Cellular and Infection Microbiology

ISSN 1664-8714
ISBN 978-2-83251-303-3
DOI 10.3389/978-2-83251-303-3

About Frontiers

Frontiers is more than just an open access publisher of scholarly articles: it is a pioneering approach to the world of academia, radically improving the way scholarly research is managed. The grand vision of Frontiers is a world where all people have an equal opportunity to seek, share and generate knowledge. Frontiers provides immediate and permanent online open access to all its publications, but this alone is not enough to realize our grand goals.

Frontiers journal series

The Frontiers journal series is a multi-tier and interdisciplinary set of open-access, online journals, promising a paradigm shift from the current review, selection and dissemination processes in academic publishing. All Frontiers journals are driven by researchers for researchers; therefore, they constitute a service to the scholarly community. At the same time, the *Frontiers journal series* operates on a revolutionary invention, the tiered publishing system, initially addressing specific communities of scholars, and gradually climbing up to broader public understanding, thus serving the interests of the lay society, too.

Dedication to quality

Each Frontiers article is a landmark of the highest quality, thanks to genuinely collaborative interactions between authors and review editors, who include some of the world's best academicians. Research must be certified by peers before entering a stream of knowledge that may eventually reach the public - and shape society; therefore, Frontiers only applies the most rigorous and unbiased reviews. Frontiers revolutionizes research publishing by freely delivering the most outstanding research, evaluated with no bias from both the academic and social point of view. By applying the most advanced information technologies, Frontiers is catapulting scholarly publishing into a new generation.

What are Frontiers Research Topics?

Frontiers Research Topics are very popular trademarks of the *Frontiers journals series*: they are collections of at least ten articles, all centered on a particular subject. With their unique mix of varied contributions from Original Research to Review Articles, Frontiers Research Topics unify the most influential researchers, the latest key findings and historical advances in a hot research area.

Find out more on how to host your own Frontiers Research Topic or contribute to one as an author by contacting the Frontiers editorial office: frontiersin.org/about/contact

The pivotal role of oral microbiota dysbiosis and microbiota-host interactions in diseases - volume II

Topic editors

Yulong Niu — Sichuan University, China

Xin Xu — Sichuan University, China

Jin Xiao — University of Rochester Medical Center, United States

Citation

Niu, Y., Xu, X., Xiao, J., eds. (2023). *The pivotal role of oral microbiota dysbiosis and microbiota-host interactions in diseases - volume II*. Lausanne: Frontiers Media SA. doi: 10.3389/978-2-83251-303-3

Table of contents

04 Experimental Periodontitis Deteriorated Atherosclerosis Associated With Trimethylamine N-Oxide Metabolism in Mice
Lingling Xiao, Lingyan Huang, Xin Zhou, Dan Zhao, Yan Wang, Haiyan Min, Shiyu Song, Weibin Sun, Qian Gao, Qingang Hu and Sijing Xie

14 Cross-Cohort Microbiome Analysis of Salivary Biomarkers in Patients With Type 2 Diabetes Mellitus
Chuqi Gao, Ying Guo and Feng Chen

25 The Crosstalk Between Saliva Bacteria and Fungi in Early Childhood Caries
Ye Tu, Zhiyan Zhou, Chang Shu, Yuan Zhou and Xuedong Zhou

37 A Mouse Periodontitis Model With Humanized Oral Bacterial Community
Lan Bai, Bo-Yan Chen, Yan Liu, Wu-Chang Zhang and Sheng-Zhong Duan

47 *Lactobacillus plantarum* Disrupts *S. mutans*–*C. albicans* Cross-Kingdom Biofilms
Yan Zeng, Ahmed Fadaak, Nora Alomeir, Tong Tong Wu, Elena Rustchenko, Shuang Qing, Jianhang Bao, Christie Gilbert and Jin Xiao

59 Oral Microbiota-Driven Cell Migration in Carcinogenesis and Metastasis
Huimin Bai, Jing Yang, Shu Meng and Chengcheng Liu

73 Diaryl Urea Derivative Molecule Inhibits Cariogenic *Streptococcus mutans* by Affecting Exopolysaccharide Synthesis, Stress Response, and Nitrogen Metabolism
Ying Liao, Mengyun Zhang, Xingnan Lin and Fuhua Yan

86 Multimodal Data Integration Reveals Mode of Delivery and Snack Consumption Outrank Salivary Microbiome in Association With Caries Outcome in Thai Children
Tong Tong Wu, Jin Xiao, Samantha Manning, Prakaimuk Saraithong, Komkham Pattanaporn, Bruce J. Paster, Tsute Chen, Shruti Vasani, Christie Gilbert, Yan Zeng and Yihong Li

101 Dental Materials for Oral Microbiota Dysbiosis: An Update
Jieyu Zhu, Wenlin Chu, Jun Luo, Jiaojiao Yang, Libang He and Jiyao Li

121 Evolutionary Relationships Between Dysregulated Genes in Oral Squamous Cell Carcinoma and Oral Microbiota
Yang Fang, Yi Yang and Chengcheng Liu

129 New feature extraction from phylogenetic profiles improved the performance of pathogen-host interactions
Yang Fang, Yi Yang and Chengcheng Liu

frontiers in Cellular and Infection Microbiology

ORIGINAL RESEARCH
published: 18 January 2022
doi: 10.3389/fcimb.2021.820535

Experimental Periodontitis Deteriorated Atherosclerosis Associated With Trimethylamine N-Oxide Metabolism in Mice

Lingling Xiao[1,3†], Lingyan Huang[1†], Xin Zhou[4], Dan Zhao[1], Yan Wang[1], Haiyan Min[5], Shiyu Song[2], Weibin Sun[1], Qian Gao[2], Qingang Hu[1*] and Sijing Xie[1*]*

[1] Nanjing Stomatological Hospital, Medical School of Nanjing University, Nanjing, China, [2] Center for Translational Medicine and Jiangsu Key Laboratory of Molecular Medicine, Medical School of Nanjing University, Nanjing, China, [3] Department of Stomatology, The Second People's Hospital of Taizhou, Taizhou, China, [4] The Affiliated Stomatological Hospital of Soochow University, Suzhou, China, [5] The Second Affiliated Hospital of Nanjing University of Chinese Medicine, Nanjing, China

OPEN ACCESS

Edited by:
Xin Xu,
Sichuan University, China

Reviewed by:
Sheng-Zhong Duan,
Shanghai Jiao Tong University, China
Akihiro Yoshida,
Matsumoto Dental University, Japan

***Correspondence:**
Sijing Xie
xiesj@nju.edu.cn
Qingang Hu
qghu@nju.edu.cn
Qian Gao
qian_gao@nju.edu.cn

[†]These authors have contributed equally to this work and share first authorship

Specialty section:
This article was submitted to Microbiome in Health and Disease, a section of the journal Frontiers in Cellular and Infection Microbiology

Received: *23 November 2021*
Accepted: *14 December 2021*
Published: *18 January 2022*

Citation:
Xiao L, Huang L, Zhou X, Zhao D, Wang Y, Min H, Song S, Sun W, Gao Q, Hu Q and Xie S (2022) Experimental Periodontitis Deteriorated Atherosclerosis Associated With Trimethylamine N-Oxide Metabolism in Mice. Front. Cell. Infect. Microbiol. 11:820535. doi: 10.3389/fcimb.2021.820535

Background: Periodontitis is considered a risk factor for atherosclerosis, but the mechanism is not clear. It was reported that oral administration of *Porphyromonas gingivalis* altered the gut microbiota in mice. Gut dysbiosis and the intestinal metabolite trimethylamine N-oxide (TMAO) were verified to be associated with atherosclerosis. Therefore, the possible TMAO-related mechanism between periodontitis and atherosclerosis needs to be explored.

Methods: Experimental periodontitis was established by oral administration of *P. gingivalis* for 2 months in ApoE$^{-/-}$ mice. Mouse hemi-mandibles were scanned using Micro-CT. Quantification of TMAO was performed using liquid chromatography–tandem mass spectrometry. Mouse feces were collected and the bacterial DNA was extracted, then the gut microbiota was analyzed using 16S rRNA genes. Atherosclerotic lesion areas were quantified. Livers, small intestines, and large intestines were analyzed for gene expression.

Results: Aggravated atherosclerosis plaques were found in experimental periodontitis mice. Plasma TMAO, a pathogenic factor of atherosclerosis, was initially found to be increased in periodontitis mice. Changes in the composition and abundance of the intestinal microflora of periodontitis mice were found. Flavin monooxygenase 3 (FMO3), the catalyzing enzyme of TMAO in the liver, was significantly increased, accompanied by an increase of IL-6 in liver, the abnormal intestinal integrity and enhanced plasma LPS. The IL-6 and LPS were verified to be able to increase FMO3 in HepG2 cells.

Conclusion: Our research discovered that experimental periodontitis in ApoE$^{-/-}$ mice induced gut dysbiosis and an increase in TMAO. These results suggest a possible mechanism by which periodontitis may accelerate atherosclerosis by influencing the intestinal microbes and the metabolism, which were triggered by inflammation of the liver and intestine.

Keywords: trimethylamine N-oxide, periodontitis, *Porphyromonas gingivalis*, gut microbiota, flavin-containing monooxygenase 3

INTRODUCTION

Periodontitis is a chronic inflammatory disease of periodontal tissues caused by dental biofilm and calculus (Pihlstrom et al., 2005). Atherosclerosis (AS) is a slowly progressive disease characterized by lipid accumulation in the outer arterial tunica intima (Xu et al., 1990). Epidemiological and biological studies indicate that periodontitis may be an important risk factor for cardiovascular disease and atherosclerosis (Socransky and Haffajee, 2005; Kebschull et al., 2010; Olivier et al., 2011). So far there are two main viewpoints about the mechanism of periodontitis related atherosclerosis. One suggested that the local inflammatory nidus in periodontal pocket could induce atherosclerosis by instigating the inflammatory cascade (Hegde and Awan, 2019). The second one proposed that an invasion of the periodontal bacteria through diseased pockets into bloodstream for atherosclerosis induction (D'Aiuto et al., 2005; Leticia et al., 2013; Kholy et al., 2015). However, the mechanism of how exactly periodontitis induces the atherosclerosis is still unclear.

Trimethylamine N-oxide, a metabolite of gut flora, has shown promise as a special indicator of atherosclerosis (Koeth et al., 2013). The circulatory TMAO may be associated with cardiovascular risks by changing enterohepatic cholesterol and bile acid metabolism that control the pathway required to eliminate cholesterol from the body (Tang and Hazen, 2014; Chistiakov et al., 2015; Wang and Zhao, 2018). Wang et al. found that TMAO promoted upregulation of multiple macrophage scavenger receptors linked to atherosclerosis and supplementation with TMAO promoted atherosclerosis in ApoE$^{-/-}$ mice (Wang et al., 2011). TMAO is converted from trimethylamine (TMA) in the liver by the oxidative effect of flavin monooxygenases (FMOs) (Schugar and Brown, 2015). TMA is a small molecule produced by the gut bacteria metabolizing some components in foods, such as choline, phosphatidylcholine, and carnitine (Wang and Zhao, 2018).

The intestine is the largest microbial habitat in the human body, holding over 1,000 microbial phylotypes, and the number is up to 100 trillion, which is 100 times the human genome (Ley et al., 2006; Rajilićstojanović et al., 2010). In the last decade, there have been studies demonstrating that gut dysbiosis is associated with atherosclerosis (Tang et al., 2017). Compared with normal controls, the plaque areas of germ-free ApoE$^{-/-}$ mice were significantly bigger after the same diet for 3–4 months (Stepankova et al., 2010), suggesting that the normal gut microbiota was protective in the development of atherosclerosis. Moreover, mice that were gavaged with cecal microbial contents from atherosclerosis-prone or atherosclerosis-resistant mice, exhibited similar symptoms with their donor mice (Gregory et al., 2015). Strikingly, a clinical study stratified the human gut microbiota into three enterotypes characterized by *Bacteroides*, *Prevotella*, and *Ruminococcus*, respectively, and the atherosclerosis patients were overrepresented in enterotype 3 represented by *Ruminococcus* (Karlsson et al., 2012). Further studies performed by a Japanese research group reported that oral administration of *Porphyromonas gingivalis* (*P. gingivalis*), a periodontal pathogen, could alter the gut microbiota and induce systemic inflammation (Arimatsu et al., 2014; Nakajima et al., 2015), thus linking the key periodontal pathogen with the gut microbiota and systemic inflammation.

Therefore, we hypothesized that periodontitis may induce gut dysbiosis and abnormal hepato-intestinal metabolism, leading to the accelerated development of atherosclerosis. In this study, *P. gingivalis* was used to generate an experimental periodontitis model in ApoE$^{-/-}$ mice. Aggravated atherosclerosis plaques, enhancement of TMAO in peripheral blood and increased FMO3, the catalyzing enzyme of TMAO in the liver, were observed in the experimental periodontitis mice, compared with the control. It may hint at a new pathway for periodontitis to promote atherosclerosis: the alterations of intestinal microbes and their metabolites originated by periodontitis.

MATERIALS AND METHODS

Mice

Ten 8-week-old male ApoE$^{-/-}$ mice, and ten 8-week-old male C57BL/6J mice were obtained from the Model Animal Research Center of Nanjing University (Nanjing, China). The mice were housed in a controlled pathogen-free environment with free access to food and water for acclimatization (Cani et al., 2008), and then randomized to two groups: the control group and the experimental periodontitis group. They were fed Western Diet (WD) consisting of 21% (w/w) fat, 0.2% cholesterol, and 0% choline (TD88137–Harlan) for an additional 8 weeks. All experimental procedures were reviewed and approved by the Institutional Animal Care and Use Committee of Nanjing University (IACUC-D2102033).

Bacterial Culture and Oral Administration

P. gingivalis strain 33277 was cultured in a Brain Heart Infusion Broth (Beyotime Biotechnology, China) in an anaerobic environment for 48 h at 37 °C. The anaerobic state was kept by AnaeroPack (Mitsubishi Gas Chemical Company, Inc, Japan) in an anaerobic jar (Oxoid, England) (Arimatsu et al., 2014). The concentration of bacteria was determined with a spectrophotometer (SpectraMax M3, Molecular Devices, USA) at an optical density of 600 nm (OD = 10^9 P. *gingivalis* per ml) (Zhang et al., 2014). A total of 10^9 CFU of live *P. gingivalis* was collected by centrifugation, and then resuspended in 100 μl Phosphate Buffered Saline (PBS) with 2% carboxymethyl cellulose (Sigma-Aldrich, America). The bacterial suspension was given to each of the five mice gingival margin of the molars 5 times a week for 8 weeks. The other five mice in the control group were sham-administrated without the *P. gingivalis*. Twenty-four hours after the final intervention, the feces were collected from the live mice, and then the mice were anesthetized for tissues collection (Arimatsu et al., 2014).

Quantification of Mandibular Alveolar Bone Resorption

The hemi-mandibles were scanned using a high-resolution Micro-CT (SkyScan1176, Bruker, Germany) for alveolar bone loss evaluation. After scanning, a set of slices were used for three-dimensional reconstructions. All images were reoriented such

that the cement-enamel junction (CEJ) and the alveolar bone crest (ABC) appeared in the Micro-CT slice that was to be analyzed. The alveolar bone loss was measured from the CEJ to the ABC of the mesial surface of the first molar on the sagittal plane (Park et al., 2007; Madeira et al., 2013).

Quantification/Histology of Atherosclerotic Lesion Area and Liver

The collected mouse hearts were embedded in tissue freezing medium (Sakura, America), and then sliced and stained with oil red O. The stained plaque area of the aortic sinus was analyzed using Image J 1.37c (National Institutes of Health, USA) (Tomoki et al., 2011). Hematoxylin–eosin-stained (H&E) sections of the aortic arch and liver were used for morphometric analysis (Kesavalu et al., 2012).

Quantification of Plasma TMAO, TMA, Choline, Creatinine, Betaine and L-Carnitine

Quantification of TMAO, TMA, Choline, Creatinine, Betaine, and L-Carnitine was performed using stable isotope dilution ultra-high-performance liquid chromatography–tandem mass spectrometry (UHPLC–MS/MS). The analysis used a Waters ACQUITY UPLC HSS T3 column (2.1 ∗ 100 mm, 1.8 um). Mobile phases A and B, respectively, comprised 0.1% formic acid and 0.1% acetonitrile in water. MS quadrupole and ion source temperatures were separately taken as 100 and 650°C. The ion transitions were m/z 76.1 → 58.1 for TMAO, m/z 60 → 40.5 for TMA, m/z 118.1 → 58.1 for Betaine, m/z 104.1 → 45 for Choline, m/z 114.1 → 44 for Creatinine and m/z 162.1 → 85 for L-Carnitine.

Lipoprotein and Serum Analysis

The mouse serum samples were collected by extracting the eyeballs, and assayed for total cholesterol (TC), triglyceride (TG), low-density lipoprotein (LDL), high-density lipoprotein (HDL), oxidized low-density lipoprotein (ox-LDL), lipopolysaccharide (LPS), interleukin (IL)-6, interleukin (IL)-1β, and tumor necrosis factor (TNF)-α. The levels of ox-LDL, LPS, IL-6, IL-1β, and TNF-α were determined by ELISA (Dakewe, China). Enzymatic colorimetry (Biosino Bio-Technology & Science Inc, China) was used for serum TC and TG analysis. The LDL and HDL concentrations were detected by the LDL/HDL-Cholesterol Kit (Biosino Bio-Technology & Science Inc, China) (Lalla et al., 2003).

Cell Culture

The HepG2 cell line was obtained from ATCC. HepG2 cells were cultured in DMEM high glucose medium (10% fetal bovine serum, 1% penicillin and streptomycin) at 37°C and 5% CO_2 saturated humidity. When the cell adherence rate reached 80 to 90%, the cells were digested with trypsin, and the cell viability was above 90% for subpassage. One day before the experiment, the cells were digested with 0.25% trypsin and inoculated with DMEM high glucose medium containing 10% fetal bovine serum into a 6-well culture plate. The agents were added after the cells were completely adhered to the wall. There were 5 wells in each group.

Analysis of Gene Expression in the Samples

The total RNA was extracted from the mouse liver, abdominal adipose, large intestine, small intestine samples, and HepG2 cells by RNAsimple Total RNA Kit (Tiangen, China). Reverse transcription PCR was carried out in the PCR Thermal Cyclers (Applied Biosystems, Thermo Fisher, America) for cDNA synthesis with PrimeScript™ RT reagent Kit with gDNA Eraser (Takara, Japan). Primers for real-time PCR were purchased from GenScript, and the primer sequences were listed in **Supplemental Table 1**. The gene expression analysis was realized finally in a final volume of 20 μl consisted by 0.5–5 ng cDNA, 900 nM each of the forward and reverse primers, and 10 μl iTaq Universal SYBR Green Supermix (Bio-Rad, America) in QuantStudio 7 Flex Real-Time PCR System (Applied Biosystems, Thermo Fisher, America). The PCR conditions were 2 min at 50°C, 10 min at 95°C followed by 40 cycles of two-step PCR denaturation at 95°C for 15 s and annealing extension at 60°C for 60 s. The relative amount of each studied mRNA was normalized to the relative quantity of glyceraldehyde-3-phosphate dehydrogenase (GAPDH) mRNA, and the data were analyzed according to the $2^{-\triangle\triangle CT}$ method (Cani et al., 2008; Nakajima et al., 2015).

DNA Extraction From Samples and Gut Microbiota Genome Sequencing

The mouse feces were collected after *P. gingivalis* administration for two months, and the bacterial DNA was extracted from feces by TIANamp Stool DNA Kit (Tiangen, China). The bacterial DNA extracted from feces was collected for gut microbiota analysis. The V3–V4 region of the 16S rRNA genes was amplified by PCR using a primer set (F: CCTAYGGGRB GCASCAG, R: GGACTACNNGGGTATCTAAT). The qualified DNA was used for sequencing analysis in Illumina HiSeq platform at the Novogene Bioinformatics Institute (Beijing, China) (Ma et al., 2018).

Statistical Analysis

The statistical analysis of phenotypic traits was performed using SPSS22. For statistical analysis, either a student t-test or one-way ANOVA was performed, and the significance level was set at P = 0.05 which was shown in the figure legends.

RESULTS

Experimental Periodontitis Caused Deteriorated Atherosclerosis and Increased TMAO in the Peripheral Blood of the ApoE$^{-/-}$ Mice

Eight week old male ApoE$^{-/-}$ mice were randomly divided into control and experimental periodontitis groups upon CMC and *P. gingivalis* administration. After 2 months of administration, the mandible specimens of the two groups were collected and scanned by Micro-CT. As shown in **Figure 1A**, the alveolar bone loss refers to the distance from the cementum-enamel junction (CEJ) to the

alveolar crest (ABC) of the first molar. The results showed that the alveolar bone height of the periodontitis group was significantly lower than that of the control, and the difference was statistically significant (P <0.05) (**Figure 1B**). The experimental periodontitis group exhibited more plaque deposition under the intima than the control group (**Figure 1C**). Analysis of the atherosclerotic plaque area revealed a significant increase in the periodontitis group versus the control group (**Figure 1D**). The H&E-stained aortic sections were used for vessel wall assessment and invading mononuclear cell observation. As shown in **Figures 1E, F**, the experimental periodontitis group exhibited the lager intimal thickness, more plaque deposition under intima and more invading monocytes throughout arterial layers than those of the control group. As shown in **Supplemental Figure 1**, experimental periodontitis had significant effects on the serum lipid profile. The cholesterol levels shifted toward atherogenic levels.

The effect of experimental periodontitis on plasma TMAO, the important indicator of atherosclerosis, and its precursors were analyzed. The plasma TMAO level increased significantly in the experimental periodontitis group, compared to the control group. However, no significant difference was observed in the level of TMA and its precursors between the two groups, except that the plasma choline level decreased in the periodontitis group (P <0.01) (**Figures 1G, H**).

Experimental Periodontitis Led to Changes in the Composition and Abundance of Intestinal Microflora

TMA, the precursor of TMAO, is a unique metabolite produced by the gut bacteria. The composition and abundance of intestinal microflora in the samples were detected by genome sequencing. There was no significant difference in the number of OTUs. The

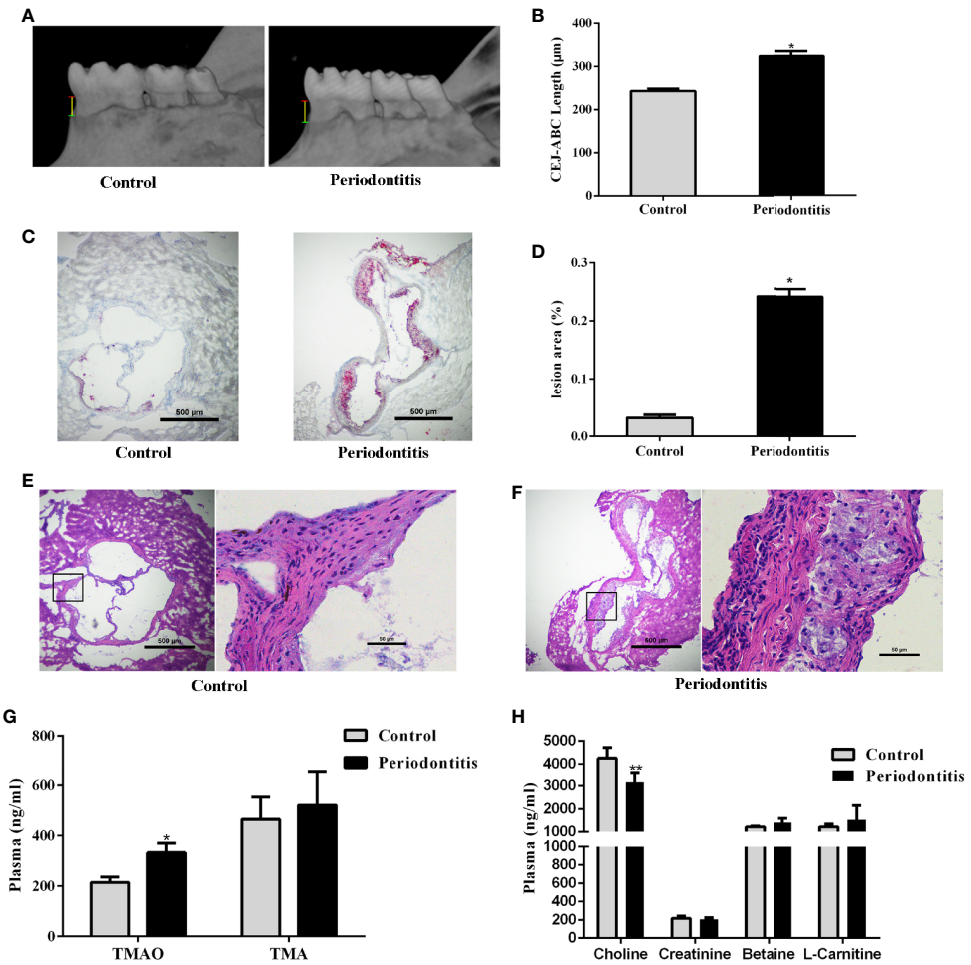

FIGURE 1 | Effect of periodontitis on alveolar bone resorption, morphologic characterization of aortic plaques, plasma TMAO/TMA levels and plasma Choline/Creatinine/Betaine/L-Carnitine levels. **(A)** hemi-mandible from each group, as reconstructed by the micro-CT. **(B)** Cemento-enamel junction (red line: CEJ)-alveolar bone crest (green line: ABC) distance to represent alveolar bone loss (yellow line). **(C)** Representative Oil-Red-O stained aortic roots from control group and periodontitis group. **(D)** aortic root lesion area quantified using Oil-Red-O staining (original magnification of 400×). **(E)** representative fields of aortic root sections in control group stained with Hematoxylin–eosin. **(F)** representative fields of aortic root sections in experimental periodontitis group stained with Hematoxylin–eosin. **(G)** TMAO and TMA levels in plasma. **(H)** Choline, Creatinine, Betaine, and L-Carnitine levels in plasma. Data are presented as mean± SEM. (n = 5/group). *P < 0.05; P < 0.01.

Chao1 index, ACE index, Shannon index, and Simpson index were lower in the periodontitis group than in the control group after a 2-month treatment (**Figure 2A**).

At the phylum level, the major 3 phyla of periodontitis and control mice were *Bacteroidetes*, *Firmicutes*, and *Proteobacteria*, and with no significant difference between the two groups (**Figure 2B**). Furthermore, the PCA analysis showed differences in microbiome composition between periodontitis and control mice (**Figure 2C**). The LEfSe analysis identified the characteristic bacteria at 2-month point. *Lachnospiraceae_NK4A136_group* and *Acetatifactor* were abundant in the periodontitis group, whereas *Rikenellaceae_RC9_gut_group* and *Mycoplasmataceae* were abundant in the control group (**Figures 2D, E**).

The analysis of different bacterial operational taxonomic units (OTUs) showed that 43 OTUs, including *Lachnospiraceae_bacterium_A4* (OTU402), *Lactobacillus_animalis* (OTU79), and *Parabacteroides_goldsteinii* (OTU147) at species level, and also *Lachnospiraceae_NK4A136_group* (OTU15, OTU471), *Mucispirillum* (OTU37), and *Ruminococcaceae_UCG-014* (OTU136), etc. at genus level, were significantly different between periodontitis model and control mice (**Figure 2F**). The full list of the OTU taxonomy is in **Supplemental Table 2**. As shown in **Figure 2G**, 37 KO ORTHOLOGY were at different levels

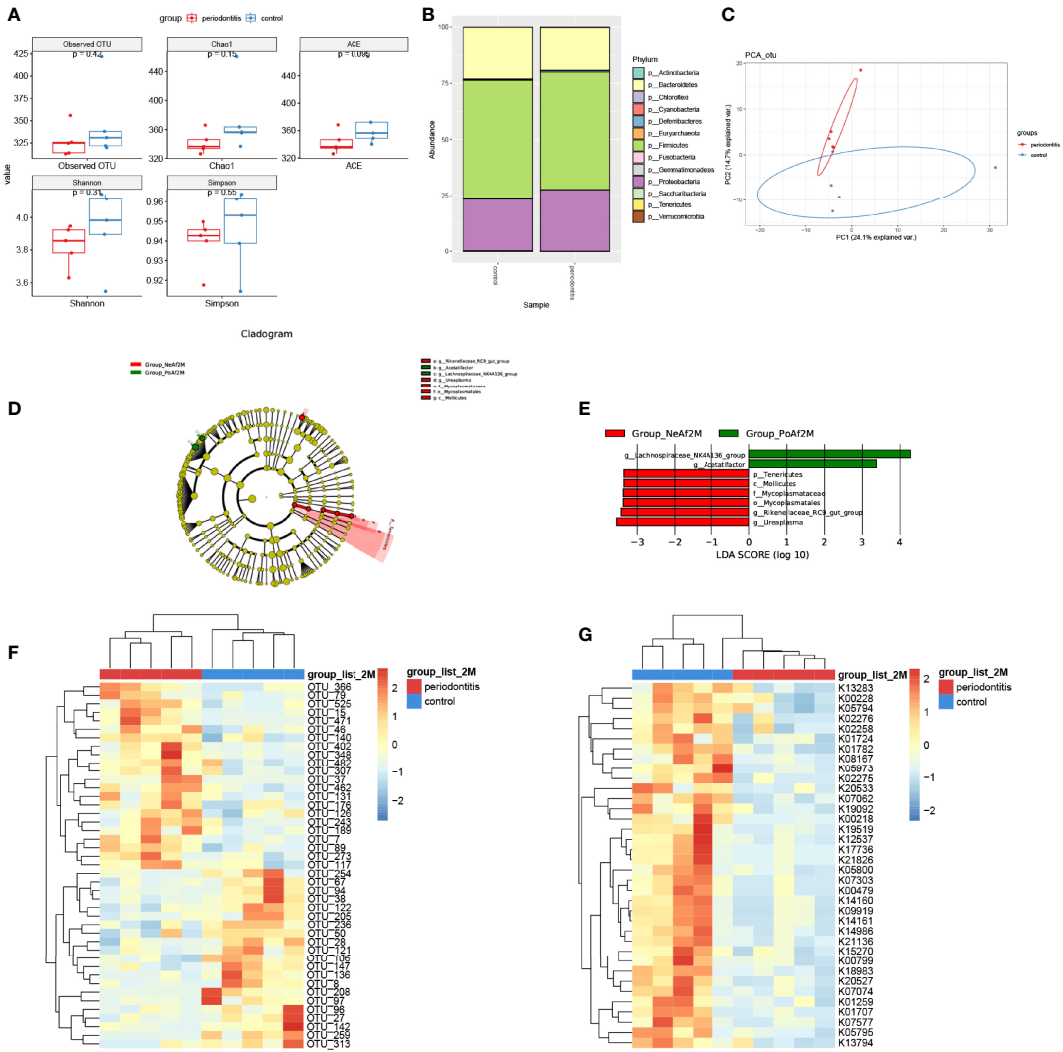

FIGURE 2 | Gut microbiota alternation in periodontitis mouse model. **(A)** boxplot showed the value of the indicated index of alpha diversity of the periodontitis group and control group after 2-month treatment of *P. gingivalis*. **(B)** stack bar plot, showed the composition of microbiota at phylum level. **(C)** PCA plot of microbial composition. **(D)** linear discriminant analysis effect size (LEfSe)-based cladogram of fecal samples. **(E)** LDA scores of fecal samples. **(F)** Heatmap of sequenced bacterial operational taxonomic unit (OTU) abundances, scaled by row. **(G)** Heatmap of KEGG KO ORTHOLOGY analyzed by Tax4Fun2, scaled by row. 2M = 2 months after administration. The taxon name is preceded by one of the following: p_, phylum; f_, family; g_, genus; s_, species. Data are presented as mean ± SEM. (n = 5/group).

between periodontitis and control mice, namely, K00108: choline dehydrogenase [EC:1.1.99.1], K00218: protochlorophyllide reductase [EC:1.3.1.33], K00228: coproporphyrinogen III oxidase [EC:1.3.3.3], etc.

Experimental Periodontitis Led to the Increased Expression of the TMA Oxidase FMO3 in the Liver, Accompanied by Abnormal Intestinal Integrity, Liver Inflammation, and Enhanced LPS in the Peripheral Blood

FMO3 is another important factor for the formation of TMAO. After the 2-month *P. gingivalis* administration, the mRNA expression of FMO3 was found to be significantly increased in the mouse livers (**Figure 3A**). Meanwhile, the expression of IL-6 (**Figure 3B**) in the liver of the periodontitis group was also enhanced. Pathological observation showed an increased lymphocyte content in the liver of the experimental periodontitis mice, compared with the control group. Experimental periodontitis also induced more steatosis, and the loss of cellular boundaries in livers (**Figure 3C**). Further blood analysis revealed that the experimental periodontitis mice had elevated LPS levels ($P < 0.05$), while changes in inflammatory factors IL-6 and TNF-α were consistent with LPS (**Figures 3D, E**).

The mRNA expression of IL-6, TNF-α, and IL-1β in the small and large intestines did not differ significantly between the two groups (**Figures 3F, G**). The expressions of tight junction proteins ZO-1, Claudin-1, and Occludin were analyzed for gut barrier function. In the small intestine, experimental periodontitis significantly downregulated ZO-1 expression

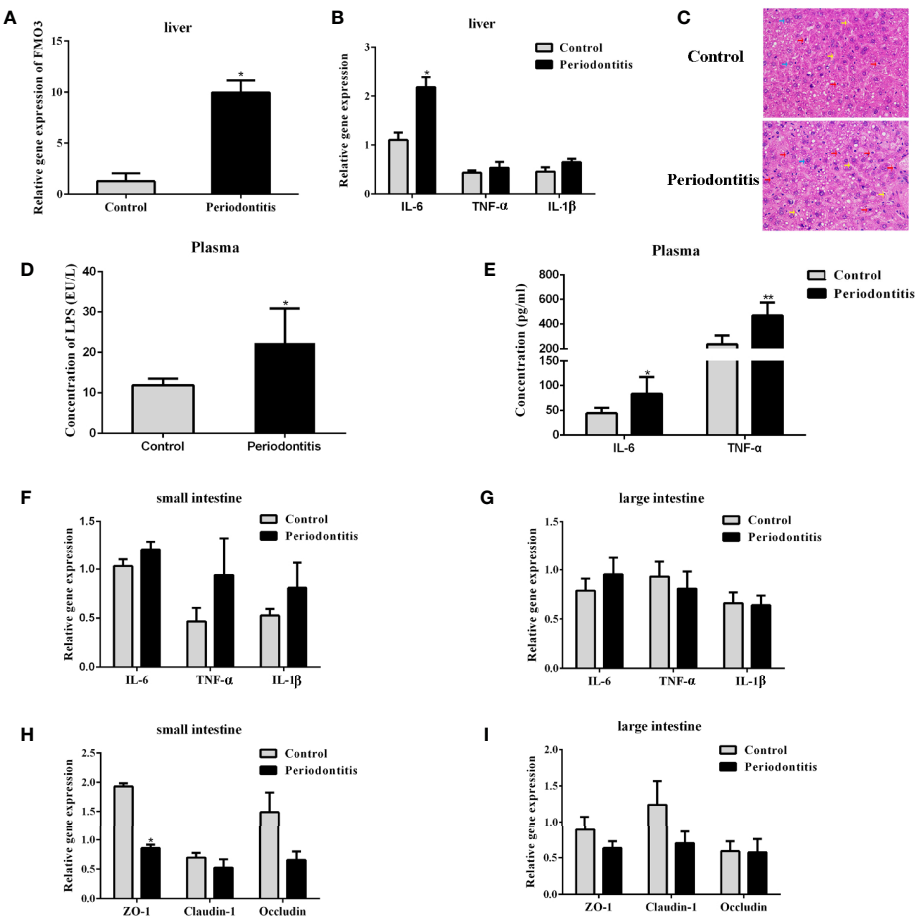

FIGURE 3 | Comparisons of lipopolysaccharide and inflammatory factor concentrations in the plasma, liver, and intestine and the expressions of FMO3 and tight junction protein between the control group and the periodontitis group. **(A)** relative gene expression levels of FMO3 in in the liver tissue. **(B)** Relative gene expression levels of inflammatory cytokines in the liver tissue. **(C)** Effects of experimental periodontitis on histopathological changes of liver hepatocytes stained with H&E (original magnification of 400×). Blue arrows: hepatic cells. Red arrows: lymphocytes. Yellow arrows: sinusoids between the plates of hepatocytes. Black arrows: fat vacuoles. **(D)** concentration of lipopolysaccharide in the plasma. **(E)** Concentration of inflammatory cytokines in the plasma. **(F, G)** relative gene expression levels of inflammatory cytokines in the small intestine and large intestine. **(H, I)** Comparisons of relative tight junction gene expression levels in the small intestine and large intestine. Data are presented as mean ± SEM. (n = 5/group). *$P < 0.05$; $P < 0.01$.

(P <0.05), and Claudin-1 and Occludin also showed less expression in experimental periodontitis mice (**Figure 3H**). These three tight junction proteins had similar decreased mRNA expressions in the large intestine at 8 weeks in the experimental periodontitis group (**Figure 3I**). The abnormal functions of intestinal immunity may create conditions for gut microbiota and its toxins like LPS to get into the bloodstream in mice.

LPS-Induced Inflammation in the Liver Resulted in Enhanced FMO3 Expression and Plasma TMAO Level

To understand the effect of LPS incitation on the FMO3 in the liver and the oxidation of TMA, 8-week-old male C57BL/6J mice were injected with LPS intraperitoneally at a dose of 5 mg/kg every 3 days for 2 weeks. The level of the inflammatory factors IL-6, IL-1β, and TNF-α in the liver increased significantly, compared to the control (**Figure 4A**). The mRNA expression of FMO3 in the liver was also increased in the LPS group (**Figure 4B**). Meanwhile, the plasma TMAO significantly increased in the LPS group compared to that in the control group, while there was no obvious effect on the level of plasma TMA and its precursors (**Figures 4C, D**).

Incitation of LPS or IL-6 to the HepG2 Cell Increased FMO3 Expression

The HepG2 cells were used to explore the direct effect of LPS and the immune effect of IL-6 on the expression of FMO3. The HepG2 cells were treated with 10, 50, and 100 μg/ml LPS, respectively, for 24 h. The mRNA expression of FMO3 increased significantly in the three LPS treatment groups, especially in the 100 μg/ml LPS group (P <0.05) (**Figure 4E**). Furthermore, a much more obvious increase of FMO3 expression was found after the treatment of HepG2 cells with 25 or 50 ng/ml IL-6 (**Figure 4F**).

DISCUSSION

In this study, we successfully established the periodontitis mouse model by oral administration of *P. gingivalis* and aggravated atherosclerosis. These results are consistent with our previous

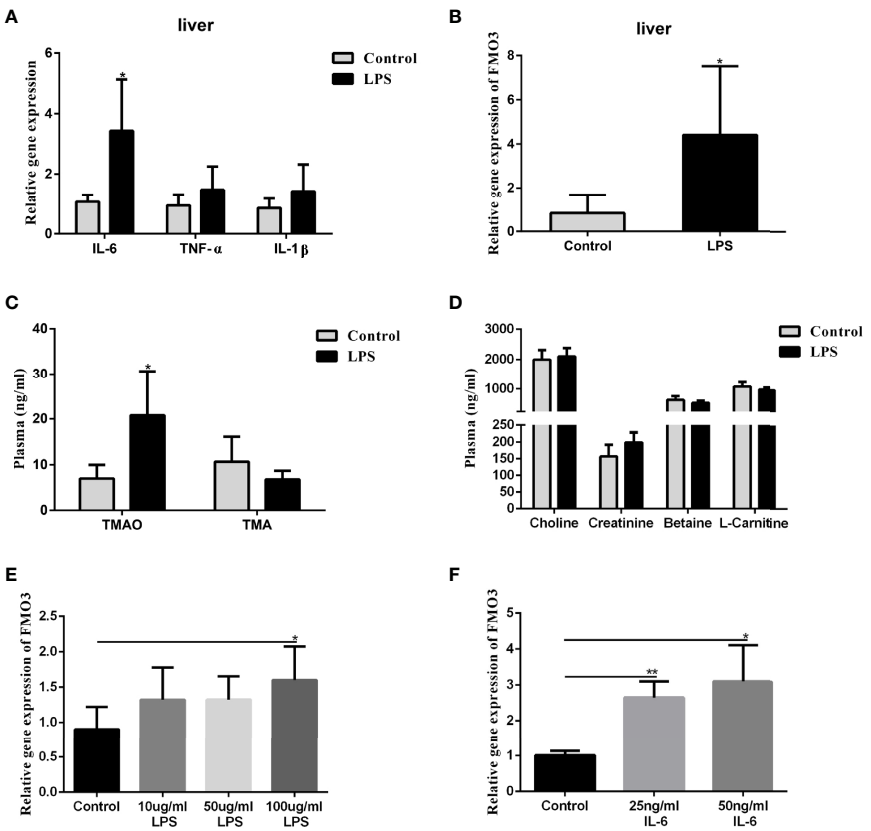

FIGURE 4 | Effect of LPS on plasma TMAO/TMA levels, plasma Choline/Creatinine/Betaine/L-Carnitine levels, and the expression of FMO3 and inflammatory factors in the liver. Effect of LPS and IL-6 stimulation on FMO3 expression in HepG2 cell. **(A)** Relative gene expression levels of inflammatory cytokines in the liver tissue. **(B)** Relative gene expression levels of FMO3 in the liver tissue. **(C)** TMAO and TMA levels in plasma. **(D)** Choline, Creatinine, Betaine, and L-Carnitine levels in plasma. **(E)** comparisons of relative gene expression levels of FMO3 in the 10, 50, and 100 μg/ml LPS-treatment HepG2 cell. **(F)** relative gene expression levels of FMO3 in the 25, 50 ng/ml IL-6-treatment HepG2 cell. Data are presented as mean ± SEM. (n = 5/group). *P <0.05; P < 0.01.

study (Yang et al., 2017), which affirmed the connection between periodontitis and general changes.

The most interesting finding was the increase of TMAO in the peripheral blood of the periodontitis mice. TMAO has been proven to be associated with cardiovascular risks by promoting inflammatory mediators, endothelial cell adhesion and foam cell formation, and decreasing reverse cholesterol efflux (Tang and Hazen, 2014; Chistiakov et al., 2015). TMAO is an oxidization product of TMA in the liver. TMA is a special metabolite of the gut microbiota. The intestinal microbiota synthesizes TMA from the choline in the diet. TMA is transported into the liver *via* the portal vein and then oxidized to TMAO by the catalytic action of FMOs. Diet, intestinal microbiota, and FMO3 are the primary factors affecting TMAO metabolism.

However, altered gut microbiota was observed in our study. When experimental periodontitis mice were compared to control mice, changes in the composition and abundance of intestinal microflora were found. The ACE index, Chao1 index, and Shannon index analysis showed that the community richness and diversity of gut microflora decreased after 2-month *P. gingivalis* administration, although the result was not statistically significant. *P. gingivalis* has shown antacid activity and may migrate to the colon and alter colon function (Sato et al., 2017). We speculated that experimental periodontitis might disturb the intestinal microflora, which would then interfere with TMA and TMAO production. Significant changes in gut bacteria, such as the *Lachnospiraceae-NK4A136_group* and *Bacteroidales_S24-7_group*, have been reported to be relevant to lipid metabolism and TMAO level (Wang et al., 2015; Skennerton et al., 2016), which may be indirect factors resulting in more serious lipid metabolism, atherosclerosis abnormalities and gut dysbiosis in experimental periodontitis mice. The microbiota and its function did change to an extent, although relationship between gut microbiota and the elevated TMAO was not very clear. The direct evidence of the relationship between the gut microbiota and TMAO needs further study.

We found that the expression of FMO3 in the liver was significantly increased and the livers of the experimental periodontitis mice were found in an inflammatory state. FMOs have been shown to regulate plasma TMAO levels effectively, and among the five members of the FMO family, FMO3 exhibits the highest specific activity towards TMA (Schugar and Brown, 2015). Our research hypothesized that this catalytic enzyme and the inflammatory response of the liver may contribute significantly to the progression of periodontitis, thereby promoting the development of atherosclerosis. The integrity disruption and inflammation of the intestine may give the channel to the bacteria and their toxins such as LPS. Furthermore, we verified the effect of IL-6 and LPS on the expression of FMO3 in the liver, and in HepG2 cells and observed the effect on the plasma TMAO level *in vivo*. It is an interesting finding that the experimental periodontitis could cause the inflammation state of the liver, and increase the FMOs. However, it still needs further research to identify. That is what we are going to focus on.

CONCLUSION

Our research found that experimental periodontitis in ApoE$^{-/-}$ mice induced gut dysbiosis, liver inflammation, and the increase in oxidase FMO3 and the intestinal metabolite TMAO. TMAO may play a key role in the development of atherosclerosis. These results suggest a possible mechanism that periodontitis induce atherosclerosis by influencing the intestinal microbes and the enterohepatic metabolism. It is possible to ameliorate the abnormality of TMAO metabolism through periodontal treatment in the future.

DATA AVAILABILITY STATEMENT

The data presented in the study are deposited in the SRA repository, accession number PRJNA784030.

ETHICS STATEMENT

The animal study was reviewed and approved by the Institutional Animal Care and Use Committee of Nanjing University (IACUC-D2102033).

AUTHOR CONTRIBUTIONS

All authors have made substantial contributions to the conception and design of this study. SX, and QG contributed to conception and design of the research. LX and LH performed the experiments and wrote the paper. YW, DZ, and XZ fed the animals, and collected data. HM and SS implemented the information analysis. WS and QH were involved in the critical discussion of the research and revising it. All authors contributed to the article and approved the submitted version.

FUNDING

This work was supported by the National Natural Science Foundation of China (81801041), Beijing, The Project of Invigorating Health Care through Science, Technology and Education (Grant No QNRC2016119) (2016–2020), Nanjing and the National Natural Science Foundation of China (82001111).

SUPPLEMENTARY MATERIAL

The Supplementary Material for this article can be found online at: https://www.frontiersin.org/articles/10.3389/fcimb.2021.820535/full#supplementary-material

REFERENCES

Arimatsu, K., Yamada, H., Miyazawa, H., Minagawa, T., Nakajima, M., Ryder, M. I., et al. (2014). Oral Pathobiont Induces Systemic Inflammation and Metabolic Changes Associated With Alteration of Gut Microbiota. *Sci. Rep.* 4 (18), 4828. doi: 10.1038/srep04828

Cani, P. D., Bibiloni, R., Knauf, C., Waget, A., Neyrinck, A. M., Delzenne, N. M., et al. (2008). Changes in Gut Microbiota Control Metabolic Endotoxemia-Induced Inflammation in High-Fat Diet-Induced Obesity and Diabetes in Mice. *Diabetes* 57 (6), 1470–1481. doi: 10.2337/db07-1403

Chistiakov, D. A., Bobryshev, Y. V., Kozarov, E., Sobenin, I. A., and Orekhov, A. N. (2015). Role of Gut Microbiota in the Modulation of Atherosclerosis-Associated Immune Response. *Front. Microbiol.* 6, 671. doi: 10.1038/nm.3145

D'Aiuto, F., Graziani, F., Tetè, S., Gabriele, M., and Tonetti, M. S. (2005). Periodontitis: From Local Infection to Systemic Diseases. *Int. J. Immunopathol. Pharmacol.* 18 (3 Suppl), 1–11.

Gregory, J. C., Buffa, J. A., Org, E., Wang, Z., Levison, B. S., Zhu, W., et al. (2015). Transmission of Atherosclerosis Susceptibility With Gut Microbial Transplantation. *J. Biol. Chem.* 290 (9), 5647–5660. doi: 10.1074/jbc.M114.618249

Hegde, R., and Awan, K. H. (2019). Effects of Periodontal Disease on Systemic Health. *Dis. Mon.* 65 (6), 185–192. doi: 10.1016/j.disamonth.2018.09.011

Karlsson, F. H., Fåk, F., Nookaew, I., Tremaroli, V., Fagerberg, B., Petranovic, D., et al. (2012). Symptomatic Atherosclerosis is Associated With an Altered Gut Metagenome. *Nat. Commun.* 3 (4), 1245. doi: 10.1038/ncomms2266

Kebschull, M., Demmer, R. T., and Papapanou, P. N. (2010). "Gum Bug, Leave My Heart Alone!"–Epidemiologic and Mechanistic Evidence Linking Periodontal Infections and Atherosclerosis. *J. Dent. Res.* 89 (9), 879–902. doi: 10.1177/0022034510375281

Kesavalu, L., Lucas, A. R., Verma, R. K., Liu, L., Dai, E., Sampson, E., et al. (2012). Increased Atherogenesis During Streptococcus Mutans Infection in ApoE-Null Mice. *J. Dent. Res.* 91 (3), 255–260. doi: 10.1177/0022034511435101

Kholy, K. E., Genco, R. J., and Dyke, T. E. V. (2015). Oral Infections and Cardiovascular Disease. *Trends Endocrinol. Metab.* 26 (6), 315–321. doi: 10.1016/j.tem.2015.03.001

Koeth, R. A., Wang, Z., Levison, B. S., Buffa, J. A., Org, E., Sheehy, B. T., et al. (2013). Intestinal Microbiota Metabolism of L-Carnitine, a Nutrient in Red Meat, Promotes Atherosclerosis. *Nat. Med.* 19 (5), 576–585. doi: 10.1038/nm.3145

Lalla, E., Lamster, I. B., Hofmann, M. A., Bucciarelli, L., Jerud, A. P., Tucker, S., et al. (2003). Oral Infection With a Periodontal Pathogen Accelerates Early Atherosclerosis in Apolipoprotein E-Null Mice. *Arterioscler. Thromb. Vasc. Biol.* 23 (8), 1405–1411. doi: 10.1161/01.ATV.0000082462.26258.FE

Leticia, R., David, H., Emil, K., Silvia, R., and Ann, P. F. (2013). Periodontal Bacterial Invasion and Infection: Contribution to Atherosclerotic Pathology. *J. Clin. Periodontol.* 40 (s14), S30–S50. doi: 10.1902/jop.2013.1340012

Ley, R. E., Peterson, D. A., and Gordon, J. I. (2006). Ecological and Evolutionary Forces Shaping Microbial Diversity in the Human Intestine. *Cell* 124 (4), 837–848. doi: 10.1016/j.cell.2006.02.017

Madeira, M. F. M., Celso Martins, Q. J., Graciela Mitre, C., Werneck, S. M. C., Daniel, C., Gustavo Pompermaier, G., et al. (2013). Platelet-Activating Factor Receptor Blockade Ameliorates Aggregatibacter Actinomycetemcomitans-Induced Periodontal Disease in Mice. *Infect. Immun.* 81 (11), 4244–4251. doi: 10.1128/IAI.01046-13

Ma, Z., He, S., Wang, X., Sun, J., Zhang, Y., Zhang, G., et al. (2018). Resequencing a Core Collection of Upland Cotton Identifies Genomic Variation and Loci Influencing Fiber Quality and Yield. *Nat. Genet.* 50 (6), 803–813. doi: 10.1038/s41588-018-0119-7

Nakajima, M., Arimatsu, K., Kato, T., Matsuda, Y., Minagawa, T., Takahashi, N., et al. (2015). Oral Administration of P. Gingivalis Induces Dysbiosis of Gut Microbiota and Impaired Barrier Function Leading to Dissemination of Enterobacteria to the Liver. *PLoS One* 10 (7), e0134234. doi: 10.1371/journal.pone.0134234

Olivier, H., Kenza, S. T., Henri, T., Jean-Luc, D., Christine, R., Yves, L., et al. (2011). Evaluating Periodontal Risk for Patients at Risk of or Suffering From Atherosclerosis: Recent Biological Hypotheses and Therapeutic Consequences. *Arch. Cardiovasc. Dis.* 104 (5), 352–358. doi: 10.1016/j.acvd.2011.02.002

Park, C., Abramson, Z. M., Jin, Q., Chang, J., Kreider, J., Goldstein, S., et al. (2007). Three-Dimensional Micro-Computed Tomographic Imaging of Alveolar Bone in Experimental Bone Loss or Repair. *J. Periodontol.* 78 (2), 273–281. doi: 10.1902/jop.2007.060252

Pihlstrom, B. L., Michalowicz, B. S., and Johnson, N. W. (2005). Periodontal Diseases. *Lancet* 366 (9499), 1809–1820. doi: 10.1016/S0140-6736(05)67728-8

Rajilićstojanović, M., Maathuis, A., Heilig, H. G. H. J., Venema, K., Vos, W. M. D., and Smidt, H. (2010). Evaluating the Microbial Diversity of an In Vitro Model of the Human Large Intestine by Phylogenetic Microarray Analysis. *Microbiol. (Read.)* 156 (11), 3270–3281. doi: 10.1099/mic.0.042044-0

Sato, K., Takahashi, N., Kato, T., Matsuda, Y., Yokoji, M., Yamada, M., et al. (2017). Aggravation of Collagen-Induced Arthritis by Orally Administered Porphyromonas Gingivalis Through Modulation of the Gut Microbiota and Gut Immune System. *Sci. Rep.* 7, 6955. doi: 10.1038/s41598-017-07196-7

Schugar, R. C., and Brown, J. M. (2015). Emerging Roles of Flavin Monooxygenase 3 in Cholesterol Metabolism and Atherosclerosis. *Curr. Opin. Lipidol.* 26 (5), 426–431. doi: 10.1097/MOL.0000000000000215

Skennerton, C. T., Haroon, M. F., Briegel, A., Shi, J., Jensen, G. J., Tyson, G. W., et al. (2016). Phylogenomic Analysis of Candidatus 'Izimaplasma' Species: Free-Living Representatives From a Tenericutes Clade Found in Methane Seeps. *Isme J.* 10 (11), 2679–2692. doi: 10.1038/ismej.2016.55

Socransky, S. S., and Haffajee, A. D. (2005). Periodontal Microbial Ecology. *Periodontol. 2000* 38 (1), 135–187. doi: 10.1111/j.1600-0757.2005.00107.x

Stepankova, R., Tonar, Z., Bartova, J., Nedorost, L., Rossman, P., Poledne, R., et al. (2010). Absence of Microbiota (Germ-Free Conditions) Accelerates the Atherosclerosis in ApoE-Deficient Mice Fed Standard Low Cholesterol Diet. *J. Atheroscler. Thromb.* 17 (8), 796–804. doi: 10.5551/jat.3285

Tang, W. H. W., and Hazen, S. L. (2014). The Contributory Role of Gut Microbiota in Cardiovascular Disease. *J. Clin. Invest.* 124 (10), 4204–4211. doi: 10.1172/JCI72331

Tang, W. H., Kitai, T., and Hazen, S. L. (2017). Gut Microbiota in Cardiovascular Health and Disease. *Circ. Res.* 120, 1183–1196. doi: 10.1161/CIRCRESAHA.117.309715

Tomoki, M., Naoki, T., Koichi, T., Yukari, A., Hirotaka, M., Sayuri, M., et al. (2011). Chronic Oral Infection With Porphyromonas Gingivalis Accelerates Atheroma Formation by Shifting the Lipid Profile. *PLoS One* 6 (5), e20240. doi: 10.1371/journal.pone.0020240

Wang, Z., Klipfell, E., Bennett, B. J., Koeth, R., Levison, B. S., Dugar, B, et al. (2011). Gut Flora Metabolism of Phosphatidylcholine Promotes Cardiovascular Disease. *Nature* 472, 57–63. doi: 10.1038/nature09922

Wang, Z., Roberts, A. B., Buffa, J. A., Levison, B. S., Zhu, W., Org, X, E., et al. (2015). Non-Lethal Inhibition of Gut Microbial Trimethylamine Production for the Treatment of Atherosclerosis. *Cell* 163 (2015), 1585–1595. doi: 10.1016/j.cell.2015.11.055

Wang, Z., and Zhao, Y. (2018). Gut Microbiota Derived Metabolites in Cardiovascular Health and Disease. *Protein Cell* 9 (5), 416–431. doi: 10.1007/s13238-018-0549-0

Xu, Q., Oberhuber, G., Gruschwitz, M., and Wick, G. (1990). Immunology of Atherosclerosis: Cellular Composition and Major Histocompatibility Complex Class II Antigen Expression in Aortic Intima, Fatty Streaks, and Atherosclerotic Plaques in Young and Aged Human Specimens. *Clin. Immunol. Immunopathol.* 56 (3), 344–359. doi: 10.1016/0090-1229(90)90155-j

Yang, J., Wu, J., Zhang, R., Yao, M., Liu, Y., Miao, L., et al. (2017). *Porphyromonas Gingivalis* Oral Infection Promote T Helper 17/Treg Imbalance in the Development of Atherosclerosis. *J. Dent. Sci.* 12 (1), 60–69. doi: 10.1016/j.jds.2016.10.003

Zhang, W., Ju, J., Rigney, T., and Tribble, G. (2014). *Porphyromonas Gingivalis* Infection Increases Osteoclastic Bone Resorption and Osteoblastic Bone Formation in a Periodontitis Mouse Model. *BMC Oral. Health* 14 (1), 89. doi: 10.1186/1472-6831-14-89

Conflict of Interest: The authors declare that the research was conducted in the absence of any commercial or financial relationships that could be construed as a potential conflict of interest.

this article, or claim that may be made by its manufacturer, is not guaranteed or endorsed by the publisher.

frontiers in Cellular and Infection Microbiology

ORIGINAL RESEARCH
published: 25 January 2022
doi: 10.3389/fcimb.2022.816526

Cross-Cohort Microbiome Analysis of Salivary Biomarkers in Patients With Type 2 Diabetes Mellitus

Chuqi Gao[1], *Ying Guo*[2] *and Feng Chen*[1]*

[1] Central Laboratory, Peking University School and Hospital of Stomatology, Beijing, China, [2] Department of Stomatology, General Hospital of Shenzhen University, Shenzhen, China

Several studies have ascertained differences in salivary microbiota between patients with type 2 diabetes mellitus (T2DM) and healthy populations. However, the predictive accuracy and reproducibility of these 16S rRNA sequencing analyses when applied to other cohorts remain enigmatic. A comprehensive analysis was conducted on the included 470 samples from five researches in publicly available databases. The discrepancy and predictive accuracy of salivary microbiota between T2DM patients and healthy populations were evaluated from multiple perspectives, followed by the identification of salivary biomarkers for DM. Next, a classification model (areas under the curves = 0.92) was developed based on a large sample. The model could be used for clinical diagnosis and prognostic monitoring and as a basis for hypothesis-driven mechanistic researches. Furthermore, the research heterogeneity across geographic regions suggested that microbiological markers might not become a uniform clinical standard in human beings. They rather identify abnormal alterations under the microbiological characteristics of a specific population.

Keywords: type 2 diabetes mellitus, biomarker, human microbiome, sequence analysis, meta-analysis, 16S

OPEN ACCESS

Edited by:
Xin Xu,
Sichuan University, China

Reviewed by:
Mythily Srinivasan,
Indiana University,
Purdue University Indianapolis,
United States
Xiaoquan Su,
Qingdao University, China

***Correspondence:**
Feng Chen
chenfeng2011@hsc.pku.edu.cn

Specialty section:
This article was submitted to Microbiome in Health and Disease, a section of the journal Frontiers in Cellular and Infection Microbiology

Received: *16 November 2021*
Accepted: *10 January 2022*
Published: *25 January 2022*

Citation:
Gao C, Guo Y and Chen F (2022) Cross-Cohort Microbiome Analysis of Salivary Biomarkers in Patients With Type 2 Diabetes Mellitus. Front. Cell. Infect. Microbiol. 12:816526. doi: 10.3389/fcimb.2022.816526

INTRODUCTION

Type 2 diabetes mellitus (T2DM), the most prevalent type of diabetes mellitus (DM), is attributed to a progressive decrease in insulin secretion and insulin resistance. It is ultimately characterized by poor glucose tolerance, hyperglycemia, and overt DM, accounting for 90-95% of DM population (Alvarenga et al., 2020). The International Diabetes Federation estimates that the prevalence of T2DM in the global adult population will exceed 10% by 2040 (Ogurtsova et al., 2017). There exist multiple diagnostic methods of DM, including fasting serum/plasma glucose tests, oral glucose tolerance tests, and interim glucose tests combined with clinical symptoms. HbA1c has been proposed as a screening and diagnostic test for DM (Higgins, 2013). However, these methods are invasive, which limits the possibility of large-scale screening. Thus, there is still an urgent need to explore easy, non-invasive, and highly accurate screening methods.

Periodontal disease is one of the common complications of DM, which has drawn attention to the oral microbiology of T2DM patients, expecting to find non-invasive biomarkers specific to DM in the oral cavity (Kocher et al., 2000). Previously, several researches have reported that specific periodontal microbes are associated with DM and that the alterations in the periodontal microbial

community are potential precursors to periodontal diseases (Long et al., 2017; Shi et al., 2020; Omori et al., 2021). DM has been documented to reduce the diversity and community stability of oral microorganisms (Sabharwal et al., 2019; Yang et al., 2020). However, there also exist multiple opposite conclusions (Casarin et al., 2013). Several studies have revealed salivary biomarkers and predictive models for T2DM (Sun et al., 2020; Liu et al., 2021). However, the predictive accuracy and reproducibility of these biomarkers and models remain poorly identified when applied to other cohorts. In conclusion, it is generally accepted that the changes in the oral microbiology are correlated with the pathogenesis of T2DM, but there has never been a consensus on the specific pathogenic microorganisms.

It is urgent to validate the associations of the human oral microbiome and DM across populations, geographic regions, and cohorts. Large-scale cross-cohort researches combine and analyze raw sequencing data from massive samples. They provide a powerful and bias-reducing method to decrease the impact of confounding factors such as epidemiological characteristics and operative techniques, realizing the uniformity of results across multiple studies worldwide. Therefore, these researches have effects comparable to multi-center large-sample studies (Thomas et al., 2019). Although microbiological researches of T2DM and periodontitis are of great interest, there have not been any large cross-cohort studies to date.

As oral microbiology has been increasingly studied, there is a research observing that the sample collection method can significantly impact the results of oral microbiome analyses (Yano et al., 2020). Traditionally, the oral microbiome in periodontal disease has been characterized by sampling subgingival plaque (Abusleme et al., 2013). However, more researches have chosen to collect saliva samples to characterize the oral microbiome due to the easy sampling. In addition to sampling, the selection of the hypervariable regions in the sequenced 16S rRNA gene has an impact on characterizing the diversity of the oral microbiome (Griffen et al., 2012). The primer pairs spanning the V3-V4 hypervariable region captured better diversity in contrast to primer pairs spanning the V1-V3 region (Castelino et al., 2017). Illumina platform is the most commonly used sequencing platform in second-generation sequencing (Pichler et al., 2018).

This research harvested 470 samples from five studies in publicly available databases, where DNA was extracted from saliva samples to amplify V3-V4 hypervariable regions in the 16S rRNA gene and conduct sequencing on the Illumina platform. A comprehensive analysis was implemented to evaluate the salivary microbial discrepancy and predictive accuracy between T2DM patients and healthy populations. Then, salivary biomarkers for T2DM were predicted and a classification model was constructed based on large-scale samples.

MATERIALS AND METHODS

Public Data Collection

The sequencing raw data of 16S rRNA of T2DM patients and healthy controls were harvested from published studies on PubMed and Embase with the inclusion of all publication dates and all languages. Analyses of this research were conducted on T2DM patients who met the inclusion criteria, and the complete oral microbiome was evaluated using 16S rRNA sequencing technology.

The inclusion criteria were as follows: (1) case-control or cross-sectional studies, or the researches published as original articles; (2) independent studies, or the most recent or informative reported results in the case of multiple reports for the same group or subgroup; (3) all samples collected as unstimulated saliva; (4) 16S rRNA sequencing using the Illumina platform, amplification of V3-V4 hypervariable region in the 16S rRNA gene; (5) the studies providing raw data of 16S rRNA sequencing for all samples. Reviews, letters to the editor, monographs, conference papers, book chapters, case reports, unpublished data, and animal studies were excluded. Also, researches were excluded if at least one of the following criteria was present: (1) the studies without a non-diabetic control group; (2) the patient with a concurrent systemic disease other than T2DM or undergoing treatment such as implant placement, crown orthodontics, or periodontal surgery; (3) the primary finding not related to T2DM.

After screening, only seven studies fully met the inclusion criteria, among which only four submitted the raw data in the Sequence Read Archive (SRA) database of National Center for Biotechnology Information (NCBI). We sent e-mails requesting raw data to the corresponding authors of the other three studies but only received data returned by Dr. Amarpreet Sabharwal. Therefore, this work included only five studies with accessible sample metadata and high-throughput sequencing performance for the V3-V4 region of the 16S rRNA gene. The raw data for four of the five studies and the independent cohort were read and downloaded from the SRA database of NCBI using the SRA Toolkit (V.2.9.2) with the following sequence numbers: PRJNA561495 by Yang et al., PRJNA601054 by Sun et al., PRJNA609009 by Liu et al., PRJNA679485 by Almeida-Santos et al, and the independent cohort with the number of PRJNA664107. The readers can download them by https://www.ncbi.nlm.nih.gov/sra/?term=PRJNA561495, https://www.ncbi.nlm.nih.gov/sra/?term=PRJNA601054, https://www.ncbi.nlm.nih.gov/sra/?term=PRJNA609009, https://www.ncbi.nlm.nih.gov/sra/?term=PRJNA679485 and https://www.ncbi.nlm.nih.gov/sra/?term=PRJNA664107.

Data Pre-Processing

The results were stored in FASTQ (referred to as fq) format file, which contained sequence information of reads and their corresponding sequencing quality information. Raw reads were firstly filtered by Trimmomatic v0.33. Then the primer sequences were identified and removed by cutadapt 1.9.1, which finally generated high-quality reads without primer sequences. Based on overlapping sequences, high-quality reads were assembled by FLASH v1.2.7, which generated clean reads. Chimeric sequences were identified and removed by UCHIME v4.2, generating effective reads.

Quality Assessment of Sequencing Data

After processing the raw data, data quality was estimated based on parameters, such as read length, counts of reads at each stage,

guanine-cytosine (GC) content, PHRED quality score threshold of 20 (Q20) and Q30 quality, and effective values. All samples had sufficient sequencing depth, except for three samples in Almeida-Santos's study. The end of the rarefaction curves showed a gentle rise, indicating that sequencing saturation was achieved for all samples and that operational taxonomic units (OTUs) covered most of the microbial species present in saliva (see **Supplementary Figure 1**).

Data Annotation and Statistical Analysis

Usearch was applied to cluster reads with similarity above 97.0%, generating OTUs (Edgar, 2013). Taxonomic annotations of feature sequences were processed by a Bayesian classifier using SILVA as a reference database (Sierra et al., 2020). Alpha and beta diversity metrics were evaluated by QIIME2 (Fung et al., 2021). In identifying T2DM versus healthy controls, the Wilcoxon rank sum test was used to determine statistical differences between groups, considering that there were only two groups which did not follow a normal distribution. Additionally, in identifying study heterogeneity among five groups, Anosim analysis was used. The randomForest in R package was applied to construct a random forest (RF) model and calculate the effect of each variable on the heterogeneity of observations at each node of the classification tree to obtain MeanDecreaseGini values. Then a 10-fold cross-validation was performed by dividing the dataset into ten parts and experimenting with nine of them in turn as the training set and one as the test set. The RF model was reconstructed using the one with the highest accuracy. The test set was trained again. Next, receiver operating characteristic (ROC) curves were plotted using the output predicted values, followed by the calculation of area under the ROC curve (AUC) values, accuracy, precision, and recall. FAPROTAX database was utilized to perform species annotation on feature sequences based on reference phylogenetic tree. Potential functions and functional genes in samples were predicted, which further revealed the difference in functions between samples or groups. The significance of difference in function abundance between samples was evaluated by G-test (the number of annotated functional genes > 20) and Fisher (the number of annotated functional genes < 20) in STAMP.

RESULTS

The Characteristics of the Large Scale Dataset

In this research, the sequencing raw data of 16S rRNA from five studies were investigated to assess differences of salivary microbiome between T2DM patients and healthy populations and to identify DM-specific biomarkers. In total, 273 samples were obtained from T2DM patients and 200 samples were collected from healthy controls. Demographic information is presented in **Table 1**, including age, sex, body mass index (BMI), and country of the subjects in each study. All samples were sequenced at sufficient depth except for 3 samples (SRR13084941, SRR13084942, and SRR13084945) from the research by Almeida-Santos et al. These samples were excluded for further analysis. A total of 21,995,091 paired-end (PE) reads were generated from the final 470 samples. After that, 17,894,743 clean reads were obtained after the quality control and assembly of the PE reads. The total number and the average number of reads per study are also recorded in **Table 1**. An average of 38,074 clean reads was generated per sample. Quality control was performed on the raw data, including the removal of the low-quality reads, the filtration based on length, and the generation of the high-quality reads. Consistent processing was conducted for all raw sequencing data on the Quantitative Insights Into Microbial Ecology platform.

The Identification of the Heterogeneity in the Potential Studies

The heterogeneity of the potential studies was explored due to the technical and biological differences among these studies. From **Figures 1A, B**, it was seen that there were significant differences in the microbial species contained in the five researches, which was tentatively speculated to be related to their geographical discrepancies. A typical phenomenon in **Figure 1B** was that the distribution of the characteristics of the three studies in Shandong, Anhui, and Sichuan was concentrated in quadrants 1, 2, and 4, whilst the study in the USA was concentrated in quadrant 3 and the study in Portugal was distributed in all the quadrants. It was thus speculated that microbial differences might also be influenced by ethnicity.

TABLE 1 | Clinical Characteristics of Large-Scale Dataset*.

	Group (N)	Age (average ± s.d)	Sex (F/M)	BMI (average ± s.d)	Total Reads	Average Reads	Country
US	DM (79)	52.99 ± 8.53	36/43	32.97 ± 8.12	5582131	39036	USA
	Control (64)	39.73 ± 14.36	40/24	27.73 ± 5.80			
Shandong	DM (70)	54.63 ± 12.13	20/50	26.63 ± 4.64	3593179	35227	China
	Control (32)	49.19 ± 8.72	16/16	24.77 ± 2.70			
Anhui	DM (75)	58.56 ± 10.46	43/32	25.67 ± 3.48	5186681	38998	China
	Control (58)	37.21 ± 13.87	41/17	22.22 ± 3.05			
Sichuan	DM (24)	47 (33–65)	11/13	25.97 ± 2.32	1652946	36732	China
	Control (21)	47.24 (35-61)	11/10	23.23 ± 2.08			
Portugal	DM (25)	62.72 ± 7.12	8/17	28.36 ± 5.20	1879806	39996	Portugal
	Control (22)	59.91 ± 8.88	6/16	26.79 ± 4.52			

The V3-V4 hypervariable region in the 16S rRNA gene was amplified in all studies.

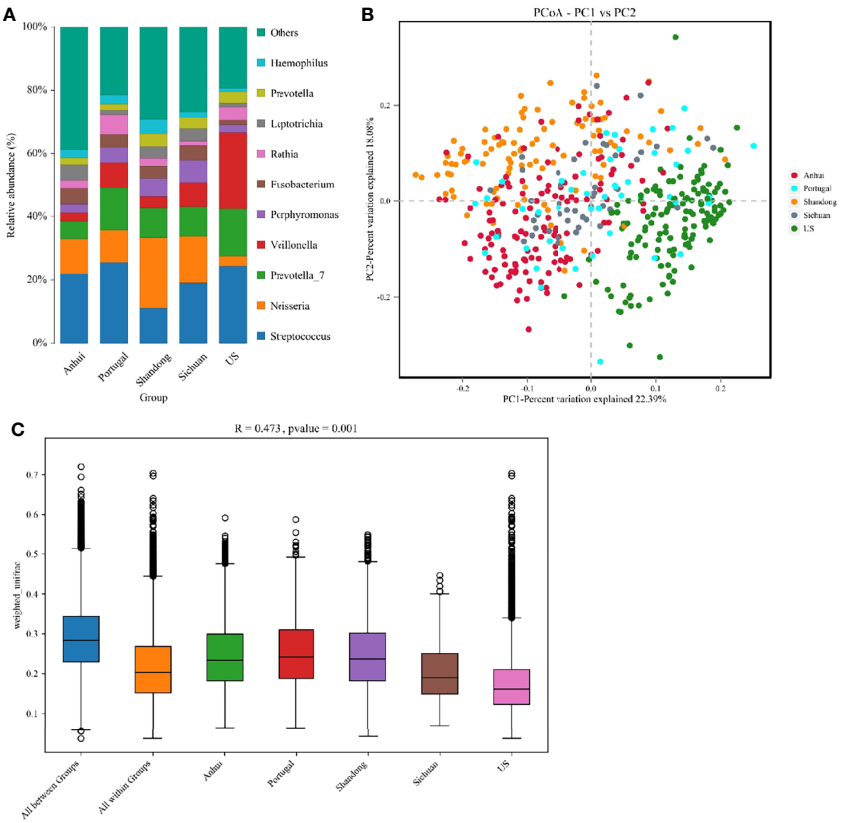

FIGURE 1 | **(A)** The structure analysis of the microbial community. The composition statistics were calculated for each sample at the phylum, order, family, genus, and species levels. This figure showed bar graphs of microbial abundance at the genus level for the five studies. **(B)** The PCoA of all samples from the five studies based on Weighted-Unifrac distances. X-axis and y-axis represented two eigenvalues that maximized the differences between samples, respectively. **(C)** R and *p* values for beta diversity based on Weighted-Unifrac distances calculated using the Anosim analysis (analysis of Similarities). The closer the R value was to 1, the greater the differences between groups were than the differences within groups; the smaller the R value, the less significant the differences between the groups. $p < 0.05$ showed high reliability of the test. The box above "All between Groups" indicated the Weighted-Unifrac distance data of the samples among all groups, while the box above "All within Groups" indicated the Weighted-Unifrac distance data of the samples within all groups. The box below represented the Weighted-Unifrac distance data of samples within different groups.

In the principal coordinate analysis (PCoA), there was no corresponding statistical test to conclude whether the differences between the different groups were significant or not. Therefore, the significance of the differences was calculated using the Anosim analysis (**Figure 1C**), in which R = 0.473 indicated significant differences between groups in the five studies ($p = 0.001$).

Salivary Microbial Differences Between T2DM Patients and Healthy Controls

A total of 197 species in 148 genera from 13 phyla, 20 orders, and 43 families were detected. There existed no significant differences in the salivary microbial community between T2DM patients and healthy controls from all aspects assessed. Alpha diversity analysis manifested no significant differences between the two groups in terms of mean Shannon, Simpson, Abundance-based Coverage Estimators (ACE), Chao1, and Phylogenetic diversity (PD) whole tree indexes (**Table 2**).

In the analysis of the beta diversity, the PCoA revealed that the saliva samples from T2DM and control groups could not be separated, suggesting insignificantly different salivary microorganisms. R = 0.027 from the Anosim analysis further verified insignificant difference between groups ($p = 0.004$) (**Figures 2A, B**). Venn diagram indicated that T2DM patients shared the same salivary "core microbiome" as the healthy populations and that the salivary microbiota of T2DM patients might not have specific characteristics compared to the control individuals (**Figure 2C**). The fully overlapping "core microbiome" also supported the further analysis of the related microbes between the two groups at the phylum, genus, and species levels.

TABLE 2 | Alpha Diversity Indicators.

	Control	DM	p value
Shannon	4.7722 ± 0.0587	4.817 ± 0.0407	0.5179
Simpson	0.9013 ± 0.0064	0.9124 ± 0.0028	0.0844
ACE	232.1372 ± 4.7197	233.271 ± 4.5195	0.8649
Chao1	233.602 ± 4.9316	235.2331 ± 4.6347	0.8127
PD whole tree	14.5491 ± 0.3559	14.407 ± 0.3075	0.7632

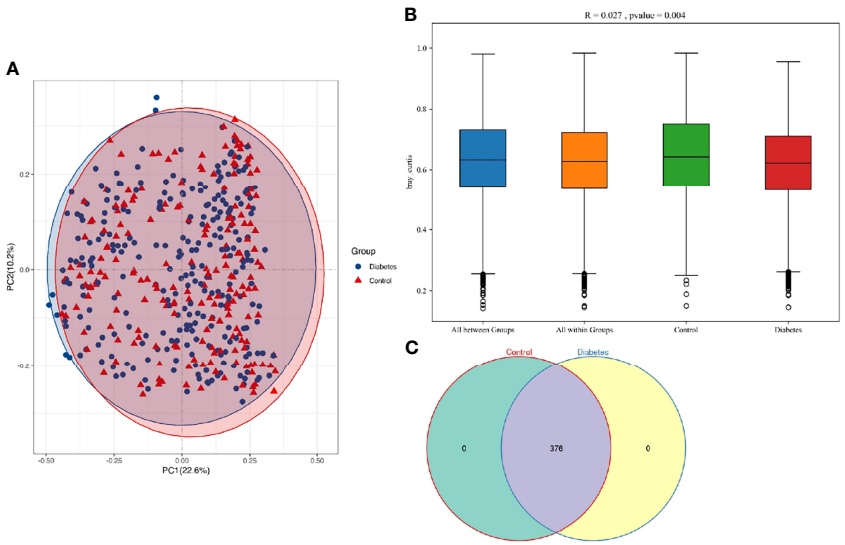

FIGURE 2 | **(A)** PCoA based on Bray-Curtis distances for all samples from T2DM patients and healthy controls (T2DM, n = 273; control, n = 197). Ellipses represented 95% confidence level. The blue and red ellipses almost overlapped, indicating insignificant differences between T2DM patients and healthy populations. **(B)** R and *p* values for the beta diversity based on Bray-Curtis distance calculated using Anosim analysis (analysis of Similarities). The closer the R value was to 1, the greater the differences between groups than the differences within groups. The smaller the R value was, the less significant the differences between them. $p < 0.05$ showed the high reliability of the test. **(C)** The numbers in each independent or overlapping region of the Venn diagram representing the number of features in each corresponding set, indicating that the "core microbiome" of T2DM patients and healthy controls overlapped completely.

The Wilcoxon rank-sum test was utilized to analyze differences in salivary microorganisms between groups from the phylum to the OTU level. At the phylum level, the salivary microbiota of T2DM patients and healthy controls was dominated by p. Firmicutes (41.74% and 39.76%), followed by p. Bacteroidetes (23.10% and 22.08%), p. Proteobacteria (17.97% and 21.31%), p. Fusobacteria (7.11% and 6.77%), and p. Actinobacteria (6.38% and 4.88%), accounting for approximately 95% of the total bacteria (**Figure 3A**). The increase of the p. Actinobacteria in T2DM patients was significant ($p = 0.001$), which was similar to the findings of Yang et al. and Long et al. (Long et al., 2017; Yang et al., 2020). We also found an elevation in the ratio of p. Firmicutes/p. Bacteroidetes (1.181 and 1.180), although this change was not significant ($p > 0.05$). The ratio of p. Firmicutes/p. Bacteroidetes has been documented to enhance in the gut of T2DM patients and be associated with the mild inflammation and the improved capacity of obtaining energy from food (Pascale et al., 2019). There is also a large-sample oral research that confirms the enhancement of this ratio in the oral cavity of T2DM patients (Chen et al., 2020).

At the genus level, the dominant genera were Streptococcus (20.41% and 20.28%), Neisseria (11.47% and 10.94%), Veillonella (11.28% and 9.53%), Prevotella_7 (10.91% and 9.82%), Porphyromonas (3.95% and 3.92%), and Rothia (3.63% and 2.70%) (**Figure 3B**), among which only the augmentation in Rothia was significant ($p < 0.001$) in T2DM patients.

The significant differences in species abundance between the two groups were analyzed at the species level. Only uncultured_bacterium_g_Rothia among the top 15 species in abundance augmented obviously [$p = 2.0 \times 10^{(-11)}$] in the T2DM patients. Besides, Prevotella_7, Veillonella, and a group of uncultured Lactobacillus elevated comparatively significantly ($p < 0.05$). The remaining species did not significantly differ between the two groups (**Supplementary Table 1**). Among the five researches, the subjects from Portugal and US had higher levels of Rothia (**Figure 1A**). To exclude the possibility that one study had a disproportionate effect on the results, these two studies were removed separately, which displayed that the elevation of Rothia remained significant [$p = 6.2 \times 10^{(-10)}$ and $p = 2.5 \times 10^{(-5)}$]. This result illustrated the general elevation of Rothia in the T2DM population. To exclude confounding factors, the separate regression analyses were implemented for the content of Rothia according to known sex, age, BMI, and smoking frequency, which exhibited insignificant linear relationship ($R < 0.05$).

To further dissect the presence of significantly different bacteria between T2DM patients and control individuals, a linear discriminant analysis (LDA) Effect Size (LEfSe) analysis was performed from the phylum to the OTU level. The Kruskal-Wallis rank-sum test was conducted for OTUs with LDA scores > 2, which depicted a significant difference ($p < 0.05$) in some OTUs between T2DM patients and healthy controls (**Figure 3C**).

The Microbial Classification Model for the Saliva With T2DM

An RF model was firstly constructed using all OTUs. Then, we evaluated the impacts of each variable on the heterogeneity of the observations at each node of the classification tree and measured the importance of the variables by MeanDecreaseGini to obtain

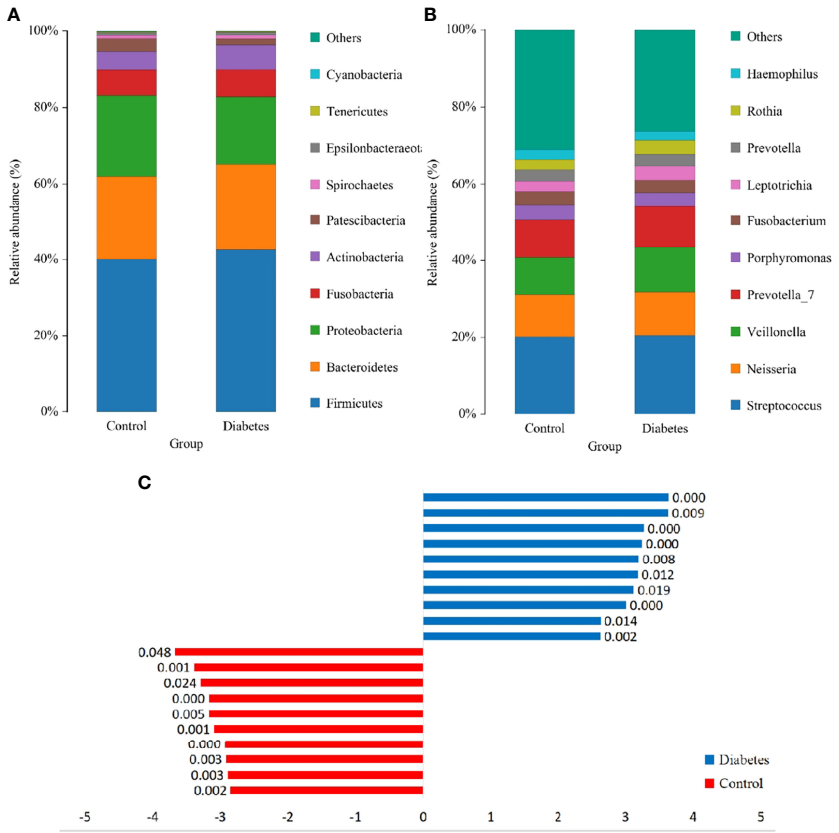

FIGURE 3 | The structure analysis of the microbial community. **(A)** and **(B)** are the bar graphs of microbial abundance at the phylum and genus levels, respectively. **(C)** LDA bar graph. Blue and red bars represented LDA values for taxa enriched in the T2DM group and those enriched in the healthy controls with *p*-values labeled next to the bars, respectively.

the top 20 key OTUs (**Figure 4A**). Among them, Rothia sp. was the most key one, which was consistent with the results of the beta diversity analysis. The next most key factors were Pseudomonas, Candidatus_Saccharimonas, Actinomyces_odontolyticus, Leptotrichia, Pasteurellaceae, Actinomyces, Prevotella_salivae, Escherichia-Shigella, and Nanoarchaeaeota.

Further, a T2DM ancillary diagnostic model was developed. The RF models were constructed based on the top 30 most important and richest OTUs and all OTUs, respectively, and were tested with 10-fold cross-validation based on OTUs. The comparison of the obtained ROC curves and AUC values revealed that the top 30 most important OTUs had higher AUC values (**Figure 4B**), which was consistent with the findings of previous studies. In addition, to determine the number of factors included in the model, the RF models containing the top 20, 30, and 40 OTUs in importance were constructed, and the obtained ROC curves and AUC values were compared. The findings demonstrated that the top 30 OTUs in importance had higher AUC values (**Figure 4C**). It was worth mentioning that the RF model was constructed using only one variable, Rothia sp., which manifested that the AUC value was still as high as 0.69. To our knowledge, no OTU has ever had such a high AUC value as an independent indicator, which again proves the importance of Rothia in the diagnosis of T2DM.

Therefore, the RF model containing the top 30 OTUs in importance were finally identified as the T2DM ancillary diagnostic model (**Supplementary Table 2**). Rothia sp. had the highest IncNodePurity value, indicating its irreplaceable importance in the model (AUC = 0.92, accuracy = 0.83, precision = 0.83, and recall = 0.89).

Inter-Study Transfer Validation of a Salivary Microbial Classification Model

To test whether the top 30 important OTUs identified were generalizable and robust across multiple studies, leave-one-dataset-out (LODO) validation and inter-study transfer validation were performed on the entire sample (**Figure 5**). The mean LODO was 0.79, demonstrating that the conclusion was general across the five studies with negligible influence of any single study. The AUC values for the inter-study transfer validation ranged from 0.37 to 0.91 with a wide span and a mean value of 0.59. The values on the diagonal were high enough, the highest of which was close to the AUC value of the RF model. This indicated that the important features identified by the RF model had good diagnostic strength when T2DM patients had similar clinical characteristics with the healthy population, such as the same geographic region. However, the lower non-diagonal

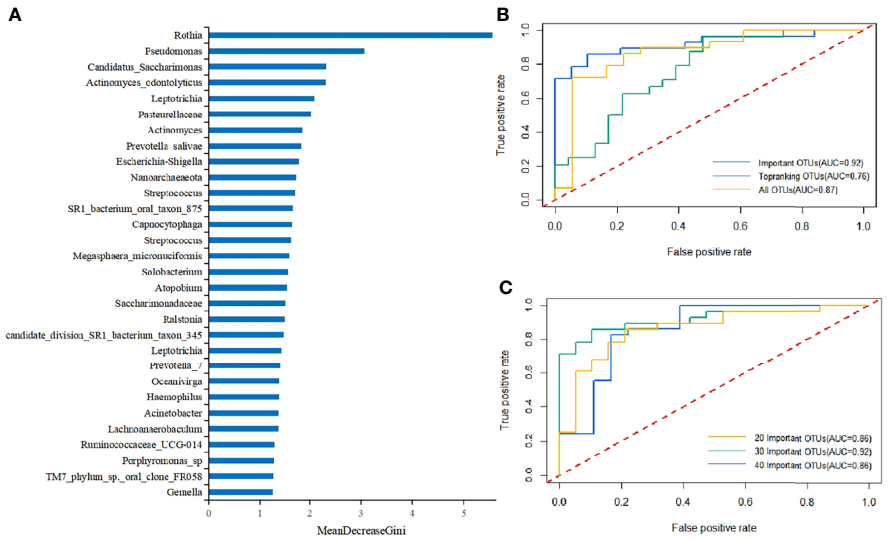

FIGURE 4 | **(A)** Key components of the RF model constructed using all OTUs to distinguish differences between T2DM patients and healthy controls (MeanDecreaseGini values represented the importance of species in the RF model). **(B)** The 10-fold cross-validation was performed on the RF model, and the model was reconstructed using the sample with the highest precision. The ROC curves and AUC values of the overall test set are shown above. The top 30 important and top-ranking OTUs were selected, respectively, where each OTU could be considered as an independent species. **(C)** The 10-fold cross-validation was performed on the RF model, and the model was reconstructed using the sample with the highest accuracy. The ROC curves and AUC values of the overall test set are shown above. 20 Important OTUs, 30 Important OTUs, and 40 Important OTUs represented the top 20, 30, and 40 OTUs in importance, respectively, where each OTU could be considered as an independent species.

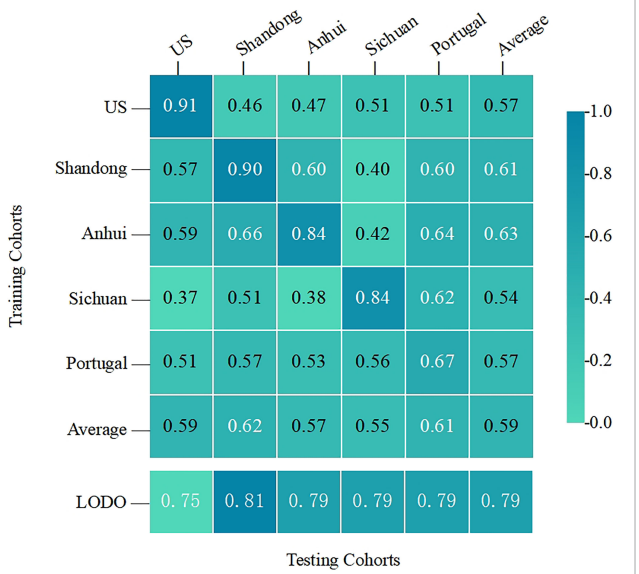

FIGURE 5 | The cross-prediction matrix thoroughly showed the AUC values of the five studies themselves and between them for the prediction of T2DM. The values on the diagonal were the results of the cross-cohort validation within each study. The non-diagonal AUC values were obtained by training the classifier on the study in each row and tested on the study in the corresponding column.

values suggested that the cross-validation within each study was generally better than that between studies. These results provided some evidence that a range of clinical characteristics represented by geographic region could severely afflict the diagnostic ability of the RF model for T2DM.

Altered Salivary Microbial Function in T2DM Patients

Currently, the Greengene database is not updated as fast as SILVA, so we used the SILVA as the reference database. However, both the commonly used Phylogenetic Investigation of Communities by Reconstruction of Unobserved States (PICRUSt) and BugBase analyses are only applicable to the Greengene database. Therefore, FAPROTAX database was applied for functional annotation prediction of all the samples, which has better prediction accuracy but may have less prediction coverage compared to PICRUSt. Human pathogen septicemia was only one significant functional gene alteration in the salivary microbiota of T2DM patients observed ($p < 0.01$) (**Supplementary Figure 2**). This evidence suggested an association between T2DM and septicemia. Human pathogens septicemia was added for reconstructing the RF model as the 31st variable, yielding an AUC value of 0.85. However, we unexpectedly found that with 31 variables, the recall improved from 0.89 to 0.93, which may be more favorable for future applications in large-scale screening. No other significant alteration had been observed in the salivary microbiota of T2DM patients.

Validation in an Independent Cohort of Subgingival Samples

46 subgingival periodontal samples with the sequence number PRJNA664107 (Diabetes n=15, Control=31) were selected as an independent cohort for validation and obtained an accuracy rate of 0.78. This rate is comparable to the accuracy of the inter-study validation, which indicates that the constructed model has good predictive power both in the included studies and outside of them.

DISCUSSION

By combining raw data from available datasets for the unified analysis, our two major findings were as follows: first, salivary microbial diversity was not significantly different between T2DM patients and healthy populations, which was confirmed by multiple statistical means. The second finding was that Rothia sp. was significantly higher in T2DM patients than in healthy population [$p = 2.0 \times 10\text{^}(-11)$], which was the joint result of the Anosim analysis, the Wilcoxon rank-sum test, the Kruskal-Wallis rank-sum test, and the RF model significant factor analysis with the exclusion of the effects of every single study. Therefore, we concluded that Rothia sp. was the most representative salivary biomarker in T2DM patients. It was worth mentioning that a significant elevation of Rothia sp. was observed in three of five included studies ($p < 0.001$), but was not specifically mentioned in the text (Sabharwal et al., 2019; Sun et al., 2020; Yang et al., 2020).

Rothia sp. belongs to p. Actinomycetes, the increase of which was also confirmed in T2DM patients. In fact, the association of p. Actinomycetes with T2DM has attracted increasing attention, but there is no consensus whether it increases or decreases in T2DM (Long et al., 2017; Matsha et al., 2020). Rothia sp. is a popular nitrate-reducing bacterium in the oral cavity and participates in the nitrate (NO3-)-nitrite (NO2-)-nitric oxide (NO) pathway, the positive impacts of which on NO activity favor the cardiovascular diseases (Vanhatalo et al., 2018). However, the discoveries of the present study suggested that this positive effect did not seem to apply to DM and that the exact role of nitrogen metabolism in the pathogenesis of DM remained to be further investigated. Prevotella sp., the next most critical biomarker of T2DM identified in this study, has been reported to be a pathogenic genus associated with insulin resistance and poor glucose tolerance (Pedersen et al., 2016).

However, the shift from a single pathogen doctrine to a microecological doctrine about inflammation and dysbiosis suggests that we should focus more on the whole picture of the flora rather than on some specific pathogen. Although Rothia sp. is of great significance in T2DM diagnosis as a common feature of T2DM patients in all geographical populations, it is still necessary to find an appropriate complementary diagnostic model to improve clinical diagnosis. Therefore, another crucial result of our work was the construction of a highly accurate T2DM prediction model based on the large sample with an AUC of 0.92, which could be applied for clinical diagnosis and prognostic monitoring.

Of the five studies included, two studies found decreased microbial alpha diversity in the saliva of T2DM patients (Sabharwal et al., 2019; Yang et al., 2020), whereas three studies observed insignificant changes (Sun et al., 2020; Almeida-Santos et al., 2021; Liu et al., 2021). However, there also exist unincluded researches elucidating that alpha diversity is elevated in T2DM patients (Casarin et al., 2013). Sun et al. and Almeida-Santos et al. also noted that the composition of the salivary microbial community in T2DM patients with periodontitis converged to that of healthy individuals after effective glycemic control (Sun et al., 2020; Almeida-Santos et al., 2021). However, the research of Yang et al. elucidated that the diversity of the salivary microbial community did not change obviously after metformin or combination therapy, which meant that treatment might not lead to flora recovery (Yang et al., 2020). In terms of the beta diversity between T2DM patients and healthy controls, three studies concluded that the differences were significant (Sabharwal et al., 2019; Sun et al., 2020; Yang et al., 2020). For example, the PCoA of Unweighted-UniFrac distance elaborated that the salivary microbiota distribution was more dispersed in non-diabetic individuals than in individuals with a history of T2DM (Yang et al., 2020). Additionally, two other studies uncovered similar distributions between groups (Almeida-Santos et al., 2021; Liu et al., 2021). However, in the present research, the differences once observed were practically offset after expanding the sample size. These contradictory results ultimately point to the conclusion that T2DM and healthy population have a similar salivary microbial composition.

Although the oral microbiome exhibited little difference in microbial diversity between T2DM patients and healthy controls, several biomarker differences were significant at each taxonomic level and these biomarkers were validated to be prevalent across the five studies, such as Rothia, on which we focused in our analysis. We found that there was indeed a difference in salivary microbial composition between T2DM patients and healthy populations, specifically in terms of biomarker content, but not diversity. It is clear that diversity is not sensitive enough in characterizing salivary microorganisms. Although Rothia as a single biomarker was valid to demonstrate differences between T2DM patients and healthy populations with a high prediction accuracy of 0.69, it was not high enough. Therefore, we attempted to construct a model with more variables in unison using the top 30 significant OTUs to capture small differences in their entirety with an accuracy of 0.92.

Through a large-scale cross-cohort study, we found that the conclusions of numerous previous 16S rRNA sequencing analyses were hasty. The argument for causality requires experiments with a logical framework that abides by Koch's Law throughout, which is currently lacking in most 16S rRNA studies. A microbiome-wide association analysis is the first step in finding the members of all floras associated with a disease. Then, the disease-associated members are isolated and cultured into pure strains or member-defined compositions, which are

inoculated into sterile animal models. Afterwards, the animals are placed under the appropriate environmental conditions to cause disease. Finally, immunological mechanisms are utilized to elucidate how these bacteria from the human body molecularly interact with the host to result in disease initiation. After this cycle, causality can be confirmed. The bacteria with proven causality and their active products can be employed as not only biomarkers for the diagnosis and early prediction but also as novel targets for disease prevention and treatment. It currently appears that only about 10% microbiota may afflict human health. Most of the oral and gut bacteria are background noise, which are virtually eliminated after the sample size is expanded in the present study. Disease-related bacteria cannot be simply found if researchers rely on various indexes of microbial diversity provided by databases and conduct classification and cutting-dimension analyses.

In addition, all five studies excluded factors (such as systemic disease and recent periodontal treatment) that assumed a significant role in confounding. And we also unveiled that the expanded sample size largely attenuated potential variations that could impact the accuracy of the results, such as oral hygiene status. As three of the five included researches did not disclose their specific clinical characteristics corresponding to the samples (including age, gender, BMI, and smoking), these clinical characteristics were not taken into account in the model. However, to mitigate the influence of these characteristics on the results, we evaluated the effects of available clinical characteristics on Rothia content. The regression analysis displayed that only the effects of age were significant ($p < 0.01$), and that the effects of gender, BMI, and smoking were not significant ($p > 0.01$). Similarly, the available results demonstrated that a range of clinical characteristics, represented by geography or ethnicity, could remarkably influence the ability of any classification models to diagnose T2DM, such as the higher Rothia sp. in US and Portugal populations (**Figure 1A**). Therefore, microbiological indicators should not be pursued to become a unified clinical standard for human beings but rather identify abnormal alterations under the microbiological characteristics of each specific population.

The diagnostic model provided by two of our included studies (in China) unraveled a substantial reduction in AUC when applied to another study (in the USA), which provided evidence for the salivary microbiological discrepancy in T2DM populations under different geographical regions. Interestingly, the study conducted by Almeida-Santos et al. has a relatively small sample size (n = 47) among the five studies. However, the microbial composition of this study was the most similar to the present study, especially the identical dominant bacteria at the phylum level (Almeida-Santos et al., 2021). The study also had the most homogeneous distribution in the PCoA, covering the quadrant, whilst the other four studies presented uneven distribution (**Figure 1B**). We strongly hypothesized that this was related to the mixed Caucasian and Yellow ancestry of Portugal, making its characteristics intermediate between those of the American and Chinese subjects.

On the other hand, the independent cohort validation has shown that salivary and subgingival microbial alterations are similar in patients with T2DM. We hypothesize that the unique microorganisms in saliva of T2DM patients are likely to originate from these eco-locations. However, our analysis unveiled that the microbial alterations characterized by saliva samples are extremely subtle and saliva samples might not be the best choice for identifying the microorganisms that could characterize T2DM patients. The oral cavity is classified into numerous different ecological sites, in which the bacteria communicate with each other through saliva, but their characteristics are totally variable. The eco-location and physicochemical environment of subgingival plaque and gingival sulcus are more specific than most of the other sites (Mark Welch et al., 2020). Therefore, the alterations may be similar in subgingival microorganisms, but are amplified. This suggests that subsequent researchers should prefer to take subgingival plaque as study subjects in order to complete oral microbiological studies related to periodontitis, although most studies have chosen to acquire saliva samples to represent the oral microbiome. Care should be taken when comparing or combining these studies to differentiate the sites sampled, such as gingival sulcus fluid and subgingival biofilm (Babaev et al., 2017; Demmer et al., 2019; Balmasova et al., 2021).

The correlation between DM and septicemia has been confirmed in several pieces of evidence (Yende and van der Poll, 2009; Schuetz et al., 2011), which explains the fact that an enhanced proportion of human pathogen septicemia functional genes is observed in the saliva of T2DM patients. The main reason for which T2DM has susceptibility to infection appears to be abnormalities of the host response, particularly of neutrophil chemotaxis, adhesion and intracellular killing, and defects that have been attributed to the effect of hyperglycemia (Koh et al., 2012). The importance of this discovery is that we added human pathogens septicemia for reconstructing the RF model as the 31st variable, yielding a recall of 0.93, which may contribute to the early prevention and monitoring of T2DM.

To the best of our knowledge, our research is the first large-sample analysis of oral microbiology in T2DM patients. We believe that as the sample size continues to expand, the salivary microbial diversity may become more similar between T2DM patients and healthy populations. Due to the unclear mechanisms of Rothia sp. in the pathogenic process of T2DM, it is not certain that its significant growth will be influenced by the larger sample size. This suggests that the positive results from prior studies are likely to be influenced by confounding factors. Multicenter clinical studies are still awaited to provide further evidence for this conjecture.

DATA AVAILABILITY STATEMENT

Publicly available datasets were analyzed in this study. This data can be found here: PRJNA561495 PRJNA601054 PRJNA609009 PRJNA679485 PRJNA664107.

AUTHOR CONTRIBUTIONS

CG and YG conceived and designed the project. CG downloaded, analyzed data, interpreted results, produced figures and drafted the manuscript. FC revised the manuscript. CG, YG, and FC all contributed to manuscript writing and editing. All authors read and approved the final manuscript.

FUNDING

This work is supported by the National Science Foundation China (grant no. 81991501) and the open project of State Key Laboratory of Oral Diseases (grant no. SKLOD2021OF03).

ACKNOWLEDGMENTS

We appreciate Dr. Amarpreet Sabharwal, Dr. Xiaoyu Sun and Dr. Yunkun Liu for providing us with the raw data from their studies, which allowed us to learn more about the salivary microbiology of diabetic patients in their regions.

SUPPLEMENTARY MATERIAL

The Supplementary Material for this article can be found online at: https://www.frontiersin.org/articles/10.3389/fcimb.2022.816526/full#supplementary-material

REFERENCES

Abusleme, L., Dupuy, A. K., Dutzan, N., Silva, N., Burleson, J. A., Strausbaugh, L. D., et al. (2013). The Subgingival Microbiome in Health and Periodontitis and its Relationship With Community Biomass and Inflammation. *ISME J.* 7 (5), 1016–1025. doi: 10.1038/ismej.2012.174

Almeida-Santos, A., Martins-Mendes, D., Gayà-Vidal, M., Pérez-Pardal, L., and Beja-Pereira, A. (2021). Characterization of the Oral Microbiome of Medicated Type-2 Diabetes Patients. *Front. Microbiol.* 12. doi: 10.3389/fmicb.2021.610370

Alvarenga, M. O. P., Miranda, G. H. N., Ferreira, R. O., Saito, M. T., Fagundes, N. C. F., Maia, L. C., et al. (2020). Association Between Diabetic Retinopathy and Periodontitis-A Systematic Review. *Front. Public Health* 8. doi: 10.3389/fpubh.2020.550614

Babaev, E. A., Balmasova, I. P., Mkrtumyan, A. M., Kostryukova, S. N., Vakhitova, E. S., Il'ina, E. N., et al. (2017). Metagenomic Analysis of Gingival Sulcus Microbiota and Pathogenesis of Periodontitis Associated With Type 2 Diabetes Mellitus. *Bull. Exp. Biol. Med.* 163 (6), 718–721. doi: 10.1007/s10517-017-3888-6

Balmasova, I. P., Olekhnovich, E. I., Klimina, K. M., Korenkova, A. A., Vakhitova, M. T., Babaev, E. A., et al. (2021). Drift of the Subgingival Periodontal Microbiome During Chronic Periodontitis in Type 2 Diabetes Mellitus Patients. *Pathogens* 10 (5), 504. doi: 10.3390/pathogens10050504

Casarin, R. C., Barbagallo, A., Meulman, T., Santos, V. R., Sallum, E. A., Nociti, F. H., et al. (2013). Subgingival Biodiversity in Subjects With Uncontrolled Type-2 Diabetes and Chronic Periodontitis. *J. Periodontal. Res.* 48 (1), 30–36. doi: 10.1111/j.1600-0765.2012.01498.x

Castelino, M., Eyre, S., Moat, J., Fox, G., Martin, P., Ho, P., et al. (2017). Optimisation of Methods for Bacterial Skin Microbiome Investigation: Primer Selection and Comparison of the 454 Versus MiSeq Platform. *BMC Microbiol.* 17 (1), 23. doi: 10.1186/s12866-017-0927-4

Chen, B., Wang, Z., Wang, J., Su, X., Yang, J., Zhang, Q., et al. (2020). The Oral Microbiome Profile and Biomarker in Chinese Type 2 Diabetes Mellitus Patients. *Endocrine* 68 (3), 564–572. doi: 10.1007/s12020-020-02269-6

Demmer, R. T., Trinh, P., Rosenbaum, M., Li, G., LeDuc, C., Leibel, R., et al. (2019). Subgingival Microbiota and Longitudinal Glucose Change: The Oral Infections, Glucose Intolerance and Insulin Resistance Study (ORIGINS). *J. Dent. Res.* 98 (13), 1488–1496. doi: 10.1177/0022034519881978

Edgar, R. C. (2013). UPARSE: Highly Accurate OTU Sequences From Microbial Amplicon Reads. *Nat. Methods* 10 (10), 996–998. doi: 10.1038/nmeth.2604

Fung, C., Rusling, M., Lampeter, T., Love, C., Karim, A., Bongiorno, C., et al. (2021). Automation of QIIME2 Metagenomic Analysis Platform. *Curr. Protoc.* 1 (9), e254. doi: 10.1002/cpz1.254

Griffen, A. L., Beall, C. J., Campbell, J. H., Firestone, N. D., Kumar, P. S., Yang, Z. K., et al. (2012). Distinct and Complex Bacterial Profiles in Human Periodontitis and Health Revealed by 16S Pyrosequencing. *ISME J.* 6 (6), 1176–1185. doi: 10.1038/ismej.2011.191

Higgins, T. (2013). HbA1c for Screening and Diagnosis of Diabetes Mellitus. *Endocrine* 43 (2), 266–273. doi: 10.1007/s12020-012-9768-y

Kocher, T., Konig, J., Borgnakke, W. S., Pink, C., and Meisel, P. (2000). Periodontal Complications of Hyperglycemia/Diabetes Mellitus: Epidemiologic Complexity and Clinical Challenge. *Periodontol* 78 (1), 59–97. doi: 10.1111/prd.12235

Koh, G. C., Peacock, S. J., van der Poll, T., and Wiersinga, W. J. (2012). The Impact of Diabetes on the Pathogenesis of Sepsis. *Eur. J. Clin. Microbiol. Infect. Dis.* 31 (4), 379–388. doi: 10.1007/s10096-011-1337-4

Liu, Y. K., Chen, V., He, J. Z., Zheng, X., Xu, X., and Zhou, X. D. (2021). A Salivary Microbiome-Based Auxiliary Diagnostic Model for Type 2 Diabetes Mellitus. *Arch. Oral. Biol.* 126, 105118. doi: 10.1016/j.archoralbio.2021.105118

Long, J., Cai, Q., Steinwandel, M., Hargreaves, M. K., Bordenstein, S. R., Blot, W. J., et al. (2017). Association of Oral Microbiome With Type 2 Diabetes Risk. *J. Periodontal. Res.* 52 (3), 636–643. doi: 10.1111/jre.12432

Mark Welch, J. L., Ramirez-Puebla, S. T., and Borisy, G. G. (2020). Oral Microbiome Geography: Micron-Scale Habitat and Niche. *Cell Host Microbe* 28 (2), 160–168. doi: 10.1016/j.chom.2020.07.009

Matsha, T. E., Prince, Y., Davids, S., Chikte, U., Erasmus, R. T., Kengne, A. P., et al. (2020). Oral Microbiome Signatures in Diabetes Mellitus and Periodontal Disease. *J. Dent. Res.* 99 (6), 658–665. doi: 10.1177/0022034520913818

Ogurtsova, K., da Rocha Fernandes, J. D., Huang, Y., Linnenkamp, U., Guariguata, L., Cho, N. H., et al. (2017). IDF Diabetes Atlas: Global Estimates for the Prevalence of Diabetes for 2015 and 2040. *Diabetes Res. Clin. Pract.* 128, 40–50. doi: 10.1016/j.diabres.2017.03.024

Omori, M., Kato-Kogoe, N., Sakaguchi, S., Kamiya, K., Fukui, N., Gu, Y. H., et al. (2021). Characterization of Salivary Microbiota in Elderly Patients With Type 2 Diabetes Mellitus: A Matched Case-Control Study. *Clin. Oral. Investig.* doi: 10.1007/s00784-021-04027-y

Pascale, A., Marchesi, N., Govoni, S., Coppola, A., and Gazzaruso, C. (2019). The Role of Gut Microbiota in Obesity, Diabetes Mellitus, and Effect of Metformin: New Insights Into Old Diseases. *Curr. Opin. Pharmacol.* 49, 1–5. doi: 10.1016/j.coph.2019.03.011

Pedersen, C., Gallagher, E., Horton, F., Ellis, R. J., Ijaz, U. Z., Wu, H., et al. (2016). Host-Microbiome Interactions in Human Type 2 Diabetes Following Prebiotic Fibre (Galacto-Oligosaccharide) Intake. *Br. J. Nutr.* 116 (11), 1869–1877. doi: 10.1017/s0007114516004086

Pichler, M., Coskun, O. K., Ortega-Arbulu, A. S., Conci, N., Worheide, G., Vargas, S., et al. (2018). A 16s rRNA Gene Sequencing and Analysis Protocol for the Illumina MiniSeq Platform. *Microbiologyopen* 7 (6), e00611. doi: 10.1002/mbo3.611

Sabharwal, A., Ganley, K., Miecznikowski, J. C., Haase, E. M., Barnes, V., and Scannapieco, F. A. (2019). The Salivary Microbiome of Diabetic and non-Diabetic Adults With Periodontal Disease. *J. Periodontol.* 90 (1), 26–34. doi: 10.1002/jper.18-0167

Schuetz, P., Castro, P., and Shapiro, N. I. (2011). Diabetes and Sepsis: Preclinical Findings and Clinical Relevance. *Diabetes Care* 34 (3), 771–778. doi: 10.2337/dc10-1185

Shi, B., Lux, R., Klokkevold, P., Chang, M., Barnard, E., Haake, S., et al. (2020). The Subgingival Microbiome Associated With Periodontitis in Type 2 Diabetes Mellitus. *ISME J.* 14 (2), 519–530. doi: 10.1038/s41396-019-0544-3

Sierra, M. A., Li, Q., Pushalkar, S., Paul, B., Sandoval, T. A., Kamer, A. R., et al. (2020). The Influences of Bioinformatics Tools and Reference Databases in Analyzing the Human Oral Microbial Community. *Genes (Basel)* 11 (8), 878. doi: 10.3390/genes11080878

Sun, X., Li, M., Xia, L., Fang, Z., Yu, S., Gao, J., et al. (2020). Alteration of Salivary Microbiome in Periodontitis With or Without Type-2 Diabetes Mellitus and Metformin Treatment. *Sci. Rep.* 10 (1), 15363. doi: 10.1038/s41598-020-72035-1

Thomas, A. M., Manghi, P., Asnicar, F., Pasolli, E., Armanini, F., Zolfo, M., et al. (2019). Metagenomic Analysis of Colorectal Cancer Datasets Identifies Cross-Cohort Microbial Diagnostic Signatures and a Link With Choline Degradation. *Nat. Med.* 25 (4), 667–678. doi: 10.1038/s41591-019-0405-7

Vanhatalo, A., Blackwell, J. R., L'Heureux, J. E., Williams, D. W., Smith, A., van der Giezen, M., et al. (2018). Nitrate-Responsive Oral Microbiome Modulates Nitric Oxide Homeostasis and Blood Pressure in Humans. *Free Radic. Biol. Med.* 124, 21–30. doi: 10.1016/j.freeradbiomed.2018.05.078

Yang, Y., Liu, S., Wang, Y., Wang, Z., Ding, W., Sun, X., et al. (2020). Changes of Saliva Microbiota in the Onset and After the Treatment of Diabetes in Patients With Periodontitis. *Aging (Albany NY)* 12 (13), 13090–13114. doi: 10.18632/aging.103399

Yano, Y., Hua, X., Wan, Y., Suman, S., Zhu, B., Dagnall, C. L., et al. (2020). Comparison of Oral Microbiota Collected Using Multiple Methods and Recommendations for New Epidemiologic Studies. *mSystems* 5 (4), e00156–20. doi: 10.1128/mSystems.00156-20

Yende, S., and van der Poll, T. (2009). Diabetes and Sepsis Outcomes–it is Not All Bad News. *Crit. Care* 13 (1), 117. doi: 10.1186/cc7707

Conflict of Interest: The authors declare that the research was conducted in the absence of any commercial or financial relationships that could be construed as a potential conflict of interest.

Publisher's Note: All claims expressed in this article are solely those of the authors and do not necessarily represent those of their affiliated organizations, or those of the publisher, the editors and the reviewers. Any product that may be evaluated in this article, or claim that may be made by its manufacturer, is not guaranteed or endorsed by the publisher.

frontiers in Cellular and Infection Microbiology

ORIGINAL RESEARCH
published: 14 February 2022
doi: 10.3389/fcimb.2022.845738

The Crosstalk Between Saliva Bacteria and Fungi in Early Childhood Caries

Ye Tu[1,2], *Zhiyan Zhou*[1,2], *Chang Shu*[3], *Yuan Zhou*[1,4*] and *Xuedong Zhou*[1,2*]

[1] State Key Laboratory of Oral Diseases & National Clinical Research Center for Oral Diseases, West China Hospital of Stomatology, Sichuan University, Chengdu, China, [2] Department of Cariology and Endodontics, West China Hospital of Stomatology, Sichuan University, Chengdu, China, [3] Department of Periodontology, Peking University School and Hospital of Stomatology, Peking University, Beijing, China, [4] Department of Pediatric Dentistry, West China Hospital of Stomatology, Sichuan University, Chengdu, China

Early childhood caries (ECC) is the most prevalent oral disease in children, which greatly affects the quality of life and health condition of the patients. Although co-infection of oral streptococci and fungi has been well recognized in the development of ECC, the correlation between other core members of oral mycobiome and ECC progression remains unclear. In the current study, saliva samples obtained from severe ECC (SECC), ECC, and caries-free children were collected, and both V3–V4 16S rRNA and ITS1 rRNA gene amplicon sequencing were performed to investigate the salivary bacterial and fungal profiles. Significant alteration of salivary fungal community in SECC/ECC children was observed compared with the caries-free control. The typing analysis determined the fungal community into five fungal types, which influenced the structure of salivary bacteria. By performing Spearman correlation analysis, carious phenotypes were positively related to *Fusobacterium* but negatively linked to *Neocosmospora*, and a significant correlation of cross-kingdom taxonomic pairs was identified. Our work demonstrated the interactions between oral bacteria and fungi at the community level, which may advance our knowledge on the etiological role of bacteria/fungi in the development of ECC and promote better management of this disease.

Keywords: microbiome, mycobiome, saliva, early childhood caries, dental caries

OPEN ACCESS

Edited by:
Jin Xiao,
University of Rochester, United States

Reviewed by:
Yuan Liu,
University of Pennsylvania, United States
Zhengwei Huang,
Shanghai Jiao Tong University, China

***Correspondence:**
Yuan Zhou
zhouyuan.0607@hotmail.com
Xuedong Zhou
zhouxd@scu.edu.cn

Specialty section:
This article was submitted to Microbiome in Health and Disease, a section of the journal Frontiers in Cellular and Infection Microbiology

Received: *30 December 2021*
Accepted: *20 January 2022*
Published: *14 February 2022*

Citation:
Tu Y, Zhou Z, Shu C, Zhou Y and Zhou X (2022) The Crosstalk Between Saliva Bacteria and Fungi in Early Childhood Caries. Front. Cell. Infect. Microbiol. 12:845738. doi: 10.3389/fcimb.2022.845738

INTRODUCTION

Early childhood caries (ECC) refers to caries occurring on deciduous dentition and is identified as one or more decayed (d), missing (m), or filled (f) surface or tooth in the primary tooth in children at 71 months of age or younger (Lis and Kuramitsu, 1997; Anil and Anand, 2017; Pierce et al., 2019). Severe ECC (SECC) is manifested as one or more cavitated, filled, or missing (due to caries) smooth surfaces in primary maxillary anterior teeth, or dmfs score ≥4 (age 3 years), ≥5 (age 4 years), or ≥6 (age 5 years), with younger onset age and higher morbidity (Drury et al., 1999). Being the most common chronic disease in children, ECC afflicts many population groups with prevalence rates ranging from

23% to 98% all over the world (Hu et al., 2011; Dye et al., 2015; Castillo et al., 2019; Pierce et al., 2019), causing heavy financial and medical burdens to the family and society (Rashewsky et al., 2012).

The etiology of ECC has been largely related to polymicrobial infection, accompanied by environmental, maternal, behavioral, and socioeconomic factors (Kim Seow, 2012; Fontana, 2015; Hemadi et al., 2017; Xiao et al., 2018). The involvement of *Streptococcus mutans* in ECC has been well recognized, largely accredited to its acidogenicity, acidurity, and capability of producing polysaccharides (Hajishengallis et al., 2017; Hemadi et al., 2017; Momeni et al., 2020). *Candida albicans* has also been demonstrated to be involved in ECC development, and its synergistic interaction with *S. mutans* greatly enhances the virulence of the biofilm (Falsetta et al., 2014; Hwang et al., 2017; Ellepola et al., 2019). Other than the extensively investigated *C. albicans*, the complicated component of oral mycobiome and the biofilm formation capacity of several fungal taxa have been discovered (Ghannoum et al., 2010; Angiolella et al., 2020; Chakraborty et al., 2020), suggesting the potential impact of fungal taxa on oral health. Furthermore, the interaction between microbiome and mycobiome has been observed in certain diseases (Hoarau et al., 2016; Azzam et al., 2020), indicating the profound influence of polymicrobial dysbiosis in disease development. However, the role of oral fungal community in ECC progression and the cross-kingdom interaction between oral bacteria and fungi still need further investigation.

The clinical validity and convenience of saliva test have been well suggested (Zhang et al., 2016; Kaczor-Urbanowicz et al., 2019; Fernandes et al., 2020), while the dental explorer which is used for plaque collecting may cause fear and anxiety in children (Leal et al., 2013), leaving a more preferable test method of saliva to kids. So far, the only few published studies involving whole oral mycobiome and ECC were either focusing solely on a fungal community without referring to oral bacteria (Fechney et al., 2019; Cui et al., 2021) or using dental plaque or oral swab samples (de Jesus et al., 2020; de Jesus et al., 2021). Hence, in the current study, we intended to 1) capture the saliva microbial (bacterial and fungal) community variation in different oral health status, 2) identify potential microbial biomarkers of healthy and ECC status, and 3) uncover the interaction between the oral microbiome and mycobiome in caries development. Results here illustrated the alteration of saliva microecosystem as caries progressed with certain taxa significantly enriched in caries children, and the potential interaction between saliva bacterial and fungal community was observed.

METHODS

Study Population, Oral Examination, and Sample Collection

The current study was approved by the Institutional Review Board of West China Hospital of Stomatology (WCHSIRB-D-2017-031). Children under 72 months of age were recruited except for those who met the following exclusion criteria: antibiotic or fluoride treatment within 3 months, mixed dentition, systemic diseases, and acute infection. The comprehensive oral examination was conducted by two professional dentists according to the WHO Basic Oral Health Survey Methods 1997 with good consistency (intra-examiner Kappa value = 0.90, inter-examiner Kappa value = 0.90). The number of carious teeth and surfaces was assessed with index variables of decayed, missing due to decay, or filled (dmfs; dmft). The diagnosis of ECC and SECC followed the instructions as previously described (Drury et al., 1999). Five milliliters of whole non-stimulated saliva was collected using the spitting method as described previously with minor modification (Navazesh, 1993). Briefly, samples were collected between 9:00 and 11:00 a.m., and participants were refrained from toothbrushing, eating, or drinking at least 2 h prior to sample collection. Participants were instructed to rest for 5 min with minimum orofacial movements and were then requested to slightly tilt the head forward to accumulate saliva in the floor of the mouth. Saliva was spitted into 50-ml centrifuge tubes every 1 min, and approximately 10 min was consumed collecting 5 ml non-stimulated saliva from children. All samples were immediately placed on dry ice and transported to a −80°C freezer for storage prior to further analysis.

DNA Extraction, Amplification, and Illumina MiSeq Sequencing

Total DNA was extracted using the TIANamp bacteria DNA Kit (Tiangen, Beijing, China), according to the protocol of the manufacturer. DNA extraction was checked on 1% agarose gel, and DNA concentration and purity were determined with NanoDrop 2000 UV–vis spectrophotometer (Thermo Scientific, Wilmington, USA). The bacterial 16S rDNA V3–V4 region and fungal ITS-1 region were amplified using primer pairs 338F (5′-ACTCCTACGGGAGGCAGCAG-3′) and 806R (5′-GGACTACHVGGGTWTCTAAT-3′) for bacteria, or ITS1F (5′-CTTGGTCATTTAGAGGAAGTAA-3′) and ITS2R (5′-GCTGCGTTCTTCATCGATGC-3′) by an ABI GeneAmp® 9700 PCR thermocycler (ABI, CA, USA). The PCR amplification of 16S rRNA and ITS gene was performed as follows: initial denaturation at 95°C for 3 min, followed by 27 cycles of denaturing at 95°C for 30 s, annealing at 55°C for 30 s and extension at 72°C for 45 s, and single extension at 72°C for 10 min, and end at 4°C. The PCR mixtures contain 5× TransStart FastPfu buffer 4 μl, 2.5 mM dNTPs 2 μl, forward primer (5 μM) 0.8 μl, reverse primer (5 μM) 0.8 μl, TransStart FastPfu DNA Polymerase 0.4 μl, BSA 0.2 μl, template DNA 10 ng, and finally ddH_2O up to 20 μl. PCR reactions were performed in triplicate. The PCR product was extracted from 2% agarose gel and purified using the AxyPrep DNA Gel Extraction Kit (Axygen Biosciences, Union City, CA, USA) according to the instructions of the manufacturer and quantified using Quantus™ Fluorometer (Promega, USA). Purified amplicons were pooled in equimolar and paired-end sequenced on an Illumina MiSeq PE300 platform/NovaSeq PE250 platform (Illumina, San Diego, USA) according to the standard protocols by Majorbio Bio-Pharm

Technology Co., Ltd. (Shanghai, China). The raw reads were deposited into the NCBI Sequence Read Archive (SRA) database (https://www.ncbi.nlm.nih.gov/bioproject/PRJNA790078, https://www.ncbi.nlm.nih.gov/bioproject/PRJNA790007).

Processing of Sequencing Data

The raw 16S and ITS1 rRNA gene sequencing reads were demultiplexed and quality-filtered by fastp version 0.20.0 (Chen et al., 2018) and merged by FLASH version 1.2.7 (Magoč and Salzberg, 2011) with the following criteria: i) the 300-bp reads were truncated at any site receiving an average quality score of <20 over a 50-bp sliding window, the truncated reads shorter than 50 bp were discarded, and reads containing ambiguous characters were also discarded; ii) only overlapping sequences longer than 10 bp were assembled according to their overlapped sequence. The maximum mismatch ratio of the overlap region is 0.2. Reads that could not be assembled were discarded; iii) samples were distinguished according to the barcode and primers, and the sequence direction was adjusted, exact barcode matching, two nucleotide mismatches in primer matching.

Operational taxonomic units (OTUs) with 99% similarity were clustered using UPARSE version 7.1 (Edgar, 2013), and chimeric sequences were identified and removed. The taxonomy of each OTU representative sequence was analyzed by RDP Classifier version 2.2 (Wang et al., 2007) against the bacterial 16S rRNA database (SILVA 138) and fungal ITS database (UNITE 8.0) under the confidence threshold of 0.7.

Bioinformatics and Statistical Analysis

Before bioinformatic analysis, sequencing reads of all samples were standardized by rarefying OTU tables to the minimum number of reads. Analyses were performed by using the online platform of Majorbio Cloud Platform (www.majorbio.com). Kruskal–Wallis *H* test and Wilcoxon rank-sum test were used to compare the differences in taxa between three groups or two groups. Alpha-diversity was calculated in terms of Shannon and Chao indexes and was compared by Wilcoxon rank-sum test. Beta-diversity was assessed by principal coordinates analysis (PCoA) using Bray–Curtis distance and permutational multivariate analysis of variance (PERMANOVA) with a permutation of 999. Analysis of similarities (ANOSIM) values were constructed in R (version 3.3.1) package "vegan" (version 2.4-3). Partial least squares discriminant analysis (PLS-DA) was performed by using R (version 3.3.1) package "mixOmics" to discriminate the community structure in different groups. Heatmaps, ternary plots, and circus plots were conducted in R (version 3.3.1) package "vegan" (version 2.4-3), ggtern plug-in, and Circos software (version 0.67-7), respectively. The relationship between microbial community and environmental factors was analyzed by redundancy analysis (RDA) using vegan package. In typing analysis, samples were clustered into five types with the highest Calinski–Harabasz (CH) index determined by the partitioning around medoids (PAM) algorithm. Linear discriminant analysis (LDA) of effect size (LEfSe) was executed to identify the significant taxa that most likely explained the differences between groups, with a threshold LDA score of 2 or greater used. For correlation analysis, Spearman's rank test was performed and results were visualized in heatmap. A p-value of <0.05 was considered statistically significant in the current study.

RESULTS

Overview of the Subjects and Samples

Fifty-five saliva samples were collected from 15 children with ECC, 22 children with SECC, and 18 CF controls, with a mean ± SD age of 45.1 ± 9.6 months. **Table 1** and **Table S1** show some characteristics of the study participants. As for the bacterial community, a total of 2,941,799 16S rRNA reads were obtained, with an average of 53,487 per sample. After rarefying the OTU table to the minimum number of reads (20,398) per sample, a total of 13,183 OTUs were identified and were assigned to 535 species and 201 genera. As for the fungal community, a total of 4,169,098 ITS reads were obtained, with an average of 75,801 per sample. After rarefying the OTU table to the minimum number of reads (19,686) per sample, a total of 15,023 OTUs were identified and were assigned to 784 species and 445 genera.

Salivary Bacterial Profile in Children With ECC

Salivary bacterial community of the current cohort mainly consisted of six phyla, namely, *Firmicutes*, *Proteobacteria*, *Bacteroidota*, *Actinobacteriota*, *Patescibacteria*, and *Fusobacteriota*. *Streptococcus* (CF: 26.32%; ECC: 25.44%; SECC: 24.12%) was the most abundant genus in the saliva sample, followed by *Neisseria* (CF: 14.63%; ECC: 14.02%; SECC: 16%), *Prevotella* (CF: 13.24%; ECC: 10.59%; SECC: 10.79%), *Veillonella* (CF: 5.349%; ECC: 7.402%; SECC: 6.243%), and *Haemophilus* (CF: 6.229%; ECC: 5.245%; SECC: 5.98%). The taxonomic profile of the top 20 most abundant bacterial genera is shown in **Figure 1A**, with mean ± SD relative abundances in each group listed in **Table S2**. Although no significant differences in the relative abundance of the top 20 bacterial genera were observed among three groups (Kruskal–Wallis; **Figure 1B**), *TM7x* in ECC children presented a significantly higher level than that in CF children (Wilcoxon rank-sum test, $p = 0.04879$). The p-values of difference statistics of the top 20 bacterial genera are listed in **Table S2**. As for taxa whose relative abundance was less than 1%, *Centipeda*, *Parvimonas*, and *Pseudopropionibacterium* also showed different relative abundance among three groups or between two groups, and p-values of difference statistics are listed in **Table S3**. We then employed ternary analysis to evaluate the taxa distribution

TABLE 1 | Demographics and carious characteristics of the study participants.

Variable	Caries severity		
	CF (n = 18)	ECC (n = 15)	SECC (n = 22)
Age (months)	40.2 ± 6.9	46.9 ± 9.2	45.1 ± 10.5
Gender (M/F)	13/5	5/10	9/13
dmfs score	0	2 ± 0.8	10.5 ± 8.1
dmft score	0	1.9 ± 0.2	6.4 ± 3.3

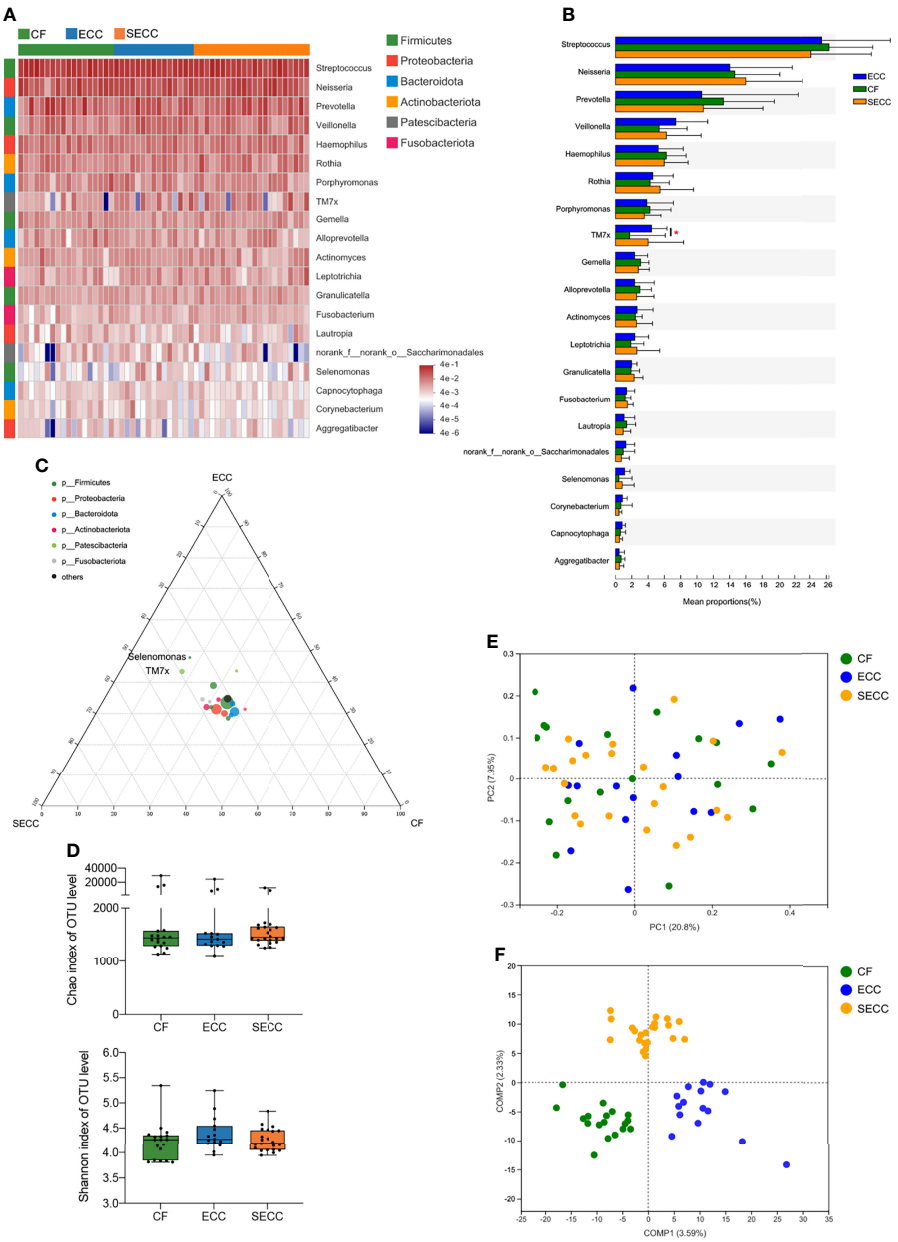

FIGURE 1 | Salivary bacterial profile in children with different health conditions. **(A)** Overview of the 20 most abundant salivary genera, and the heatmap plot presents the common logarithm of relative abundance. **(B)** Statistical comparison of the relative abundance of the 20 most abundant genera (Kruskal–Wallis, among three groups; Wilcoxon rank-sum test, within two groups; $^*p < 0.05$). **(C)** The relative occurrence of genera (circles) in samples with different oral health conditions. **(D)** Alpha-diversity indices for richness (Chao index, Kruskal–Wallis, $p = 0.351$) and diversity (Shannon index, Kruskal–Wallis, $p = 0.351$) of the bacterial community on the OTU level. **(E)** Principal coordinates analysis (PCoA) plots of Bray–Curtis dissimilarities at the OTU level (PERMANOVA, $p = 0.771$). **(F)** Partial least square discriminant analysis (PLS-DA) plot of saliva microbiota. CF, caries free; ECC, early childhood caries; OTU, operational taxonomic unit; PCoA, principal coordinates analysis; PERMANOVA, permutational multivariate analysis of variance; PLS-DA, partial least square discriminant analysis; SECC, severe early childhood caries.

corresponding to different oral health conditions, and a quite narrow distribution of bacterial genera was observed (**Figure 1C**). *TM7x* and *Selenomonas*, whose relative abundance was more than 1% in at least one group, were found enriched in caries samples. No significant difference in richness (Chao index, Kruskal–Wallis, $p = 0.351$; **Figure 1D**), alpha-diversity (Shannon index, Kruskal–Wallis, $p = 0.351$; **Figure 1D**), or beta-diversity (Bray–Curtis, PERMANOVA, $p = 0.771$; **Figure 1E**) existed among the CF, ECC, and SECC groups. ANOSIM also indicated no significant difference of bacterial structure within groups (**Table 2**). However, PLS-DA suggested an obviously different structure of overall saliva bacteria among three groups (**Figure 1F**).

Salivary Fungal Profile in Children With ECC

Ascomycota and *Basidiomycota* constituted the majority of salivary fungal community at the phylum level. *Candida* (CF: 32.49%; ECC: 32.45%; SECC: 24.91%) was the most abundant fungal genus, and *Cladosporium* (CF: 7.368%; ECC: 7.156%; SECC: 7.81%), *Aspergillus* (CF: 3.638%; ECC: 8.364%; SECC: 5.873%), *Wallemia* (CF: 1.178%; ECC: 6.06%; SECC: 2.634%), and *Malassezia* (CF: 5.088%; ECC: 1.772%; SECC: 1.773%) were also enriched in the saliva samples. The taxonomic profile of the top 20 most abundant fungal taxa is shown in **Figure 2A**, and mean ± SD relative abundances in each group are listed in **Table S4**. In the top 20 fungal taxa, *Agaricus* showed significantly different levels among three groups (Kruskal–Wallis, $p = 0.04708$), presenting higher relative abundance in either ECC or SECC group than that in the CF group (Wilcoxon rank-sum test, $p = 0.02608$ and $p = 0.02014$, respectively) (**Figure 2B**). The *p*-values of difference statistics are listed in **Table S4**. As for fungal taxa whose relative abundance was less than 1%, *unclassified_o:Hypocreales*, *Bjerkandera*, *Mycosphaerella*, *Subulicystidium*, *Neoascochyta*, and *Psathyrella* also showed significant difference in relative abundance among three groups or between healthy and caries samples, and *p*-values of difference statistics are listed in **Table S5**. Ternary analysis revealed a dispersed distribution of fungal genera, indicating that certain taxa might be relevant to healthy or caries status (**Figure 2C**). *Aspergillus*, *Wallemia*, *Agaricus*, and *Geotrichum*, whose mean relative abundances were more than 1%, were found enriched in carries samples. Beyond our expectation, there was no obvious difference in *Candida* level among healthy and caries samples, indicating the potential caries-promoting effect of fungal genera other than *Candida*. Although no significant difference in richness (Chao index, Kruskal–Wallis, $p = 0.886$; **Figure 2D**), alpha-diversity (Shannon index, Kruskal–Wallis, $p = 0.823$; **Figure 2D**), or beta-diversity (Bray–Curtis, PERMANOVA, $p = 0.304$; **Figure 2E**) was observed within three groups, ANOSIM revealed remarkable variations of salivary fungal structure between SECC and other two groups (**Table 2**). PLS-DA also indicated a distinct fungal structure among three groups (**Figure 2F**).

Association Between Saliva Fungal Types and Oral Health Status

Since insignificant bacterial variations but notable fungal alterations were detected within healthy and caries samples, we intended to further focus on the association between saliva fungi and oral health status. By executing PAM and PCoA in terms of Bray–Curtis distance, the fungal community of all samples was clustered into five types at the genus level (**Figure 3A**). Typing analysis revealed that 55.56% (10/18) CF samples owned the type 2 fungal community, while this fungal type occurred in only 26.67% (4/15) ECC samples and 27.27% (6/22) SECC samples. No CF sample possessed the type 3 fungal community, which was found in 20.00% (3/15) ECC samples and 13.64% (3/22) SECC samples. The type 4 fungal community was detected in 13.33% (2/15) ECC samples and up to 40.91% (9/22) SECC samples, but was found in only one CF sample. Type 1 and type 5 fungal communities were evenly distributed in the healthy and caries cases. The distinctive composition and structure indicated the uniqueness of the five fungal types (Bray–Curtis, PERMANOVA, $p = 0.001$; **Figure 3B**), even though type 3 and type 4 were both clustered from caries-related samples. To reflect the sample condition that each fungal type prevailed over, we designated type 2 as health-related type (H type), type 3 and type 4 as caries-related type 1 (C-1 type) and caries-related type 2 (C-2 type), and type 1 and type 5 as general type 1 (G-1 type) and general type 2 (G-2 type). After eliminating *unclassified_k:Fungi*, we found that five fungal types were dominated by different genera: *Candida* followed by *Cladosporium* and *Cutaneotrichosporon* (H type), *Aspergillus* followed by *Candida* and *Wallemia* (C-1 type), *Candida* followed by *Aspergillus* and *Trichosporon* (C-2 type), *Cladosporium* followed by *Candida* and *Malassezia* (G-1 type), and *Candida* followed by *Cladosporium* and *Agaricus* (G-2 type), and other less abundant genera were also distinctive in different types (**Table S6**). Since all five types possessed a relatively high abundance of *Candida*, we came up with the hypothesis that it might be the fungal taxa other than *Candida* that led to the different oral health conditions in the current cohort. The typing analysis was also executed on the bacterial community at the genus level in terms of Bray–Curtis distance, with no obvious association between bacterial types and oral health status being observed (**Figure S1** and **Table S7**).

Due to the pathogenetic roles of certain bacteria in ECC onset, we intended to investigate whether saliva fungi can impact bacterial profile. The fungal type corresponding to each sample was considered as an affecting factor, and host factors including age, gender, dmfs score, dmft score, and fungal type were assessed regarding their influence on the bacterial community by performing RDA. RDA revealed that fungal type was the only

TABLE 2 | The calculations and *p*-values of ANOSIM and Adonis of salivary bacteria and fungi.

		Bray–Curtis ANOSIM		Adonis	
		Statistic	***p*-value**	r^2	***p*-value**
Bacteria	Among three groups	–0.0045	0.522	0.0309	0.764
	CF vs. ECC	0.0136	0.291	0.0322	0.362
	ECC vs. SECC	–0.0383	0.779	0.0161	0.975
	CF vs. SECC	0.0097	0.299	0.0228	0.555
Fungi	Among three groups	0.0477	0.052	0.0393	0.283
	CF vs. ECC	–0.0193	0.634	0.0261	0.742
	ECC vs. SECC	0.0945	0.05	0.0331	0.136
	CF vs. SECC	0.0576	0.046	0.0294	0.174

CF, caries free; ECC, early childhood caries; SECC, severe early childhood caries.

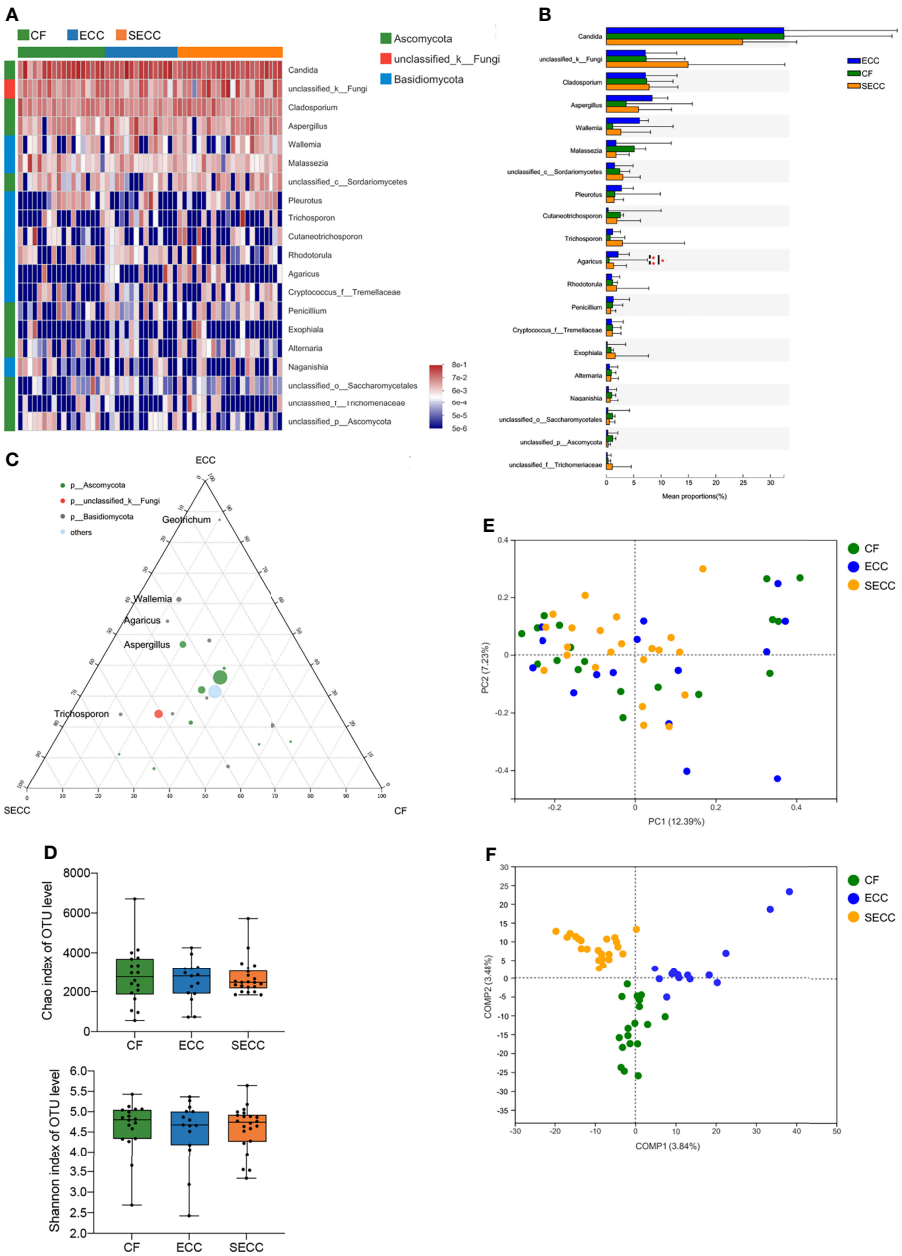

FIGURE 2 | Salivary fungal profile in children with different health conditions. **(A)** Overview of the 20 most abundant salivary genera, and the heatmap presents the common logarithm of relative abundance. **(B)** Statistical comparison of the relative abundance of the 20 most abundant genera (Kruskal–Wallis, among three groups; Wilcoxon rank-sum test, within two groups; $^*p < 0.05$). **(C)** The relative occurrence of genera (circles) in samples with different oral health conditions. **(D)** Alpha-diversity indices for richness (Chao index, Kruskal–Wallis, $p = 0.886$) and diversity (Shannon index, Kruskal–Wallis, $p = 0.823$) of the fungal community on the OTU level. **(E)** PCoA plots of Bray–Curtis dissimilarities at the OTU level (PERMANOVA, $p = 0.304$). **(F)** PLS-DA plot of saliva microbiota. CF, caries free; ECC, early childhood caries; OTU, operational taxonomic unit; PCoA, principal coordinates analysis; PERMANOVA, permutational multivariate analysis of variance; PLS-DA, partial least square discriminant analysis; SECC, severe early childhood caries.

factor that significantly affected the bacterial community structure ($r^2 = 0.1118, p = 0.044$), with its close relationship to the distribution of *Prevotella*, a potential bacterial biomarker of ECC (**Figure 3C** and **Table 3**). Thus, we came up with the opinion that the oral fungal community can influence bacterial profiles, and this cross-kingdom interaction may result in different oral health status.

Potential Crosstalk Between the Oral Microbiome and Mycobiome in Children With ECC

Since we detected the possible relationship between the oral fungal and bacterial community, we intended to identify the specialized taxa that distinguished samples from healthy to caries

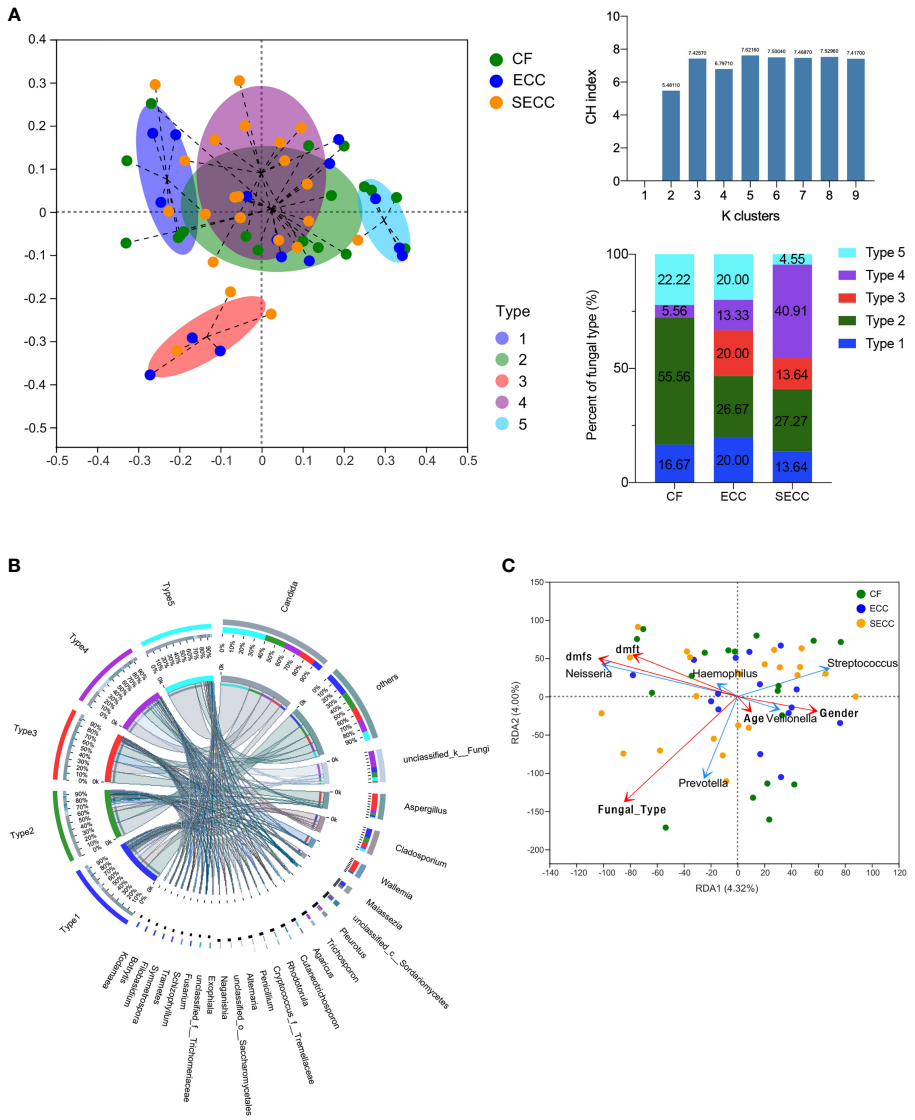

FIGURE 3 | Association between salivary fungi and oral health condition and salivary bacterial profile. **(A)** The distribution of samples based on the highest CH indices using the PAM algorithm (Bray–Curtis distance) and the proportions of five fungal types in three groups. **(B)** Profiles of each fungal type at the genus level. **(C)** Correlation between salivary bacterial community structure and host factors by using RDA. CF, caries free; CH indices, Calinski–Harabasz indices; ECC, early childhood caries; PAM, partitioning around medoids; RDA, redundancy analysis; SECC, severe early childhood caries.

conditions. Samples were divided into five groups as previously clustered by typing analysis. For a better consistency within the actual health state and dominant fungal type of each cluster, we removed the CF sample in the caries-related cluster, as well as ECC or SECC samples in the health-related cluster. We then used LEfSe to identify the taxa that significantly differed between health and caries samples, and bacterial or fungal genera with LDA scores of 2 or greater were confirmed and shown in **Figures 4A, B**, respectively. As for the bacterial community, *Streptococcus* was enriched in the health-related type community, while *Actinomyces*, *Prevotella*, and *Fusobacteria* were enriched in the caries-related type community. As for the fungal community, a wealth of taxa was found assembling in caries-related type community. Focusing on the prevailing taxa, we eliminated the genera whose relative abundances were less than 1%, remaining 5 bacterial genera and 21 fungal genera. The correlation between filtered taxa and host properties was then determined by using Spearman correlation analysis. It was found that the bacterial taxon *Fusobacterium* was positively related to dmfs score, dmft score, and caries severity, while the negative correlations between either *unclassified_o:Malasseziales* or *Neocosmospora* and caries phenotypes were figured out (**Figure 4C** and **Table S8**). Thus, we deduced that *Fusobacterium* plays an important role in caries onset, whereas *unclassified_o:Malasseziales* and *Neocosmospora* may represent good oral health condition. The relationship between filtered

TABLE 3 | The calculations and *p*-values of redundancy analysis.

	RDA1	RDA2	r^2	*p*-values
Age	0.7267	–0.6869	0.0015	0.964
Gender	0.9913	–0.1319	0.0239	0.547
dmfs	–0.9789	0.2044	0.0788	0.099
dmft	–0.9543	0.2989	0.0488	0.254
Fungal_Type	–0.7945	–0.6072	0.1118	0.044

bacterial and fungal taxa was further assessed, revealing 17 significant correlation in cross-kingdom pairs (**Figure 4D** and **Table S9**). As for health-related taxa, fungal taxa *Leptospora* was positively related to bacterial taxa *Streptococcus* ($p = 0.042$), while negative correlations between *Naganishia* and *Leptospora* and caries-related *Prevotella* ($p = 0.00044$; $p = 0.011$) were observed. Of note, the significant negative correlation between *Neocosmospora* enriched in CF samples and *Fusobacterium* on behalf of caries was revealed ($p = 0.024$), reconfirming the opposite roles they played in different oral health conditions. As for caries-related taxa, fungal taxa including *Hannaella*, *Vishniacozyma*, *unclassified_f:Metschnikowiaceae*, and *Lepista* were found positively related to bacterial taxa *Actinomyces* or *Bergeyella* ($p = 0.023$; $p = 0.035$; $p = 0.012$; $p = 0.022$).

DISCUSSION

In the current study, we investigated the salivary bacterial and fungal profiles in children with good oral health, ECC, and SECC. Most studies involving ECC were largely focused on oral bacteria or pathogenic *C. albicans* (Xiao et al., 2018; Alkhars et al., 2021; Baker et al., 2021; de Jesus et al., 2021). Here, we noticed the novel correlation between integral oral mycobiome and microbiome, figuring out potential taxonomic biomarkers which may lead to different oral health conditions in children. The fungal community was found distinguished into five types on behalf of different oral health status and significantly affected the bacterial profile. By analyzing the correlation between enriched taxa and carious indexes, we found *Neocosmospora* and *Fusobacterium* could be considered as potential biomarkers of good oral health and caries risk, respectively. Therefore, we concluded that the joint effect of salivary fungi and bacteria may play important roles in caries progression, and the impact of oral mycobiome on oral health deserved further investigation.

ECC is the most common disease of children with high prevalence worldwide, presenting as one or more decayed, missing, or filled tooth/surfaces in the primary tooth (Casamassimo et al., 2009; Anil and Anand, 2017). It has been substantiated that the co-infection of *S. mutans* and *C. albicans*, accompanied by bad oral hygiene, genetic factor, and immunological factor, led to the onset of ECC (Xiao et al., 2018) and, meanwhile, resulted in the dysbiosis of the oral microbiome (Kressirer et al., 2018; Xiao et al., 2018; Baker et al., 2021). Numerous studies have investigated the changes of the oral bacterial community in caries children compared with CF children, detecting decreased bacterial diversity as well as identifying certain discriminatory taxa including *Streptococcus*, *Prevotella*, *Veillonella*, *Neisseria*, and *Rothia* that were associated with caries (Wang et al., 2019; de Jesus et al., 2020; Baker et al., 2021; de Jesus et al., 2021). To our surprise, no significant difference of bacterial alpha- or beta-diversity based on caries status existed in the present cohort, although the non-distinctive alpha-diversity was also reported by Grier et al. and Agnello et al. (Agnello et al., 2017; Grier et al., 2021). Among the bacteria genera with high relative abundance, only *TM7x* was found enriched in children with ECC, whose strong co-occurrence with caries risk has been previously noticed (Kalpana et al., 2020; Baker et al., 2021).

In recent years, researchers have gradually attached more attention to the relationship between oral fungi and caries development. Most ITS-based investigations were focused on the dental plaque, revealing an increased fungal load, decreased community diversity, and enrichment of several taxa including *C. albicans*, *Candida dubliniensis*, *Candida sake*, *Cryptococcus neoformans*, and *Nigrospora oryzae* in samples from subjects with caries, while *Malassezia globose*, *Bipolaris sorokiniana*, *Mycosphaerella*, and *Trichosporon* were more relevant to CF status (Baraniya et al., 2020; de Jesus et al., 2020; O'Connell et al., 2020; Cui et al., 2021). *In vitro*, despite the well-recognized synergistic interaction between *S. mutans* and *C. albicans*, *M. globose* enriched in CF subjects has demonstrated its inhibitory properties against *S. mutans* (Baraniya et al., 2020). In the present study, we observed high relative abundances of *Candida*, *Cladosporium*, *Aspergillus*, and *Malassezia* across subjects with or without caries, which have been consistently identified as core human oral mycobiome in previous studies (Ghannoum et al., 2010; Fechney et al., 2019; Baraniya et al., 2020). Significant differences of beta-diversity and distribution of fungal colonies were noticed, indicating a higher colony sensitivity toward oral health conditions than that of the bacterial community. The obvious enrichment of *Candida* did not exist in caries samples, and previous studies also failed to detect the increased abundance of *C. albicans* in children with caries (Fechney et al., 2019; de Jesus et al., 2020), which suggests the potential pathogenic impact of other fungi in ECC development. The fungal community was determined into five discriminative fungal types *via* typing analysis, and types were designated as general type, health-related type, and caries-related type according to the prevalence in CF or caries samples. Previous studies have observed that certain *Candida* species can influence caries risk by affecting oral bacteria profile (Xiao et al., 2018; de Jesus et al., 2020; Alkhars et al., 2021). By performing RDA, we also verified the significant impact of fungal types on bacterial profile. RDA further revealed the

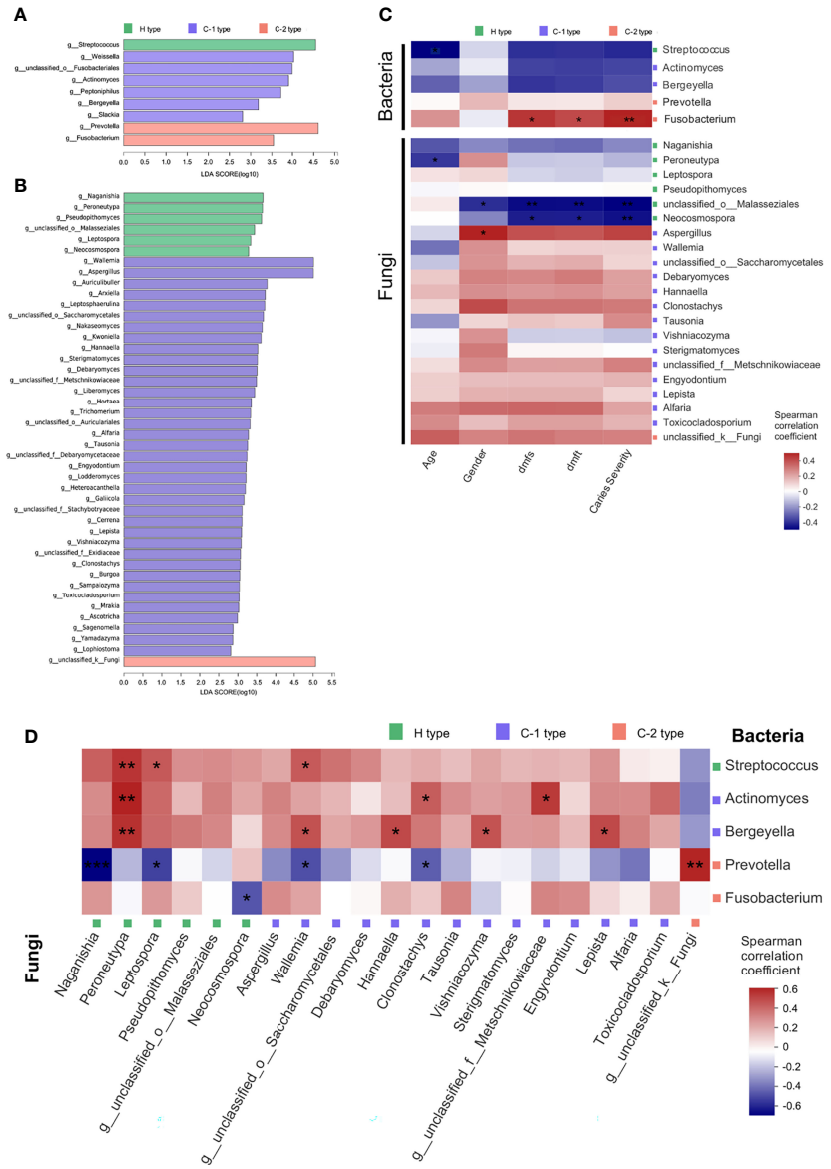

FIGURE 4 | Potential crosstalk between the oral microbiome and mycobiome in children with different oral health status. **(A)** LDA scores of distinct salivary bacteria among groups at the genus level. **(B)** LDA scores of distinct salivary fungi among groups at the genus level. **(C)** Spearman rank correlation between host properties and abundances of distinct salivary bacteria and fungi. **(D)** Spearman rank correlation between distinct salivary bacteria and fungi. *$p < 0.05$, ** < 0.01, ***$p < 0.001$. C-1 type, caries-related type 1; C-2 type, caries-related type 2; dmfs, decayed, missing, or filled surfaces; dmft, decayed, missing, or filled teeth; H type, health-related type; LDA, linear discriminant analysis.

positive correlation between fungal types and the distribution of *Prevotella*, a critical biomarker of ECC onset with great contribution to acid production (Yang et al., 2012; Teng et al., 2015; Wang et al., 2019; Baker et al., 2021). Surprisingly, although *Neisseria* has long been found associated with good oral health (Baker et al., 2021; Qudeimat et al., 2021), the strong positive correlation between *Neisseria* and either dmfs or dmft score was observed in the present study, indicating its potential cariogenic capabilities such as sugar metabolism, acid production, and acid tolerance in caries risk (Xiao et al., 2021).

Typing analysis also clustered saliva samples into five groups, three of which were dominated by CF or caries samples, being termed as health-related cluster or caries-related clusters. In order to precisely lock on the symbolic taxa of healthy or caries condition, we firstly filtered samples by eliminating those whose actual health status was not concordant to the cluster type. The characteristic genera of either health-related cluster or caries-related clusters were then identified by executing LEfSe, and taxa with relative abundance above 1% were retained for further evaluation. The relationship between filtered taxa and

host properties was assessed by Spearman correlation analysis. Being the member of the "orange" complex in subgingival plaque, *Fusobacterium* was traditionally regarded as a critical periodontal pathogen (Socransky et al., 1998), while increasing studies have noticed its enrichment and predictive potentiality on ECC occurrence (Zhu et al., 2018; Chen et al., 2021). Here, a significant positive correlation between *Fusobacterium* and caries indexes was observed, re-emphasizing its possible roles in caries progression. On the contrary, *unclassified_o:Malasseziales* and *Neocosmospora* were identified as negatively correlated to caries indexes. *Malassezia* is a commonly detected fungus of human skin and oral cavity (Gaitanis et al., 2012; Baraniya et al., 2020) and was previously found significantly enriched in CF children (Baraniya et al., 2020). *Neocosmospora* is an originally reported oral health-relevant fungus in current research, which includes groups of taxa that were previously assigned to the *Fusarium solani* complex discovered from plants, humans, and animals (Sandoval-Denis et al., 2018). It was revealed that galactose oxidase secreted by *Fusarium* species can convert substrates into the aldehyde forms and concomitantly produce hydrogen peroxide, and its ability in inhibiting *S. mutans* has been demonstrated (Lis and Kuramitsu, 1997). Further Spearman correlation analysis substantiated the significant negative correlation between *Fusobacterium* and *Neocosmospora*, indicating their opposite effects in maintaining CF condition or developing caries. In addition, although a number of studies have verified the promoting effects of *S. mutans* in ECC progression (Momeni et al., 2020; Xiao et al., 2020; Baker et al., 2021), *Streptococcus* was found to be a characteristic in the CF sample and, meanwhile, negatively related to carious indexes in the present study, indicating the complicated roles that the *Streptococcus* species played in caries risk, and the intricate prevalence of *Streptococcus* species has also been reported by AlEraky et al. (2021).

Caution should be taken when applying current evidence. Firstly, community analysis was restrained at the genus level due to the shallow sequencing depth, which provided a less-precise profile of community variation and was unable to lock on the exact species or subspecies that are closely related to ECC risk. On account of the small sample size, we did not conduct random forest model with receiving operational curve (ROC) analysis to test the discriminatory power of genera signature, leaving a less demonstration quality of the results. The limitations above remind us of a larger-scale cohort and the employment of whole metagenome sequencing and metabolomics analysis in future studies. Although saliva samples are easy to collect, the distinctive taxonomic profiles between saliva and dental plaque have been observed in previous research (Cui et al., 2021; de Jesus et al., 2021), suggesting a further investigation of plaque microorganisms in predicting ECC, for the closer contact of plaque with the dental surface may result in a higher sensitivity in predicting ECC compared with that of saliva samples. Besides, attention need to be paid to the cross-kingdom interactions in ECC progression, and the mechanisms of *Neocosmospora* in inhibiting cariogenic taxa are worthy of future investigation.

DATA AVAILABILITY STATEMENT

The datasets presented in this study can be found in online repositories. The names of the repository and accession numbers can be found below: NCBI; accession numbers: PRJNA790078 and PRJNA790007.

ETHICS STATEMENT

The studies involving human participants were reviewed and approved by the Institutional Review Board of West China Hospital of Stomatology. Written informed consent to participate in this study was provided by the legal guardian/next of kin of the participants. Written informed consent was obtained from the legal guardian/next of kin of the minor(s) for the publication of any potentially identifiable images or data included in this article.

AUTHOR CONTRIBUTIONS

YZ and XZ contributed to the study design and critically revised the manuscript. YT contributed to the conception, bioinformatic analysis, data interpretation, and manuscript drafting. ZZ and CS contributed to the sample collection, data acquisition, and data analysis. All authors contributed to the article and approved the submitted version.

FUNDING

This study was supported by the National Natural Science Foundation of China (81870754, 81700964).

ACKNOWLEDGMENTS

We thank the parents and the participants.

SUPPLEMENTARY MATERIAL

The Supplementary Material for this article can be found online at: https://www.frontiersin.org/articles/10.3389/fcimb.2022.845738/full#supplementary-material

REFERENCES

Agnello, M., Marques, J., Cen, L., Mittermuller, B., Huang, A., Chaichanasakul Tran, N., et al (2017). Microbiome Associated With Severe Caries in Canadian First Nations Children. *J. Dent. Res.* 96 (12), 1378–1385. doi: 10.1177/0022034517718819

AlEraky, D. M., Madi, M., El Tantawi, M., AlHumaid, J., Fita, S., AbdulAzeez, S., et al (2021). Predominance of non-Streptococcus Mutans Bacteria in Dental Biofilm and its Relation to Caries Progression. *Saudi J. Biol. Sci.* 28 (12), 7390–7395. doi: 10.1016/j.sjbs.2021.08.052

Alkhars, N., Zeng, Y., Alomeir, N., Al Jallad, N., Wu, T. T., Aboelmagd, S., et al (2021). Oral Candida Predicts Streptococcus Mutans Emergence in

Underserved US Infants. *J. Dent. Res.* 101 (1), 54–62. doi: 10.1177/00220345211012385

Angiolella, L., Rojas, F., Mussin, J., Greco, R., Sosa, M. L. A., Zalazar, L., et al (2020). Biofilm Formation, Adherence, and Hydrophobicity of M. Sympodialis, M. Globosa and M. Slooffiae From Clinical Isolates and Normal Skinvirulence Factors of M. Sympodialis, M. Globosa and M. Slooffiae. *Med. Mycol.* 58 (8), 1162–1168. doi: 10.1093/mmy/myaa017

Anil, S., and Anand, P. S. (2017). Early Childhood Caries: Prevalence, Risk Factors, and Prevention. *Front. Pediatr.* 5, 157. doi: 10.3389/fped.2017.00157

Azzam, S. Z., Cayme, G. J., and Martinez, L. R. (2020). Polymicrobial Interactions Involving Fungi and Their Importance for the Environment and in Human Disease. *Microb. Pathog.* 140, 103942. doi: 10.1016/j.micpath.2019.103942

Baker, J. L., Morton, J. T., Dinis, M., Alvarez, R., Tran, N. C., Knight, R., et al (2021). Deep Metagenomics Examines the Oral Microbiome During Dental Caries, Revealing Novel Taxa and Co-Occurrences With Host Molecules. *Genome Res.* 31 (1), 64–74. doi: 10.1101/gr.265645.120

Baraniya, D., Chen, T., Nahar, A., Alakwaa, F., Hill, J., Tellez, M., et al (2020). Supragingival Mycobiome and Inter-Kingdom Interactions in Dental Caries. *J. Oral. Microbiol.* 12 (1), 1729305. doi: 10.1080/20002297.2020.1729305

Casamassimo, P. S., Thikkurissy, S., Edelstein, B. L., and Maiorini, E. (2009). Beyond the Dmft: The Human and Economic Cost of Early Childhood Caries. *J. Am. Dent. Assoc.* 140 (6), 650–657. doi: 10.14219/jada.archive.2009.0250

Castillo, J. L., Palma, C., and Cabrera-Matta, A. (2019). Early Childhood Caries in Peru. *Front. Public Health* 7, 337. doi: 10.3389/fpubh.2019.00337

Chakraborty, T., Tóth, Z., Tóth, R., Vágvölgyi, C., and Gácser, A. (2020). Iron Metabolism, Pseudohypha Production, and Biofilm Formation Through a Multicopper Oxidase in the Human-Pathogenic Fungus Candida Parapsilosis. *mSphere* 5 (3), e00227-20. doi: 10.1128/mSphere.00227-20

Chen, Y., Dou, G., Wang, D., Yang, J., Zhang, Y., Garnett, J. A., et al (2021). Comparative Microbial Profiles of Caries and Black Extrinsic Tooth Stain in Primary Dentition. *Caries Res.* 55 (4), 310–321. doi: 10.1159/000517006

Chen, S., Zhou, Y., Chen, Y., and Gu, J. (2018). Fastp: An Ultra-Fast All-in-One FASTQ Preprocessor. *Bioinformatics* 34 (17), i884–ii90. doi: 10.1093/bioinformatics/bty560

Cui, Y., Wang, Y., Zhang, Y., Pang, L., Zhou, Y., Lin, H., et al (2021). Oral Mycobiome Differences in Various Spatial Niches With and Without Severe Early Childhood Caries. *Front. Pediatr.* 9, 748656. doi: 10.3389/fped.2021.748656

de Jesus, V. C., Khan, M. W., Mittermuller, B. A., Duan, K., Hu, P., Schroth, R. J., et al (2021). Characterization of Supragingival Plaque and Oral Swab Microbiomes in Children With Severe Early Childhood Caries. *Front. Microbiol.* 12, 683685. doi: 10.3389/fmicb.2021.683685

de Jesus, V. C., Shikder, R., Oryniak, D., Mann, K., Alamri, A., Mittermuller, B., et al (2020). Sex-Based Diverse Plaque Microbiota in Children With Severe Caries. *J. Dent. Res.* 99 (6), 703–712. doi: 10.1177/0022034520908595

Drury, T. F., Horowitz, A. M., Ismail, A. I., Maertens, M. P., Rozier, R. G., and Selwitz, R. H. (1999). Diagnosing and Reporting Early Childhood Caries for Research Purposes. A Report of a Workshop Sponsored by the National Institute of Dental and Craniofacial Research, the Health Resources and Services Administration, and the Health Care Financing Administration. *J. Public Health Dent.* 59 (3), 192–197. doi: 10.1111/j.1752-7325.1999.tb03268.x

Dye, B. A., Hsu, K. L., and Afful, J. (2015). Prevalence and Measurement of Dental Caries in Young Children. *Pediatr. Dent.* 37 (3), 200–216.

Edgar, R. C. (2013). UPARSE: Highly Accurate OTU Sequences From Microbial Amplicon Reads. *Nat. Methods* 10 (10), 996–998. doi: 10.1038/nmeth.2604

Ellepola, K., Truong, T., Liu, Y., Lin, Q., Lim, T. K., Lee, Y. M., et al (2019). Multi-Omics Analyses Reveal Synergistic Carbohydrate Metabolism in Streptococcus Mutans-Candida Albicans Mixed-Species Biofilms. *Infect. Immun.* 87 (10), e00339-19. doi: 10.1128/IAI.00339-19

Falsetta, M. L., Klein, M. I., Colonne, P. M., Scott-Anne, K., Gregoire, S., Pai, C. H., et al (2014). Symbiotic Relationship Between Streptococcus Mutans and Candida Albicans Synergizes Virulence of Plaque Biofilms In Vivo. *Infect. Immun.* 82 (5), 1968–1981. doi: 10.1128/IAI.00087-14

Fechney, J. M., Browne, G. V., Prabhu, N., Irinyi, L., Meyer, W., Hughes, T., et al (2019). Preliminary Study of the Oral Mycobiome of Children With and Without Dental Caries. *J. Oral. Microbiol.* 11 (1), 1536182. doi: 10.1080/20002297.2018.1536182

Fernandes, L. L., Pacheco, V. B., Borges, L., Athwal, H. K., de Paula Eduardo, F., Bezinelli, L., et al (2020). Saliva in the Diagnosis of COVID-19: A Review and New Research Directions. *J. Dent. Res.* 99 (13), 1435–1443. doi: 10.1177/0022034520960070

Fontana, M. (2015). The Clinical, Environmental, and Behavioral Factors That Foster Early Childhood Caries: Evidence for Caries Risk Assessment. *Pediatr. Dent.* 37 (3), 217–225.

Gaitanis, G., Magiatis, P., Hantschke, M., Bassukas, I. D., and Velegraki, A. (2012). The Malassezia Genus in Skin and Systemic Diseases. *Clin. Microbiol. Rev.* 25 (1), 106–141. doi: 10.1128/CMR.00021-11

Ghannoum, M. A., Jurevic, R. J., Mukherjee, P. K., Cui, F., Sikaroodi, M., Naqvi, A., et al (2010). Characterization of the Oral Fungal Microbiome (Mycobiome) in Healthy Individuals. *PloS Pathog.* 6 (1), e1000713. doi: 10.1371/journal.ppat.1000713

Grier, A., Myers, J. A., O'Connor, T. G., Quivey, R. G., Gill, S. R., and Kopycka-Kedzierawski, D. T. (2021). Oral Microbiota Composition Predicts Early Childhood Caries Onset. *J. Dent. Res.* 100 (6), 599–607. doi: 10.1177/0022034520979926

Hajishengallis, E., Parsaei, Y., Klein, M. I., and Koo, H. (2017). Advances in the Microbial Etiology and Pathogenesis of Early Childhood Caries. *Mol. Oral. Microbiol.* 32 (1), 24–34. doi: 10.1111/omi.12152

Hemadi, A. S., Huang, R., Zhou, Y., and Zou, J. (2017). Salivary Proteins and Microbiota as Biomarkers for Early Childhood Caries Risk Assessment. *Int. J. Oral. Sci.* 9 (11), e1. doi: 10.1038/ijos.2017.35

Hoarau, G., Mukherjee, P. K., Gower-Rousseau, C., Hager, C., Chandra, J., Retuerto, M. A., et al (2016). Bacteriome and Mycobiome Interactions Underscore Microbial Dysbiosis in Familial Crohn's Disease. *mBio* 7 (5), e01250-16. doi: 10.1128/mBio.01250-16

Hu, D. Y., Hong, X., and Li, X. (2011). Oral Health in China–trends and Challenges. *Int. J. Oral. Sci.* 3 (1), 7–12. doi: 10.4248/IJOS11006

Hwang, G., Liu, Y., Kim, D., Li, Y., Krysan, D. J., and Koo, H. (2017). Candida Albicans Mannans Mediate Streptococcus Mutans Exoenzyme GtfB Binding to Modulate Cross-Kingdom Biofilm Development In Vivo. *PloS Pathog.* 13 (6), e1006407. doi: 10.1371/journal.ppat.1006407

Kaczor-Urbanowicz, K. E., Wei, F., Rao, S. L., Kim, J., Shin, H., Cheng, J., et al (2019). Clinical Validity of Saliva and Novel Technology for Cancer Detection. *Biochim. Biophys. Acta Rev. Cancer* 1872 (1), 49–59. doi: 10.1016/j.bbcan.2019.05.007

Kalpana, B., Prabhu, P., Bhat, A. H., Senthilkumar, A., Arun, R. P., Asokan, S., et al (2020). Bacterial Diversity and Functional Analysis of Severe Early Childhood Caries and Recurrence in India. *Sci. Rep.* 10 (1), 21248. doi: 10.1038/s41598-020-78057-z

Kim Seow, W. (2012). Environmental, Maternal, and Child Factors Which Contribute to Early Childhood Caries: A Unifying Conceptual Model. *Int. J. Paediatr. Dent.* 22 (3), 157–168. doi: 10.1111/j.1365-263X.2011.01186.x

Kressirer, C. A., Chen, T., Lake Harriman, K., Frias-Lopez, J., Dewhirst, F. E., Tavares, M. A., et al (2018). Functional Profiles of Coronal and Dentin Caries in Children. *J. Oral. Microbiol.* 10 (1), 1495976. doi: 10.1080/20002297.2018.1495976

Leal, A. M., Serra, K. G., Queiroz, R. C., Araújo, M. A., and Maia Filho, E. M. (2013). Fear and/or Anxiety of Children and Parents Associated With the Dental Environment. *Eur. J. Paediatr. Dent.* 14 (4), 269–272.

Lis, M., and Kuramitsu, H. K. (1997). Galactose Oxidase-Glucan Binding Domain Fusion Proteins as Targeting Inhibitors of Dental Plaque Bacteria. *Antimicrob. Agents Chemother.* 41 (5), 999–1003. doi: 10.1128/AAC.41.5.999

Magoč, T., and Salzberg, S. L. (2011). FLASH: Fast Length Adjustment of Short Reads to Improve Genome Assemblies. *Bioinformatics* 27 (21), 2957–2963. doi: 10.1093/bioinformatics/btr507

Momeni, S. S., Beno, S. M., Baker, J. L., Edlund, A., Ghazal, T., Childers, N. K., et al (2020). Caries-Associated Biosynthetic Gene Clusters in Streptococcus Mutans. *J. Dent. Res.* 99 (8), 969–976. doi: 10.1177/0022034520914519

Navazesh, M. (1993). Methods for Collecting Saliva. *Ann. N. Y. Acad. Sci.* 694, 72–77. doi: 10.1111/j.1749-6632.1993.tb18343.x

O'Connell, L. M., Santos, R., Springer, G., Burne, R. A., Nascimento, M. M., and Richards, V. P. (2020). Site-Specific Profiling of the Dental Mycobiome Reveals Strong Taxonomic Shifts During Progression of Early-Childhood Caries. *Appl. Environ. Microbiol.* 86 (7), e02825-19. doi: 10.1128/AEM.02825-19

Pierce, A., Singh, S., Lee, J., Grant, C., Cruz de Jesus, V., and Schroth, R. J. (2019). The Burden of Early Childhood Caries in Canadian Children and Associated Risk Factors. *Front. Public Health* 7, 328. doi: 10.3389/fpubh.2019.00328

Qudeimat, M. A., Alyahya, A., Karched, M., Behbehani, J., and Salako, N. O. (2021). Dental Plaque Microbiota Profiles of Children With Caries-Free and Caries-Active Dentition. *J. Dent.* 104, 103539. doi: 10.1016/j.jdent.2020.103539

Rashewsky, S., Parameswaran, A., Sloane, C., Ferguson, F., and Epstein, R. (2012). Time and Cost Analysis: Pediatric Dental Rehabilitation With General Anesthesia in the Office and the Hospital Settings. *Anesth. Prog.* 59 (4), 147–153. doi: 10.2344/0003-3006-59.4.147

Sandoval-Denis, M., Guarnaccia, V., Polizzi, G., and Crous, P. W. (2018). Symptomatic Citrus Trees Reveal a New Pathogenic Lineage in Fusarium and Two New Neocosmospora Species. *Persoonia* 40, 1–25. doi: 10.3767/persoonia.2018.40.01

Socransky, S. S., Haffajee, A. D., Cugini, M. A., Smith, C., and Kent, R. L.Jr. (1998). Microbial Complexes in Subgingival Plaque. *J. Clin. Periodontol.* 25 (2), 134–144. doi: 10.1111/j.1600-051X.1998.tb02419.x

Teng, F., Yang, F., Huang, S., Bo, C., Xu, Z. Z., Amir, A., et al (2015). Prediction of Early Childhood Caries *via* Spatial-Temporal Variations of Oral Microbiota. *Cell Host Microbe* 18 (3), 296–306. doi: 10.1016/j.chom.2015.08.005

Wang, Q., Garrity, G. M., Tiedje, J. M., and Cole, J. R. (2007). Naive Bayesian Classifier for Rapid Assignment of rRNA Sequences Into the New Bacterial Taxonomy. *Appl. Environ. Microbiol.* 73 (16), 5261–5267. doi: 10.1128/AEM.00062-07

Wang, Y., Wang, S., Wu, C., Chen, X., Duan, Z., Xu, Q., et al (2019). Oral Microbiome Alterations Associated With Early Childhood Caries Highlight the Importance of Carbohydrate Metabolic Activities. *mSystems* 4 (6), e00450-19. doi: 10.1128/mSystems.00450-19

Xiao, J., Fiscella, K. A., and Gill, S. R. (2020). Oral Microbiome: Possible Harbinger for Children's Health. *Int. J. Oral. Sci.* 12 (1), 12. doi: 10.1038/s41368-020-0082-x

Xiao, J., Grier, A., Faustoferri, R. C., Alzoubi, S., Gill, A. L., Feng, C., et al (2018). Association Between Oral Candida and Bacteriome in Children With Severe ECC. *J. Dent. Res.* 97 (13), 1468–1476. doi: 10.1177/0022034518790941

Xiao, X., He, S., He, F., Wu, X., and Zheng, Y. (2021). Metagenomic Analysis Reveals Neisseria Bacilliformis Variation in the Early Childhood Caries Plaque Microbiome. *Evid. Based Complement. Alternat. Med.* 2021, 2774772. doi: 10.1155/2021/2774772

Yang, F., Zeng, X., Ning, K., Liu, K. L., Lo, C. C., Wang, W., et al (2012). Saliva Microbiomes Distinguish Caries-Active From Healthy Human Populations. *Isme J.* 6 (1), 1–10. doi: 10.1038/ismej.2011.71

Zhang, C. Z., Cheng, X. Q., Li, J. Y., Zhang, P., Yi, P., Xu, X., et al (2016). Saliva in the Diagnosis of Diseases. *Int. J. Oral. Sci.* 8 (3), 133–137. doi: 10.1038/ijos.2016.38

Zhu, C., Yuan, C., Ao, S., Shi, X., Chen, F., Sun, X., et al (2018). The Predictive Potentiality of Salivary Microbiome for the Recurrence of Early Childhood Caries. *Front. Cell Infect. Microbiol.* 8, 423. doi: 10.3389/fcimb.2018.00423

Conflict of Interest: The authors declare that the research was conducted in the absence of any commercial or financial relationships that could be construed as a potential conflict of interest.

Publisher's Note: All claims expressed in this article are solely those of the authors and do not necessarily represent those of their affiliated organizations, or those of the publisher, the editors and the reviewers. Any product that may be evaluated in this article, or claim that may be made by its manufacturer, is not guaranteed or endorsed by the publisher.

frontiers in Cellular and Infection Microbiology

ORIGINAL RESEARCH
published: 22 February 2022
doi: 10.3389/fcimb.2022.842845

A Mouse Periodontitis Model With Humanized Oral Bacterial Community

Lan Bai[1,2,3†], *Bo-Yan Chen*[1,2,3†], *Yan Liu*[2,3], *Wu-Chang Zhang*[2,3*] *and Sheng-Zhong Duan*[1,2,3*]

[1] Department of Periodontology, Shanghai Ninth People's Hospital, Shanghai Jiao Tong University School of Medicine, Shanghai, China, [2] Laboratory of Oral Microbiota and Systemic Diseases, Shanghai Ninth People's Hospital, College of Stomatology, Shanghai Jiao Tong University School of Medicine, Shanghai, China, [3] National Center for Stomatology, National Clinical Research Center for Oral Diseases, Shanghai Key Laboratory of Stomatology, Shanghai, China

Increasing evidence suggests that periodontitis, characterized by oral dysbiosis, is a critical player in the progression of multiple systemic diseases in humans. However, there is still a lack of a proper mouse model of periodontitis with the colonization of human periodontitis-associated bacteria. We here established a new mouse periodontitis model by combining ligation of the second molars with application of subgingival plaques from periodontitis patients. Using 16S rRNA gene sequencing and Taxonomic classification, we found that human periodontitis-associated bacteria efficiently colonized in the mouse model and were enriched in both ligature silk and mouse saliva. Furthermore, the well-recognized periodontal pathogens including *Porphyromonas gingivalis*, *Fusobacterium nucleatum*, *Prevotella intermedia*, and *Tannerella forsythia* were enriched in the new model, but not in ligature-induced periodontitis model or Sham mice. The human periodontitis-associated bacteria potently aggravated mouse periodontitis, as demonstrated by more severe bone resorption and higher expression of inflammatory and osteoclastogenesis genes. In summary, the new mouse periodontitis model paves the way for studying human periodontitis-associated bacteria in oral diseases and systemic diseases.

Keywords: periodontitis, mouse model, subgingival plaque, saliva, 16S rRNA sequencing

OPEN ACCESS

Edited by:
Xin Xu,
Sichuan University, China

Reviewed by:
Feng Chen,
Peking University, China
Lanjing Zhang,
Rutgers University, United States

****Correspondence:***
Sheng-Zhong Duan
duansz@shsmu.edu.cn
Wu-Chang Zhang
zhangwuchang104@hotmail.com

†These authors share first authorship

Specialty section:
This article was submitted to Microbiome in Health and Disease, a section of the journal Frontiers in Cellular and Infection Microbiology

Received: *24 December 2021*
Accepted: *31 January 2022*
Published: *22 February 2022*

Citation:
Bai L, Chen B-Y, Liu Y, Zhang W-C and Duan S-Z (2022) A Mouse Periodontitis Model With Humanized Oral Bacterial Community. Front. Cell. Infect. Microbiol. 12:842845. doi: 10.3389/fcimb.2022.842845

INTRODUCTION

Human periodontitis-associated bacteria cause local destruction of periodontal tissue and are also tightly linked to the progression of multiple systemic diseases. Periodontitis (PD) is a biofilm-induced chronic inflammatory disease of the tooth-supporting tissues, which destroys gingiva and alveolar bone, eventually causes teeth loss (Brown LJ and Löe, 1989). The number of new periodontitis cases is about 701/100,000 each year, and periodontitis becomes the 6th most prevalent diseases all over the world (Kassebaum et al., 2014). Some studies suggest that the dysbiosis of oral microecology not only causes periodontitis, but affects other organs (Hajishengallis, 2015). Accumulating evidence has linked periodontal disease with cardiovascular diseases, metabolic diseases, and cancers (Michaud et al., 2017; Polak and Shapira, 2018; Sanz et al., 2020). Although increasing attentions are paid on the human oral dysbiosis during understanding

the pathogenesis of systemic diseases, there is no proper mouse model of periodontitis with the colonization of human periodontitis-associated microbiota.

The microbiota of the human oral cavity consists of a myriad of bacterial species, which normally exist in commensal harmony with the host (Mysak et al., 2014). The dominant flora in oral cavity of periodontitis patients is massively different from those in healthy people. The current concept of the etiology of periodontitis is that bacterial components of the biofilm initiate the inflammatory cascade, including infiltration of immune cells and production of inflammatory mediators in the periodontal tissue (Bage et al., 2010). It has been demonstrated that *Porphyromonas gingivalis*, *Tannerella forsythia*, and *Treponema denticola* are closely related to periodontitis progression (Socransky et al., 1998), and that *Synergistes*, *Filifactor*, and *Mycoplasma* also take part in periodontal disease (Shi et al., 2015). Besides causing tooth loss, periodontal pathogens have a systemic impact through a variety of mechanisms. These include bacteremia caused by the translocation of periodontal pathogens into the systemic circulation and endotoxemias due to the lipopolysaccharides of the periodontal-pathogenic bacteria.

For particular purposes, some mouse periodontitis models including inoculation of well recognized periodontal pathogens, LPS injection, and ligation of molars have been constructed (Blasco-Baque et al., 2017; Costa et al., 2021). Ligation of molars is a classical mouse periodontitis model, making great contributions to the elucidation of mechanisms of periodontitis. However, these models cannot meet the currently increasing demands in the field, such as screening the human periodontal pathogens critical for systemic diseases. Previous studies suggested that *Bifidobacteria*, which was common bacteria in human oral microflora, was not detected in mouse oral cavity (Mackie et al., 1999). Furthermore, the dominancy of *Staphylococcus* species in the mouse was not found in the human oral microflora (Paster et al., 2006; Keijser et al., 2008). Moreover, even within the common bacterial orders, the actual families, and species were often different between mice and humans (Hasegawa et al., 2010). Therefore, the current experimental animal and *in vivo* models cannot fully summarize the human situation, despite that these models can effectively address particular aspects of the disease.

In this study, we aimed to establish a mouse model of periodontitis with colonization of human periodontitis-associated oral microbiota. We combined the ligature-induced mouse periodontitis (LIP) with transplantation of subgingival plaque from periodontitis patients. Firstly, we used 5-0 silk suture ligaturing mouse second molars. We then transplanted subgingival plaque of periodontitis patients on the silk suture. Finally, we analyzed the alveolar bone resorption and the composition of microbiota. The results suggested that we successfully established a mouse periodontitis model, whose composition of oral bacteria was similar to periodontitis patients.

METHODS

Subject Recruitment

This study was approved by the Ethics Committee of Shanghai Ninth People's Hospital, Shanghai Jiao Tong University School of Medicine. Informed consent was signed by all subjects before enrollment. All medical data were collected according to clinical standard procedures.

The clinical periodontal examination was performed by a single trained examiner before the collection of subgingival plaque (SP). Severe PD was diagnosed used the following criteria (Timmerman et al., 1998): 1) gum bleeding within 15 seconds after probing; 2) at least one site with periodontal pocket depth > 5mm; 3) at least one site with attachment loss > 4mm. Patients who had taken any antibiotic or probiotic, smoke, or had undergone periodontal therapy in the previous 6 months were excluded.

Sample Collection

SP were collected from six sites showing the deepest probing depth of each patient. All SP samples were stored in 20% glycerin at -80°C until further processing.

Animals

Male C57/B6J adult mice (8~10w) were used for experiments. And all experiments were repeated more than three times. The mice were randomly divided into three groups: Sham group (n=3), LIP group (n=3), and LIP+SP group (n=6). LIP was established by 5/0 silk suture around the bilateral maxillary second molars of mice (Abe and Hajishengallis, 2013). All SP samples were mixed and centrifuged at 5,000g for 5 minutes. Then, precipitate was resuspended in sterile 20% glycerin and was divided into tubes (the number of tubes was same as the quantity of patients). Again, centrifuged at 5,000g for 5 minutes, the pellets were resuspended in 1 ml sterile 2% carboxymethylcellulose (CMC). Application of SP (100μl per mouse) or 2% CMC to mouse teeth began on the next day, once every two days for 14 days (totally 7 times). Oral swabs of each mouse were collected one day before sacrificing. Four weeks after ligation, mice were euthanized, silk sutures, gingiva, and maxilla were collected. Mice in Sham group were ligated for 4 hours before being sacrificed. Mice were excluded if they died after the operation.

The animal experiments were approved by the Institutional Review and Ethics Board of Ninth People's Hospital, Shanghai Jiao Tong University School of Medicine.

Micro-CT Analysis

Maxillary bone and teeth were collected and fixed in 4% phosphate-buffered paraformaldehyde for 72 h. Then, the maxillae were processed for micro-computed tomography (CT) scanning using Bruker SkyScan 1176 (SkyScan) at a voxel resolution of 9 μm. Measurements were performed on the lingual sides of the maxillary second molar. The distance from the cementoenamel junction (CEJ) to the alveolar bone crest (ABC) was measured. Bone mineral density (BMD) and bone volume/total volume (BV/TV) were also measured.

Histology

The maxillae were fixed in 4% phosphate-buffered paraformaldehyde for 72 h, then decalcified in 10% EDTA solution for 4 weeks. The EDTA solution was changed daily

until decalcified. Maxillae were embedded in paraffin and cut into 5μm sections, which were then prepared for hematoxylin and eosin (HE) staining. HE staining was conducted according to routine protocols. The staining was observed under a microscope and photographed with 50X and 100X lens.

Quantitative RT-PCR

Gingiva RNA was extracted using Trizol (Life Technologies/Thermo Fisher Scientific) and cDNA was synthesized using reverse transcription kits (Takara, Shiga, Japan). QRT-PCR was performed with a SYBR Green PCR Master Mix (Takara) on a LightCycler480II system (Roche Diagnosticscs, Indianapolis, IN, USA). The sequences for the primers are listed. Il1β forward primer, 5′-GAAATGCCACCTTTTGACAGTG-3′, reverse primer, 5′-TGGATGCTCTCATCAGGACAG-3′. Il17a forward primer, TTTAACTCCCTTGGCGCAAAA, reverse primer, CTTTCCCTCCGCATTGACAC. Rankl forward primer, CAGCATCGCTCTGTTCCTGTA, reverse primer, CTGCGTTTTCATGGAGTCTCA.

High-Throughput Sequencing and Processing

Silk sutures, saliva swabs, and SP were used for high-throughput Sequencing. The genomic DNA was extracted and the bacteria was identified by 16S ribosomal RNA (rRNA) sequencing. PCR amplification of the nearly full-length bacterial 16S rRNA genes was performed using the forward primer 27F 5'-AGAGTTTGATCMTGGCTCAG-3' and the reverse primer 1492R 5'-ACCTTGTTACGACTT-3'. The PCR products were quantified with PicoGreen dsDNA Assay Kit (Invitrogen, Carlsbad, USA) and sequenced on PacBio Sequel platform at Shanghai Personal Biotechnology Co., Ltd (Shanghai, China).

Procession of the sequencing data was performed on QIIME2 platform. Analysis of sequencing data was based on amplicon sequence variants (ASVs) (Bokulich et al., 2018). After chimera detection, high-quality sequences with 97% similarity were clustered into the same ASV. Classification of ASVs was performed based on the Greengenes Database.

Data Analysis

Richness and a-diversity were measured by Chao1 and Shannon indices based on the species profiles (Chao, 1984; Shannon, 1948). Beta diversity was visualized using principal coordinate analysis (PCoA) based on the Bray-Curtis distances. Taxa abundances at the species levels were compared among groups by MEGAN (Huson et al., 2011). LEfSe (Linear discriminant analysis effect size) was performed to detect differentially abundant taxa across groups using the default parameters (Segata et al., 2011). Venn diagram was generated to visualize the shared and unique species among groups using R package "Venn Diagram", based on the occurrence of species across groups regardless of their relative abundance (Zaura et al., 2009).

Statistics

All data were shown as mean ± SEM. Statistical analysis was performed using Prism 5.0 (GraphPad Software, La Jolla, CA, USA). The differences between means of two experimental groups were analyzed by unpaired Student's *t* test or non-parametric test. Values of $p \leq 0.05$ were considered statistically significant.

RESULTS

Human Periodontitis-Causing Bacteria Efficiently Colonize in the Mouse Model

To establish the mouse model of periodontitis with colonization of human periodontitis-associated oral microbiota, we combined the ligature-induced mouse periodontitis with transplantation of subgingival plaque from periodontitis patients. In detail, we first ligatured the second molar with silk suture in mice, and then applied the bacteria, dissolved in 2% carboxymethylcellulose, on the ligature silk once every other day. The whole period of model construction was 4 weeks (**Figure 1A**). Lastly, 16S rRNA gene sequencing and taxonomic classification were carried out for unbiased measurement of bacterial composition and abundance in human subgingival plaque, mouse saliva and ligature silk.

We first compared the numbers of same bacteria in the ligature silk and saliva as in human subgingival plaque in both LIP and LIP + SP groups. As showed by Venn diagrams, 40 and 80 species of bacteria were shared by the ligature silk and human subgingival plaque in LIP and LIP + SP mice respectively. Meanwhile, 42 and 121 species of bacteria are same in the saliva and subgingival plaque in LIP and LIP + SP mice respectively (**Figure 1B**). Consistently, the analysis of bacterial composition showed similar results. The bacterial compositions in the ligature silk (**Figure 1C**) and saliva (**Figure 1D**) were significantly more comparable to those in human subgingival plaque in LIP + SP mice versus LIP mice. It is interesting that the well-known periodontal pathogenic bacteria including *Porphyromonas gingivalis* (*P.g*), *Fusobacterium nucleatum* (*F.n*), *Prevotella intermedia (P.i)*, and *Tannerella forsythia* (*T.f*) were markedly colonized in LIP + SP mice, but not in LIP mice. Then, we analyzed the sample diversity using principal coordinate analysis (PCoA). In LIP + SP group, the bacterial composition of saliva is more similar to the SP compared with silk sutures (**Figure 1E**). These results cumulatively demonstrated that the transplantation of human subgingival plaque significantly promoted the enrichment of human periodontitis-causing bacteria in mouse periodontitis model.

Pathogenic Bacteria of Human Periodontitis Are Enriched in the Ligature Silk in the Mouse Model

We further analyzed the change of bacterial composition on ligature silks by sequentially comparing LIP with Sham mice, and LIP + SP with LIP mice. As expected, LIP groups of mice showed significantly higher diversity of subgingival bacteria in comparison with sham mice, and human subgingival plaque transplantation further markedly enlarged the increase of bacterial diversity (**Figure 2A**). PCoA based on Bray-Curtis distance was performed to determine β-diversity (between-sample diversity) of bacteria composition on ligature silks, which demonstrated the potent distinction among Sham, LIP,

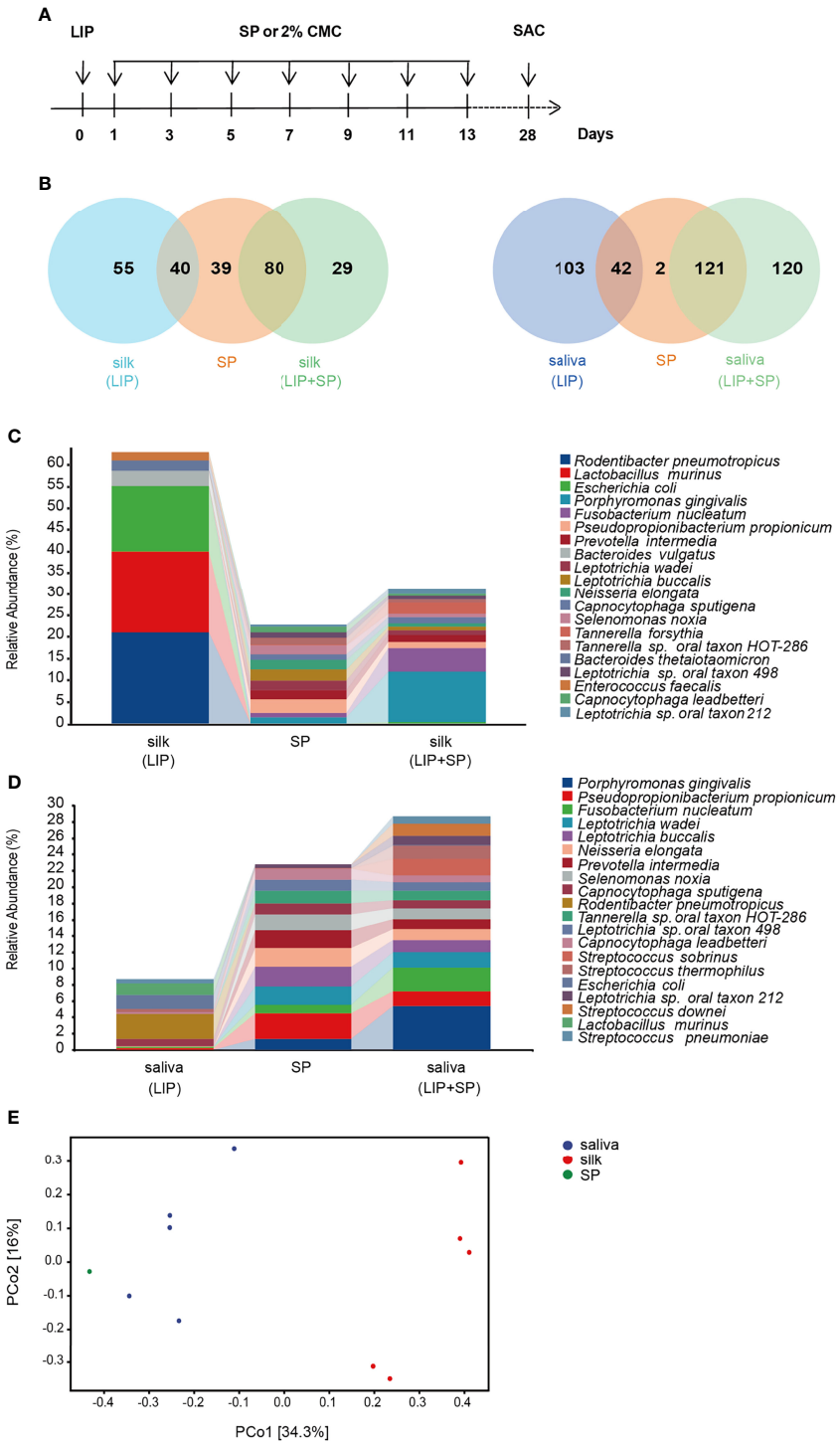

FIGURE 1 | Human periodontitis-causing bacteria efficiently colonize in the mouse model. **(A)** Schematic illustration of experimental design. LIP, ligature-induced periodontitis. SP, subgingival plaques from patients with periodontitis. CMC, carboxymethylcellulose, and SAC, sacrifice. **(B)** The Venn diagrams showing the overlapped and different bacteria species between mouse silk ligature and human subgingival plaque (left), and between human subgingival plaque and mouse saliva (right). **(C)** Taxonomic composition of bacterial community at species level in mouse silk ligature and human subgingival plaque. **(D)** Taxonomic composition of bacterial community at species level in mouse saliva and human subgingival plaque. **(E)** β-diversity of SP and saliva, silk ligature bacteria at species level in LIP + SP group, assessed by principal coordinate analysis (PCoA) based on bray–curtis distance. (n = 5:5).

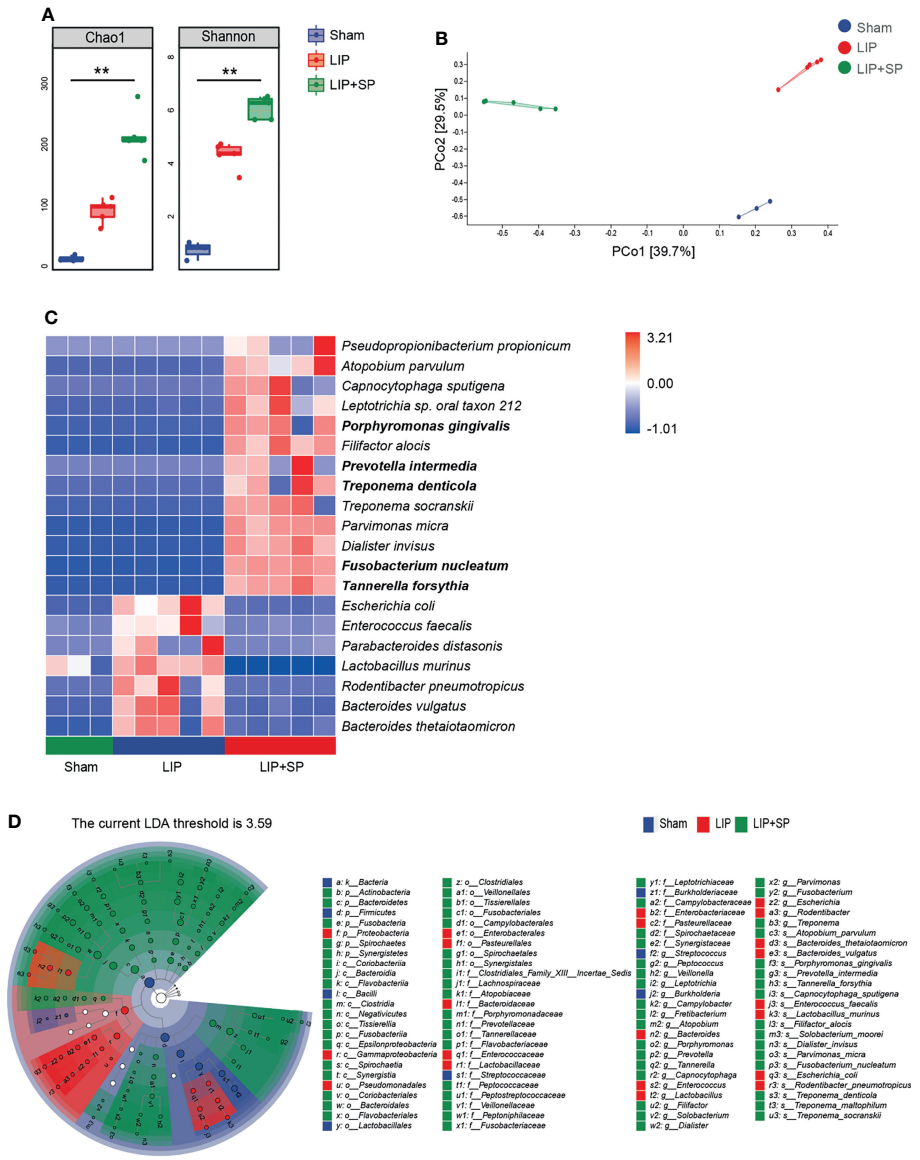

FIGURE 2 | Pathogenic bacteria of human periodontitis are enriched in the ligature silk in the mouse model. Bacterial community of ligature silks from Sham, LIP, and LIP + SP group mice were analyzed using 16S rRNA gene sequencing. **(A)** α-diversity of bacteria on ligature silks assessed by Chao1 and Shannon indices. **(B)** β-diversity of bacteria on ligature silk assessed by principal coordinate analysis (PCoA) based on Bray–Curtis distance of bacteria at species level. **(C)** The heat map of the relative abundance of the top 20 most abundant species of bacteria on ligature silks. **(D)** Taxonomic cladogram of bacteria on ligature silk using LEfSe (LDA = 3.59). The values represent means ± SEM (n = 3:5:5). **P < 0.01.

and LIP + SP groups of mice (**Figure 2B**). Furthermore, the Heatmap of relative abundances of bacteria species showed that thirteen species of bacteria were massively enriched in the LIP + SP group. Some of these bacteria are periodontal pathogens, including *Porphyromonas gingivalis (P.g), Prevotella intermedia (P.i), Treponema denticola (T.d)*, and *Fusobacterium nucleatum (F.n)*, while they were detected at extremely low abundance in Sham and LIP groups (**Figure 2C**). We next employed linear discriminant analysis effect size (LEfSe) to identify taxa that discriminate microbial composition among three groups of mice. Again, it was shown that the periodontitis-causing bacteria species including *P.g, P.i, T.d, F.n* and *T.f* were more enriched in ligature silk of LIP+SP mice versus Sham and LIP mice (**Figure 2D**).

Pathogenic Bacteria of Human Periodontitis Are Enriched in the Mouse Saliva

By the same strategies, we analyzed the differences of bacteria composition and abundance in saliva among Sham, LIP and LIP +

SP groups of mice. The alpha diversity, illustrated by the Chao1 and the Shannon indices, was significantly increased by LIP + SP treatment compared to LIP treatment or no treatment (**Figure 3A**). In the PCoA analysis for β-diversity, the dots of LIP + SP group were far away from the dots of Sham and LIP group, demonstrating the significant divergence in their bacteria composition (**Figure 3B**). We used the Heatmap to show the top 20 most abundant bacteria species in saliva (**Figure 3C**). In LIP + SP group, the compositions of microbial species markedly differed from those in Sham and LIP groups. At the species level, the relative abundances of *F.n*, *P.g*, *P.i*, and *S.n*, which had been shown the close association with periodontal diseases, were sharply increased by human subgingival bacteria transplantation. LEfSe analysis consistently illustrated that these periodontal pathogenic bacteria were significantly enriched in saliva of LIP + SP group mice (**Figure 3D**).

Human Periodontitis-Associated Bacteria Worsen Periodontitis in Mice

To measure effects of the colonized periodontitis-associated bacteria on periodontal tissue in our mouse model, Micro-CT analysis, H&E staining, and real time QPCR assay were

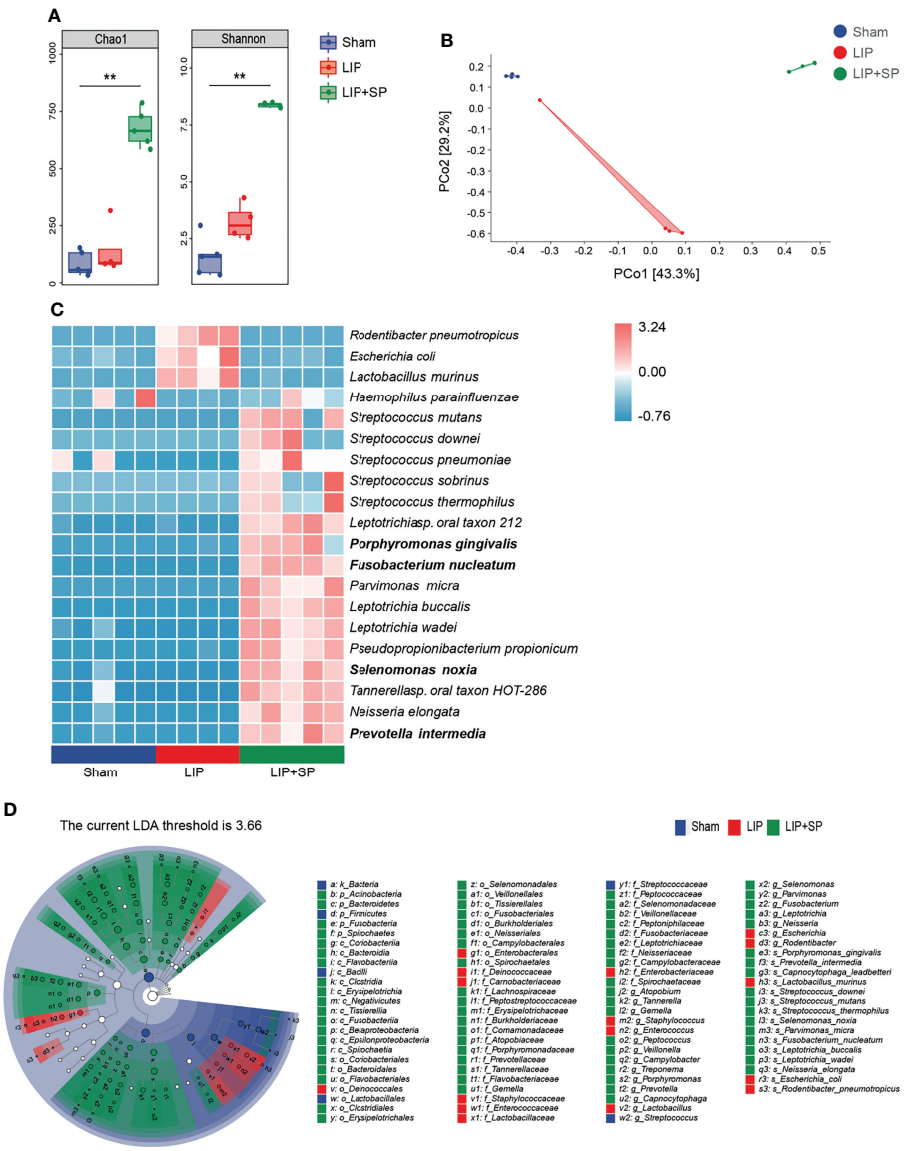

FIGURE 3 | Pathogenic bacteria of human periodontitis are enriched in the mouse saliva. Saliva bacteria from Sham, LIP, and LIP + SP group mice were analyzed using 16S rRNA gene sequencing. **(A)** α-diversity of saliva bacteria assessed by Chao1 and Shannon indices. **(B)** β-diversity of saliva bacteria at species level, assessed by principal coordinate analysis (PCoA) based on Bray–Curtis distance. **(C)** The heat map of the relative abundance of the top 20 most abundant bacteria species in mouse saliva. **(D)** Taxonomic cladogram of saliva bacteria using LEfSe (LDA = 3.65). LDA, Linear Discriminant Analysis. The values represent means ± SEM (n = 5:4:5). **P < 0.01.

performed. The reconstruction images of maxilla showed that LIP caused significant loss of alveolar bone, and the loss was further aggravated by additional treatment of human subgingival plaque (**Figures 4A, B**). As a result, percentage of bone volume (BV) to total volume (TV) was significantly decreased by LIP, and BV/TV was much lower in LIP + SP group versus LIP group (**Figure 4C**). Consistently, there was a significant decline in maxilla bone mineral density (BMD) in both LIP and LIP + SP groups, and the decrease was much greater in LIP + SP group than that in LIP group (**Figure 4D**). In both LIP and LIP + SP groups, hematoxylin–eosin (H&E) staining of maxilla sections showed marked destruction of periodontal tissue around the second molar (**Figure 4E**). In addition, the mRNA levels of inflammatory genes including interleukin-1b (*Il1b*) and interleukin-17a (*Il17*a), and osteoclastogenesis gene, receptor activator of NF-κB ligand (*Rankl*), were substantially higher in the LIP + SP group than those in LIP group. Similarly, the expression of these genes was significantly higher in both periodontitis group versus in Sham group (**Figure 4F**).

DISCUSSION

Human periodontitis-associated bacteria cause local destruction of periodontal tissue and are also tightly linked to the progression of multiple systemic diseases. However, there is still a lack of proper mouse model of periodontitis with the colonization of human periodontitis-associated microbiota. Here, we created a new mouse model to simulate the clinical situation by transplanting SP on silk sutures, which was used to ligate mouse molars to induce periodontitis. In this model, the composition of mouse periodontal bacteria matched better with that of periodontitis patients.

Previous studies established PD model by silk ligature or specific periodontal bacteria, which induced chronic periodontal disease and systemic inflammation. However, it failed to simulate the original periodontal bacterial composition of PD. The composition of normal oral flora of humans and animals is different (Hasegawa et al., 2010). In the silk suture ligation-induced periodontal model, the main periodontal pathogens are changed, which play a role in the process of periodontitis. This conclusion was supported by in our study that the microbiota composition of the LIP group was totally different from SP. Periodontitis is mainly caused by the imbalance of multiple microbial floras (Socransky et al., 1998). The use of a specific bacterium does not reflect the role of other bacteria in periodontitis, especially the host immune response. Different bacteria are associated with particular function in innate responses and the generation of distinct T-cell subsets (David Jarrossay et al., 2001). For example, Toll-like receptor 2 can recognize *P.g*, *T.f*, *P.i*, and *T.d*. Besides, *Aggregatibacter*, *actinomycetemcomitans*, and *Veillonella parvula* are the pathogens of Toll-like receptor 4 (Cekici et al., 2014). Lastly, periodontitis can affect other systemic diseases (such as cardiovascular diseases, metabolic diseases, and cancers). The possible mechanism includes direct colonization of bacteria on target organs (Costa et al., 2021). The method of using silk sutures to ligate or smear a single bacteria cannot effectively locate the colonized bacteria. As a result, the experimental model *in vivo* is not always appropriate for mimicking clinical settings.

Different types of animals, including mice, rats, dogs, and non-human primates, have been used to establish periodontitis models. However, mice are still the most convenient, cost-effective and versatile models. Advantages of the mice as a model include the considerable background information on their immune system, a wide range of genetically engineered strains (e.g., gene knockouts for key immune receptors or signaling molecules) and availability of high-quality immunochemical and cellular reagents (Graves et al., 2008). Ligation of maxillary second molars in mice is a common periodontitis modeling method. Many articles on periodontitis models have adopted the method of ligating maxillary second molars (Li et al., 2021). Compared with first molars, ligating the second molar is more solid and suture is not easy to slip off. The maxillary third molar is too small and more difficult to operate. In addition, the second molar is adjacent to the first and third molar, where periodontal pathogens can colonize the adjacent teeth.

To our knowledge, this work is the first one to establish a sustained model to simulate the clinical situation. Ligation of second molars combining with patients' plaques can establish a 'two hit' model. This two-hit mouse model of PD has its unique merits. Ligation of molars is not only convenient and time-saving but also facilitates the accumulation of bacteria. In other ligation-induced periodontal models, researchers usually choose two weeks to study how PD affects systemic diseases (Kitamoto et al., 2020). However, these studies might not be representative of the oral health condition and the oral microbiome composition. In this study, we sacrifice mice and harvest samples after ligation for four weeks, which is enough for patients' bacteria colonizing. In contrast to single periodontal pathogens, patients' plaques have complex microflora, which is more representative to simulate periodontitis patients' oral condition.

We observed significant microbial alterations in oral cavity of LIP + SP group mice. Salivary microbiota showed higher richness than that of silk suture of LIP + SP group mice. In comparison with silk sutures, saliva provides larger space, more diverse nutrients, and mobile liquid environment. The different microbiota enriched in the ligation suture and saliva is probably due to the difference of local environment between saliva and ligature silk sutures. Besides, bacteria species of LIP + SP are far more than those of LIP and Sham groups. This is likely because there is more bacterial diversity in subjects with periodontal disease (Abusleme et al., 2013). Furthermore, the dominant pathogens of periodontitis include 'red complex' (P. g, T. d, and T. f) and 'orange complex' (F. n and P. i, etc.) (Hajishengallis and Lamont, 2012), and the progression of periodontitis is mainly caused by the dominant pathogens. Single periodontal pathogen may not cause disease as expected. Previous study illustrates that P. g is not a potent stand-alone inducer of inflammation. *In vitro* and vivo, P. g often induces contradictory hosts responses. For example, P. g lipopolysaccharide can antagonize toll-like receptor 4, unlike other highly pro-inflammatory lipopolysaccharides from most gram-negative bacteria. Also, in the absence of commensal bacteria, P. g fails to induce periodontitis when used as a mono-infection in germ-free mice (Hajishengallis and Lamont, 2012).

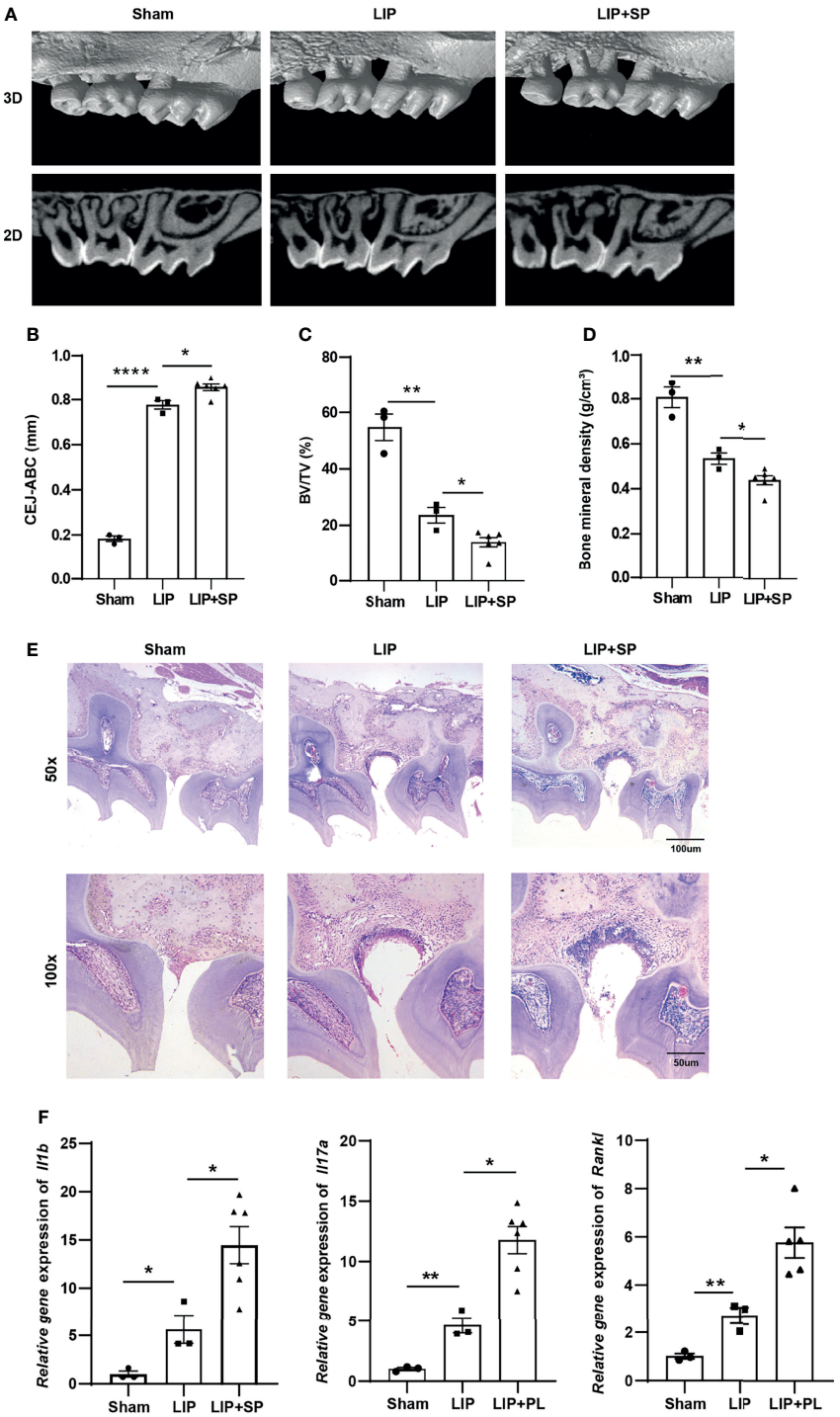

FIGURE 4 | Transplantation of human periodontitis-associated bacteria worsens periodontitis in mice. **(A)** Representative images of Micro–computed tomography scanning of left maxilla from the indicated groups of mice. Both three-dimensional volume (Upper panels) and multiplanar reconstruction (Lower panels) are shown. **(B)** Quantification of the distance from cementoenamel junction (CEJ) to alveolar bone crest (ABC). **(C)** The ratio of bone volume (BV) to total volume (TV) of maxilla surrounding the second molar. **(D)** Bone mineral density (BMD) (g/cm^3) of maxilla surrounding the second molar. **(E)** Representative hematoxylin–eosin (H&E) staining images of periodontal tissue showing the pathogenic alteration. **(F)** QRT-PCR analyses of inflammatory and osteoclastogenesis gene expression. *Gapdh* was used as internal references. The values represent means ± SEM (n = 3:3:6) from three independent experiments. ns, not significant. *P < 0.05, **P < 0.01, ****P < 0.0001.

Therefore, application of SP is a better choice than specific pathogen to induce periodontitis.

CONCLUSION

In summary, we established a 'two-hit' periodontitis model which combined ligation of mouse molars with subgingival plaques from periodontitis patients. The microbiota composition of silk suture and saliva was similar to that of patients' subgingival plaques. Additionally, using this animal model, we found that subgingival plaques exacerbated ligation-induced periodontitis and promoted gingiva inflammation.

DATA AVAILABILITY STATEMENT

The datasets presented in this study can be found in online repositories. The names of the repository/repositories and accession number(s) can be found below: https://www.ncbi.nlm.nih.gov/bioproject/PRJNA793991.

ETHICS STATEMENT

The protocol was approved by the Institutional Review and Ethics Board of Shanghai Ninth People's Hospital, Shanghai Jiao Tong University School of Medicine. The patients/participants provided their written informed consent to participate in this study. The animal study was reviewed and approved by Institutional Review and Ethics Board of Ninth People's Hospital, Shanghai Jiao Tong University School of Medicine.

AUTHOR CONTRIBUTIONS

S-ZD and W-CZ designed and supervised the project. LB, B-YC, and YL collected the clinical samples, performed the statistical analyses, and wrote the manuscript. S-ZD and W-CZ read and revised the manuscript. All authors contributed to the article and approved the submitted version.

FUNDING

This work was supported by grants from the National Natural Science Foundation of China (81991503, 81991500, 81921002) and the Innovative Research Team of High-Level Local Universities in Shanghai (Oral-Gut Ecology and Major Chronic Diseases, SHSMU-ZDCX20212500).

REFERENCES

Abe, T., and Hajishengallis, G. (2013). Optimization of the Ligature-Induced Periodontitis Model in Mice. *J. Immunol. Methods* 394 (1-2), 49–54. doi: 10.1016/j.jim.2013.05.002

Abusleme, L., Dupuy, A. K., Dutzan, N., Silva, N., Burleson, J. A., Strausbaugh, L. D., et al. (2013). The Subgingival Microbiome in Health and Periodontitis and its Relationship With Community Biomass and Inflammation. *ISME J.* 7 (5), 1016–1025. doi: 10.1038/ismej.2012.174

Bage, T., Lindberg, J., Lundeberg, J., Modeer, T., and Yucel-Lindberg, T. (2010). Signal Pathways JNK and NF-Kappab, Identified by Global Gene Expression Profiling, are Involved in Regulation of TNFalpha-Induced mPGES-1 and COX-2 Expression in Gingival Fibroblasts. *BMC Genomics* 11, 241. doi: 10.1186/1471-2164-11-241

Blasco-Baque, V., Garidou, L., Pomie, C., Escoula, Q., Loubieres, P., Le Gall-David, S., et al. (2017). Periodontitis Induced by Porphyromonas Gingivalis Drives Periodontal Microbiota Dysbiosis and Insulin Resistance via an Impaired Adaptive Immune Response. *Gut* 66 (5), 872–885. doi: 10.1136/gutjnl-2015-309897

Bokulich, N. A., Kaehler, B. D., Rideout, J. R., Dillon, M., Bolyen, E., Knight, R., et al. (2018). Optimizing Taxonomic Classification of Marker-Gene Amplicon Sequences With QIIME 2's Q2-Feature-Classifier Plugin. *Microbiome* 6 (1), 90. doi: 10.1186/s40168-018-0470-z

Brown LJ, O. R., and Löe, H. (1989). Periodontal Diseases in the U.S. @ in 1981: Prevalence, Severity, Extent, and Role in Tooth Mortality. *J. Periodontol.* 60 (7), 363–370. doi: 10.1902/jop.1989.60.7.363

Cekici, A., Kantarci, A., Hasturk, H., and Van Dyke, T. E. (2014). Inflammatory and Immune Pathways in the Pathogenesis of Periodontal Disease. *Periodontol. 2000* 64 (1), 57–80. doi: 10.1111/prd.12002

Chao, A. (1984). Nonparametric Estimation of the Number of Classes in a Population. *Scand. J. Stat.* 11 (4), 265–270.

Costa, M. J. F., de Araujo, I. D. T., da Rocha Alves, L., da Silva, R. L., Dos Santos Calderon, P., Borges, B. C. D., et al. (2021). Relationship of Porphyromonas Gingivalis and Alzheimer's Disease: A Systematic Review of Pre-Clinical Studies. *Clin. Oral. Investig.* 25 (3), 797–806. doi: 10.1007/s00784-020-03764-w

David Jarrossay, G. N., Colonna, M., and Lanzavecchia, F. S. (2001). Specialization and Complementarity in Microbialmolecule Recognition by Human Myeloid Andplasmacytoid Dendritic Cells. *Eur. J. Immunol.* 31 (11), 3388–3393. doi: 10.1002/1521-4141(200111)31:11<3388::AID-IMMU3388>3.0.CO;2-Q

Graves, D. T., Fine, D., Teng, Y. T., Van Dyke, T. E., and Hajishengallis, G. (2008). The Use of Rodent Models to Investigate Host-Bacteria Interactions Related to Periodontal Diseases. *J. Clin. Periodontol.* 35 (2), 89–105. doi: 10.1111/j.1600-051X.2007.01172.x

Hajishengallis, G. (2015). Periodontitis: From Microbial Immune Subversion to Systemic Inflammation. *Nat. Rev. Immunol.* 15 (1), 30–44. doi: 10.1038/nri3785

Hajishengallis, G., and Lamont, R. J. (2012). Beyond the Red Complex and Into More Complexity: The Polymicrobial Synergy and Dysbiosis (PSD) Model of Periodontal Disease Etiology. *Mol. Oral. Microbiol.* 27 (6), 409–419. doi: 10.1111/j.2041-1014.2012.00663.x

Hasegawa, M., Osaka, T., Tawaratsumida, K., Yamazaki, T., Tada, H., Chen, G. Y., et al. (2010). Transitions in Oral and Intestinal Microflora Composition and Innate Immune Receptor-Dependent Stimulation During Mouse Development. *Infect. Immun.* 78 (2), 639–650. doi: 10.1128/IAI.01043-09

Kassebaum, N. J., Bernabe, E., Dahiya, M., Bhandari, B., Murray, C. J., and Marcenes, W. (2014). Global Burden of Severe Periodontitis in 1990-2010: A Systematic Review and Meta-Regression. *J. Dent. Res.* 93 (11), 1045–1053. doi: 10.1177/0022034514552491

Keijser, B. J., Zaura, E., Huse, S. M., van der Vossen, J. M., Schuren, F. H., Montijn, R. C., et al. (2008). Pyrosequencing Analysis of the Oral Microflora of Healthy Adults. *J. Dent. Res.* 87, 1016–1020. doi: 10.1177/154405910808701104

Kitamoto, S., Nagao-Kitamoto, H., Jiao, Y., Gillilland, M. G., 3rd, Hayashi, A., Imai, J., et al. (2020). The Intermucosal Connection Between the Mouth and Gut in Commensal Pathobiont-Driven Colitis. *Cell* 182 (2), 447–462 e414. doi: 10.1016/j.cell.2020.05.048

Li, L., Bao, J., Chang, Y., Wang, M., Chen, B., and Yan, F. (2021). Gut Microbiota May Mediate the Influence of Periodontitis on Prediabetes. *J. Dent. Res.*, 100 (12), 1387–1396. 220345211009449. doi: 10.1177/00220345211009449

Mackie, RI, Sghir, A, and Gaskins, HR (1999). Developmental Microbial Ecology of the Neonatal Gastrointestinaltract. *Am J Clin Nutr*. 69 (5), 1035S–1045S. doi: 10.1093/ajcn/69.5.1035s

Michaud, D. S., Fu, Z., Shi, J., and Chung, M. (2017). Periodontal Disease, Tooth Loss, and Cancer Risk. *Epidemiol. Rev.* 39 (1), 49–58. doi: 10.1093/epirev/mxx006

Mysak, J., Podzimek, S., Sommerova, P., Lyuya-Mi, Y., Bartova, J., Janatova, T., et al. (2014). Porphyromonas Gingivalis: Major Periodontopathic Pathogen Overview. *J. Immunol. Res.* 2014, 476068. doi: 10.1155/2014/476068

Paster, B. J., Olsen, I., Aas, J. A., and Dewhirst, F. E. (2006). The Breadth of Bacterial Diversity in the Human Periodontal Pocket and Other Oral Sites. *Periodontol. 2000* 42, 80–87. doi: 10.1111/j.1600-0757.2006.00174.x

Polak, D., and Shapira, L. (2018). An Update on the Evidence for Pathogenic Mechanisms That may Link Periodontitis and Diabetes. *J. Clin. Periodontol.* 45 (2), 150–166. doi: 10.1111/jcpe.12803

Sanz, M., Marco Del Castillo, A., Jepsen, S., Gonzalez-Juanatey, J. R., D'Aiuto, F., Bouchard, P., et al. (2020). Periodontitis and Cardiovascular Diseases: Consensus Report. *J. Clin. Periodontol.* 47 (3), 268–288. doi: 10.1111/jcpe.13189

Segata, N., Izard, J., Waldron, L., Gevers, D., Miropolsky, L., Garrett, W. S., et al. (2011). Metagenomic Biomarker Discovery and Explanation. *Genome Biol.* 12 (6), R60. doi: 10.1186/gb-2011-12-6-r60

Shannon, C. E. (1948). A Mathematical Theory of Communication. *Bell. Syst. Tech. J.* 27 (3), 379–423. doi: 10.1002/j.1538-7305.1948.tb01338.x

Shi, B., Chang, M., Martin, J., Mitreva, M., Lux, R., Klokkevold, P., et al. (2015). Dynamic Changes in the Subgingival Microbiome and Their Potential for Diagnosis and Prognosis of Periodontitis. *mBio* 6 (1), e01926–e01914. doi: 10.1128/mBio.01926-14

Socransky, S. S., Haffajee, A. D., Cugini, M. A., Smith, C., and Kent, R.L. (1998). Microbial Complexes in Subgingival Plaque. *J. Clin. Periodontol.* 25, 134–144. doi: 10.1111/j.1600-051X.1998.tb02419.x

Timmerman, M. F., van der Weijden, G. A., Armand, S., Abbas, F., Winkel, E. G., Van Winkelhoff, A. J., et al. (1998). Untreated Periodontal Disease in Indonesian Adolescents. Clinical and Microbiological Baseline Data. *J. Clin. Periodontol.* 25 (3), 215–224. doi: 10.1111/j.1600-051x.1998.tb02431.x

Zaura, E., Keijser, B. J., Huse, S. M., and Crielaard, W. (2009). Defining the Healthy "Core Microbiome" of Oral Microbial Communities. *BMC Microbiol.* 9, 259. doi: 10.1186/1471-2180-9-259

Huson, D. H., Mitra, S., Ruscheweyh, H. J., Weber, N., and Schuster, S. C. (2011). Integrative Analysis of Environmental Sequences using MEGAN4. *Genome Res* 21 (9), 1552–1560. doi: 10.1101/gr.120618.111

Conflict of Interest: The authors declare that the research was conducted in the absence of any commercial or financial relationships that could be construed as a potential conflict of interest.

Publisher's Note: All claims expressed in this article are solely those of the authors and do not necessarily represent those of their affiliated organizations, or those of the publisher, the editors and the reviewers. Any product that may be evaluated in this article, or claim that may be made by its manufacturer, is not guaranteed or endorsed by the publisher.

frontiers in Cellular and Infection Microbiology

ORIGINAL RESEARCH
published: 22 March 2022
doi: 10.3389/fcimb.2022.872012

Lactobacillus plantarum Disrupts *S. mutans–C. albicans* Cross-Kingdom Biofilms

Yan Zeng[1], *Ahmed Fadaak*[1], *Nora Alomeir*[1], *Tong Tong Wu*[2], *Elena Rustchenko*[3], *Shuang Qing*[4], *Jianhang Bao*[1], *Christie Gilbert*[5] *and Jin Xiao*[1]*

[1] Eastman Institute for Oral Health, University of Rochester Medical Center, Rochester, NY, United States, [2] Department of Biostatistics and Computational Biology, University of Rochester Medical Center, Rochester, NY, United States, [3] Department of Biochemistry and Biophysics, University of Rochester Medical Center, Rochester, NY, United States, [4] University of Rochester River Campus, Rochester, NY, United States, [5] Microbiology and Immunology, University of Rochester Medical Center, Rochester, NY, United States

Dental caries, an ecological dysbiosis of oral microflora, initiates from the virulent biofilms formed on tooth surfaces where cariogenic microorganisms metabolize dietary carbohydrates, producing acid that demineralizes tooth enamel. Forming cariogenic biofilms, *Streptococcus mutans* and *Candida albicans* are well-recognized and emerging pathogens for dental caries. Recently, probiotics have demonstrated their potential in treating biofilm-related diseases, including caries. However, limited studies have assessed their effect on cariogenic bacteria–fungi cross-kingdom biofilm formation and their underlying interactions. Here, we assessed the effect of four probiotic *Lactobacillus strains (Lactobacillus rhamnosus* ATCC 2836, *Lactobacillus plantarum* ATCC 8014, *Lactobacillus plantarum* ATCC 14917, and *Lactobacillus salivarius* ATCC 11741) on *S. mutans* and *C. albicans* using a comprehensive multispecies biofilm model that mimicked high caries risk clinical conditions. Among the tested probiotic species, *L. plantarum* demonstrated superior inhibition on the growth of *C. albicans* and *S. mutans*, disruption of virulent biofilm formation with reduced bacteria and exopolysaccharide (EPS) components, and formation of virulent microcolonies structures. Transcriptome analysis (RNA sequencing) further revealed disruption of *S. mutans* and *C. albicans* cross-kingdom interactions with added *L. plantarum*. Genes of *S. mutans* and *C. albicans* involved in metabolic pathways (e.g., EPS formation, carbohydrate metabolism, glycan biosynthesis, and metabolism) were significantly downregulated. More significantly, genes related to *C. albicans* resistance to antifungal medication (ERG4), fungal cell wall chitin remodeling (CHT2), and resistance to oxidative stress (CAT1) were also significantly downregulated. In contrast, *Lactobacillus* genes *plnD*, *plnG*, and *plnN* that contribute to antimicrobial peptide plantaricin production were significantly upregulated. Our novel study findings support further assessment of the potential role of probiotic *L. plantarum* for cariogenic biofilm control.

Keywords: *Streptococcus mutans*, *Candida albicans*, dental caries, multispecies biofilms, cross-kingdom interactions, *Lactobacillus plantarum*

OPEN ACCESS

Edited by:
Sarah Maddocks, Cardiff Metropolitan University, United Kingdom

Reviewed by:
Ruijie Huang, Sichuan University, China
Yuan Liu, University of Pennsylvania, United States

***Correspondence:**
Jin Xiao
jin_xiao@urmc.rochester.edu

Specialty section:
This article was submitted to Microbiome in Health and Disease, a section of the journal Frontiers in Cellular and Infection Microbiology

Received: *09 February 2022*
Accepted: *23 February 2022*
Published: *22 March 2022*

Citation:
Zeng Y, Fadaak A, Alomeir N, Wu TT, Rustchenko E, Qing S, Bao J, Gilbert C and Xiao J (2022) Lactobacillus plantarum Disrupts S. mutans–C. albicans Cross-Kingdom Biofilms. Front. Cell. Infect. Microbiol. 12:872012. doi: 10.3389/fcimb.2022.872012

1 INTRODUCTION

Dental caries, an ecological dysbiosis of oral microflora, initiates from the virulent biofilms formed on tooth surfaces where cariogenic bacteria and fungi metabolize dietary carbohydrates, produce acid, and lead to irreversible consequences—demineralization of tooth enamel (Bowen, 2016). *Streptococcus mutans* is a well-known cariogenic pathogen due to its acidogenicity, aciduricity, and capability of synthesizing the dental plaque extracellular matrix (Bowen et al., 2018). Moreover, research also revealed the cariogenic role of oral *Candida*, in that it is acidogenic, aciduric, and capable of dissolving hydroxyapatite and leads to more severe dental caries when infected together with *S. mutans* in the rat model (Falsetta et al., 2014; Du et al., 2021). Children with oral *Candida albicans* presented with >5 times greater odds of experiencing early childhood caries (ECC) than children without this yeast strain (Xiao et al., 2018b). The presence of *C. albicans* in the oral cavity of preschool children was associated with oral bacterial dysbiosis with an abundance of taxa with greater virulence and more conducive for ECC (Xiao et al., 2018a). Furthermore, the emergence of *S. mutans* by 1 year was 3.5 times higher in infants with early colonization of oral *Candida* than those free of oral *Candid*a (Alkhars N et al., 2021). Therefore, regulating *S. mutans* and *C. albicans* simultaneously in the oral cavity sheds new light on caries prevention.

Probiotic therapy has the potential to prevent and treat dental caries (Zaura and Twetman, 2019). The most commonly used probiotics include *Lactobacilli* and *Bifidobacterium*, both of which produce lactic acid and other bioactive substances, including hydrogen peroxide, carbon peroxide, bacteriocins, and adhesion inhibitors that could potentially affect the growth of cariogenic microorganisms (Meurman, 2005). Several studies have reported the inhibitory effect of probiotics on *S. mutans* and *C. albicans*; for instance, *Lactobacillus rhamnosus*, *Lactobacillus reuteri*, *Lactobacillus casei*, *Lactobacillus plantarum*, and *Lactobacillus salivarius* inhibit the growth of *S. mutans in vitro* and *in vivo* (Laleman et al., 2014; Wasfi et al., 2018; Zhang et al., 2020a); *L. rhamnosus*, *L. casei*, *Lactobacillus paracasei*, *Lactobacillus fermentum*, and *Lactobacillus acidophilus* inhibit *C. albicans* biofilms (Matsubara et al., 2016; Rossoni et al., 2018; Panariello et al., 2021).

Since the coexistence of *S. mutans* and *C. albicans* in the oral cavity leads to a more pathogenic microbial eco-community and potentially elevates the caries risk of individuals (Koo et al., 2018; Du et al., 2021), an ideal probiotic regimen is to control *S. mutans* and *C. albicans* simultaneously. Intriguingly, our previous study revealed that the abundance of *L. plantarum* in dental plaques was three-fold higher in children without *C. albicans* compared to those with carriage of *C. albicans*, indicating a potential antagonistic interaction between *L. plantarum* and *C. albicans* (Xiao et al., 2018a). Moreover, Srivastava et al. reported that the supernatant of *L. plantarum* 108 inhibited the duo-species biofilm formation by *S. mutans* and *C. albicans* (Srivastava et al., 2020). Zhang et al. demonstrated that *L. plantarum* CCFM8724 could decrease the carriage of *S. mutans* and *C. albicans* in rat's oral cavity and reduce caries score in rats (Zhang et al., 2020b). The abovementioned study findings support a better understanding of the interactions between *L. plantarum*, *S. mutans*, and *C. albicans* in multispecies biofilms. In the present study, we evaluated the effect of four probiotic *Lactobacillus strains* (two *L. plantarum*, *L. salivarius*, and *L. rhamnosus*) on the growth of *S. mutans* and *C. albicans*, in planktonic and cariogenic biofilm settings that simulate high caries risk clinical conditions. We used a comprehensive biofilm evaluation model and RNA-Seq analysis to reveal species interactions.

2 MATERIALS AND METHODS

2.1 Bacterial Strains and Starter Preparation

The microorganisms used in the study were *S. mutans* UA159, *C. albicans* SC5314, *L. rhamnosus* ATCC 2836, *L. plantarum* ATCC 8014, *L. plantarum* ATCC 14917, and *L. salivarius* ATCC 11741. C. *albicans*, *S. mutans*, and *Lactobacillus* were recovered from frozen stock using YPD agar (BD Difco™, San Jose, CA, USA, 242720), blood agar (TSA with sheep blood, Thermo Scientific™, Waltham, MA, USA, R01202), and MRS agar (BD Difco™, 288210), respectively. After 48 h of incubation, 3–5 colonies of each species were inoculated into 10 ml of broth for overnight incubation (5% CO_2, 37°C). *C. albicans* was grown in YPD broth (BD Difco™, 242820); *S. mutans* was grown in TSBYE broth (3% Tryptic Soy, 0.5% Yeast Extract Broth, BD Bacto™ 286220 and Gibco™ 212750) with 1% glucose; and *Lactobacillus* spp. were grown in MRS broth (BD Difco™, 288130). On the following day, 0.5 ml of the overnight starters was added to individual glass tubes with fresh broth and incubated for 3–4 h to reach the mid-exponential phase with desirable optical density. The morning starters were then ready for the preparation of planktonic and biofilm models described below.

2.2 Planktonic Model

Interactions between *C. albicans*, *S. mutans*, and *Lactobacillus* species were first evaluated in planktonic conditions; see **Figure S1A** for the study flow. The inoculation quantity of *C. albicans* (10^3 CFU/ml) and *S. mutans* (10^5 CFU/ml) was chosen to simulate high caries risk conditions in the clinical setting. The inoculation quantity of the four *Lactobacillus* (10^8 CFU/ml) is the lower dose of the probiotics used in the commercial probiotic products (10^9–10^{12} CFU as a single dosage). *C. albicans*, *S. mutans*, and one of the *Lactobacilli* were grown in 10 ml TSBYE broth with 1% glucose for 20 h (5% CO_2, 37°C). Additionally, a dose-titration effect of *L. plantarum* 14917 (10^4–10^7 CFU/ml inoculation) was assessed. The growth of each microorganism and pH values were measured at multiple time points.

2.3 Mixed-Species Biofilm Model

We then used a mixed-species biofilm model to assess the effect of *Lactobacilli* on the biofilm formation by *S. mutans* and *C. albicans*; see **Figure S1B** for the study flow. The biofilm was formed on saliva-coated hydroxyapatite discs (0.50″ diameter ×

0.05″ thickness, Clarkson Chromatography Products, Inc., South Williamsport, PA), the method detailed previously (Xiao et al., 2012). The discs were placed in a vertical position using a custom-made disc holder to mimic the caries-prone smooth tooth surfaces in the oral cavity (Xiao et al., 2012).

The mixture of *S. mutans*, *C. albicans*, and *Lactobacilli* was inoculated in 2.8 ml of TSBYE broth with 0.1% (w/v) sucrose and incubated at 37°C and 5% CO_2. During the first 24 h, the organisms were grown undisturbed to allow initial biofilm formation. At 24 h, the biofilms were transferred to a fresh culture medium containing 1% (w/v) sucrose or 1% (w/v) glucose to induce cariogenic challenges, while an additional set of biofilms was grown with 0.1% sucrose. The culture medium was replaced every 24 h until the end of the experimental period (72 h). *Lactobacilli* (10^8 CFU/ml) was added to the fresh culture medium daily. The culture medium pH was measured at selected time points. The biofilms underwent microbiological, dry-weight, and confocal imaging assays at 24, 48, and 72 h, transcriptome analysis *via* RNA-Seq at 48 h, and qRT-PCR validation at 48, 50, and 52 h. The methods are detailed previously (Xiao et al., 2012) and are shown in **Appendix 1**. Duplicated discs were used in each run. Independent assays were repeated three times.

2.4 Inhibition of *C. albicans* and *S. mutans* by *L. plantarum* Supernatant

The supernatant of *L. plantarum* 8014 and 14917 overnight culture was harvested and sterilized with a vacuum filter system (0.22 μm PES, Corning™ Disposable Vacuum Filter Systems, USA). *S. mutans* and *C. albicans* with a range of concentration ($10^{1\text{-}8}$ for *S. mutans* and $10^{1\text{-}6}$ for *C. albicans*) were treated with the supernatant of *L. plantarum* and allowed to grow for 24 h in TSBYE with 1% glucose or 1% sucrose condition in 96-well plates. Clear culture indicated no growth of microorganisms.

2.5 Transcriptome Analysis by RNA-seq

2.5.1 RNA Library Preparation and Sequencing

The mass of biofilms was harvested from four discs for each condition. The discs were immersed in RNAlater (Applied Biosystems/Ambion, Austin, TX, USA) for 1 h, followed by biomass removal with a spatula. RNAs were extracted and purified with MasterPure complete DNA and RNA purification kit (Epicentre, Lucigen, WI, USA). The raw RNA product was quantified using NanoDrop One Microvolume UV-Vis Spectrophotometer (Thermo Scientific™, Wilmington, DE, USA). rRNA depletion was performed using Ribo-Zero rRNA Removal Kit (Illumina, San Diego, CA, USA). The RNA sequencing library was prepared using NEBNext Ultra RNA Library Prep Kit for Illumina by following the manufacturer's recommendations (NEB, Ipswich, MA, USA). The sequencing libraries were multiplexed and clustered on one lane of a flow cell and loaded on the Illumina HiSeq instrument according to the manufacturer's instructions.

The RNA sequencing library was prepared using the NEBNext Ultra RNA Library Prep Kit for Illumina by following the manufacturer's recommendations (NEB, Ipswich, MA, USA). Briefly, enriched RNAs were fragmented for 15 min at 94°C. First- and second-strand cDNAs were synthesized. The cDNA fragments were end repaired and adenylated at 3′ ends, and a universal adapter was ligated to cDNA fragments, followed by index addition and library enrichment with limited cycle PCR. Sequencing libraries were validated using the Agilent TapeStation 4200 (Agilent Technologies, Palo Alto, CA, USA) and quantified by using the Qubit 2.0 Fluorometer (Invitrogen, Carlsbad, CA) as well as by quantitative PCR (Applied Biosystems, Carlsbad, CA, USA).

The sequencing libraries were multiplexed and clustered on one lane of a flow cell and loaded on the Illumina HiSeq instrument according to the manufacturer's instructions. The samples were sequenced using a 2x150 paired-end (PE) configuration. Image analysis and base calling were conducted using the HiSeq Control Software (HCS). Raw sequence data generated from Illumina HiSeq were converted into FASTQ files and demultiplexed using Illumina's bcl2fastq 2.17 software. The sequence reads of all samples in the study are deposited in the NCBI Sequence Read Archive (SRA) as a study under the accession number of PRJNA809829. One mismatch was allowed for index sequence identification. After demultiplexing, sequence data were checked for overall quality and yield. The sequence reads were trimmed to remove possible adapter sequences and nucleotides with poor quality using Trimmomatic v.0.36. The STAR aligner v.2.5.2b (Dobin et al., 2013) was used to map the trimmed reads to the reference genomes. Unique gene hit counts were calculated by using feature Counts from the Subread package v.1.5.2. Only unique reads within exon regions were counted. Gene hit counts were extracted, and the gene hit count table was used for downstream differential expression analysis.

Using DESeq2, a comparison of gene expression between the groups of samples was performed. The Wald test was used to generate p-values and Log2 fold changes. *S. mutans* and *C. albicans* genes with adjusted p-values (false discovery rate (FDR) p-values) < 0.05 and absolute log2 fold changes > 2 and *L. plantarum* 14917 genes with FDR p-values < 0.05 and absolute log2 fold changes > 1 were called differentially expressed genes (DEGs) for each comparison. A gene ontology (GO) analysis was performed on the statistically significant set of genes by implementing the software GeneSCF v1.1 (Subhash and Kanduri, 2016). The GO list was used to cluster the set of genes based on their biological process and determine their statistical significance. A principal component analysis (PCA) was performed using the "plotPCA" function within the DESeq2 R package. The plot shows the samples in a 2D plane spanned by their first two principal components. The top 500 genes, selected by the highest row variance, were used to generate the plot. Volcano plots were created by VolcaNoseR (https://huygens.science.uva.nl/VolcaNoseR) (Goedhart and Luijsterburg, 2020). Kyoto Encyclopedia of Genes and Genomes pathways were generated by KEGG mapper (genome.jp) and Cytoscape software version 3.8.2.

2.5.2 Real-Time Reverse Transcription Polymerase Chain Reaction

Then cDNAs were synthesized using 0.2 μg of purified RNA and the Bio-Rad iScript cDNA synthesis kit (Bio-Rad Laboratories,

Inc., Hercules, CA). The resulting cDNA and negative controls were amplified by quantitative amplification conditions using Applied Biosystems™ PowerTrack™ SYBR Green Master Mix and a QuantStudio™ 3 Real-Time PCR System (Thermo Fisher Scientific, USA). Each 20-μl reaction mixture included template cDNA, 10 μM each primer, and 2× SYBR Green Mix (containing SYBR Green and Taq DNA Polymerase). Unique core genes of *S. mutans*, *C. albicans*, and *L. plantarum* were used as internal reference for comparative expression calculation: *gyrA* for *S. mutans* genes (Zeng and Burne, 2013); ACT1 for *C. albicans*, and *ropB* for *L. plantarum*.

2.6 Statistical Analysis

To compare the abundance of *S. mutans*, *C. albicans*, and *Lactobacillus* spp. in planktonic and biofilm conditions, the CFU values were first converted to natural log values; zero values remained to be zero. The log values were compared between each group treated with *Lactobacillus* spp. to the control group using the Mann–Whitney U test after assessing the normality of data. For other measurements, such as biomass (bacteria and EPS), number and size of microcolonies, and pH value of the biofilms at specific time points, normality tests were performed first. For normally distributed data, the comparisons between groups were tested using the t-test for two groups and one-way ANOVA for more than two groups followed by *post hoc* test. For data that were not normally distributed, Kruskal–Wallis was used to compare the outcomes of more than two groups, and the Mann–Whitney U test was used for a two-group comparison. Statistical tests were two-sided with a significant level of 5%. IBM SPSS was used for statistical analyses.

3 RESULTS

3.1 Inhibition of *C. albicans* and *S. mutans* by *Lactobacilli* in Planktonic Condition

All four *Lactobacillus* spp. significantly inhibited the growth of *C. albicans* by 1 log at 6 h and 2 logs at 20 h (**Figure 1A**) in planktonic conditions. All tested *Lactobacilli* significantly inhibited the growth of *S. mutans* at 6 and 20 h (**Figure 1B**). In contrast to the inhibited growth of *C. albicans* and *S. mutans*, the growth of *Lactobacilli* in multispecies conditions was not different from their growth in a single *Lactobacillus* species condition (**Figure 1C**). The culture medium pH dropped faster with the addition of *Lactobacilli* spp., but reached the same acidity (~4) at 20 h across all conditions ($p > 0.05$, **Figure S2A**). Worth noting is that a dose-dependent effect was seen, as shown in **Figure S3**; the minimal inoculum of *L. plantarum* 14917 that demonstrated inhibition on the growth of *S. mutans* and *C. albicans* was 10^8 CFU/ml.

3.2 Inhibition of *C. albicans* and *S. mutans* by *Lactobacillus* in Multispecies Biofilms

The growth of *C. albicans* and *S. mutans* was significantly inhibited by *L. salivarius* 11741, *L. plantarum* 8014, *and L. plantarum* 14917 in multispecies biofilms (**Figures 1D–L**). Interestingly, rich sucrose conditions (1% sucrose vs. 0.1% sucrose) enhanced the performance of *Lactobacillus* spp. Intriguingly, *L. plantarum* 8014 and 14917 inhibited *S. mutans* to non-detectable levels (<20 CFU/ml) as early as 48 h, and the inhibitory effect remained until 72 h, whereas *L. rhamnosus* did not inhibit the growth of *S. mutans* growth except in 1% glucose conditions. The dynamic changes in microorganism composition in each condition were plotted, as shown in **Figure S4**. In the biofilms treated with *L. salivarius* 11741, *L. plantarum* 8014, and *L. plantarum* 14917 (1% sucrose and 1% glucose conditions), *Lactobacilli* became the dominant species after 48 h. The pH of the culture medium (**Figures S2B–D**) was significantly lower with added *Lactobacilli* at 24, 48, and 72 h, compared to the control group ($p < 0.05$).

3.3 Inhibition of Cariogenic Biofilm Formation by *L. plantarum*

Since *L. plantarum* 8014 and 14917 demonstrated the better inhibition of *C. albicans* and *S. mutans* in planktonic and biofilm conditions, these two strains advanced to the biofilm structural analysis. *L. plantarum* 8014 and 14917 significantly reduced cariogenic biofilm formation measured by bacteria and EPS biomass and biofilm dry weight ($p < 0.05$), compared to the control group (*C. albicans–S. mutans* duo-species biofilm). The 72-h biofilms are shown in **Figure 2**, and the dynamic changes of biofilm formation from 24 to 72 h are shown in **Figure S5**. The vertical distributions of bacteria and EPS further demonstrate the altered biofilm assembly (**Figure S6**). The control group formed the thickest biofilms in 1% sucrose conditions, with the bulk of the biofilm accumulated at around 150–250 μm above the biofilm–HA disc interface (**Figures S6D, E**). Conversely, the biofilms treated by *L. plantarum* 14917 were the thinnest and had the least horizontal converge, with approximately 15% coverage of bacteria and 19% EPS at the most abundant layer (20 μm above the biofilm–HA disc interface).

Microcolonies are considered virulent and functional structures of biofilm. Surface-attached and free-floating microcolonies were identified in the biofilms. Well-formed mushroom-shaped microcolonies formed in the control group (**Figure 2A**). Microcolonies formed with added *L. plantarum* 14917 were less structured, with less bacteria components enmeshed with EPS (**Figure 2E**) ($p < 0.05$). Furthermore, biofilms treated with *L. plantarum* 14917 had significantly fewer surface-attached and free-floating microcolonies, with reduced size (**Figure 2F**).

3.4 Inhibition on *C. albicans* and *S. mutans* Growth by *L. plantarum* Supernatant

The supernatant of *L. plantarum* 14917 demonstrated antibacterial and antifungal activity against *C. albicans* and *S. mutans* (**Table S5**). Specifically, the supernatant of *L. plantarum* 14917 inhibited the growth of *S. mutans* with a starting concentration equal or lower than 10^4 CFU/ml in 1% sucrose conditions, and the growth of *C. albicans* with a starting concentration equal or lower than 10^1 CFU/ml in 1% sucrose conditions. The supernatant of *L. plantarum* 8014 had no

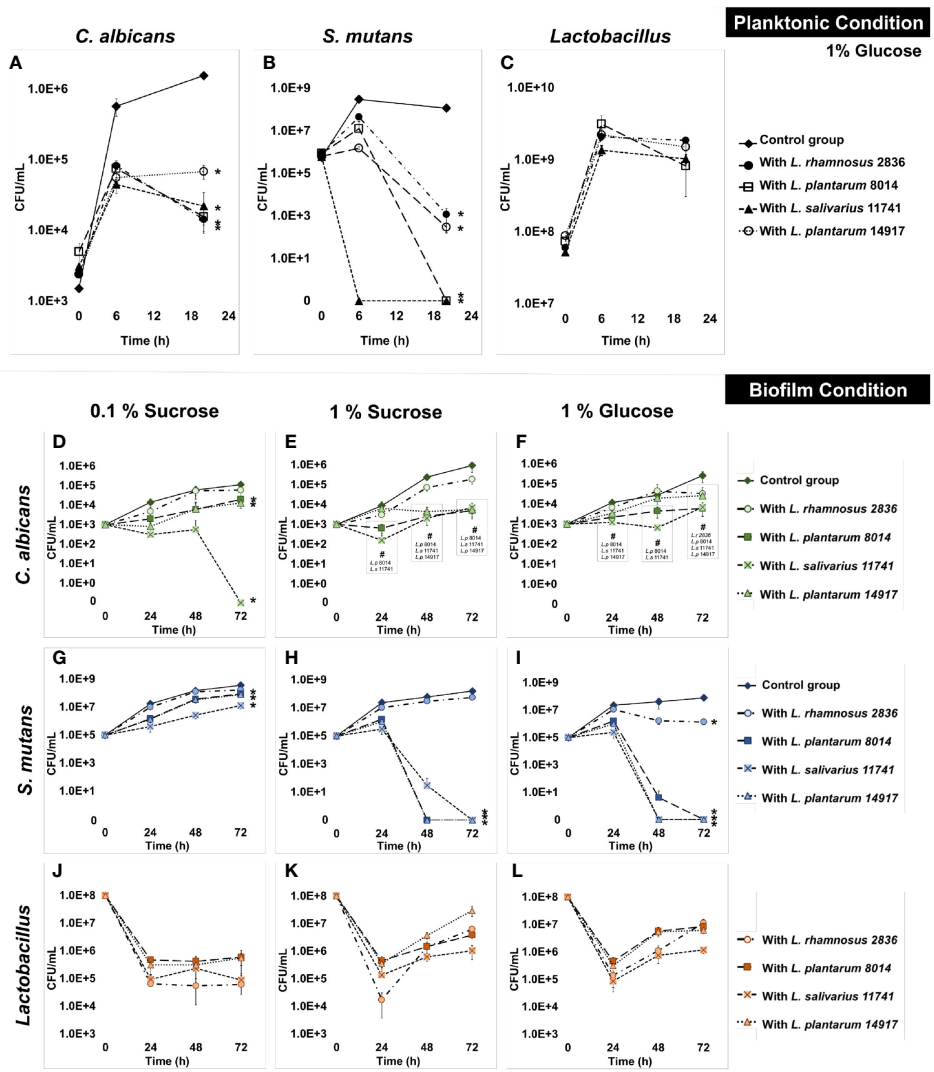

FIGURE 1 | Inhibition of *C. albicans* and *S. mutans* by *Lactobacilli* in multispecies biofilms. The growth curves of *C. albicans*, *S. mutans*, and *Lactobacilli* in multispecies planktonic and biofilm conditions are plotted. The control group consists of *C. albicans* and *S. mutans*. The group with added *Lactobacilli* was marked as "with *Lactobacillus*". **(A)** *Lactobacilli* significantly inhibited the growth of *C. albicans* by 1 log after 6 h and 1–2 logs after a 20-h incubation. **(B)** *Lactobacilli* significantly inhibited the growth of *S. mutans* at 6 and 20 h. *S. mutans* was inhibited to non-detectable level (<20 CFU/ml) after a 20-h incubation with *L. plantarum* 8014 and *L. salivarius* 11741. **(C)** *Lactobacilli* maintained a stable growth in all groups. **(D–L)** The growth curves of *C. albicans*, *S. mutans*, and *Lactobacilli* in multispecies biofilm conditions are plotted. **(D–F)** *Lactobacilli (L. plantarum* and *L. salivarius)* inhibited the growth of *C. albicans* in high-sucrose conditions (1%) by 72 h, a 3-log reduction compared to the control group. No difference of *C. albicans* growth was detected with the addition of *L. rhamnosus* in all sugar conditions. **(G–I)** *Lactobacilli (L. plantarum* and *L. salivarius)* inhibit the growth of *S. mutans* in high-sugar conditions (1% sucrose and 1% glucose). Significantly, *L. plantarum* 8014 and 14917 inhibited *S. mutans* in the biofilms to non-detectable level (<20 CFU/ml) as early as 48 h, and the treated biofilms remained non-detectable *S. mutans* (<20 CFU/ml) at 72 h. *L. rhamnosus* had poor performance on inhibiting the growth of *S. mutans* growth in all sugar conditions. **(J–L)** *Lactobacilli* maintained a stable growth in all groups. * Indicates that the CFU values of the multispecies biofilms were significantly less than the control group at all follow-up time points ($p < 0.05$). # Indicates that the CFU values of the multispecies biofilms were significantly less than the control group at specific marked time points ($p < 0.05$).

inhibitory effect on *C. albicans*. The inhibitory effect was identified as bacteriostatic and fungistatic.

3.5 Transcriptomic Analysis

The principal component analysis (PCA) (**Figure S8**) and the hierarchical clustering analysis (**Figure S9**) indicated distinctive transcriptomic profiles of biofilms treated with *L. plantarum* 14917. Overall, 441 genes of *S. mutans* and 232 genes of *C. albicans* had a differential expression between *L. plantarum* 14917-treated multispecies biofilm and the control group, while 391 genes of *L. plantarum* 14917 were differentially expressed between the multispecies group and *L. plantarum* 14917 single-species biofilms (**Figure 3** and **Tables S2–4**). These differentially expressed genes are defined as DEGs.

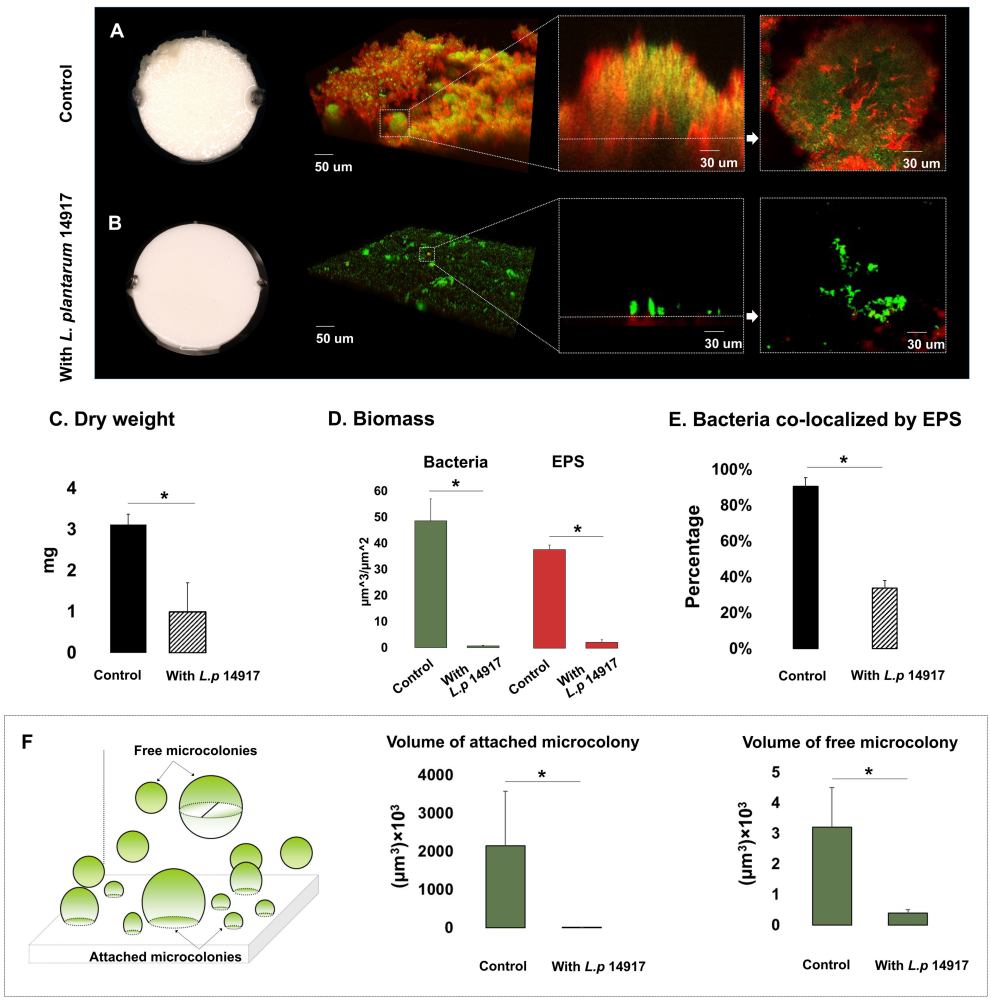

FIGURE 2 | Morphogenesis, 3D architecture, and quantitative measurement of microcolonies in 72-h multispecies biofilms (1% sucrose condition). The 72-h biofilms of the control group (*C. albicans* and *S. mutans*) and experimental groups (with *L. plantarum* 14917*)* in 1% sucrose condition were visualized using a two-photon laser confocal microscope. The three-dimensional structure of the biofilms was rendered using Amira software. The green color indicates bacteria and the red color indicates the exopolysaccharides (EPS). *L. plantarum* 14917 dramatically reduced biofilm formation, compared to the control group **(A, B)**. Biofilm dry weight was significantly reduced with added *L. plantarum* 14917 **(C)**. *$p < 0.05$. The biomass of the two biofilm components, bacteria and exopolysaccharides (EPS), was calculated using image-processing software COMSTAT (Heydorn et al., 2000). Both *L. plantarum* 14917 significantly reduced the biomass of bacteria and EPS **(D)**. The confocal images indicate the cross-sectional and sagittal views of microcolonies formed in the control group (*S. mutans* and *C. albicans* duo-species) and with added *L. plantarum* 14917. Well-formed mushroom-shaped microcolonies were seen in the control group, and the largest size microcolonies were seen in the *S. mutans* and *C. albicans* duo-species biofilm. Microcolonies formed with added *L. plantarum* 14917 were much less structured. Bacterial components were less encapsulated with EPS. The amount of co-localization between bacteria and EPS was calculated using DUOSTAT **(E)**, which was consistent with the findings revealed in the images (*$p < 0.05$). The surface-attached and free-floating microcolonies were evaluated using COMSTAT and DUOSTAT software. Panel **(F)** illustrates that biofilms treated by *L. plantarum* 14917 had significantly reduced microcolony size ($p > 0.05$; ANOVA, comparison for all pairs using Tukey–Kramer HSD).

The validation results from the quantitative real-time reverse transcription polymerase chain reaction (qRT-PCR) for selected genes of interest were consistent with the RNA-Seq data (**Figure 3**). Worth noting is that genes related to *C. albicans* resistance to antifungal medication (ERG4), fungal cell wall chitin remodeling (CHT2), and resistance to oxidative stress (CAT1) were significantly downregulated when treated with *L. plantarum* 14917.

KEGG pathway analyses were further performed with 441 *S. mutans* DEGs, 232 C. *albicans* DEGs, and 391 *L. plantarum* 14917 DEGs, resulting in 33 pathways for *S. mutans*, 66 pathways for *C. albicans*, and 31 pathways for *L. plantarum* 14917. Transcriptomic analysis revealed the disruption of *S. mutans* and *C. albicans* cross-kingdom interactions with added *L. plantarum*. Genes of *S. mutans* (**Figure 4**) and *C. albicans* (**Figure 5**) involved in metabolic pathways (e.g., EPS formation, carbohydrate metabolism, glycan biosynthesis, and metabolism) were significantly downregulated. In contrast, genes of *L. plantarum* 14917 in the pathways of genetic information processing, environmental information processing, cellular

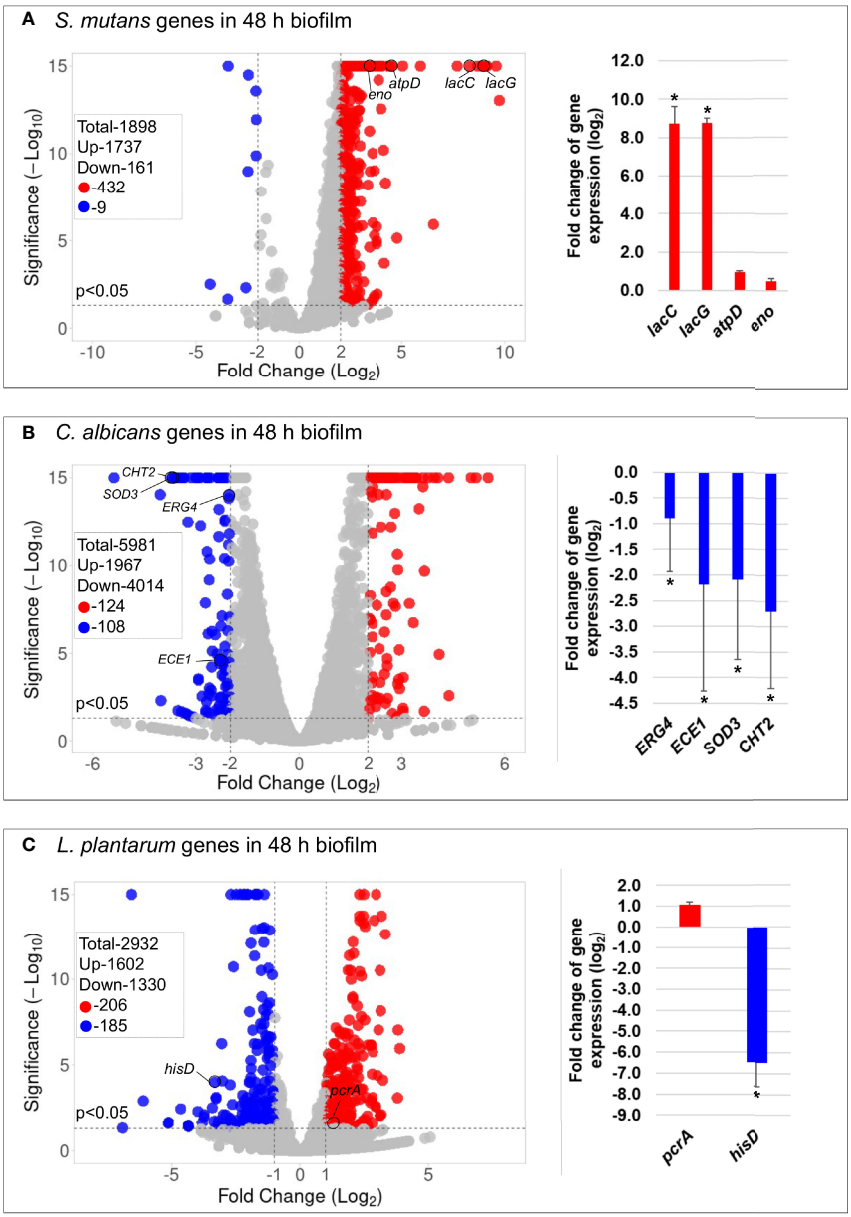

FIGURE 3 | Comparison of transcriptome profiling between multispecies biofilms treated with *L. plantarum* 14917 and their controls. **(A)** Volcano plots from transcriptome analysis of *S. mutans* in multispecies (*L. plantarum* 14917 + *S. mutans* + *C. albicans*) biofilm (48 h, 1% sucrose) compared to *S. mutans* in duo-species (*S. mutans* + *C. albicans*) biofilm. **(B)** *C. albicans* in multispecies biofilm compared to *C. albicans* in duo-species biofilm. **(C)** *L. plantarum* 14917 in multispecies biofilm compared to *L. plantarum* 14917 single-species biofilms. Data represent three independent replicates of each condition. qRT-PCR validation results of selected genes are shown on the right side of each volcano plots. * Indicates that the expression of genes in the multispecies biofilms was significantly different from that in the control group ($p < 0.05$).

processes, and metabolism (lipid, carbohydrate, glycan, energy) were significantly upregulated (**Figure S10**).

To determine the transcriptomic dynamic changes in genes of interest during specific stages of biofilm formation, particularly with the significant drop of pH value in the culture media, qRT-PCR was performed for biofilms at 50 and 52 h (2 and 4 h after culture medium change, **Figure S11**). *S. mutans* genes related to EPS formation (*gtfB* and *gtfC*) were significantly downregulated at 50 h. Genes related to *C. albicans* resistance fungal cell wall chitin remodeling (CHT2) and resistance to oxidative stress (CAT1) were also significantly downregulated following culture medium change. *Lactobacillus* genes *plnD*, *plnG*, and *plnN* that contribute to antimicrobial peptide plantaricins were significantly upregulated.

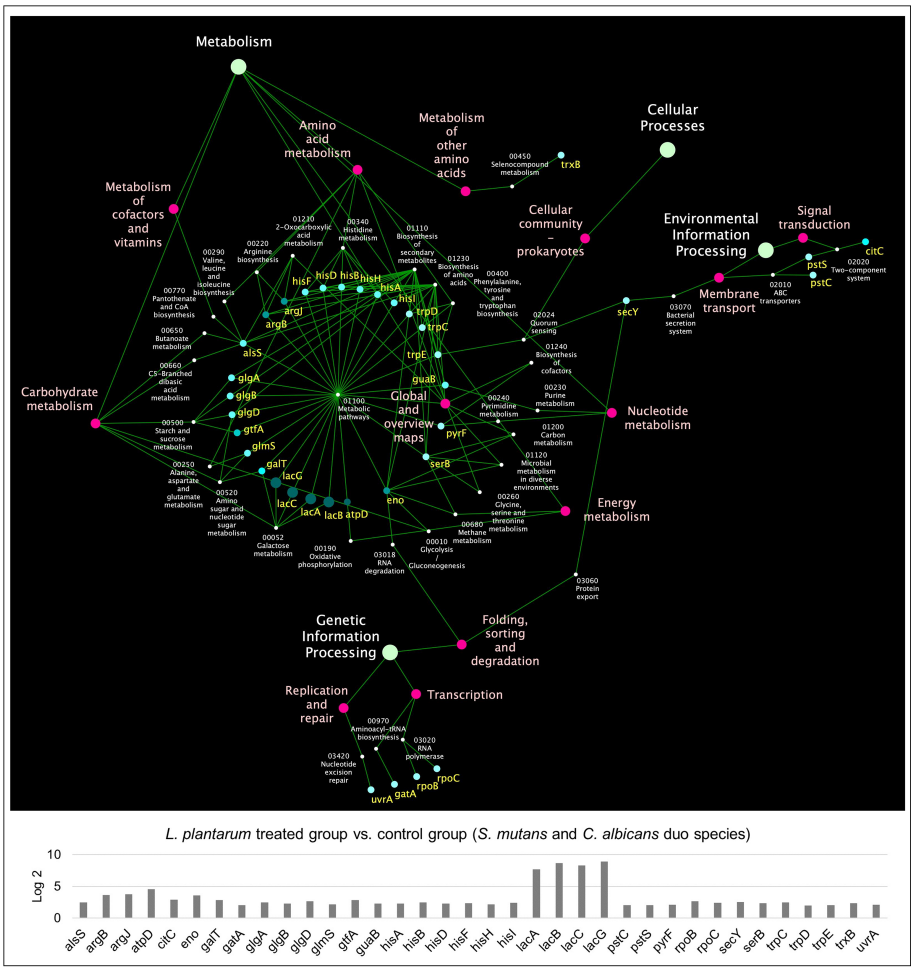

FIGURE 4 | KEGG pathway network for *S. mutans* differentially expressed genes between the multispecies and duo-species biofilms. The genes of *S. mutans* differentially expressed genes between the comparison groups with FDR p-values < 0.05 and log2 fold changes > 2 were defined as DEGs and are listed in **Supplementary Table 2**. Overall, 33 impacted pathways were found for 441 *S. mutans* DEGs. The fold change of the DEGs involved in the identified pathways is shown in the lower panel.

4 DISCUSSION

We used a comprehensive approach to examine the inhibitory effect of probiotic *Lactobacilli* on the growth of *C. albicans* and *S. mutans* in cariogenic mixed-species biofilms. Among the four tested *Lactobacillus* spp., *L. plantarum* 14917 exhibited superior inhibitory properties, whereas *L. rhamnosus*, a commonly used probiotic in commercial products, was not capable of inhibiting the growth of *C. albicans* and *S. mutans* in cariogenic biofilms. *L. plantarum* has various potential pharmaceutical usages with recent adoption in clinical studies and trials to prevent and treat respiratory diseases, irritable bowel syndrome, depression, etc. (Arasu et al., 2016). The following mechanisms suggest its antifungal and antibiofilm activities observed in our study.

1) Production of plantaricins. Bacteriocins, antimicrobial molecules, produced by *L. plantarum* are known as plantaricins (Sabo et al., 2014). Not surprisingly, most *pln* genes (*plnD*, *plnG*, *plnN*, and *plnEF*) that encode plantaricins by *L. plantarum* were upregulated in our multispecies biofilms in comparison to *L. plantarum* 14917 single-species biofilms. The only exception is *plnA*. *plnA* functions as a peptide pheromone that induces transcription of *pln* genes organized in the following five operons: *plnABCD*, *plnEFI*, *plnJKLR*, *plnMNOP*, and *plnGHSTUV* (Diep et al., 2003). The possible reason for the downregulation of *plnA* still needs more exploration. Moreover, culture medium was changed at 48 h in our model. The expressions of *plnD*, *plnG*, *plnN*, *plnA*, and *plnEF* at 52 h were lower than 50 h, possibly due to the availability of culture medium sources and the pH-related expression difference.

2) Altered fitness and virulence of *S. mutans* with the addition of *L. plantarum* 14917. First, *S. mutans* upregulates specific adaptation mechanisms (e.g., F-ATPase system, fatty acid biosynthesis) to cope with acidic environments (Baker et al., 2017). Among the F-ATPase system, *atpD* has a critical function

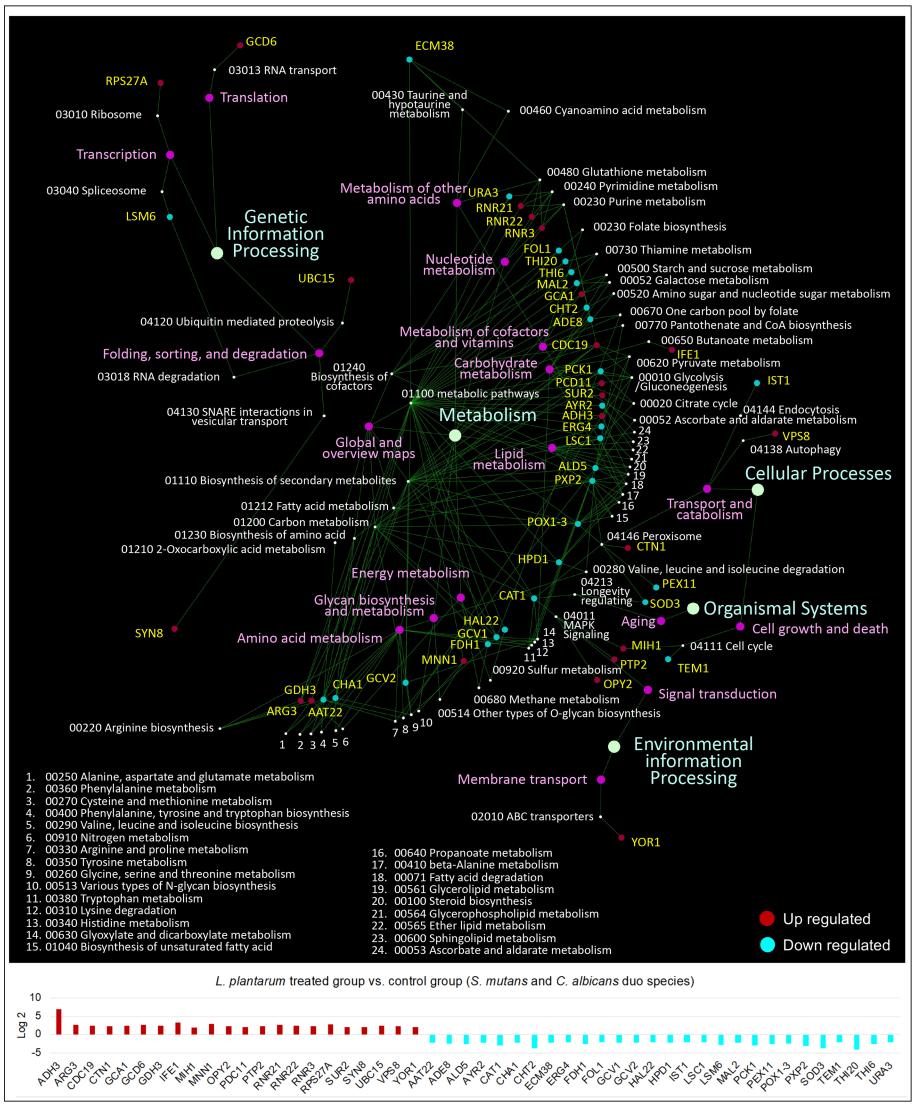

FIGURE 5 | KEGG pathway network for *C. albicans* differentially expressed genes between the multispecies and duo-species biofilms. The genes of *C. albicans* that differentially expressed between the comparison groups with FDR p-values < 0.05 and log2 fold changes > 2 were defined as DEGs and are listed in **Supplementary Table 3**. Overall, 66 impacted pathways were found for 232 C. *albicans* DEGs. The fold change of the DEGs involved in the identified pathways is shown in the lower panel.

in the assembly of the ATPase complex and is highly induced at low pH (Kuhnert et al., 2004). With added *L. plantarum* 14917, *atpD* was upregulated at the 48-h biofilm but downregulated at the 50- and 52-h biofilm. Second, *S. mutans* genes that are associated with glucan synthesis and remodeling (*gtfBC*, *dexA*) and glucan-binding (*gbpB)* are usually more expressed in multispecies conditions, resulting in more abundant EPS formation in biofilms and dental plaques (Bowen and Koo, 2011). When treated with *L. plantarum* 14917, *gtfBC* of *S. mutans* were downregulated, explaining significantly reduced biofilm biomass and thickness. Third, *S. mutans lac* genes are associated with galactose metabolism and are upregulated in the presence of *C. albicans* (He et al., 2017). The addition of *L. plantarum* 14917 further enhanced the upregulation of *S. mutans lacCG*, possibly due to the relief of catabolite repression. Furthermore, studies have indicated that some probiotic lactobacilli have an ability to co-aggregate with *S. mutans* (Keller et al., 2011) and *C. albicans* (do Carmo et al., 2016), which might explain the inhibition of adhesion to the HA disc.

3) Altered *C. albicans* virulence. Significantly, several virulence genes of *C. albicans* were downregulated with added *L. plantarum* 14917: a) genes related to hyphal growth and adhesion to host cells, including the hyphal wall protein 1 gene (HWP1) and the extent of cell elongation gene 1 (ECE1) (Wang et al., 2017; Lohse et al., 2018). The inhibition of *C. albicans* switching from yeast to hyphal form was observed in planktonic

conditions when treated with *L. plantarum* 14917 (**Figure S12**). b) Superoxide dismutase 3 gene (SOD3), a copper fist transcription factor; c) regulator of copper transport protein gene (CTR1); d) chitinase 2 precursor gene (CHT2) that relates to cell wall chitin remodeling (McCreath et al., 1995); and e) ergosterol biosynthesis of ERG4, a gene related to antifungal medication resistance (Copping et al., 2005).

4) Production of other antimicrobial products such as hydrogen peroxide and lactic acid. Hydrogen peroxide is a commonly suggested antimicrobial compound produced from *Lactobacilli* (Zhang et al., 2018); the inhibition of *S. mutans* in the biofilm conditions could be a result of reduced transcription of polysaccharide intercellular adhesions. Lactic acid inhibits the growth and production of virulence factors of bacteria (Zhang et al., 2018). Despite aciduric characteristics of *S. mutans* and *C. albicans*, the presence of *Lactobacilli* further decreased the pH, compared to the control group, which might affect the expression of virulence factors of *S. mutans* and *C. albicans*.

5) Sugar metabolism. The ability of *L. plantarum* to colonize different niches is associated with its ability to ferment a variety of sugars and compete against other microorganisms (Garcia-Gonzalez et al., 2021). Sucrose metabolism might be an important ecological fitness determinant of *L. plantarum* in the competitive growth in multiple-species biofilm (Yin et al., 2018). Our study revealed an interesting finding that *L. plantarum* could inhibit *S. mutans* and *C. albicans* in high-sucrose (1%) conditions but not in low-sucrose (0.1%) conditions. The pH-dependent plantaricin antimicrobial activity could be the partial reason, since plantaricin was most active at pH 5.0 (Kato et al., 1994), which is the culture medium acidity seen in 1% sucrose (pH~5), not in 0.1% sucrose (pH~6.5). In addition, *L. plantarum* exhibits remarkable genetic and phenotypic diversity, particularly in strain-specific carbohydrate utilization capacities (Fuhren et al., 2020). A previous study demonstrated that strain-specific phenotypes and strain genotypes are associated with utilization of isomaltose and other oligosaccharides (Fuhren et al., 2020). Therefore, we speculate that *L. plantarum* inhibits *S. mutans* and *C. albicans* in high-sucrose conditions due to the utilization of sugar resources and related phenotypic presentation. Future efforts should investigate the genetic traits of *L. plantarum* related to this phenomenon.

Worth noting is that our study results revealed antimicrobial properties of the overnight culture supernatant of *L. plantarum*, which supports further analysis of the supernatant in identifying active antimicrobial compounds. Furthermore, we demonstrated the dose-dependent inhibition of *L. plantarum* on the growth of *S. mutans* and *C. albicans*, where a threshold (10^8 CFU/ml) of *L. plantarum* is needed to demonstrate the inhibitory effect in our mixed-species model that mimicked high risk for dental caries. More interestingly, an ecological shift of the microbial community was seen in our model. Despite the inhibition of *S. mutans* and *C. albicans* by a high dose of *L. plantarum* ($\geq 10^8$ CFU/ml), a low dose of L. plantarum (104–6 CFU/ml) promoted the growth of *S. mutans* and *C. albicans* in 1% glucose planktonic conditions (**Figure S3**), which warrants further understanding of the mechanistic interaction between *L. plantarum* and other species.

Moreover, further studies are needed to assess the efficacy of inhibition of *L. plantarum* on clinical isolates of *S. mutans* and *C. albicans*. Animal studies are also warranted to test the efficacy and side effects of using probiotics in caries prevention and optimizing dosage and delivery methods. Subsequently, clinical trials combined with observation of overall oral microflora changes with probiotics will provide a deeper understanding of utilizing probiotic regimens to create and maintain oral microbial homeostasis and prevent dental caries.

5 CONCLUSIONS

L. plantarum demonstrated superior inhibition on the growth of *C. albicans* and *S. mutans*, disruption of virulent biofilm structure with reduced EPS, and virulent microcolony formation. Transcriptomic analysis further revealed disruption of *S. mutans–C. albicans* cross-kingdom interactions with added *L. plantarum*. Our study findings laid a critical foundation for future assessment of using *L. plantarum* 14917 as a novel caries prevention strategy in animal and clinical studies.

DATA AVAILABILITY STATEMENT

The sequence reads of all samples in the study are deposited in the NCBI Sequence Read Archive (SRA) as a study under the accession number of PRJNA809829.

AUTHOR CONTRIBUTIONS

YZ and JX contributed to the conception, design, data acquisition, analysis, and interpretation, drafting, and critical revision of the manuscript. TW contributed to data acquisition, analysis, and interpretation, drafting, and critical revision of the manuscript. AF, NA, ER, SQ, JB, and CG contributed to data acquisition, data interpretation, and critical review of the manuscript. All authors have read and approved the final version of the manuscript and agree to be accountable for all aspects of the work.

FUNDING

JX's research was supported by NIDCR (K23DE027412). TW's work is supported by a grant from the National Science Foundation NSF-CCF-1934962. The funding agencies had no role in the study design, data collection, analyses, decision to publish, or preparation of the manuscript.

SUPPLEMENTARY MATERIAL

The Supplementary Material for this article can be found online at: https://www.frontiersin.org/articles/10.3389/fcimb.2022.872012/full#supplementary-material

REFERENCES

Alkhars N, Z. Y., Alomeir, N., Al Jallad, N., Wu, T. T., Aboelmagd, S., Youssef, M., et al. (2021). Oral Candida Predicts Streptococcus Mutans Emergence in Underserved US Infants. *J. Dental Res.* 101 (1), 54–62. doi: 10.1177/00220345211012385

Arasu, M. V., Al-Dhabi, N. A., Ilavenil, S., Choi, K. C., and Srigopalram, S. (2016). In Vitro Importance of Probiotic Lactobacillus Plantarum Related to Medical Field. *Saudi J. Biol. Sci.* 23 (1), S6–s10. doi: 10.1016/j.sjbs.2015.09.022

Baker, J. L., Faustoferri, R. C., and Quivey, R. G. (2017). Acid-Adaptive Mechanisms of Streptococcus Mutans-the More We Know, the More We Don't. *Mol. Oral. Microbiol.* 32 (2), 107–117. doi: 10.1111/omi.12162

Bowen, W. H. (2016). Dental Caries - Not Just Holes in Teeth! A Perspective. *Mol. Oral. Microbiol.* 31 (3), 228–233. doi: 10.1111/omi.12132

Bowen, W. H., Burne, R. A., Wu, H., and Koo, H. (2018). Oral Biofilms: Pathogens, Matrix, and Polymicrobial Interactions in Microenvironments. *Trends Microbiol.* 26 (3), 229–242. doi: 10.1016/j.tim.2017.09.008

Bowen, W. H., and Koo, H. (2011). Biology of Streptococcus Mutans-Derived Glucosyltransferases: Role in Extracellular Matrix Formation of Cariogenic Biofilms. *Caries Res.* 45 (1), 69–86. doi: 10.1159/000324598

Copping, V. M., Barelle, C. J., Hube, B., Gow, N. A., Brown, A. J., and Odds, F. C. (2005). Exposure of Candida Albicans to Antifungal Agents Affects Expression of SAP2 and SAP9 Secreted Proteinase Genes. *J. Antimicrob. Chemother.* 55 (5), 645–654. doi: 10.1093/jac/dki088

Diep, D. B., Myhre, R., Johnsborg, O., Aakra, A., and Nes, I. F. (2003). Inducible Bacteriocin Production in Lactobacillus is Regulated by Differential Expression of the Pln Operons and by Two Antagonizing Response Regulators, the Activity of Which is Enhanced Upon Phosphorylation. *Mol. Microbiol.* 47 (2), 483–494. doi: 10.1046/j.1365-2958.2003.03310.x

Dobin, A., Davis, C. A., Schlesinger, F., Drenkow, J., Zaleski, C., Jha, S., et al. (2013). STAR: Ultrafast Universal RNA-Seq Aligner. *Bioinformatics* 29 (1), 15–21. doi: 10.1093/bioinformatics/bts635

do Carmo, M. S., Noronha, F. M., Arruda, M. O., Costa, E. P., Bomfim, M. R., Monteiro, A. S., et al. (2016). Lactobacillus Fermentum ATCC 23271 Displays In Vitro Inhibitory Activities Against Candida Spp. *Front. Microbiol.* 7. doi: 10.3389/fmicb.2016.01722

Du, Q., Ren, B., He, J., Peng, X., Guo, Q., Zheng, L., et al. (2021). Candida Albicans Promotes Tooth Decay by Inducing Oral Microbial Dysbiosis. *ISME J.* 15 (3), 894–908. doi: 10.1038/s41396-020-00823-8

Falsetta, M. L., Klein, M. I., Colonne, P. M., Scott-Anne, K., Gregoire, S., Pai, C. H., et al. (2014). Symbiotic Relationship Between Streptococcus Mutans and Candida Albicans Synergizes Virulence of Plaque Biofilms. *In Vivo Infect. Immun.* 82 (5), 1968–1981. doi: 10.1128/iai.00087-14

Fuhren, J., Rosch, C., Ten Napel, M., Schols, H. A., and Kleerebezem, M. (2020). Synbiotic Matchmaking in Lactobacillus Plantarum: Substrate Screening and Gene-Trait Matching To Characterize Strain-Specific Carbohydrate Utilization. *Appl. Environ. Microbiol.* 86 (18), aem.asm.org 1-17. doi: 10.1128/AEM.01081-20

Garcia-Gonzalez, N., Battista, N., Prete, R., and Corsetti, A. (2021). Health-Promoting Role of Lactiplantibacillus Plantarum Isolated From Fermented Foods. *Microorganisms* 9 (2), 349. doi: 10.3390/microorganisms9020349

Goedhart, J., and Luijsterburg, M. S. (2020). VolcaNoseR is a Web App for Creating, Exploring, Labeling and Sharing Volcano Plots. *Sci. Rep.* 10 (1), 20560. doi: 10.1038/s41598-020-76603-3

He, J., Kim, D., Zhou, X., Ahn, S. J., Burne, R. A., Richards, V. P., et al. (2017). RNA-Seq Reveals Enhanced Sugar Metabolism in Streptococcus Mutans Co-Cultured With Candida Albicans Within Mixed-Species Biofilms. *Front. Microbiol.* 8. doi: 10.3389/fmicb.2017.01036

Heydorn, A., Nielsen, A. T., Hentzer, M., Sternberg, C., Givskov, M., Ersboll, B. K., et al. (2000). Quantification of Biofilm Structures by the Novel Computer Program COMSTAT. *Microbiology* 146, 2395–2407. doi: 10.1099/00221287-146-10-2395

Kato, T., Matsuda, T., Ogawa, E., Ogawa, H., Kato, H., Doi, U., et al. (1994). Plantaricin-149, a Bacteriocin Produced by Lactobacillus-Plantarum Nric-149. *J. Fermentation Bioeng.* 77 (3), 277–282. doi: 10.1016/0922-338x(94)90234-8

Keller, M. K., Hasslof, P., Stecksen-Blicks, C., and Twetman, S. (2011). Co-Aggregation and Growth Inhibition of Probiotic Lactobacilli and Clinical Isolates of Mutans Streptococci: An In Vitro Study. *Acta Odontol. Scand.* 69 (5), 263–268. doi: 10.3109/00016357.2011.554863

Koo, H., Andes, D. R., and Krysan, D. J. (2018). Candida-Streptococcal Interactions in Biofilm-Associated Oral Diseases. *PloS Pathog.* 14 (12), e1007342. doi: 10.1371/journal.ppat.1007342

Kuhnert, W. L., Zheng, G. L., Faustoferri, R. C., and Quivey, R. G. (2004). The F-ATPase Operon Promoter of Streptococcus Mutans Is Transcriptionally Regulated in Response to External pH. *J. Bacteriol.* 186 (24), 8524–8528. doi: 10.1128/jb.186.24.8524-8528.2004

Laleman, I., Detailleur, V., Slot, D. E., Slomka, V., Quirynen, M., and Teughels, W. (2014). Probiotics Reduce Mutans Streptococci Counts in Humans: A Systematic Review and Meta-Analysis. *Clin. Oral. Investig* 18 (6), 1539–1552. doi: 10.1007/s00784-014-1228-z

Lohse, M. B., Gulati, M., Johnson, A. D., and Nobile, C. J. (2018). Development and Regulation of Single- and Multi-Species Candida Albicans Biofilms. *Nat. Rev. Microbiol.* 16 (1), 19–31. doi: 10.1038/nrmicro.2017.107

Matsubara, V. H., Wang, Y., Bandara, H., Mayer, M. P. A., and Samaranayake, L. P. (2016). Probiotic Lactobacilli Inhibit Early Stages of Candida Albicans Biofilm Development by Reducing Their Growth, Cell Adhesion, and Filamentation. *Appl. Microbiol. Biotechnol.* 100 (14), 6415–6426. doi: 10.1007/s00253-016-7527-3

McCreath, K. J., Specht, C. A., and Robbins, P. W. (1995). Molecular Cloning and Characterization of Chitinase Genes From Candida Albicans. *Proc. Natl. Acad. Sci. U. S. A.* 92 (7), 2544–2548. doi: 10.1073/pnas.92.7.2544

Meurman, J. H. (2005). Probiotics: Do They Have a Role in Oral Medicine and Dentistry? *Eur. J. Oral. Sci.* 113 (3), 188–196. doi: 10.1111/j.1600-0722.2005.00191.x

Panariello, B. H. D., Klein, M. I., Dias, L. M., Bellini, A., Costa, V. B., Barbugli, P. A., et al. (2021). Lactobacillus Casei Reduces the Extracellular Matrix Components of Fluconazole-Susceptible Candida Albicans Biofilms. *Biofouling* 37 (9-10), 1006–1021. doi: 10.1080/08927014.2021.2001645

Rossoni, R. D., de Barros, P. P., de Alvarenga, J. A., Ribeiro, F. C., Velloso, M. D. S., Fuchs, B. B., et al. (2018). Antifungal Activity of Clinical Lactobacillus Strains Against Candida Albicans Biofilms: Identification of Potential Probiotic Candidates to Prevent Oral Candidiasis. *Biofouling* 34 (2), 212–225. doi: 10.1080/08927014.2018.1425402

Sabo, S. D., Vitolo, M., Gonzalez, J. M. D., and Oliveira, R. P. D. (2014). Overview of Lactobacillus Plantarum as a Promising Bacteriocin Producer Among Lactic Acid Bacteria. *Food Res. Int.* 64, 527–536. doi: 10.1016/j.foodres.2014.07.041

Srivastava, N., Ellepola, K., Venkiteswaran, N., Chai, L. Y. A., Ohshima, T., and Seneviratne, C. J. (2020). Lactobacillus Plantarum 108 Inhibits Streptococcus Mutans and Candida Albicans Mixed-Species Biofilm Formation. *Antibiotics (Basel)* 9 (8). doi: 10.3390/antibiotics9080478

Subhash, S., and Kanduri, C. (2016). GeneSCF: A Real-Time Based Functional Enrichment Tool With Support for Multiple Organisms. *BMC Bioinf.* 17, 365. doi: 10.1186/s12859-016-1250-z

Wang, S., Wang, Q. Y., Yang, E. C., Yan, L., Li, T., and Zhuang, H. (2017). Antimicrobial Compounds Produced by Vaginal Lactobacillus Crispatus Are Able to Strongly Inhibit Candida Albicans Growth, Hyphal Formation and Regulate Virulence-Related Gene Expressions. *Front. Microbiol.* 8. doi: 10.3389/fmicb.2017.00564

Wasfi, R., Abd El-Rahman, O. A., Zafer, M. M., and Ashour, H. M. (2018). Probiotic Lactobacillus Sp. Inhibit Growth, Biofilm Formation and Gene Expression of Caries-Inducing Streptococcus Mutans. *J. Cell Mol. Med.* 22 (3), 1972–1983. doi: 10.1111/jcmm.13496

Xiao, J., Grier, A., Faustoferri, R. C., Alzoubi, S., Gill, A. L., Feng, C., et al. (2018a). Association Between Oral Candida and Bacteriome in Children With Severe ECC. *J. Dental Res.* 97 (13), 1468–1476. doi: 10.1177/0022034518790941

Xiao, J., Huang, X., Alkhers, N., Alzamil, H., Alzoubi, S., Wu, T. T., et al. (2018b). Candida Albicans and Early Childhood Caries: A Systematic Review and Meta-Analysis. *Caries Res.* 52 (1-2), 102–112. doi: 10.1159/000481833

Xiao, J., Klein, M. I., Falsetta, M. L., Lu, B., Delahunty, C. M., Yates, J. R., et al. (2012). The Exopolysaccharide Matrix Modulates the Interaction Between 3D Architecture and Virulence of a Mixed-Species Oral Biofilm. *PLoS Pathog.* 8 (4), e1002623. doi: 10.1371/journal.ppat.1002623

Yin, X. C., Heeney, D. D., Srisengfa, Y. T., Chen, S. Y., Slupsky, C. M., and Marco, M. L. (2018). Sucrose Metabolism Alters Lactobacillus Plantarum Survival and Interactions With the Microbiota in the Digestive Tract. *FEMS Microbiol. Ecol.* 94 (7), fiy084. doi: 10.1093/femsec/fiy084

Zaura, E., and Twetman, S. (2019). Critical Appraisal of Oral Pre- and Probiotics for Caries Prevention and Care. *Caries Res.* 53 (5), 514–526. doi: 10.1159/000499037

Zeng, L., and Burne, R. A. (2013). Comprehensive Mutational Analysis of Sucrose-Metabolizing Pathways in Streptococcus Mutans Reveals Novel Roles for the Sucrose Phosphotransferase System Permease. *J. Bacteriol.* 195 (4), 833–843. doi: 10.1128/JB.02042-12

Zhang, G., Lu, M., Liu, R., Tian, Y., Vu, V. H., Li, Y., et al. (2020a). Inhibition of Streptococcus Mutans Biofilm Formation and Virulence by Lactobacillus Plantarum K41 Isolated From Traditional Sichuan Pickles. *Front. Microbiol.* 11. doi: 10.3389/fmicb.2020.00774

Zhang, Z. W., Lv, J. L., Pan, L., and Zhang, Y. G. (2018). Roles and Applications of Probiotic Lactobacillus Strains. *Appl. Microbiol. Biotechnol.* 102 (19), 8135–8143. doi: 10.1007/s00253-018-9217-9

Zhang, Q., Qin, S., Xu, X., Zhao, J., Zhang, H., Liu, Z., et al. (2020b). Inhibitory Effect of Lactobacillus Plantarum CCFM8724 Towards Streptococcus Mutans- and Candida Albicans-Induced Caries in Rats. *Oxid. Med. Cell Longev.* 2020, 4345804. doi: 10.1155/2020/4345804

Conflict of Interest: The authors declare that the research was conducted in the absence of any commercial or financial relationships that could be construed as a potential conflict of interest.

frontiers | Frontiers in Cellular and Infection Microbiology

REVIEW
published: 29 April 2022
doi: 10.3389/fcimb.2022.864479

Oral Microbiota-Driven Cell Migration in Carcinogenesis and Metastasis

Huimin Bai[1†], *Jing Yang*[2†], *Shu Meng*[1*] *and Chengcheng Liu*[1*]

[1] State Key Laboratory of Oral Diseases, National Clinical Research Center for Oral Diseases, Department of Periodontics, West China School & Hospital of Stomatology, Sichuan University, Chengdu, China, [2] State Key Laboratory of Oral Diseases, National Clinical Research Center for Oral Diseases, Department of Cariology and Endodontics, West China School & Hospital of Stomatology, Sichuan University, Chengdu, China

The oral cavity harbors approximately 1,000 microbial species, and both pathogenic and commensal strains are involved in the development of carcinogenesis by stimulating chronic inflammation, affecting cell proliferation, and inhibiting cell apoptosis. Moreover, some substances produced by oral bacteria can also act in a carcinogenic manner. The link between oral microbiota and chronic inflammation as well as cell proliferation has been well established. Recently, increasing evidence has indicated the association of the oral microbiota with cell migration, which is crucial in regulating devastating diseases such as cancer. For instance, increased cell migration induced the spread of highly malignant cancer cells. Due to advanced technologies, the mechanistic understanding of cell migration in carcinogenesis and cancer metastasis is undergoing rapid progress. Thus, this review addressed the complexities of cell migration in carcinogenesis and cancer metastasis. We also integrate recent findings on the molecular mechanisms by which the oral microbiota regulates cell migration, with emphasis on the effect of the oral microbiota on adhesion, polarization, and guidance. Finally, we also highlight critical techniques, such as intravital microscopy and superresolution microscopy, for studies in this field.

Keywords: oral microbiota, cell migration, EMT, carcinogenesis, metastasis

OPEN ACCESS

Edited by:
Jin Xiao,
University of Rochester, United States

Reviewed by:
Masae Kuboniwa,
Osaka University, Japan
Panagiotis Mistriotis,
Auburn University, United States

****Correspondence:***
Shu Meng
dreamingsue@163.com
Chengcheng Liu
liuchengcheng519@163.com

[†]These authors have contributed equally to this work

Specialty section:
This article was submitted to Microbiome in Health and Disease, a section of the journal Frontiers in Cellular and Infection Microbiology

Received: *28 January 2022*
Accepted: *04 April 2022*
Published: *29 April 2022*

Citation:
Bai H, Yang J, Meng S and Liu C (2022) Oral Microbiota-Driven Cell Migration in Carcinogenesis and Metastasis. Front. Cell. Infect. Microbiol. 12:864479. doi: 10.3389/fcimb.2022.864479

INTRODUCTION

An eclectic and diverse assemblage of microbiota inhabits different sites within the oral cavity, such as teeth, saliva, and oral mucosal surfaces (Lamont et al., 2018). Distinct microbial communities accumulate in these sites through successive colonization events. Since van Leeuwenhoek made the first observation of oral bacteria in dental plaques using primitive microscopes in 1683, our knowledge of oral microbiology has burgeoned. Investigations of the oral microbiota in health and diseases are currently undergoing rapid progress due to the development of techniques (Willis and Gabaldon, 2020). The oral microbial community is a complex and dynamic entity, and shifts in these communities contribute to both oral diseases (e.g., dental caries, periodontitis) and systemic diseases (e.g., diabetes mellitus, cardiovascular disease) (Kleinstein et al., 2020; Hajishengallis and Lamont, 2021). Interestingly, the carcinogenic effect of the microbiome in various organs has been revealed by studies in germ-free animals (Scott et al., 2019). Recently, the microbiome has been considered an influential environmental factor modulating carcinogenesis (Scott et al., 2019; Irfan et al., 2020). *Helicobacter pylori* is the most known bacterial carcinogen (Alipour, 2021). There is

also increasing evidence indicating a correlation of some specific species with cancer, including *Porphyromonas gingivalis*, *Treponema denticola*, *Fusobacterium* sp., *Streptococcus* sp., *Peptostreptococcus* sp., *Prevotella* sp., and *Capnocytophaga* (Fitzsimonds et al., 2020). In some cases, a dysbiotic community results from a shift in microbial composition rather than a specific organism associated with the carcinogenic process (Irfan et al., 2020). The current strategies to study the role of the oral microbiome in cancer have predominantly focused on detecting microbial communities present or populational shifts in specific samples and investigating host responses to specific microbial challenges, such as immunological responses, inflammatory responses, and cell proliferation. The potentially oncogenic oral bacteria and possible mechanisms of their action on the carcinogenesis of cells have been systematically reviewed (Whitmore and Lamont, 2014; Fitzsimonds et al., 2020; Irfan et al., 2020; Lamont et al., 2022). In summary, oral microbiota participate in cancer mainly *via* the following mechanisms: (1) stimulating chronic inflammation; (2) inducing mutagenesis, oncogene activation, and angiogenesis; (3) facilitating cell proliferation and inhibiting cellular apoptosis; and (4) producing carcinogens.

In cancer biology, the microbiome is considered an influential environmental factor modulating the carcinogenic process (Scott et al., 2019). Cell migration is an essential physiological process for the immune response, wound repair, and tissue regeneration, while abnormal cell migration is found in devastating diseases such as tumor formation and metastasis. An increasing number of studies have shown that cell migration can be induced by oral bacteria, such as *P. gingivalis* and *Fusobacterium nucleatum*. The latest study found that the tyrosine phosphatase (Ltp1) of *P. gingivalis* is secreted and facilitates *P. gingivalis*-induced proliferation, migration, and the epithelial to mesenchymal transition (EMT) of gingival epithelial cells by targeting the regulator of growth and cell cycle (RGCC). Three distinct activities occurring either simultaneously or independently are involved in cell migration: protrusion, attachment, and traction. There is a complex and discrepant scenario of these activities depending on conditions and migration types. Taking epithelial cells as an example, slow-moving epithelial cells are characterized by slipping of adhesion and retrograde actin flow, while fast-moving epithelial cells have more gripping adhesions and rapid protrusion (Jurado et al., 2005). Single-cell migration and collective cell migration are two main types of cell migration. Studies have demonstrated that epithelial cells either migrate collectively or undergo EMT, thus migrating as single mesenchymal cells (Lu and Lu, 2021). Migration and EMT are highly compatible and facilitate each other involved in development, wound healing, and cancer metastasis (Son and Moon, 2010; Stone et al., 2016). For example, cell migration induced the spread of highly malignant cancer cells (Mosier et al., 2021). Moreover, carcinoma cells migrate into adjacent tissues and invade the lymphatic system and blood vessels and then seeds in distant organs (Christiansen and Rajasekaran, 2006).

Therefore, cell migration is a potential linkage between oral microbiota and carcinogenesis. Recently, investigations in this field have attracted more attention. However, the mechanisms underlying how the oral microbiota participates in regulating cell migration remain to be elucidated. To contribute to the understanding of this issue, this review summarizes the role of cell migration in carcinogenesis and cancer metastasis and focuses on the mechanisms employed by oral microbiota for regulating cell migration. Finally, we introduced critical techniques in the field of cell migration investigation to arouse exciting science over the next decade.

CELL MIGRATION

Cell Migration and EMT

EMT is a cellular biological process involved in tumor cell invasion and metastasis, which was first discovered by Elizabeth Hay during gastrulation in vertebrate embryos in 1982 (Greenburg and Hay, 1982). EMT has been traditionally defined as a process by which epithelial cells lose their vestiges of epithelial origin (e.g., cell–cell adhesion and cell polarity) while migrating and invading into mesenchymal stem cells (Stemmler et al., 2019). Research findings in recent years have found that EMT is not a binary process; there is the hybrid E/M phenotype of cells that originate from epithelial cells in the progression of cancer, known as partial, incomplete, or hybrid EMT (Bakir et al., 2020). The hybrid EMT has been demonstrated to be involved in various human primary cancers (e.g., head and neck cancer) and carcinosarcomas (e.g, esophageal carcinosarcomas) (Pastushenko and Blanpain, 2019). Theoretical and experimental efforts have provided crucial insights into the mechanisms of EMT and the coupling between EMT and other biological processes, such as cell migration, the cell cycle and apoptosis (Lovisa et al., 2015; Aiello et al., 2018; Li et al., 2019; Prakash et al., 2019). The relationship between EMT and cell migration has attracted increasing interest (Aiello et al., 2018; Li et al., 2019). In general, EMT is an important biological process for epithelial-derived cells to acquire migration and invasion during cancer development, especially during metastasis. There is mounting evidence that cancer cells exploit EMT to increase their migratory and invasive ability during the initial stage of the metastatic cascade. Furthermore, the correlation between EMT and migration is type-dependent. A highly specialized epithelial cell is relatively fixed and possesses a low migration ability due to cell–cell adhesions and the apico-basal surface. Therefore, achieving complete mesenchymal transformation is a prerequisite for the migration of a single epithelial cell. During EMT, epithelial cells gain features such as cell elongation, motility, and invasion, coordinated by reorganization of the actin cytoskeleton. In turn, cell migration occurs, which gives rise to single tumor cells capable of crossing basement membranes and invading blood vessels. This process has been utilized by many breast and colorectal cancer cell lines (Aiello et al., 2018). However, the invasion of cancer cells is usually visualized as the migration of groups of cells. The hybrid state of EMT has been associated with increased invasion and collective cell migration, in which cells retain cell–cell adhesion with each

other and possess mesenchymal features, such as increased motility and loss of apical–basal polarity. For instance, Campbell *et al.* demonstrated that the hybrid EMT driven by *Snail* induced collective cell migration and seeded polyclonal metastases in *Drosophila* intestinal tumors (Campbell et al., 2019). Overall, cells that undergo EMT obtain increased migratory ability. Key pathways and cellular events that participate in controlling EMT are also considered to be important factors that regulate cell migration.

Three mechanisms of action have been suggested regarding EMT. The first is deconstructing cell junctions and polarity. The typical characteristics of polarized epithelial cells are tight junctions, adhesive junctions, desmosomes, and gap junctions. Over the years, numerous studies have elucidated that the junction complex plays a vital role in EMT as a medium for polarizing cell–cell contact as well as an anchor point for the actin cytoskeleton. Actin-binding proteins (ABPs) and Rho family GTPases participate in regulating the actin cytoskeleton by controlling the polymerization and disintegration of actin filaments (Tokuraku et al., 2020). Adhesive junctions can anchor capillary basal microtubule arrays and participate in collective cell migration *via* the interaction between E-cadherin and discoidin domain receptor 1 (DDR1) (Gadiya and Chakraborty, 2018). Microtubules and intermediate filaments are also critical for EMT by influencing cell motility, cell shape, intracellular trafficking, and forces to support protrusion (Datta et al., 2021). The second mechanism attributed to EMT is cytoskeletal changes and motility. Active remodeling of the cytoskeleton is crucial for the transformation of cells into a more motile phenotype, thereby promoting EMT (Amack, 2021; Leggett et al., 2021). In the third mechanism, mast regulators regulating gene expression that contribute to the repression of epithelial phenotype and activation of the mesenchymal phenotype drive EMT, including Snail, Slug, Twist1, Zeb1 and Zeb2 (Stemmler et al., 2019).

Cell Migration in Carcinogenesis

Since Pott noticed the association between exposure to soot in chimneys and scrotal cancer in 1775, which is considered the first research describing the cause of cancer, an explosion of research evidence on the etiology of cancer has occurred rapidly. The mechanism of carcinogenesis is a complicated process involving the regulation of various levels and pathways. Exogenous substances (e.g., chemicals) or endogenous signals (e.g., reactive intermediates generated from cellular pathways) can lead to mutations in proto-oncogenes or tumor suppressors (Patterson et al., 2018). The biological characteristics, pathways or genetic alterations during cell migration may also be related to cancer. For instance, the Abl family of tyrosine kinases can modulate actin cytoskeleton arrangement through activation of cell-surface receptors that are critical for cell motility and migration (Bradley and Koleske, 2009). They also play an important role in the progression of leukemia and solid tumors. ABL1 has been identified as an oncogene in leukemia. The upregulation and activation of ABL can also be observed in solid tumors (Greuber et al., 2013).

It has been gradually noticed that actin also exists in the nucleus (Rando et al., 2002). Actin in cytoplasm is the main provider for driving force at the front edge and responsible for the contraction of the cell body at the rear edge. Recent studies have found that increasing the level of nuclear actin monomer inhibited cell migration by regulating serum response factor (SRF) and TEA Domain (TEAD) transcription factors expression (Mcneill et al., 2020). Cell migration can be accelerated when the polymerization of nuclear membrane and actin filament is prevented (Fracchia et al., 2020). ABPs combine with actin to make it pass through the nucleus. Actin cytoskeleton dynamics are the basis of cell migration. The polymerization and degradation of actin filaments influenced by ABPs is an essential step of cell migration. ABP can regulate cell activity mediated by actin elaborately (Tokuraku et al., 2020). Additionally, ABPs induce the production of invasive structures such as filopodia (Wang et al., 2017). Meanwhile, actin and ABPs are involved in the process of carcinogenesis. Nuclear actin, as an important part of the chromatin complex, may affect DNA transcription and repair. The levels of actin and ABPs may be connected to chromatin remodeling and upregulation of oncogenes (Izdebska et al., 2020). Different kinds of ABPs in the nucleus (i.e., α-actinin-4, nerspin and cofilin) are associated with the expression of genes responsible for tumorigenesis and influence tumorigenic phenotypes (An et al., 2016; Sur-Erdem et al., 2020).

During cell migration, it is necessary for migrating cells to reduce cell rigidity and pass through narrow intercellular spaces. Genomic changes, including temporary nuclear envelope rupture, DNA damage and genomic rearrangements, can be observed in the process of immune and cancer cell migration (Denais et al., 2016; Raab et al., 2016). DNA damage is an important first step in carcinogenesis. When the replication of damaged DNA takes place before DNA repair tools come into play or the damage process occurs at a high frequency, nuclear deformation-associated genomic instability may lead to various cellular responses, ultimately leading to cancer (Basu, 2018). In the case of other cell migration, it is still necessary to discuss whether DNA will be damaged mechanically and then cause carcinogenesis.

Cancer Cell Migration in Metastasis

Cancer cell migration is a critical parameter in metastatic dissemination, which allows the cells to detach from the primary tumor, migrate through the extracellular matrix (ECM), enter the lymphatic vessels or the bloodstream, spread within the tissues and then undergo metastatic growth in distant organs. The same principles of cell migration were employed by cancer cells and nonneoplastic cells (e.g., keratinocytes, fibroblasts) as mentioned above. Histopathological evidence has indicated that cancer cells spread within tissues in diverse patterns. They can disseminate using amoeboid- or mesenchymal-type cell migration or collective migration, which expand into solid cell strands, sheets, files, or clusters. Moreover, multiple forms usually exist simultaneously. Amoeboid-like cells often migrate alone or in streams.

Mesenchymal-type cells tend to switch between various modes, including single-cell, in streams and collective migration (Clark and Vignjevic, 2015). For instance, oral squamous cell carcinoma (OSCC) exhibits predominantly collective cell migration when explanted *in vitro*. However, most solid stromal tumors disseminate *via* individual cells. Overall, these patterns are regulated by the molecular repertoire of cancer cells, which mainly includes integrins, matrix-degrading enzymes, cell–cell adhesion molecules and cell–cell communication. Increased contractility mediated by the Rho pathway in cancer cells migrating individually facilitates amoeboid-like migration (Sahai and Marshall, 2003). Under most conditions, the lower the differentiation stage is, the more likely the cancer cells are to spread through a single cell.

In collective migration, cell clusters retain intercellular connections and combine with ECM through integrins, cadherin, gap junctions, etc. (Shih and Yamada, 2012; Yang et al., 2019). Partial retention of epithelial characteristics and partial EMT allow cells to migrate as clusters (Shih and Yamada, 2012; Cheung and Ewald, 2016; Liao et al., 2021). Cells in migrating clusters are usually divided into two groups: leader cells and follower cells. Leader cells sense the cancer microenvironment and create a low-resistance migration path (Vilchez Mercedes et al., 2021). The traction generated by leader cells can be transmitted along with cell–cell junctions to enable the migration of follower cells (Bazellières et al., 2015). Bronsert found that cells at the metastasis front rarely expressed mesenchymal morphology or EMT markers and speculated that single-cell migration is rare or even absent in most epithelial tumors (Bronsert et al., 2014). Collective cell migration may play a key role in the process of cancer cell metastasis. Moreover, cancer seeding by collective migration has a worse clinical prognosis because of its greater metastatic and proliferative potential (Hou et al., 2012; Aceto et al., 2014).When tumor cells need to pass through the narrow channel of extracellular space in dense three-dimensional matrices, they can establish the polarized distribution of Na^+/H^+ pump and aquaporin, thus resulting in the inflow of water at the front of cells and the outflow of water at the back of cells, resulting in net cell displacement (Stroka et al., 2014). The method that adjusts the volume through water infiltration provides another possible cell migration mechanism that does not require actin polymerization.

ORAL MICROBIOTA AND CELL MIGRATION

Oral Bacteria Regulating Cell Migration

The oral cavity contains one of the greatest microbiological reservoirs in the human body. The dynamic and finely balanced relationship between the oral microbiome and the host is of great importance to human health (Hajishengallis and Lamont, 2021). Bacteria are the largest contributor to the oral resident microbiota, 94% of which is composed of six major phyla (Firmicutes, Bacteroidetes, Proteobacteria, Actinobacteria, Spirochaetes and Fusobacteria), and 6% contains other phyla (Zhang et al., 2018). Accumulating data support a role for oral bacterial infection in the migration of various types of cells, mainly epithelial cells, and cancer cells. The effect may vary depending on the infection method, time, and cell type (**Table 1**).

P. gingivalis, the key etiological agent in periodontitis, can successfully invade oral epithelial cells and live intracellularly. It adheres and internalizes to oral cells by modulating host signaling cascades such as phosphorylation/dephosphorylation of molecules and changes in the cell cytoskeleton (Andrian et al., 2006). For instance, *P. gingivalis* can induce gingival epithelial cells to undergo autophagy and traffic into autophagosome vacuoles to protect itself from targeted lysosome degradation mediated by selective ubiquitin (Lee et al., 2018). *P. gingivalis* expresses virulence and releases outer membrane vesicles (OMVs), which are involved in the communication between bacteria and the host. In general, *P. gingivalis*, its derivatives (e.g., heated-killed or conditioned medium from bacteria) and secreted substances (OMVs and Ltp1) can promote the migration of oral epithelial cells and OSCC cells (Inaba et al., 2014; Ha et al., 2015; Ha et al., 2016; Geng et al., 2017; Lee et al., 2017; Abdulkareem et al., 2018a; Hoppe et al., 2019; Ohshima et al., 2019; Kamarajan et al., 2020; Fitzsimonds et al., 2021; Liu et al., 2021a; Liu et al., 2021b). Comprehensive analysis of the host transcription response to *P. gingivalis* infection showed the mode of increased cell migration (Geng et al., 2019). The colonization of *P. gingivalis* has been identified as a risk factor for OSCC and is related to prognosis (Ganly et al., 2019). However, the inhibitory effect has also been observed in some studies (Laheij et al., 2013; Bhattacharya et al., 2014). This may suggest that bacterial challenge may hinder the re-epithelialization process and lead to delayed healing after the barrier function of the gingival epithelium is destroyed. We speculated that the possible reason for such a diametrically opposed situation is the relatively short infection time or different sources and locations of cells. It may also be due to differences in protocols between continuous infection and long-term culture with a short infection followed by a medium change. When serial infection experiments with *P. gingivalis* are performed *in vitro*, cells often float alive due to strong protease activity.

As a symbiotic bacterium, *F. nucleatum* is commonly found in the oral cavity. It expresses a variety of adhesins, such as FadA, on the surface to adhere to and invade host cells. Similarly, *F. nucleatum* can also release extracellular vesicles (EVs) or OMVs (Liu et al., 2019; Liu et al., 2021). Studies have shown that infection with *F. nucleatum* ATCC 25586 and heated-killed *F. nucleatum* ATCC 10953 promotes OSCC cell migration and invasion *in vitro* (Abdulkareem et al., 2018a; Kamarajan et al., 2020; Shao et al., 2021). The effect of its derivatives, secretions and virulence factors on cell migration still needs further study.

Butyric acid (BA), a short-chain fatty acid, is produced by periodontopathic bacteria, such as *P. gingivalis* and *F. nucleatum.* Large amounts of BA have been detected in the oral cavities of patients with periodontal disease. BA from periodontopathic bacteria does not directly affect the migration of ameloblastomas but has an indirect influence through the expression of epidermal

TABLE 1 | Summary of oral bacteria affecting cell migration.

Bacteria species	Cell types	Infection conditions	Effect on cell migration	Ref
P. gingivalis ATCC 33277	human immortalized oral epithelial cells (HIOECs)	MOI=1, 24 h repeatedly in 5, 10, 15, and 23 weeks	promote	(Geng et al., 2017)
	primary human oral epithelial cells (OECs)	MOI=10 and 100, 120 h	promote	(Lee et al., 2017)
	primary gingival keratinocytes	MOI=10, 24 h	inhibit	(Bhattacharya et al., 2014)
	Human telomerase immortalized gingival keratinocytes (TIGK)	MOI=100,1 h, followed by 23 h in fresh medium	promote	(Fitzsimonds et al., 2021)
	TIGK	MOI=100, 24 h	promote	(Ohshima et al., 2019)
	Human immortalized oral keratinocyte cell line OKF6/hTERT-1	MOI=100, 24 h	promote	(Hoppe et al., 2019)
	human OSCC cell lines, UM-SCC-14A (floor of mouth) and HSC-3 (tongue)	MOI=10,50,100,2 h	promote	(Kamarajan et al., 2020)
	SAS and Ca9-22 cells	MOI=1, 24 h	promote	(Inaba et al., 2014)
	OSC-20 and SAS cells	MOI=100,3 h	promote	(Ha et al., 2016)
	Human esophageal cancer cell lines NE6-T, KYSE-30 and KYSE-150	MOI=10, 48 h	promote	(Liang et al., 2020; Qi et al., 2020)
secreted gingipains of *P. gingivalis* ATCC33277	human embryonic microglia clone 3 (HMC3) cell line	MOI=1,12 h	promote	(Nonaka and Nakanishi, 2020)
Outer membrane vesicles (OMVs) of *P. gingivalis* ATCC 33277	OSCC cell line (HSC-3)	6 h	promote	(Liu et al., 2021b)
Ltp1 of *P. gingivalis* ATCC 33277	TIGK	MOI=100, 6 h	promote	(Liu et al., 2021a)
Heat-killed *P. gingivalis* ATCC 33277	OSCC cell line(H400)	MOI=100, 8 d	promote	(Abdulkareem et al., 2018a)
P. gingivalis W83	human buccal epithelial cell line HO-1-N-1	MOI=10,100, 17 h	inhibit	(Laheij et al., 2013)
heat-killed *P. gingivalis* W83	human buccal epithelial cell line HO-1-N-1	MOI=100, 1000,17 h	inhibit	(Laheij et al., 2013)
conditioned medium from *P. gingivalis* W83	human buccal epithelial cell line HO-1-N-1	MOI=100,17 h	inhibit	(Laheij et al., 2013)
P. gingivalis strain 381	Ca9-22 OSCC cells	MOI=100, 2 h	promote	(Ha et al., 2015)
F. nucleatum ATCC 25586	primary gingival keratinocytes	MOI=10:1, 24 h	inhibit	(Bhattacharya et al., 2014)
	human OSCC cell lines, UM-SCC-14A (floor of mouth) and HSC-3 (tongue)	MOI=10,50,100,2 h	promote	(Kamarajan et al., 2020)
	Colorectal cancer cell lines (HCT-116, LoVo)	MOI=100, 12 h and 24 h	promote	(Chen et al., 2020; Xu et al., 2021a)
Heat-killed *F. nucleatum* ATCC 10953	OSCC cell line(H400)	MOI=100, 8 d	promote	(Abdulkareem et al., 2018a)
	OSCC cell line(HOC621 cells)	MOI=10, 3 h	promote	(Shao et al., 2021)
Heat-killed *F. nucleatum* JCM8532	OSCC cell line(HOC621 cells)	MOI=10, 3 h	promote	(Shao et al., 2021)
Live or heat-killed *F. nucleatum* JCM11024	OSCC cell line(HOC621 cells)	MOI=10, 3 h	promote	(Shao et al., 2021)
Live or heat-killed *F. nucleatum* ATCC23726	OSCC cell line(HOC621 cells)	MOI=10, 3 h	promote	(Shao et al., 2021)
T. denticola ATCC35405	human OSCC cell lines, UM-SCC-14A (floor of mouth) and HSC-3 (tongue)	MOI=10,50,100,2 h	promote	(Kamarajan et al., 2020)
P. intermedia ATCC 25611 *T. forsythia* ATCC 43037	human buccal epithelial cell line HO-1-N-1	MOI=10,100 or 1000, 17 h	inhibit	(Laheij et al., 2013)

(Continued)

TABLE 1 | Continued

Bacteria species	Cell types	Infection conditions	Effect on cell migration	Ref
Conditioned medium from *Streptococcus mitis* LMG 14557 (MOI 100, 1000) and heat-killed *Streptococcus mitis* LMG 14557 Conditioned medium from *Prevotella nigrescens* ATCC 33563 ((MOI=100,1000) heat-killed *Prevotella nigrescens* ATCC 33563 (MOI 10, 100, 1000) Heat-killed *Prevotella intermedia* ATCC 25611 (MOI 100, 1000) *Tannerella forsythia* ATCC 43037 (MOI 50, 500)				

Periodontal pathogens Porphyromonas gingivalis and Fusobacterium nucleatum promote tumor progression in an oral-specific chemical carcinogenesis model.

growth factor (EGF) and transforming growth factor β1 (TGF-β1) (Ishikawa et al., 2020). Other oral bacteria are also related to cell migration. Oral streptococci, such as *Streptococcus gordonii*, is an important component of the oral microbiome. *S. gordonii* has been considered an early colonizer to host tissues. It can resist ZEB2 induction by *P. gingivalis* and then inhibit cell migration (Ohshima et al., 2019). The specific molecular mechanism of oral bacteria related to cell migration, interaction between different kinds of bacteria and its effect on cell migration deserve further study.

There is already evidence that oral bacteria can spread to other body sites through the bloodstream or digestive tract and participate in a variety of systemic diseases (Fiorillo et al., 2019). It may affect the pathogenesis and progression of diseases *via* cell migration and metastasis. *P. gingivalis* increases the migration of esophageal squamous cell carcinoma (Liang et al., 2020; Qi et al., 2020). *F. nucleatum* has been found to be enriched in colorectal cancer (CRC) tissue and acts as a pro-carcinogenic bacterium (Wang et al., 2021). It promotes CRC cancer migration *in vitro* and metastasis *in vivo* (Chen et al., 2020; Xu et al., 2021a). In addition, the metastases in mice in which breast cancer developed after infection with *F. nucleatum* were larger than those in the control group (Parhi et al., 2020). *P. gingivalis* has been found in the brains of Alzheimer's disease patients and is involved in the disease process (Dominy et al., 2019). Gingipains, cysteine proteases secreted by *P. gingivalis*, induces cell migration and membrane ruffling in the human embryonic microglia clone 3 (HMC3) cell line through the protease-activated receptor 2 (PAR2)/ERK1/2 pathway (Nonaka and Nakanishi, 2020). This signaling pathway may be necessary for embryonic microglial cells to move into the infection sites.

Emerging Link Between Oral Virus/Fungi and Cell Migration

Dental professionals are usually familiar with viruses present or cause symptoms in the oral cavity. In a broad sense, they can both be defined as oral viruses. There is not always a clear distinction between them. For example, viruses that induce symptoms affecting oral tissues can be present in the oral cavity following replication and release from other tissues or the blood circulation. Prolonged infection of certain viral genes can insert into host DNA as proto-oncogenes to turn them into oncogenes, leading to malignant transformation (Young et al., 2016; Warburton et al., 2018). There is emerging evidence that Epstein–Barr virus (EBV), as an oncogenic virus, promotes OSCC progression. P53 can promote the emergence of leader cells and then coordinate the migration of epithelial cells (Kozyrska et al., 2022). EBV decreases the stability of P53 and increases the expression of matrix metalloproteinase (MMP) through CTAR family proteins/programmed cell death protein 1 ligand, thereby promoting OSCC cell metastasis and tumorigenesis (Radaic and Kapila, 2021). Human papillomavirus (HPV) is detectable in 40-70% of oropharyngeal cancer (OPC) and 20% of non-OPC, almost the HPV16 subtype (Mehanna et al., 2013). The relationship between HPV and cervical cancer has been generally acknowledged. HPV16 can lead to enhanced migration and invasion of cervical cancer cells *in vitro* and in a mouse model (Hu et al., 2015; Wang et al., 2019).

Fungi are common, albeit minor, members of the oral microbiota, which are structurally and metabolically distinct from other oral microorganisms, such as bacteria and viruses. They have varied cell morphologies, including yeast, hyphae, pseudo hyphae, and chlamydospores. Although filamentous fungi can rarely be isolated from the oral cavity, yeast can be cultured from the saliva of approximately 40% of individuals, such as *Candida tropicalis*, *Candida dubliniensis*, and *Candida glabrata*. The most frequent oral fungal infection is *Candida albicans*. *C. albicans* significantly increased in OSCC patients compared with the control group (Hong et al., 2020). *C. albicans* can enhance the migratory ability of oral keratinocytes through activation of the ERK/focal adhesion kinase (FAK) pathway (Shi et al., 2009). Exposure to different concentrations of *C. glabrata and Candida kefyr* (MOI=1,10) was found to inhibit human buccal epithelial cell migration *in vitro* (Haverman et al., 2017). This inhibitory effect may play a role in the process of ulcerative mucositis.

THE MECHANISMS OF ORAL MICROBIOTA REGULATING CELL MIGRATION

Migration is a multistep process. First, the cells are polarized in response to the migration-promoting stimulus, and then the

membrane protrusions extend in the direction of the stimulus (Lauffenburger and Horwitz, 1996). Then, the adhesion of the protrusions to the ECM produces traction, which allows the movement of the cell, disassembly of the adhesion points and retraction of the back of the cell (Ridley et al., 2003). Collective and single-cell migration share these broad mechanistic characteristics (Yang et al., 2019). Studies have found that oral microbes mainly regulate cell migration by affecting cell adhesion, polarization, guidance, etc. (**Figure 1**).

Adhesion

Intercellular adhesion is mediated by different types of junction complexes, including tight junctions, adhesive junctions, gap junctions and desmosomes (Rusu and Georgiou, 2020). Oral microbiota can degrade epithelial cell tight junction proteins in an MMP-dependent manner or by affecting the activity of transcription factors (Ha et al., 2015). The shape of infected cells became slender, indicating absent contact inhibition, and cell junctions were weakened under a transmission electron microscope (Geng et al., 2017). MMP is involved in focal degradation of type IV collagen, breakdown of basement membrane and release of cell adhesion (Strutz et al., 2002). MMP-1, MMP-2, MMP-3, MMP-7 and MMP-9 were upregulated following exposure to *P. gingivalis* stimulation (Ha et al., 2016; Lee et al., 2017). One mechanism is that gingipains of *P. gingivalis* process the proenzyme of MMP-9 into active MMP-9 to promote cell migration and invasion (Inaba et al., 2014; Inaba et al., 2015). This process is regulated by the PAR4, p38/HSP27, ERK1/2-Ets1, and PAR2/NF-κB pathways (Inaba et al., 2014; Inaba et al., 2015). *P. gingivalis* could also activate the expression of MMP-2 and MMP-9 by increasing the transcription of nicotinamide N-methyltransferase (NNMT) and Gas6 (Tang et al., 2011; Geng et al., 2017).

E-cadherin, the central protein of cell–cell adherens junctions, is downregulated by a series of transcription factors (Slug, Snail, JAG1, Notch, Zeb1 and Zeb2) (Wu and Zhou, 2010). *P. gingivalis* can significantly enhance the activity of these transcription factors (Geng et al., 2017). Moreover, *P. gingivalis* infection could inhibit the expression of E-cadherin and increase the expression of Snail in oral epithelial cells by upregulating the transcription of colon cancer associated transcript 1 (CCAT1) and growth arrest specific 6 (Gas6) (Jiang et al., 2015; Guo and Hua, 2017). HPV-16 may also facilitate the migration and metastasis potential of cervical cancer through altered cadherin switching (Hu et al., 2015).

Polarization and Guidance

Polarity is characteristic of epithelial cells. In polarized epithelial cells, the intercellular junction complex is located asymmetrically. The spatial asymmetry of these complexes is mediated by a class of evolutionarily conserved proteins, which can be divided into three functional groups: the Crumbs2 complex, Scribble complex and Par complex. The apical domain is related to the Crumbs complex, the basolateral domain is composed of the Scribble complex, and the subapical region of the apical-basal boundary is related to the Par complex, which is composed of Par3, Par6, and atypical protein kinase C and Cdc42.

In single-cell migration, migrating epithelial cells tend to lose apical-basal polarity and rearrange their actin cytoskeleton (Gibieža and Petrikaitė, 2021). The protusions of the leading edge drive the cell to orientally migrate, and the main force of migrating is generated by the lamellipodia. Myoslin II and Rho catalyze the formation of new cell-ECM adhesion (focal

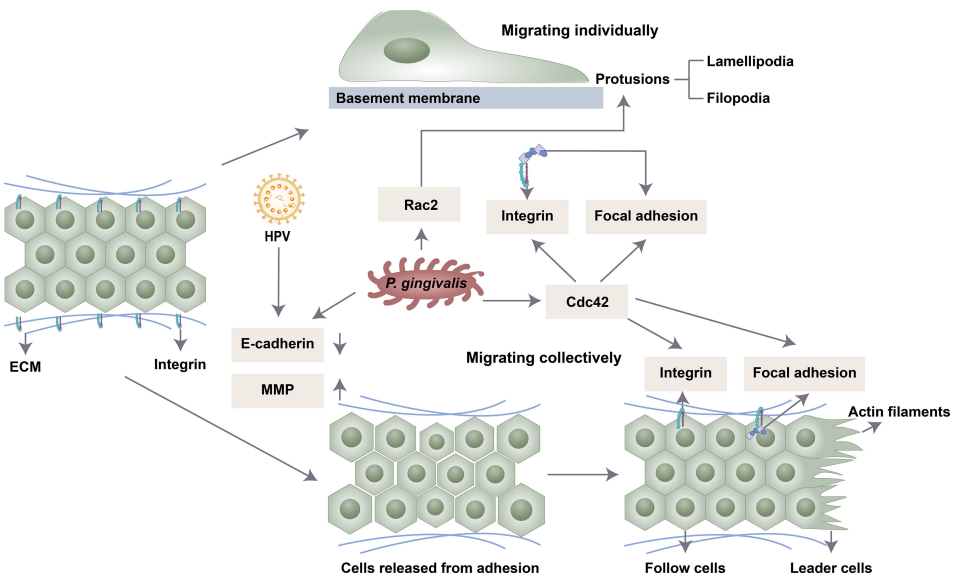

FIGURE 1 | Possible mechanisms by which oral microbiota influence cell migration. *P. gingivalis* and HPV 16 release intercellular adhesions by downregulating E-cadherin and upregulating MMP. *P. gingivalis* enhances the expression of Cdc42 and Rac2 to induce the front and back polarity that is crucial for cell migration. *P. gingivalis* drives cell clusters to move orientally through the formation of integrin and focal adhesion.

adhesions) during lamellipodia extension. The stress fibers are joined to mature focal adhesions, connecting the cell to the ECM. In collective migration, cells in different positions show different expression patterns. The simple case is front/rear polarization. The leading cells with a mesenchymal phenotype guide the following cells to retain epithelial characteristics. This process is coordinated by cell-ECM and cell–cell interactions.

Rho family GTPases include RhoA, Rac and Cdc42 proteins, which participate in the formation of cytoskeletal components by inducing the accumulation of F-actin in the front of the cell (Ridley, 1999). Rho GTPases regulate cytoskeletal actin rearrangement and thus cell dynamics (Sahai and Marshall, 2003; Lawson and Ridley, 2018). Polar proteins regulated by GTPase enzymes of the Rho family induce the formation of the front and rear axes (Capuana et al., 2020). Rac protein is closely related to the formation of lamellipodia and cell migration. The Rho-dependent localization of myosin IIB in the back of the cell is necessary for the maintenance of front and back polarity and tail contraction during the process of mesenchymal migration (Vicente-Manzanares et al., 2008). Cdc42 mainly produces front and back polarity. The local activation of Cdc42 and its spatial gradient in nonpolarized cells drive the formation of the initial protruding front under uniform chemotaxis stimulation (Yang et al., 2016). When the apical junction complex is destroyed, Cdc42 and the polar protein complex relocate from the tight junction area to the front and induce the centrosome and Golgi to relocate to the front of the cell, promoting the growth of microtubules to the front of the cell and subsequent cell migration (Burute et al., 2017). Therefore, at the front end, Cdc42 and Rac promote actin polymerization, thereby promoting the formation of protrusions such as filopodia or lamelia. Increased actin reorganization and Cdc42 and Rac activity are observed in OSCC (Iwai et al., 2010). *P. gingivalis* enhanced the expression of Rac2 and Cdc42 in platelets and neutrophils (Börgeson et al., 2011; Senini et al., 2019). *P. gingivalis* fimbriae induced transendothelial migration of monocytes by activating Rac1 and PI3K (Harokopakis et al., 2006). Its effect on oral epithelial cells needs further study.

Integrin alpha V and FAK signals help mediate cell migration (Trepat et al., 2012).Cell migration depends on the binding of integrins to the ECM, which activates downstream signaling, including FAK phosphorylation and mitogen-activated protein kinase (MAPK), to recruit focal contacts. Several integrins, such as beta-6 integrin, can facilitate cell migration through actin cytoskeletal reorganization and cell polarization. *P. gingivalis* inhibits the induction of integrin beta-3 and -6 and the cell migratory process in oral keratinocytes (Bhattacharya et al., 2014). Periodontal pathogens (*P. gingivalis, F. nucleatum*, and *T. denticola*) promote OSCC cell migration through the activation of integrin alpha V and FAK (Kamarajan et al., 2020). The E6 protein of HPV could also promote actin cytoskeleton assembly through β1-integrin signaling (Holloway and Storey, 2014).

EMT

The other strategy employed by oral microbiota to manipulate cell migration is modulating the EMT process (**Figure 2**). Specifically, microbial dysbiosis results in the degradation of epithelial tight junction proteins, enhances mesenchymal characteristics, and induces at least a portion of the EMT process. For instance, *P. gingivalis* regulates epithelial barrier function through the degradation of E-cadherin (Sztukowska

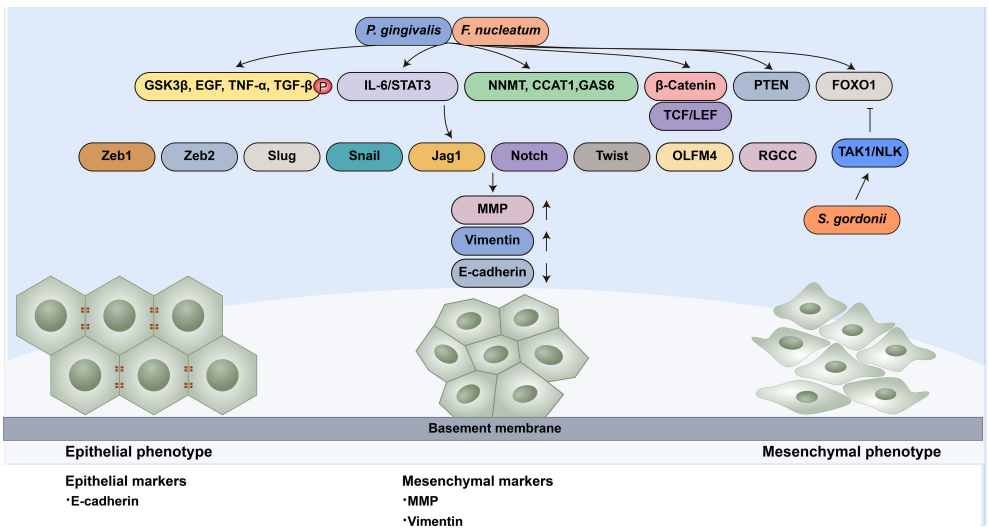

FIGURE 2 | Oral microbiota guide epithelial-mesenchymal transition of normal epithelial cells. EMT-associated transcription factors (Zeb1, Zeb2, Slug, Snail, Jag1, Notch, Twist, OLFM4 and RGCC) can induce epithelial cells to undergo partial or complete mesenchymal transformation by downregulating epithelial markers (such as E-cadherin) and upregulating mesenchymal markers (MMP and Vimentin). *P. gingivalis* and *F. nucleatum* enhance the expression of EMT-associated transcription factors through diverse pathways: (1) the phosphorylation of GSK-3β, EGF, TNF-α and TGF-β1; (2) the activation of the IL-6/STAT3 pathway; (3) the upregulation of NNMT, CCAT1 and GAS6;(4) the nuclear translocation of β-catenin and further activation TCF/LEF promoter elements; (5) the activation of PTEN; and (6) the upregulation of FOXO1 *S. gordonii* can resist EMT-associated factor induction by *P. gingivalis* by suppressing FOXO1 and activating the TAK1-NLK negative regulatory pathway.

et al., 2016; Abdulkareem et al., 2018a). *P. gingivalis* and *F. nucleatum* could also enhance the expression of EMT-associated transcription factors (Zeb1, Zeb2, Slug, Snail, Jag1, Notch, Twist, OLFM4 and RGCC) in oral epithelial cells and OSCC cells through diverse pathways, including the phosphorylation of glycogen synthase kinase-3β (GSK-3β), EGF, tumor necrosis factor-α (TNF-α) and TGF-β1 (Bhattacharya et al., 2014; Sztukowska et al., 2016; Abdulkareem et al., 2018a; Abdulkareem et al., 2018b). *S. gordonii* can resist ZEB2 induction by *P. gingivalis* by suppressing FOXO1 and activating the TAK1-NLK negative regulatory pathway (Ohshima et al., 2019). *F. nucleatum* can activate the signal transducer and activator of transcription 3 (STAT3) signaling pathway, which can increase the expression of EMT-associated genes (E-cadherin, Snail and Twist) (Huang et al., 2011; Wang et al., 2020). The upregulation of partial EMT genes is also observed in *F. nucleatum*-infected OSCC cells (Shao et al., 2021).

Wnt/β-catenin facilitates EMT in cancer progression (Liu et al., 2017; Li et al., 2021). β-catenin in the nucleus binds to the T cell factor/lymphoid enhancer factor (TCF/LEF) transcription factor, the major end point mediators of Wnt/β-catenin signaling, to activate EMT. Vimentin is the target of Wnt/β-catenin signaling. The nuclear translocation of β-catenin and activation of vimentin can be observed in OSCC cells, which are related to poor prognosis (Chaw et al., 2012). The gingipains of *P. gingivalis* modulate the β-catenin pathway in gingival epithelial cells and the disassociation of the β-catenin destruction complex composed of scaffolding proteins and the kinases GSK3β and Casein Kinase 1α (CK1α). It can induce nuclear translocation of β-catenin and further activate TCF/LEF promoter elements (Zhou et al., 2015).

It has been proven that several genes are positively relevant to cell migratory and invasive ability, such as CCAT1, NNMT and Gas6. CCAT1 and Gas6 can downregulate E-cadherin and upregulate EMT-associated transcription factors, such as Snail and Twist (Jiang et al., 2015; Guo and Hua, 2017). The mRNA expression of NNMT, CCAT1 and GAS6 was increased in *P. gingivalis*-infected oral epithelial cells (Geng et al., 2017).

Others

Keratin 7 (KRT7) is a type II cytokeratin and is involved in cell motile activity. It has been proven to be relevant to lymph node metastasis and poor prognosis in CRC (Bayrak et al., 2011; Hrudka et al., 2021). *F. nucleatum* upregulates the long noncoding RNA KRT7-antisense and stabilizes KRT7 mRNA *via* the NF-κB pathway (Chen et al., 2020). HPV-16 enhances actin polymerization by downregulating alpha-actinin-4 (ACTN4), leading to enhanced migration and invasion (Tentler et al., 2019; Wang et al., 2019).

CRITICAL TECHNIQUES FOR INVESTIGATING CELL MIGRATION

With the development of new microscopy methods and fluorescent reagents specifically used for cell imaging, microscopy technology plays a central role in the research of cell biophysics. Optical microscopes allow us to view cell structures with previously unattainable spatial and temporal resolution and to image living cells in tissues and animals. Improvements in electron microscopy technology allow us to understand the molecular structure of organelles in cells in more detail. In recent years, an increasing number of technologies have emerged, such as video real-time microscopy, confocal microscopy, multiphoton microscopy, intravital microscopy, superresolution fluorescence microscopy, electrochemiluminescence microscopy, and traction force microscopy, which make the observation and analysis of cell migration more accurate and intuitive (Horwitz, 2016).

Most biological research relies on conventional experimental techniques, and static analysis is only allowed at certain time points *in vitro*. Visualizing cell dynamics in organisms can provide opportunities to study key biological phenomena *in vivo*. However, electron microscopy is usually not suitable for live or wet samples due to the need for vacuum operation conditions. Soon after the first compound microscope was invented in 1595, the intravital microscope (IVM) was used for physiological research. IVM can be combined with a variety of optical systems, such as confocal and multiphoton microscopy, to conduct deeper observations of tissues and directly observe the biological structure and dynamic behavior of objects, including single cells and living animals. With these characteristics, IVM can be used to visualize the biological morphology of various fields, such as vascular biology, immunology, stem cell biology and oncology (Choo et al., 2020). For instance, in the field of oncology, IVM can be used to observe the single-cell behavior of cancer cells and immune cells during tumor progression and metastasis (Ng et al., 2008; Pinner et al., 2009; Gabriel et al., 2018; Kuo et al., 2019). To overcome the obstacle of the traditional IVM that the limited frame rate cannot accurately observe the rapid dynamic behavior of cells, a real-time IVM capable of video image scanning (over 30 frames/sec) has been invented to visualize faster cell movement and further study cell functions and the interactions between cells (Padera et al., 2002). Moreover, the Boyden chamber assay and scratch wound assay are standard techniques for studying cell invasion and migration, but both techniques have their own limitations. The Boyden chamber assay is difficult and time-consuming, while the scratch wound assay has low repeatability. The real-time video microscope can be introduced into the incubator to generate real-time images of cell migration, which can provide accurate quantitative data for wound healing and is used to provide automatic real-time analysis of cell migration, which improves repeatability (Jain et al., 2012). This video microscope-based scratch experiment has proven to be a reliable technique for evaluating cell migration and invasion (Guy et al., 2017).

In addition, superresolution fluorescence microscopy, harmonic generation microscopy, electrochemiluminescence microscopy, and traction force microscopy are all powerful tools for studying cell migration. The5 superresolution microscope overcomes the limitations of conventional optical microscopes in resolution, dimensionality, quantification, and imaging speed. It can be used to observe the cellular processes of

single cells with nanometer-level resolution, contributing to the understanding of rapid cell dynamics with a more visualized subcellular and molecular scale. Increasing methods have been developed to achieve superresolution, such as stimulated emission depletion (STED), structured illumination microscopy (SIM), photoactivation localization microscopy (PALM), stochastic optical reconstruction microscopy (STORM), and superresolution optical fluctuation imaging (SOFI) (Feng et al., 2018). These realize the nanoscale, visualization and quantitative analysis of signaling pathway molecules such as membrane proteins (Xu et al., 2021b). Second harmonic generation (SHG) is a second-order nonlinear optical process. Two photons interacting with nonlinear optical materials, such as collagen, combine to form a new photon whose frequency is twice that of the original photon, and the wavelength is halved (Wolf et al., 2009). SHG microscopy is a high-resolution nondestructive imaging method that represents an ideal method for detecting the geometry of collagen in natural and/or connective tissues. It has been used to study the morphology of fibrous collagen in a variety of tissues, which helps to understand the structure of collagen in tissues under normal or abnormal conditions. Unlike SHG microscopy, which requires specific asymmetry of the imaging structure, third harmonic generation (THG) is a combination of three photons converted into a photon with one third of the excitation wavelength and three times the energy. Therefore, compared to SHG, the application range of THG is wider. The combination of SHG or THG with fluorescence detection and intravital microscopy provides more details about tissue-tissue and cell-tissue interactions, which helps to simulate the migration of tumor cells in the tissue in a specific environment (Weigelin et al., 2012). Electrochemiluminescence microscopy can provide a clear visual contrast between the adhesion site and the noncontact domain so that the former can be selected and displayed in a label-free manner to image the cell matrix adhesion of the moving cell clusters to study the movement of cells in collective migration (Ding et al., 2020). Traction force microscopy is an experimental technique used to quantify the contractile force produced by adherent cells by placing the cells on a flexible material, such as polyethylene glycol or polyacrylamide gel with a known elastic modulus, track the displacement of the substrate caused by the cell contraction, and then convert it into a traction field (Hur et al., 2020). Traction force microscopy with integrated microfluidics can precisely control physical and chemical stimulation to detect the migration speed, traction and intercellular tension of cell clusters under different chemical gradients (Jang et al., 2019).

In the limited three-dimensional (3D) space, the situation of cell migration is more complex, which is difficult to observe by traditional methods. New engineering model systems, such as hydrogels and microchannel assays provide new insights into 3D cell migration. The synthesized hydrogel can independently modulate the hardness, composition, degradability, or other characteristics to analyze the role of a single characteristic of ECM in cell migration (Trappmann et al., 2017). Therefore, it provides a platform to see how cancer cells respond to different biochemical and mechanical signals. Other types of cells can also be introduced into these hydrogels to simultaneously observe cell-matrix and cell-cell interactions (Katz and West, 2022). Confined microchannel approach can introduce and adjust the interface geometry to explore changes in cytoskeleton, adhesion, and regulatory proteins induced by different experimental microenvironments (Mak et al., 2011). Polydimethylsiloxane (PDMS) microchannel devices are also widely used to study migration in 3D confinement. Microchannel system allows direct and real-time imaging and explores the mechanism of migration under confined conditions without shear stress. Microchannel coated with different ECM proteins can be applied to explore cells' response to external gradients. In addition, the limited migration space *in vivo* can also be simulated by grooved substrates, micropatterned lines and islands, vertical confinement, patterned gels, and so on (Paul et al., 2016).

SUMMARY

Studies have shown that the oral microbiota can regulate the carcinogenic process of cells, and this process may involve abnormal cell migration. Partial or complete EMT is related to increased migratory ability and participates in cancer invasion and metastasis. Specific genetic changes and signaling pathway activation during cell migration may also be seen in EMT, tumorigenic phenotypes and cancer metastasis. Collective migration is the main form of cancer invasion, and it is associated with worse prognosis. Oral microbial dysbiosis is related to abnormal cell migration of oral epithelial cells. Increasing evidence has shown that *P. gingivalis*, *F. nucleatum*, *Streptococci* and their virulence factors regulate cell migration, whose effects vary with infection methods, time, and cell types. Some oral viruses and fungi can affect cell migration, and further study is needed. The oral microbiota also participates in systemic diseases through cell migration. The mechanism by which the oral microbiota regulates cell migration includes cell adhesion, polarization, guidance, EMT, etc. real-time microscopy, superresolution microscopy, harmonic microscopy and traction microscopy are widely used to observe and analyze the migration process. We expect that with further development of microscope imaging technology, the relevant mechanism can be observed more intuitively and accurately.

AUTHOR CONTRIBUTIONS

HB and JY drafted the manuscript. SM and CL edited and added valuable insights to the manuscript. All authors approved the final manuscript and agreed to be accountable for all aspects of the work.

FUNDING

This study was supported by the National Natural Science Foundation of China (82071108).

REFERENCES

Abdulkareem, A. A., Shelton, R. M., Landini, G., Cooper, P. R., and Milward, M. R. (2018a). Periodontal Pathogens Promote Epithelial-Mesenchymal Transition in Oral Squamous Carcinoma Cells *In Vitro*. *Cell Adh. Migr.* 12, 127–137. doi: 10.1080/19336918.2017.1322253

Abdulkareem, A. A., Shelton, R. M., Landini, G., Cooper, P. R., and Milward, M. R. (2018b). Potential Role of Periodontal Pathogens in Compromising Epithelial Barrier Function by Inducing Epithelial-Mesenchymal Transition. *J. Periodontal Res.* 53, 565–574. doi: 10.1111/jre.12546

Aceto, N., Bardia, A., Miyamoto, D. T., Donaldson, M. C., Wittner, B. S., Spencer, J. A., et al. (2014). Circulating Tumor Cell Clusters are Oligoclonal Precursors of Breast Cancer Metastasis. *Cell* 158, 1110–1122. doi: 10.1016/j.cell.2014.07.013

Aiello, N. M., Maddipati, R., Norgard, R. J., Balli, D., Li, J., Yuan, S., et al. (2018). EMT Subtype Influences Epithelial Plasticity and Mode of Cell Migration. *Dev. Cell* 45, 681–695.e684. doi: 10.1016/j.devcel.2018.05.027

Alipour, M. (2021). Molecular Mechanism of Helicobacter Pylori-Induced Gastric Cancer. *J. Gastrointest. Cancer* 52, 23–30. doi: 10.1007/s12029-020-00518-5

Amack, J. D. (2021). Cellular Dynamics of EMT: Lessons From Live *In Vivo* Imaging of Embryonic Development. *Cell Commun. Signal* 19, 79. doi: 10.1186/s12964-021-00761-8

Andrian, E., Grenier, D., and Rouabhia, M. (2006). Porphyromonas Gingivalis-Epithelial Cell Interactions in Periodontitis. *J. Dent. Res.* 85, 392–403. doi: 10.1177/154405910608500502

An, H. T., Yoo, S., and Ko, J. (2016). α-Actinin-4 Induces the Epithelial-to-Mesenchymal Transition and Tumorigenesis *via* Regulation of Snail Expression and β-Catenin Stabilization in Cervical Cancer. *Oncogene* 35, 5893–5904. doi: 10.1038/onc.2016.117

Bakir, B., Chiarella, A. M., Pitarresi, J. R., and Rustgi, A. K. (2020). EMT, MET, Plasticity, and Tumor Metastasis. *Trends Cell Biol.* 30, 764–776. doi: 10.1016/j.tcb.2020.07.003

Basu, A. K. (2018). DNA Damage, Mutagenesis and Cancer. *Int. J. Mol. Sci.* 19, 970. doi: 10.3390/ijms19040970

Bayrak, R., Yenidünya, S., and Haltas, H. (2011). Cytokeratin 7 and Cytokeratin 20 Expression in Colorectal Adenocarcinomas. *Pathol. Res. Pract.* 207, 156–160. doi: 10.1016/j.prp.2010.12.005

Bazellières, E., Conte, V., Elosegui-Artola, A., Serra-Picamal, X., Bintanel-Morcillo, M., Roca-Cusachs, P., et al. (2015). Control of Cell-Cell Forces and Collective Cell Dynamics by the Intercellular Adhesome. *Nat. Cell Biol.* 17, 409–420. doi: 10.1038/ncb3135

Bhattacharya, R., Xu, F., Dong, G., Li, S., Tian, C., Ponugoti, B., et al. (2014). Effect of Bacteria on the Wound Healing Behavior of Oral Epithelial Cells. *PloS One* 9, e89475. doi: 10.1371/journal.pone.0089475

Börgeson, E., Lönn, J., Bergström, I., Brodin, V. P., Ramström, S., Nayeri, F., et al. (2011). Lipoxin A_4 Inhibits Porphyromonas Gingivalis-Induced Aggregation and Reactive Oxygen Species Production by Modulating Neutrophil-Platelet Interaction and CD11b Expression. *Infect. Immun.* 79, 1489–1497. doi: 10.1128/IAI.00777-10

Bradley, W. D., and Koleske, A. J. (2009). Regulation of Cell Migration and Morphogenesis by Abl-Family Kinases: Emerging Mechanisms and Physiological Contexts. *J. Cell Sci.* 122, 3441–3454. doi: 10.1242/jcs.039859

Bronsert, P., Enderle-Ammour, K., Bader, M., Timme, S., Kuehs, M., Csanadi, A., et al. (2014). Cancer Cell Invasion and EMT Marker Expression: A Three-Dimensional Study of the Human Cancer-Host Interface. *J. Pathol.* 234, 410–422. doi: 10.1002/path.4416

Burute, M., Prioux, M., Blin, G., Truchet, S., Letort, G., Tseng, Q., et al. (2017). Polarity Reversal by Centrosome Repositioning Primes Cell Scattering During Epithelial-To-Mesenchymal Transition. *Dev. Cell* 40, 168–184. doi: 10.1016/j.devcel.2016.12.004

Campbell, K., Rossi, F., Adams, J., Pitsidianaki, I., Barriga, F. M., Garcia-Gerique, L., et al. (2019). Collective Cell Migration and Metastases Induced by an Epithelial-to-Mesenchymal Transition in Drosophila Intestinal Tumors. *Nat. Commun.* 10, 2311. doi: 10.1038/s41467-019-10269-y

Capuana, L., Bostrom, A., and Etienne-Manneville, S. (2020). Multicellular Scale Front-to-Rear Polarity in Collective Migration. *Curr. Opin. Cell Biol.* 62, 114–122. doi: 10.1016/j.ceb.2019.10.001

Chaw, S. Y., Abdul Majeed, A., Dalley, A. J., Chan, A., Stein, S., and Farah, C. S. (2012). Epithelial to Mesenchymal Transition (EMT) Biomarkers–E-Cadherin, Beta-Catenin, APC and Vimentin–in Oral Squamous Cell Carcinogenesis and Transformation. *Oral. Oncol.* 48, 997–1006. doi: 10.1016/j.oraloncology.2012.05.011

Chen, S., Su, T., Zhang, Y., Lee, A., He, J., Ge, Q., et al. (2020). Fusobacterium Nucleatum Promotes Colorectal Cancer Metastasis by Modulating KRT7-As/Krt7. *Gut Microbes* 11, 511–525. doi: 10.1080/19490976.2019.1695494

Cheung, K. J., and Ewald, A. J. (2016). A Collective Route to Metastasis: Seeding by Tumor Cell Clusters. *Science* 352, 167–169. doi: 10.1126/science.aaf6546

Choo, Y. W., Jeong, J., and Jung, K. (2020). Recent Advances in Intravital Microscopy for Investigation of Dynamic Cellular Behavior *In Vivo*. *BMB Rep.* 53, 357–366. doi: 10.5483/BMBRep.2020.53.7.069

Christiansen, J. J., and Rajasekaran, A. K. (2006). Reassessing Epithelial to Mesenchymal Transition as a Prerequisite for Carcinoma Invasion and Metastasis. *Cancer Res.* 66, 8319–8326. doi: 10.1158/0008-5472.CAN-06-0410

Clark, A. G., and Vignjevic, D. M. (2015). Modes of Cancer Cell Invasion and the Role of the Microenvironment. *Curr. Opin. Cell Biol.* 36, 13–22. doi: 10.1016/j.ceb.2015.06.004

Datta, A., Deng, S., Gopal, V., Yap, K. C., Halim, C. E., Lye, M. L., et al. (2021). Cytoskeletal Dynamics in Epithelial-Mesenchymal Transition: Insights Into Therapeutic Targets for Cancer Metastasis. *Cancers (Basel)* 13, 1882. doi: 10.3390/cancers13081882

Denais, C. M., Gilbert, R. M., Isermann, P., Mcgregor, A. L., Te Lindert, M., Weigelin, B., et al. (2016). Nuclear Envelope Rupture and Repair During Cancer Cell Migration. *Science* 352, 353–358. doi: 10.1126/science.aad7297

Ding, H., Guo, W., and Su, B. (2020). Imaging Cell-Matrix Adhesions and Collective Migration of Living Cells by Electrochemiluminescence Microscopy. *Angew. Chem. Int. Ed. Engl.* 59, 449–456. doi: 10.1002/anie.201911190

Dominy, S. S., Lynch, C., Ermini, F., Benedyk, M., Marczyk, A., Konradi, A., et al. (2019). Porphyromonas Gingivalis in Alzheimer's Disease Brains: Evidence for Disease Causation and Treatment With Small-Molecule Inhibitors. *Sci. Adv.* 5, eaau3333. doi: 10.1126/sciadv.aau3333

Feng, H., Wang, X., Xu, Z., Zhang, X., and Gao, Y. (2018). Super-Resolution Fluorescence Microscopy for Single Cell Imaging. *Adv. Exp. Med. Biol.* 1068, 59–71. doi: 10.1007/978-981-13-0502-3_6

Fiorillo, L., Cervino, G., Laino, L., D'amico, C., Mauceri, R., Tozum, T. F., et al. (2019). Porphyromonas Gingivalis, Periodontal and Systemic Implications: A Systematic Review. *Dent. J. (Basel)* 7, 114. doi: 10.3390/dj7040114

Fitzsimonds, Z. R., Liu, C., Stocke, K. S., Yakoumatos, L., Shumway, B., Miller, D. P., et al. (2021). Regulation of Olfactomedin 4 by Porphyromonas Gingivalis in a Community Context. *Isme J.* 15, 2627–2642. doi: 10.1038/s41396-021-00956-4

Fitzsimonds, Z. R., Rodriguez-Hernandez, C. J., Bagaitkar, J., and Lamont, R. J. (2020). From Beyond the Pale to the Pale Riders: The Emerging Association of Bacteria With Oral Cancer. *J. Dent. Res.* 99, 604–612. doi: 10.1177/0022034520907341

Fracchia, A., Asraf, T., Salmon-Divon, M., and Gerlitz, G. (2020). Increased Lamin B1 Levels Promote Cell Migration by Altering Perinuclear Actin Organization. *Cells* 9, 2161. doi: 10.3390/cells9102161

Gabriel, E. M., Fisher, D. T., Evans, S., Takabe, K., and Skitzki, J. J. (2018). Intravital Microscopy in the Study of the Tumor Microenvironment: From Bench to Human Application. *Oncotarget* 9, 20165–20178. doi: 10.18632/oncotarget.24957

Gadiya, M., and Chakraborty, G. (2018). Signaling by Discoidin Domain Receptor 1 in Cancer Metastasis. *Cell Adh. Migr.* 12, 315–323. doi: 10.1080/19336918.2018.1520556

Ganly, I., Yang, L., Giese, R. A., Hao, Y., Nossa, C. W., Morris, L. G. T., et al. (2019). Periodontal Pathogens are a Risk Factor of Oral Cavity Squamous Cell Carcinoma, Independent of Tobacco and Alcohol and Human Papillomavirus. *Int. J. Cancer* 145, 775–784. doi: 10.1002/ijc.32152

Geng, F., Liu, J., Guo, Y., Li, C., Wang, H., Wang, H., et al. (2017). Persistent Exposure to Porphyromonas Gingivalis Promotes Proliferative and Invasion Capabilities, and Tumorigenic Properties of Human Immortalized Oral Epithelial Cells. *Front. Cell Infect. Microbiol.* 7, 57. doi: 10.3389/fcimb.2017.00057

Geng, F., Wang, Q., Li, C., Liu, J., Zhang, D., Zhang, S., et al. (2019). Identification of Potential Candidate Genes of Oral Cancer in Response to Chronic Infection With Porphyromonas Gingivalis Using Bioinformatical Analyses. *Front. Oncol.* 9, 91. doi: 10.3389/fonc.2019.00091

Gibieža, P., and Petrikaitė, V. (2021). The Regulation of Actin Dynamics During Cell Division and Malignancy. *Am. J. Cancer Res.* 11, 4050–4069.

Greenburg, G., and Hay, E. D. (1982). Epithelia Suspended in Collagen Gels can Lose Polarity and Express Characteristics of Migrating Mesenchymal Cells. *J. Cell Biol.* 95, 333–339. doi: 10.1083/jcb.95.1.333

Greuber, E. K., Smith-Pearson, P., Wang, J., and Pendergast, A. M. (2013). Role of ABL Family Kinases in Cancer: From Leukaemia to Solid Tumours. *Nat. Rev. Cancer* 13, 559–571. doi: 10.1038/nrc3563

Guo, X., and Hua, Y. (2017). CCAT1: An Oncogenic Long Noncoding RNA in Human Cancers. *J. Cancer Res. Clin. Oncol.* 143, 555–562. doi: 10.1007/s00432-016-2268-3

Guy, J. B., Espenel, S., Vallard, A., Battiston-Montagne, P., Wozny, A. S., Ardail, D., et al. (2017). Evaluation of the Cell Invasion and Migration Process: A Comparison of the Video Microscope-Based Scratch Wound Assay and the Boyden Chamber Assay. *J. Vis. Exp.* 17, 56337. doi: 10.3791/56337

Hajishengallis, G., and Lamont, R. J. (2021). Polymicrobial Communities in Periodontal Disease: Their Quasi-Organismal Nature and Dialogue With the Host. *Periodontol. 2000* 86, 210–230. doi: 10.1111/prd.12371

Ha, N. H., Park, D. G., Woo, B. H., Kim, D. J., Choi, J. I., Park, B. S., et al. (2016). Porphyromonas Gingivalis Increases the Invasiveness of Oral Cancer Cells by Upregulating IL-8 and MMPs. *Cytokine* 86, 64–72. doi: 10.1016/j.cyto.2016.07.013

Harokopakis, E., Albzreh, M. H., Martin, M. H., and Hajishengallis, G. (2006). TLR2 Transmodulates Monocyte Adhesion and Transmigration *via* Rac1- and PI3K-Mediated Inside-Out Signaling in Response to Porphyromonas Gingivalis Fimbriae. *J. Immunol.* 176, 7645–7656. doi: 10.4049/jimmunol.176.12.7645

Haverman, T. M., Laheij, A., De Soet, J. J., De Lange, J., and Rozema, F. R. (2017). Candida and Porphyromonas Gingivalis: The Effect on Wound Closure *In Vitro*. *J. Oral. Microbiol.* 9, 1328266. doi: 10.1080/20002297.2017.1328266

Ha, N. H., Woo, B. H., Kim, D. J., Ha, E. S., Choi, J. I., Kim, S. J., et al. (2015). Prolonged and Repetitive Exposure to Porphyromonas Gingivalis Increases Aggressiveness of Oral Cancer Cells by Promoting Acquisition of Cancer Stem Cell Properties. *Tumour Biol.* 36, 9947–9960. doi: 10.1007/s13277-015-3764-9

Holloway, A., and Storey, A. (2014). A Conserved C-Terminal Sequence of High-Risk Cutaneous Beta-Human Papillomavirus E6 Proteins Alters Localization and Signalling of Beta1-Integrin to Promote Cell Migration. *J. Gen. Virol.* 95, 123–134. doi: 10.1099/vir.0.057695-0

Hong, B. Y., Hoare, A., Cardenas, A., Dupuy, A. K., Choquette, L., Salner, A. L., et al. (2020). The Salivary Mycobiome Contains 2 Ecologically Distinct Mycotypes. *J. Dent. Res.* 99, 730–738. doi: 10.1177/0022034520915879

Hoppe, T., Kraus, D., Probstmeier, R., Jepsen, S., and Winter, J. (2019). Stimulation With Porphyromonas Gingivalis Enhances Malignancy and Initiates Anoikis Resistance in Immortalized Oral Keratinocytes. *J. Cell Physiol.* 234, 21903–21914. doi: 10.1002/jcp.28754

Horwitz, R. (2016). Cellular Biophysics. *Biophys. J.* 110, 993–996. doi: 10.1016/j.bpj.2016.02.002

Hou, J. M., Krebs, M. G., Lancashire, L., Sloane, R., Backen, A., Swain, R. K., et al. (2012). Clinical Significance and Molecular Characteristics of Circulating Tumor Cells and Circulating Tumor Microemboli in Patients With Small-Cell Lung Cancer. *J. Clin. Oncol.* 30, 525–532. doi: 10.1200/JCO.2010.33.3716

Hrudka, J., Fišerová, H., Jelínková, K., Matěj, R., and Waldauf, P. (2021). Cytokeratin 7 Expression as a Predictor of an Unfavorable Prognosis in Colorectal Carcinoma. *Sci. Rep.* 11, 17863. doi: 10.1038/s41598-021-97480-4

Huang, C., Yang, G., Jiang, T., Zhu, G., Li, H., and Qiu, Z. (2011). The Effects and Mechanisms of Blockage of STAT3 Signaling Pathway on IL-6 Inducing EMT in Human Pancreatic Cancer Cells *In Vitro*. *Neoplasma* 58, 396–405. doi: 10.4149/neo_2011_05_396

Hur, S. S., Jeong, J. H., Ban, M. J., Park, J. H., Yoon, J. K., and Hwang, Y. (2020). Traction Force Microscopy for Understanding Cellular Mechanotransduction. *BMB Rep.* 53, 74–81. doi: 10.5483/BMBRep.2020.53.2.308

Hu, D., Zhou, J., Wang, F., Shi, H., Li, Y., and Li, B. (2015). HPV-16 E6/E7 Promotes Cell Migration and Invasion in Cervical Cancer *via* Regulating Cadherin Switch *In Vitro* and *In Vivo*. *Arch. Gynecol. Obstet.* 292, 1345–1354. doi: 10.1007/s00404-015-3787-x

Inaba, H., Amano, A., Lamont, R. J., and Murakami, Y. (2015). Involvement of Protease-Activated Receptor 4 in Over-Expression of Matrix Metalloproteinase 9 Induced by Porphyromonas Gingivalis. *Med. Microbiol. Immunol.* 204, 605–612. doi: 10.1007/s00430-015-0389-y

Inaba, H., Sugita, H., Kuboniwa, M., Iwai, S., Hamada, M., Noda, T., et al. (2014). Porphyromonas Gingivalis Promotes Invasion of Oral Squamous Cell Carcinoma Through Induction of Prommp9 and its Activation. *Cell Microbiol.* 16, 131–145. doi: 10.1111/cmi.12211

Irfan, M., Delgado, R. Z. R., and Frias-Lopez, J. (2020). The Oral Microbiome and Cancer. *Front. Immunol.* 11, 591088. doi: 10.3389/fimmu.2020.591088

Ishikawa, T., Terashima, J., Shimoyama, Y., Ohashi, Y., Mikami, T., Takeda, Y., et al. (2020). Effects of Butyric Acid, a Bacterial Metabolite, on the Migration of Ameloblastoma Mediated by Laminin 332. *J. Oral. Sci.* 62, 435–438. doi: 10.2334/josnusd.19-0380

Iwai, S., Yonekawa, A., Harada, C., Hamada, M., Katagiri, W., Nakazawa, M., et al. (2010). Involvement of the Wnt-Beta-Catenin Pathway in Invasion and Migration of Oral Squamous Carcinoma Cells. *Int. J. Oncol.* 37, 1095–1103. doi: 10.3892/ijo_00000761

Izdebska, M., Zielińska, W., Hałas-Wiśniewska, M., and Grzanka, A. (2020). Involvement of Actin and Actin-Binding Proteins in Carcinogenesis. *Cells* 9, 2245. doi: 10.3390/cells9102245

Jain, P., Worthylake, R. A., and Alahari, S. K. (2012). Quantitative Analysis of Random Migration of Cells Using Time-Lapse Video Microscopy. *J. Vis. Exp.*, 63, e3585. doi: 10.3791/3585

Jang, H., Kim, J., Shin, J. H., Fredberg, J. J., Park, C. Y., and Park, Y. (2019). Traction Microscopy With Integrated Microfluidics: Responses of the Multi-Cellular Island to Gradients of HGF. *Lab. Chip* 19, 1579–1588. doi: 10.1039/C9LC00173E

Jiang, T., Liu, G., Wang, L., and Liu, H. (2015). Elevated Serum Gas6 Is a Novel Prognostic Biomarker in Patients With Oral Squamous Cell Carcinoma. *PloS One* 10, e0133940. doi: 10.1371/journal.pone.0133940

Jurado, C., Haserick, J. R., and Lee, J. (2005). Slipping or Gripping? Fluorescent Speckle Microscopy in Fish Keratocytes Reveals Two Different Mechanisms for Generating a Retrograde Flow of Actin. *Mol. Biol. Cell* 16, 507–518. doi: 10.1091/mbc.e04-10-0860

Kamarajan, P., Ateia, I., Shin, J. M., Fenno, J. C., Le, C., Zhan, L., et al. (2020). Periodontal Pathogens Promote Cancer Aggressivity *via* TLR/MyD88 Triggered Activation of Integrin/FAK Signaling That is Therapeutically Reversible by a Probiotic Bacteriocin. *PloS Pathog.* 16, e1008881. doi: 10.1371/journal.ppat.1008881

Katz, R. R., and West, J. L. (2022). Reductionist Three-Dimensional Tumor Microenvironment Models in Synthetic Hydrogels. *Cancers (Basel)* 14, 1225. doi: 10.3390/cancers14051225

Kleinstein, S. E., Nelson, K. E., and Freire, M. (2020). Inflammatory Networks Linking Oral Microbiome With Systemic Health and Disease. *J. Dent. Res.* 99, 1131–1139. doi: 10.1177/0022034520926126

Kozyrska, K., Pilia, G., Vishwakarma, M., Wagstaff, L., Goschorska, M., Cirillo, S., et al. (2022). P53 Directs Leader Cell Behavior, Migration, and Clearance During Epithelial Repair. *Science* 375, eabl8876. doi: 10.1126/science.abl8876

Kuo, C. W., Chueh, D. Y., and Chen, P. (2019). Real-Time *In Vivo* Imaging of Subpopulations of Circulating Tumor Cells Using Antibody Conjugated Quantum Dots. *J. Nanobiotechnology* 17, 26. doi: 10.1186/s12951-019-0453-7

Laheij, A. M., De Soet, J. J., Veerman, E. C., Bolscher, J. G., and Van Loveren, C. (2013). The Influence of Oral Bacteria on Epithelial Cell Migration *In Vitro*. *Mediators Inflamm.* 2013, 154532. doi: 10.1155/2013/154532

Lamont, R. J., Fitzsimonds, Z. R., Wang, H., and Gao, S. (2022). Role of Porphyromonas Gingivalis in Oral and Orodigestive Squamous Cell Carcinoma. *Periodontol. 2000.* 89, 154–165. doi: 10.1111/prd.12425

Lamont, R. J., Koo, H., and Hajishengallis, G. (2018). The Oral Microbiota: Dynamic Communities and Host Interactions. *Nat. Rev. Microbiol.* 16, 745–759. doi: 10.1038/s41579-018-0089-x

Lauffenburger, D. A., and Horwitz, A. F. (1996). Cell Migration: A Physically Integrated Molecular Process. *Cell* 84, 359–369. doi: 10.1016/S0092-8674(00)81280-5

Lawson, C. D., and Ridley, A. J. (2018). Rho GTPase Signaling Complexes in Cell Migration and Invasion. *J. Cell Biol.* 217, 447–457. doi: 10.1083/jcb.201612069

Lee, J., Roberts, J. S., Atanasova, K. R., Chowdhury, N., Han, K., and Yilmaz, O. (2017). Human Primary Epithelial Cells Acquire an Epithelial-Mesenchymal-Transition Phenotype During Long-Term Infection by the Oral Opportunistic Pathogen, Porphyromonas Gingivalis. *Front. Cell Infect. Microbiol.* 7, 493. doi: 10.3389/fcimb.2017.00493

Lee, K., Roberts, J. S., Choi, C. H., Atanasova, K. R., and Yilmaz, Ö. (2018). Porphyromonas Gingivalis Traffics Into Endoplasmic Reticulum-Rich-Autophagosomes for Successful Survival in Human Gingival Epithelial Cells. *Virulence* 9, 845–859. doi: 10.1080/21505594.2018.1454171

Leggett, S. E., Hruska, A. M., Guo, M., and Wong, I. Y. (2021). The Epithelial-Mesenchymal Transition and the Cytoskeleton in Bioengineered Systems. *Cell Commun. Signal* 19, 32. doi: 10.1186/s12964-021-00713-2

Liang, G., Wang, H., Shi, H., Zhu, M., An, J., Qi, Y., et al. (2020). Porphyromonas Gingivalis Promotes the Proliferation and Migration of Esophageal Squamous Cell Carcinoma Through the miR-194/GRHL3/PTEN/Akt Axis. *ACS Infect. Dis.* 6, 871–881. doi: 10.1021/acsinfecdis.0c00007

Liao, C., Wang, Q., An, J., Long, Q., Wang, H., Xiang, M., et al. (2021). Partial EMT in Squamous Cell Carcinoma: A Snapshot. *Int. J. Biol. Sci.* 17, 3036–3047. doi: 10.7150/ijbs.61566

Li, C. F., Chen, J. Y., Ho, Y. H., Hsu, W. H., Wu, L. C., Lan, H. Y., et al. (2019). Snail-Induced Claudin-11 Prompts Collective Migration for Tumour Progression. *Nat. Cell Biol.* 21, 251–262. doi: 10.1038/s41556-018-0268-z

Liu, C. C., Cai, D. L., Sun, F., Wu, Z. H., Yue, B., Zhao, S. L., et al. (2017). FERMT1 Mediates Epithelial-Mesenchymal Transition to Promote Colon Cancer Metastasis *via* Modulation of β-Catenin Transcriptional Activity. *Oncogene* 36, 1779–1792. doi: 10.1038/onc.2016.339

Liu, J., Hsieh, C. L., Gelincik, O., Devolder, B., Sei, S., Zhang, S., et al. (2019). Proteomic Characterization of Outer Membrane Vesicles From Gut Mucosa-Derived Fusobacterium Nucleatum. *J. Proteomics* 195, 125–137. doi: 10.1016/j.jprot.2018.12.029

Liu, L., Liang, L., Yang, C., Zhou, Y., and Chen, Y. (2021c). Extracellular Vesicles of Fusobacterium Nucleatum Compromise Intestinal Barrier Through Targeting RIPK1-Mediated Cell Death Pathway. *Gut Microbes* 13, 1–20. doi: 10.1080/19490976.2021.1902718

Liu, D., Liu, S., Liu, J., Miao, L., Zhang, S., and Pan, Y. (2021b). sRNA23392 Packaged by Porphyromonas Gingivalis Outer Membrane Vesicles Promotes Oral Squamous Cell Carcinomas Migration and Invasion by Targeting Desmocollin-2. *Mol. Oral. Microbiol.* 36, 182–191. doi: 10.1111/omi.12334

Liu, C., Stocke, K., Fitzsimonds, Z. R., Yakoumatos, L., Miller, D. P., and Lamont, R. J. (2021a). A Bacterial Tyrosine Phosphatase Modulates Cell Proliferation Through Targeting RGCC. *PloS Pathog.* 17, e1009598. doi: 10.1371/journal.ppat.1009598

Li, T. H., Zhao, B. B., Qin, C., Wang, Y. Y., Li, Z. R., Cao, H. T., et al. (2021). IFIT1 Modulates the Proliferation, Migration and Invasion of Pancreatic Cancer Cells *via* Wnt/β-Catenin Signaling. *Cell Oncol. (Dordr)* 44, 1425–1437. doi: 10.1007/s13402-021-00651-8

Lovisa, S., Lebleu, V. S., Tampe, B., Sugimoto, H., Vadnagara, K., Carstens, J. L., et al. (2015). Epithelial-To-Mesenchymal Transition Induces Cell Cycle Arrest and Parenchymal Damage in Renal Fibrosis. *Nat. Med.* 21, 998–1009. doi: 10.1038/nm.3902

Lu, P., and Lu, Y. (2021). Born to Run? Diverse Modes of Epithelial Migration. *Front. Cell Dev. Biol.* 9, 704939. doi: 10.3389/fcell.2021.704939

Mak, M., Reinhart-King, C. A., and Erickson, D. (2011). Microfabricated Physical Spatial Gradients for Investigating Cell Migration and Invasion Dynamics. *PloS One* 6, e20825. doi: 10.1371/journal.pone.0020825

Mcneill, M. C., Wray, J., Sala-Newby, G. B., Hindmarch, C. C. T., Smith, S. A., Ebrahimighaei, R., et al. (2020). Nuclear Actin Regulates Cell Proliferation and Migration *via* Inhibition of SRF and TEAD. *Biochim. Biophys. Acta Mol. Cell Res.* 1867, 118691. doi: 10.1016/j.bbamcr.2020.118691

Mehanna, H., Beech, T., Nicholson, T., El-Hariry, I., Mcconkey, C., Paleri, V., et al. (2013). Prevalence of Human Papillomavirus in Oropharyngeal and Nonoropharyngeal Head and Neck Cancer–Systematic Review and Meta-Analysis of Trends by Time and Region. *Head Neck* 35, 747–755. doi: 10.1002/hed.22015

Mosier, J. A., Schwager, S. C., Boyajian, D. A., and Reinhart-King, C. A. (2021). Cancer Cell Metabolic Plasticity in Migration and Metastasis. *Clin. Exp. Metastasis* 38, 343–359. doi: 10.1007/s10585-021-10102-1

Ng, L. G., Mrass, P., Kinjyo, I., Reiner, S. L., and Weninger, W. (2008). Two-Photon Imaging of Effector T-Cell Behavior: Lessons From a Tumor Model. *Immunol. Rev.* 221, 147–162. doi: 10.1111/j.1600-065X.2008.00596.x

Nonaka, S., and Nakanishi, H. (2020). Secreted Gingipains From Porphyromonas Gingivalis Induce Microglia Migration Through Endosomal Signaling by Protease-Activated Receptor 2. *Neurochem. Int.* 140, 104840. doi: 10.1016/j.neuint.2020.104840

Ohshima, J., Wang, Q., Fitzsimonds, Z. R., Miller, D. P., Sztukowska, M. N., Jung, Y. J., et al. (2019). Streptococcus Gordonii Programs Epithelial Cells to Resist ZEB2 Induction by Porphyromonas Gingivalis. *Proc. Natl. Acad. Sci. U .S. A.* 116, 8544–8553. doi: 10.1073/pnas.1900101116

Padera, T. P., Stoll, B. R., So, P. T., and Jain, R. K. (2002). Conventional and High-Speed Intravital Multiphoton Laser Scanning Microscopy of Microvasculature, Lymphatics, and Leukocyte-Endothelial Interactions. *Mol. Imaging* 1, 9–15. doi: 10.1162/153535002753395662

Parhi, L., Alon-Maimon, T., Sol, A., Nejman, D., Shhadeh, A., Fainsod-Levi, T., et al. (2020). Breast Cancer Colonization by Fusobacterium Nucleatum Accelerates Tumor Growth and Metastatic Progression. *Nat. Commun.* 11, 3259. doi: 10.1038/s41467-020-16967-2

Pastushenko, I., and Blanpain, C. (2019). EMT Transition States During Tumor Progression and Metastasis. *Trends Cell Biol.* 29, 212–226. doi: 10.1016/j.tcb.2018.12.001

Patterson, A. D., Gonzalez, F. J., Perdew, G. H., and Peters, J. M. (2018). Molecular Regulation of Carcinogenesis: Friend and Foe. *Toxicol. Sci.* 165, 277–283. doi: 10.1093/toxsci/kfy185

Paul, C. D., Hung, W. C., Wirtz, D., and Konstantopoulos, K. (2016). Engineered Models of Confined Cell Migration. *Annu. Rev. BioMed. Eng.* 18, 159–180. doi: 10.1146/annurev-bioeng-071114-040654

Pinner, S., Jordan, P., Sharrock, K., Bazley, L., Collinson, L., Marais, R., et al. (2009). Intravital Imaging Reveals Transient Changes in Pigment Production and Brn2 Expression During Metastatic Melanoma Dissemination. *Cancer Res.* 69, 7969–7977. doi: 10.1158/0008-5472.CAN-09-0781

Prakash, V., Carson, B. B., Feenstra, J. M., Dass, R. A., Sekyrova, P., Hoshino, A., et al. (2019). Ribosome Biogenesis During Cell Cycle Arrest Fuels EMT in Development and Disease. *Nat. Commun.* 10, 2110. doi: 10.1038/s41467-019-10100-8

Qi, Y. J., Jiao, Y. L., Chen, P., Kong, J. Y., Gu, B. L., Liu, K., et al. (2020). Porphyromonas Gingivalis Promotes Progression of Esophageal Squamous Cell Cancer *via* TGFbeta-Dependent Smad/YAP/TAZ Signaling. *PloS Biol.* 18, e3000825. doi: 10.1371/journal.pbio.3000825

Raab, M., Gentili, M., De Belly, H., Thiam, H. R., Vargas, P., Jimenez, A. J., et al. (2016). ESCRT III Repairs Nuclear Envelope Ruptures During Cell Migration to Limit DNA Damage and Cell Death. *Science* 352, 359–362. doi: 10.1126/science.aad7611

Radaic, A., and Kapila, Y. L. (2021). The Oralome and its Dysbiosis: New Insights Into Oral Microbiome-Host Interactions. *Comput. Struct. Biotechnol. J.* 19, 1335–1360. doi: 10.1016/j.csbj.2021.02.010

Rando, O. J., Zhao, K., Janmey, P., and Crabtree, G. R. (2002). Phosphatidylinositol-Dependent Actin Filament Binding by the SWI/SNF-Like BAF Chromatin Remodeling Complex. *Proc. Natl. Acad. Sci. U .S. A.* 99, 2824–2829. doi: 10.1073/pnas.032662899

Ridley, A. J. (1999). Rho Family Proteins and Regulation of the Actin Cytoskeleton. *Prog. Mol. Subcell. Biol.* 22, 1–22. doi: 10.1007/978-3-642-58591-3_1

Ridley, A. J., Schwartz, M. A., Burridge, K., Firtel, R. A., Ginsberg, M. H., Borisy, G., et al. (2003). Cell Migration: Integrating Signals From Front to Back. *Science* 302, 1704–1709. doi: 10.1126/science.1092053

Rusu, A. D., and Georgiou, M. (2020). The Multifarious Regulation of the Apical Junctional Complex. *Open Biol.* 10, 190278. doi: 10.1098/rsob.190278

Sahai, E., and Marshall, C. J. (2003). Differing Modes of Tumour Cell Invasion Have Distinct Requirements for Rho/ROCK Signalling and Extracellular Proteolysis. *Nat. Cell Biol.* 5, 711–719. doi: 10.1038/ncb1019

Scott, A. J., Alexander, J. L., Merrifield, C. A., Cunningham, D., Jobin, C., Brown, R., et al. (2019). International Cancer Microbiome Consortium Consensus Statement on the Role of the Human Microbiome in Carcinogenesis. *Gut* 68, 1624–1632. doi: 10.1136/gutjnl-2019-318556

Senini, V., Amara, U., Paul, M., and Kim, H. (2019). Porphyromonas Gingivalis Lipopolysaccharide Activates Platelet Cdc42 and Promotes Platelet Spreading and Thrombosis. *J. Periodontol.* 90, 1336–1345. doi: 10.1002/JPER.18-0596

Shao, W., Fujiwara, N., Mouri, Y., Kisoda, S., Yoshida, K., Yoshida, K., et al. (2021). Conversion From Epithelial to Partial-EMT Phenotype by Fusobacterium Nucleatum Infection Promotes Invasion of Oral Cancer Cells. *Sci. Rep.* 11, 14943. doi: 10.1038/s41598-021-94384-1

Shih, W., and Yamada, S. (2012). N-Cadherin-Mediated Cell-Cell Adhesion Promotes Cell Migration in a Three-Dimensional Matrix. *J. Cell Sci.* 125, 3661–3670. doi: 10.1242/jcs.103861

Shi, J., Zeng, X., Zhou, M., and Chen, Q. (2009). Activation of ERK-FAK Signaling Pathway and Enhancement of Cell Migration Involved in the Early Interaction Between Oral Keratinocytes and Candida Albicans. *Mycopathologia* 167, 1–7. doi: 10.1007/s11046-008-9142-z

Son, H., and Moon, A. (2010). Epithelial-Mesenchymal Transition and Cell Invasion. *Toxicol. Res.* 26, 245–252. doi: 10.5487/TR.2010.26.4.245

Stemmler, M. P., Eccles, R. L., Brabletz, S., and Brabletz, T. (2019). Non-Redundant Functions of EMT Transcription Factors. *Nat. Cell Biol.* 21, 102–112. doi: 10.1038/s41556-018-0196-y

Stone, R. C., Pastar, I., Ojeh, N., Chen, V., Liu, S., Garzon, K. I., et al. (2016). Epithelial-Mesenchymal Transition in Tissue Repair and Fibrosis. *Cell Tissue Res.* 365, 495–506. doi: 10.1007/s00441-016-2464-0

Stroka, K. M., Jiang, H., Chen, S. H., Tong, Z., Wirtz, D., Sun, S. X., et al. (2014). Water Permeation Drives Tumor Cell Migration in Confined Microenvironments. *Cell* 157, 611–623. doi: 10.1016/j.cell.2014.02.052

Strutz, F., Zeisberg, M., Ziyadeh, F. N., Yang, C. Q., Kalluri, R., Muller, G. A., et al. (2002). Role of Basic Fibroblast Growth Factor-2 in Epithelial-Mesenchymal Transformation. *Kidney Int.* 61, 1714–1728. doi: 10.1046/j.1523-1755.2002.00333.x

Sur-Erdem, I., Hussain, M. S., Asif, M., Pınarbası, N., Aksu, A. C., and Noegel, A. A. (2020). Nesprin-1 Impact on Tumorigenic Cell Phenotypes. *Mol. Biol. Rep.* 47, 921–934. doi: 10.1007/s11033-019-05184-w

Sztukowska, M. N., Ojo, A., Ahmed, S., Carenbauer, A. L., Wang, Q., Shumway, B., et al. (2016). Porphyromonas Gingivalis Initiates a Mesenchymal-Like Transition Through ZEB1 in Gingival Epithelial Cells. *Cell Microbiol.* 18, 844–858. doi: 10.1111/cmi.12554

Tang, S. W., Yang, T. C., Lin, W. C., Chang, W. H., Wang, C. C., Lai, M. K., et al. (2011). Nicotinamide N-Methyltransferase Induces Cellular Invasion Through Activating Matrix Metalloproteinase-2 Expression in Clear Cell Renal Cell Carcinoma Cells. *Carcinogenesis* 32, 138–145. doi: 10.1093/carcin/bgq225

Tentler, D., Lomert, E., Novitskaya, K., and Barlev, N. A. (2019). Role of ACTN4 in Tumorigenesis, Metastasis, and EMT. *Cells* 8, 1427. doi: 10.3390/cells8111427

Tokuraku, K., Kuragano, M., and Uyeda, T. Q. P. (2020). Long-Range and Directional Allostery of Actin Filaments Plays Important Roles in Various Cellular Activities. *Int. J. Mol. Sci.* 21, 3209. doi: 10.3390/ijms21093209

Trappmann, B., Baker, B. M., Polacheck, W. J., Choi, C. K., Burdick, J. A., and Chen, C. S. (2017). Matrix Degradability Controls Multicellularity of 3D Cell Migration. *Nat. Commun.* 8, 371. doi: 10.1038/s41467-017-00418-6

Trepat, X., Chen, Z., and Jacobson, K. (2012). Cell Migration. *Compr. Physiol.* 2, 2369–2392. doi: 10.1002/cphy.c110012

Vicente-Manzanares, M., Koach, M. A., Whitmore, L., Lamers, M. L., and Horwitz, A. F. (2008). Segregation and Activation of Myosin IIB Creates a Rear in Migrating Cells. *J. Cell Biol.* 183, 543–554. doi: 10.1083/jcb.200806030

Vilchez Mercedes, S. A., Bocci, F., Levine, H., Onuchic, J. N., Jolly, M. K., and Wong, P. K. (2021). Decoding Leader Cells in Collective Cancer Invasion. *Nat. Rev. Cancer* 21, 592–604. doi: 10.1038/s41568-021-00376-8

Wang, S., Liu, Y., Li, J., Zhao, L., Yan, W., Lin, B., et al. (2021). Fusobacterium Nucleatum Acts as a Pro-Carcinogenic Bacterium in Colorectal Cancer: From Association to Causality. *Front. Cell Dev. Biol.* 9, 710165. doi: 10.3389/fcell.2021.710165

Wang, Q., Song, R., Zhao, C., Liu, H., Yang, Y., Gu, S., et al. (2019). HPV16 E6 Promotes Cervical Cancer Cell Migration and Invasion by Downregulation of NHERF1. *Int. J. Cancer* 144, 1619–1632. doi: 10.1002/ijc.31876

Wang, H., Tao, L., Jin, F., Gu, H., Dai, X., Ni, T., et al. (2017). Cofilin 1 Induces the Epithelial-Mesenchymal Transition of Gastric Cancer Cells by Promoting Cytoskeletal Rearrangement. *Oncotarget* 8, 39131–39142. doi: 10.18632/oncotarget.16608

Wang, Q., Yu, C., Yue, C., and Liu, X. (2020). Fusobacterium Nucleatum Produces Cancer Stem Cell Characteristics *via* EMT-Resembling Variations. *Int. J. Clin. Exp. Pathol.* 13, 1819–1828.

Warburton, A., Redmond, C. J., Dooley, K. E., Fu, H., Gillison, M. L., Akagi, K., et al. (2018). HPV Integration Hijacks and Multimerizes a Cellular Enhancer to Generate a Viral-Cellular Super-Enhancer That Drives High Viral Oncogene Expression. *PloS Genet.* 14, e1007179. doi: 10.1371/journal.pgen.1007179

Weigelin, B., Bakker, G. J., and Friedl, P. (2012). Intravital Third Harmonic Generation Microscopy of Collective Melanoma Cell Invasion: Principles of Interface Guidance and Microvesicle Dynamics. *Intravital* 1, 32–43. doi: 10.4161/intv.21223

Whitmore, S. E., and Lamont, R. J. (2014). Oral Bacteria and Cancer. *PloS Pathog.* 10, e1003933. doi: 10.1371/journal.ppat.1003933

Willis, J. R., and Gabaldon, T. (2020). The Human Oral Microbiome in Health and Disease: From Sequences to Ecosystems. *Microorganisms* 8, 308. doi: 10.3390/microorganisms8020308

Wolf, K., Alexander, S., Schacht, V., Coussens, L. M., Von Andrian, U. H., Van Rheenen, J., et al. (2009). Collagen-Based Cell Migration Models *In Vitro* and *In Vivo*. *Semin. Cell Dev. Biol.* 20, 931–941. doi: 10.1016/j.semcdb.2009.08.005

Wu, Y., and Zhou, B. P. (2010). Snail: More Than EMT. *Cell Adh. Migr.* 4, 199–203. doi: 10.4161/cam.4.2.10943

Xu, C., Fan, L., Lin, Y., Shen, W., Qi, Y., Zhang, Y., et al. (2021a). Fusobacterium Nucleatum Promotes Colorectal Cancer Metastasis Through miR-1322/CCL20 Axis and M2 Polarization. *Gut Microbes* 13, 1980347. doi: 10.1080/19490976.2021.1980347

Xu, X., Wang, Y., Choi, W. S., Sun, X., and Godbout, R. (2021b). Super Resolution Microscopy Reveals DHA-Dependent Alterations in Glioblastoma Membrane Remodelling and Cell Migration. *Nanoscale* 13, 9706–9722. doi: 10.1039/D1NR02128A

Yang, H. W., Collins, S. R., and Meyer, T. (2016). Locally Excitable Cdc42 Signals Steer Cells During Chemotaxis. *Nat. Cell Biol.* 18, 191–201. doi: 10.1038/ncb3292

Yang, Y., Zheng, H., Zhan, Y., and Fan, S. (2019). An Emerging Tumor Invasion Mechanism About the Collective Cell Migration. *Am. J. Transl. Res.* 11, 5301–5312.

Young, L. S., Yap, L. F., and Murray, P. G. (2016). Epstein-Barr Virus: More Than 50 Years Old and Still Providing Surprises. *Nat. Rev. Cancer* 16, 789–802. doi: 10.1038/nrc.2016.92

Zhang, Y., Wang, X., Li, H., Ni, C., Du, Z., and Yan, F. (2018). Human Oral Microbiota and its Modulation for Oral Health. *BioMed. Pharmacother.* 99, 883–893. doi: 10.1016/j.biopha.2018.01.146

Zhou, Y., Sztukowska, M., Wang, Q., Inaba, H., Potempa, J., Scott, D. A., et al. (2015). Noncanonical Activation of β-Catenin by Porphyromonas Gingivalis. *Infect. Immun.* 83, 3195–3203. doi: 10.1128/IAI.00302-15

Conflict of Interest: The authors declare that the research was conducted in the absence of any commercial or financial relationships that could be construed as a potential conflict of interest.

Publisher's Note: All claims expressed in this article are solely those of the authors and do not necessarily represent those of their affiliated organizations, or those of the publisher, the editors and the reviewers. Any product that may be evaluated in this article, or claim that may be made by its manufacturer, is not guaranteed or endorsed by the publisher.

frontiers | Frontiers in Cellular and Infection Microbiology

ORIGINAL RESEARCH
published: 10 May 2022
doi: 10.3389/fcimb.2022.904488

Diaryl Urea Derivative Molecule Inhibits Cariogenic *Streptococcus mutans* by Affecting Exopolysaccharide Synthesis, Stress Response, and Nitrogen Metabolism

Ying Liao[1], *Mengyun Zhang*[2], *Xingnan Lin*[3*†] *and Fuhua Yan*[4*†]

[1] Department of Pediatric Dentistry, Nanjing Stomatological Hospital, Medical School of Nanjing University, Nanjing, China, [2] Nanjing Stomatological Hospital, Medical School of Nanjing University, Nanjing, China, [3] School/Hospital of Stomatology, Zhejiang Chinese Medical University, Hangzhou, China, [4] Department of Periodontology, Nanjing Stomatological Hospital, Medical School of Nanjing University, Nanjing, China

OPEN ACCESS

Edited by:
Xin Xu,
Sichuan University, China

Reviewed by:
Zhengwei Huang,
Shanghai Jiao Tong University, China
Yuan Liu,
University of Pennsylvania, United States

***Correspondence:**
Fuhua Yan
yanfh@nju.edu.cn
Xingnan Lin
linxingnan@126.com

[†]These authors share last authorship

Specialty section:
This article was submitted to Microbiome in Health and Disease, a section of the journal Frontiers in Cellular and Infection Microbiology

Received: 25 March 2022
Accepted: 11 April 2022
Published: 10 May 2022

Citation:
Liao Y, Zhang M, Lin X and Yan F (2022) Diaryl Urea Derivative Molecule Inhibits Cariogenic Streptococcus mutans by Affecting Exopolysaccharide Synthesis, Stress Response, and Nitrogen Metabolism. Front. Cell. Infect. Microbiol. 12:904488. doi: 10.3389/fcimb.2022.904488

Different small molecules have been developed to target cariogenic bacteria *Streptococcus mutans*. Based on target-based designing and *in silico* screening, a novel diaryl urea derivative, 1,3-bis[3,5-bis(trifluoromethyl)phenyl]urea (BPU), has previously been found effective in inhibiting the growth of *S. mutans*. However, the exact mechanism remains unclear. This current study aimed to explore the antimicrobial and antibiofilm effects of BPU on *S. mutans* and locate key enzymes and biological processes affected by the molecule *via in silico* molecular docking analysis and transcriptomic profile. Our *in vitro* results confirmed that BPU was capable of inhibiting planktonic growth as well as biofilm formation of *S. mutans*. The virtual binding analysis predicted that the molecule had strong binding potentials with vital enzymes (3AIC and 2ZID) involved in extracellular exopolysaccharide (EPS) synthesis. The predicted inhibitive binding was further confirmed by *in vitro* quantification of EPS, which found a decreased amount of EPS in the biofilms. The transcriptomic profile also found differential expression of genes involved in EPS synthesis. Moreover, the transcriptomic profile implied alterations in stress response and nitrogen metabolism in *S. mutans* treated with BPU. Examination of differentially expressed genes involved in these biological processes revealed that altered gene expression could contribute to impaired growth, biofilm formation, and competitiveness of *S. mutans*. In conclusion, the novel diaryl urea derivative BPU can inhibit the virulence of *S. mutans* by affecting different biological processes and serves as a potent anti-caries agent.

Keywords: dental caries, *Streptococcus mutans*, transcriptomic study, small molecules, stress response, nitrogen metabolism

INTRODUCTION

The prevention and treatment of dental caries have long been associated with the interference of cariogenic bacteria in the oral cavity. Traditional anti-caries agents, including fluoride and antibiotics, have been reported to contribute to local and systematic toxicity, as well as drug resistance (Liao et al., 2017; Qiu et al., 2020). Novel anti-caries chemicals are required to inhibit the growth and metabolism of cariogenic microorganisms while exerting limited side effects.

Various small molecules have been developed to target cariogenic microorganisms including the notorious species, *Streptococcus mutans* (Cui et al., 2019; Yang et al., 2021). These small molecules usually have unique structures to target specific metabolic pathways and vital enzymes in bacterial cells (Zhang et al., 2015). Different approaches, including drug repositioning, library screening, natural products screening, and target-based designing, have been applied to identify small molecules that have anti-caries potentials (Yang et al., 2021). Among them, target-based designing and *in silico* screening from the small-molecule library have been of special interest, as they provide hits with good specificity and high throughput (Younson and Kelly, 2004; Nijampatnam et al., 2016; Nijampatnam et al., 2021).

Based on the abovementioned methods, a previous study identified a series of small molecules that have the potential to enhance fluoride toxicity in bacterial cells (Nelson et al., 2015). One of the small molecules, 1,3-bis[3,5-bis(trifluoromethyl) phenyl]urea (BPU; **Figure 1A**), was found to be especially effective in inhibiting the growth of *Escherichia coli* and *S. mutans* when used in combination with fluoride (Nelson et al., 2015). The enhanced antimicrobial ability was suggested to be associated with the trifluoromethyl substituents on the aryl rings, which facilitate fluoride/chloride uptake and/or retention (Busschaert et al., 2012; Nelson et al., 2015). Further investigation of the molecule structure reveals that the trifluoromethyl substituents are not the only structure related to antimicrobial effects. The diaryl rings in the small molecule contribute as hydrogen-bond donors and have been proved to be able to bind and inhibit specific bacterial proteins including DNA gyrase B and penicillin-binding protein 1a (Limban et al., 2020; Sroor et al., 2021). Moreover, similar urea derivatives have been used to target pathogenic bacteria such as *Staphylococcus aureus*, *Pseudomonas aeruginosa*, and *Enterococcus faecalis* (Wu, 1965; Gunduz et al., 2020). The preliminary structure investigation indicated that BPU has the potential to exert an inhibitive effect against *S. mutans* alone and act as a novel anti-caries agent. However, no *in vitro* result has been reported to support the antimicrobial effect of BPU alone on *S. mutans*. Also, the exact inhibition site and affected biological processes remain unknown.

In this study, we investigated the antimicrobial and antibiofilm effects of the novel diaryl urea derivative, namely, BPU, against *S. mutans* UA159. *In silico* molecular docking analysis was applied to predict the binding potential and binding site of the small molecule with different proteins in *S. mutans* cells. Transcriptomic analysis was performed to validate the predictions and locate major biological processes that were affected by the small molecule.

MATERIALS AND METHODS

In Silico Molecular Docking

The three-dimensional structure of BPU was downloaded from PubChem (Cas no. 3824-74-6). The structure was geometrically optimized and energy minimized using ChemBio3D Ultra 14.0 software. A total of 20 proteins originating from *S. mutans* were selected for *in silico* molecular docking (**Table 1**). These proteins were selected because they have been reported to be associated with the virulence of *S. mutans* and their crystal structures were available online. Crystal structures of targeted proteins were obtained from Protein Data Bank (PDB) with accession codes. The protein structures were processed step by step including the removal of original ligands and water molecules, the addition of polar hydrogen atoms, and charge calculation and distribution using PyMOL v2.3.0 and AutoDocktools v1.5.6. Docking analysis was performed using AotoDock Vina v1.1.2 with default parameters. Results with the strongest protein–ligand interactions were visualized and analyzed with PyMOL v2.3.0 and LigPlot v2.2.4.

Experimental Chemicals, Bacterial Strain, and Growth Conditions

Different amount of BPU (Sigma-Aldrich, CA, USA) was dissolved in acetonitrile (Aladdin, Nanjing, China) for *in vitro* studies. *S. mutans* UA159 was obtained from the State Key Laboratory of Oral Disease (Sichuan University, Chengdu, China). Bacteria were routinely grown in brain heart infusion (BHI) broth (BD, NJ, USA) or on BHI agar plates at 37°C anaerobically (10% H_2, 5% CO_2, and 85% N_2). For biofilm formation, 1% sucrose (Sigma-Aldrich, CA, USA) was added to the BHI broth.

Planktonic Growth Assay

The antimicrobial effect of BPU on planktonic *S. mutans* UA159 was tested using a growth curve. *S. mutans* UA159 was incubated in BHI broth until the early log phase (OD_{600} = 0.2). Bacterial cells were pelleted and resuspended with fresh BHI broth containing 1, 2, 5, 10, 20, and 50 μg/ml of BPU. For blank control, fresh BHI broth containing the same volume of acetonitrile was used to resuspend bacterial cells. Resuspensions measuring 200 μl were then added into wells of a sterile 96-well microplate. The microplate was sealed with a transparent sealer and incubated at 37°C for 12 h. Growth was monitored by recording the optical density at 600 nm (OD_{600}) every 30 min with Spectra MaxM3 (Molecular Devices, CA, USA).

Crystal Violet Assay

The biomass of *S. mutans* biofilms with or without BPU treatment was quantified with a crystal violet staining assay. *S. mutans* UA159 was incubated until mid-log phase (OD_{600} = 0.5),

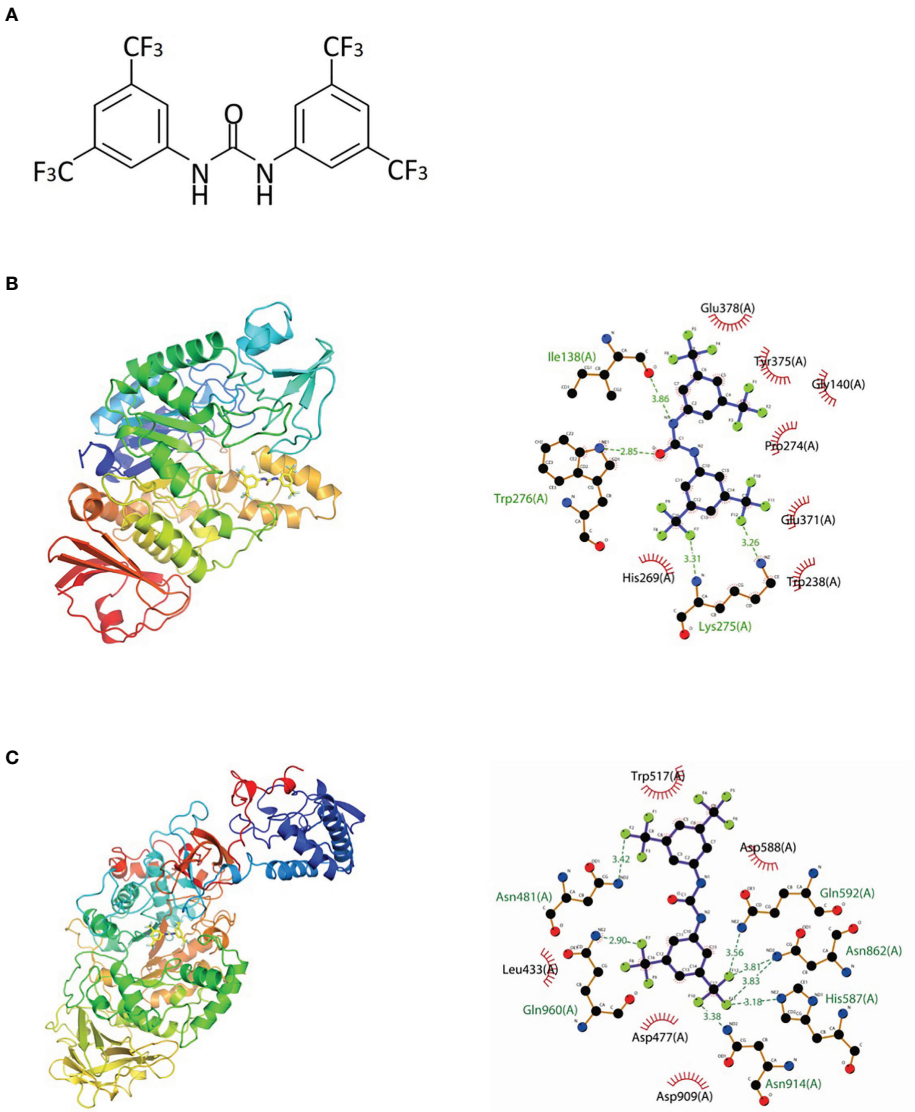

FIGURE 1 | Chemical structure and molecular docking analysis. **(A)** Chemical structure of 1,3-bis[3,5-bis(trifluoromethyl)phenyl]urea (BPU) molecule. **(B, C)** Predicted binding mode (left, 3D; right, 2D) of BPU molecule with 2ZID **(B)** and 3AIC **(C)**. Hydrogen bond is shown with green dashed lines (right). Hydrophobic interaction is shown with red "eyelashes".

pelleted, and resuspended with fresh BHI broth supplemented with 1% (w/w) sucrose (BHIS). Resuspensions were transferred to a sterile 96-well microplate, and BPU was added to reach different final concentrations (1, 2, 5, 10, 20, and 50 μg/ml). The same volume of acetonitrile was added to the control group. After anaerobic incubation at 37°C for 24 h, all wells were washed with sterile phosphate-buffered saline (PBS) to remove loose cells. Biofilms attached to the bottom of the wells were fixed with 4% paraformaldehyde (Sigma-Aldrich, CA, USA) for 15 min followed by staining with 0.01% crystal violet solution (Adamas, Shanghai, China) for 8 min. Solutions were then removed, and biofilms were again washed with PBS twice. Acetic acid (33% v/v, Sigma-Aldrich, CA, USA) was added to each well to destain for 10 min. The destaining solution was then transferred to a new 96-well plate, and OD_{575} was recorded with Spectra MaxM3.

Biofilm Formation on Saliva-Coated Hydroxyapatite Discs

Biofilms of *S. mutans* UA159 were formed on saliva-coated hydroxyapatite (sHA) discs using a previously described method with a few modifications (Wang et al., 2020). Briefly, HA discs (8 mm in diameter and 2 mm in thickness; Baiameng Bioactive Materials, Chengdu, China) were sonicated in deionized water for 10 min and sterilized at 121°C for 15 min before use. Clarified saliva was prepared by centrifuging whole

TABLE 1 | Proteins selected for molecular docking study.

PDB accession	Annotation
5UQZ	Glucan binding protein C
3BJV	Putative phosphotransferase system enzyme IIA (PtxA)
6CAM	Glucan binding protein C (sucrose-dependent)
3CZC	Putative phosphotransferase system enzyme IIB (PtxB)
3QE5	C-germinal region of Antigen I/II
3AIE	Glucansucrase
3OPU	C-terminal domain of surface protein (SpaP)
2HVV	dCMP deaminase
3AIC	Glucosyltransferase (GtfC)
4TSH	Surface protein adhesin P1
3EXT	3-Keto-L-gulonate 6-phosphate decarboxylase
2ZID	Dextran glucosidase (DexB)
2RI0	Glucosamine 6-phosphate deaminase (NagB)
3L8R	Putative phosphotransferase system, cellobiose-specific IIA (PtcA)
2NQ5	Methyltransferase
3OIX	Putative dihydroorotate dehydrogenase
5ZA3	C-terminal domain of response regulator (VicR)
3PN8	Putative 6-phospho-beta-glucosidase
6TZL	Surface protein adhesin (SspB)
3K8U	Peptidase domain of putative ABC transporter, ATP-binding protein (ComA)
3M7V	Phosphopentomutase (DeoB)

unstimulated saliva of a healthy human donor at 4,000 rpm for 20 min at 4°C, followed by filtration through 0.22-μm polyethersulfone membrane (Koo et al., 2010). The sterile HA discs were placed into 24-well plates. Each well contained clarified saliva mixed with the same volume of desorption buffer (containing 500 mM of KCl, 10 mM of $CaCl_2$, 1 mM of $MgCl_2$, 6.2 mM of K_2HPO_4, and 14 mM of KH_2PO_4). After incubation in clarified saliva and desorption buffer at 37°C for 30 min, the sHA discs were ready for use.

S. mutans UA159 was incubated in BHI broth until the mid-log phase (OD_{600} = 0.5). Cells were then pelleted and resuspended in BHIS. Resuspended bacterial cells were transferred to sterile 24-well plates with different concentrations of BPU or the same volume of acetonitrile. The abovementioned sHA discs were placed in each well. Plates were incubated anaerobically at 37°C for 24 h. Biofilms formed on the surface of sHA discs were used for further examinations.

Scanning Electron Microscopy

Twenty-four-hour biofilms attached to the surface of sHA discs were harvested and washed twice with cysteine peptone water (CPW; containing yeast extract, peptone, sodium chloride, and cysteine HCl, pH 7.2). Biofilms were fixed with 2.5% glutaraldehyde (Adamas, Shanghai, China) at 4°C overnight, followed by serial dehydration with ethanol (30%, 40%, 50%, 60%, 70%, 80%, 90%, and 100%). Samples were dried and coated with gold before observation with SEM (Quanta 400 FEG, FEI, Hillsboro, OR, USA).

pH Drop Examination

Acid production of *S. mutans* biofilms was examined with a pH drop of the supernatant. Culture media of the abovementioned biofilms measuring 2 ml formed on sHA discs were taken at 0, 4, 8, 12, and 24 h and centrifuged at 4°C at 4,000 rpm for 10 min. The pH of the supernatant was measured with an electronic pH meter (FiveEasy Plus, FE28-standard, Mettler-Toledo, Schwerzenbach, Switzerland).

Confocal Laser Scanning Microscopy Analysis

A commercial LIVE/DEAD BacLight Viability Kit (Life Technologies, NY, USA) was used to stain viable and dead cells in 24-h biofilms. *S. mutans* biofilms formed on sHA discs were harvested after 24-h incubation. The staining of bacterial cells was processed according to the manufacturer's instructions. Viable cells and dead cells were respectively stained with SYTO 9 (excitation, 480 nm; emission, 500 nm) and propidium iodide (PI; excitation, 490 nm; emission, 635 nm). Samples were observed with confocal laser scanning microscopy (CLSM; NikonA1; Nikon Inc., Tokyo, Japan). Images were taken at an interval of 10 μm. Integrated fluorescence density was quantified with ImageJ software (v1.48, National Institutes of Health, USA).

Water-Insoluble Exopolysaccharide Determination

Production of water-insoluble exopolysaccharide (EPS) by *S. mutans* biofilms was examined qualitatively by fluorescence staining and quantitatively by the anthrone–sulfuric method (Tang et al., 2019). For fluorescence staining, Alexa Fluor 647 (Life Technologies, NY, USA) was used to label EPS, and SYTO 9 was used to label bacterial cells. Alexa Fluor 647 was added to the BHIS medium at the beginning of 24-h biofilm formation. Biofilms were stained with SYTO 9 at the end of the 24-h biofilm formation experiment. Samples were then observed using CLSM with the same procedure as live/dead staining.

To quantify EPS synthesis with the anthrone–sulfuric method, 24-h biofilms were harvested and scraped from sHA discs and washed with PBS buffer. The planktonic cells and suspension were removed by centrifuging the mixture at 4,000 rpm for 10 min at 4°C. The precipitate was mixed with 0.4 mol/L of NaOH and incubated for 2 h at 37°C. The mixture was centrifuged again, and the suspension was collected and transferred to a new EP tube. The suspension was mixed with three volumes of the anthrone–sulfuric acid reagent (Macklin, Shanghai, China) and heated on a heat block at 95°C for 5 min until the reaction was complete. The solution was cooled to room temperature before being transferred to a new 96-well plate. Absorbance at 625 nm was recorded, and the amount of polysaccharide was calculated according to the standard curve.

RNA Sequencing and Data Analysis

For transcriptomic analysis, *S. mutans* UA159 was grown in BHI until the log phase (OD_{600} = 0.5). Cells were harvested and resuspended with fresh BHI. Cells were challenged with either a final concentration of 2 μg/ml of BPU or the same volume of acetonitrile for 1 h. This concentration was chosen mainly based on results from crystal violet assay to make sure that there was enough BPU to induce significant alterations in gene expression,

while potential toxicity was kept as low as possible. Samples were then harvested with centrifugation and kept at −80°C until used. Total RNA was extracted using TRIzol reagent (Invitrogen, OR, USA). The concentration and quality of RNA were determined with Nanodrop 2000 spectrophotometer (Thermo Scientific, MA, USA). rRNA was removed from total RNA using Zymo-Seq RiboFree Total RNA Library Kit. cDNA library was constructed by Shanghai Personal Biotechnology Co. Ltd (Shanghai, China). RNA sequencing was performed on Novaseq 6000 platform (Illumina, San Diego, CA, USA).

Data were filtered and controlled for quality before analysis. Filtered reads were mapped to the *S. mutans* UA159 reference genome (RefSeq NC_004350.2) using Bowtie 2 (version 2.2.6). Differentially expressed genes (DEGs) were recognized as transcripts with $|\log_2\text{FoldCHange}| > 1$ and $p < 0.05$. Differential expression analysis was performed using DESeq (version 1.30.0). All DEGs were annotated by searching the Gene Ontology (GO) databases. All genes were mapped to terms in the GO database, and numbers of differentially enriched genes in each term were calculated. GO enrichment analysis was performed using the topGO R package on the differential genes. GO terms with significantly enriched differential genes ($p < 0.05$ according to the hypergeometric distribution method) were identified to determine the main biological functions of DEGs. Three individual samples were sequenced for each group.

Statistical Analyses

Data were analyzed using Prism (version 9.0.0). All experiments were performed at least in triplicate. Student's *t*-test or one-way ANOVA was employed to compare data from two or more groups. A *p*-value of <0.05 was considered statistically significant.

RESULTS

In Silico Screening for Potential Binding Site

The binding potentials of BPU with 20 selected proteins originating from *S. mutans* are shown in **Table 2**. A higher absolute value indicates a stronger binding ability. Proteins with the highest scores were 3M7V (phosphopentomutase), 2ZID (dextran glucosidase), and 3AIC (glucosyltransferase). These three proteins were further visualized to predict the binding mode. Hydrogen bond and hydrophobic interaction acted as the main interaction forces. We further examined the potential binding sites occupied by the BPU molecule. While there was not enough information on 3M7V, we did find interesting results for 2ZID and 3AIC (**Figure 1**). The molecule can bind several vital amino acid residues of 2ZID, which were involved in the active binding pocket (Lys 275, His269, and Pro274), recognition of substrate (Glu371), and high level of enzyme activity toward long-chain substrates (Trp238) (Hondoh et al., 2008). Also, the molecule may competitively bind several conserved amino acid residues of 3AIC (His587, Asp588, Asp477, Asn481, and Asp909), which were responsible for the recognition of glucosyl moiety of the primary sucrose (Ito et al., 2011). One of the amino acid residues (Gln592) bound by the molecule was found to be involved in the catalytic domains of 3AIC (Ito et al., 2011).

TABLE 2 | Binding potential with selected proteins (kcal/mol).

PDB accession	Binding potential	PDB accession	Binding potential	PDB accession	Binding potential
3M7V	−10.3	2HVV	−8.7	3QE5	−7.6
2ZID	−9.6	2NQ5	−8.7	3L8R	−7.4
3AIC	−9.6	6CAM	−8.6	3OPU	−7.2
6TZL	−9.5	4TSH	−8.5	5ZA3	−6.8
3AIE	−9.5	3OIX	−8.4	3K8U	−6.6
2RI0	−9	5UQZ	−8.1	3PN8	−6.5
3BJV	−8.8	3EXT	−7.6	3CZC	−5.6

PDB, Protein Data Bank.

Inhibition of Planktonic Growth

Compared to the control groups (treated with deionized water or acetonitrile), incubation with different levels of BPU significantly inhibited the growth of planktonic *S. mutans* UA159 in BHI broth (**Figure 2**). With a trace amount of drug in the culture (1 μg/ml), hardly any growth could be noticed in the bacterial culture.

Inhibition of Biofilm Formation and Acid Production

Biomass of *S. mutans* UA159 biofilms treated with different levels of BPU was determined with crystal violet assay. As shown in **Figure 3A**, no significant difference was noticed between groups treated with deionized water and acetonitrile. Treatment of 1 μg/ml of BPU resulted in the loss of half of the biomass as compared to the control groups. Higher concentrations of BPU almost completely inhibited biofilm formation. Similar results were visualized with SEM examination (**Figure 3B**). Biofilms on sHA discs treated with 1 and 2 μg/ml of BPU were much thinner as compared to the control group. While biofilms of the control group appeared dense and highly stereoscopic, biofilms treated with BPU seemed plainer with more porous structures and less extracellular matrix in the system (**Figure 3B**).

CLSM also found severe inhibition of biofilm formation and maturation by BPU (**Figure 4**). Strong green fluorescence in the control group (treated with acetonitrile) indicated a large number of viable cells in the biofilms. Biofilms treated with BPU exhibited significantly less green fluorescence and enhanced red fluorescence as compared to the control group (**Figure 4A**). Quantified mean fluorescence intensity confirmed that the signal of green fluorescence was remarkably lower in BPU-treated groups when compared with the control group (**Figure 4B**).

Figure 5 shows the pH change of the supernatant of *S. mutans* biofilms treated with or without BPU within 24 h. As expected, biofilms treated with acetonitrile (control) were able to decrease environmental pH from 7.40 to 3.58 ± 0.03 within 24 h. Once treated with BPU, very little pH drop was noticed. At 24 h, pH of supernatant was similar for the 1 μg/ml and 2 μg/ml groups (pH 6.84 ± 0.08 and 6.87 ± 0.02, respectively).

Inhibition of Exopolysaccharide Synthesis by *Streptococcus mutans* Biofilms

EPS synthesis by *S. mutans* biofilms was examined using CLSM analysis and the anthrone–sulfuric method. CLSM images clearly showed that treatment of 1 and 2 μg/ml of BPU disrupted the ability of biofilms to synthesize EPS. Along with the decrease in EPS, the number of bacterial cells in biofilms also reduced significantly (**Figure 6**). While the control group exhibited thick, dense bacterial aggregations, groups treated with BPU appeared to be more dispersed with much thinner structures and fewer extracellular matrix connections (**Figure 6**).

The amount of EPS synthesized by biofilms treated with or without BPU was further examined using the anthrone–sulfuric method. Groups treated with deionized water and acetonitrile synthesized 0.53 ± 0.06 and 0.51 ± 0.06 mg/ml of EPS, respectively. The amount of EPS from two experimental groups (treated with 1 and 2 μg/ml of BPU) was both below the detection limit.

Transcriptomic Analysis of *Streptococcus mutans* Treated With Diaryl Urea Derivative

Transcriptomic analysis revealed that a total of 701 DEGs were identified in the experimental group, including 270 upregulated genes and 431 downregulated genes. GO enrichment analysis indicated that a total of 68 GO terms involved in molecular function and biological processes were affected. A rich factor was calculated for 20 GO terms with the smallest false discovery rate (FDR) values (**Figure 7**). The results showed that GO term unfolded protein binding, protein folding, and exonuclease activity had the largest rich factors. A directed acyclic graph (DAG) was used to further display the relationship of the enriched GO terms. In cellular component, while not statistically significant, most differences were found in the cytoplasm (GO: 0005737), extracellular region (GO: 0005578), cell wall (GO: 0005618), and primosome complex (GO: 1990077). In molecular function, the difference was mostly concentrated in exonuclease activity (GO: 0004527), unfolded protein binding (GO: 0051082), and nucleic acid binding (GO: 0003676). In biological process, genes associated with protein folding (GO: 0006437), regulation of primary metabolic process (GO: 0080090), regulation of nitrogen compound metabolic process (GO: 0051171), and cellular nitrogen compound metabolic process (0031323) were most significantly differentially expressed (**Figure 7**).

We further looked into DEGs related to the regulation of metabolic processes and DEGs related to the regulation of macromolecule metabolic processes (**Supplementary Figures 1, 2**; **Supplementary Tables 1, 2**). Eleven genes involved in the regulation of metabolic process were upregulated, and 59 genes were downregulated. Most of them were associated with transcriptional regulation, sucrose metabolism, and nitrogen metabolism. For regulation of macromolecule metabolic process, 10 genes were upregulated and 58 downregulated. Among them were genes involved in EPS synthesis (*sacR*, *scrR*, and *msmR*), stress tolerance (*rex*, *perR*, *spxA*, *clpE*, and *ciaR*), and nitrogen metabolism (*glnB*, *glnR*, *ciaR*, and *clpE*).

Differential expression of genes associated with protein functions of 3AIC, 2ZID, and 3M7V was also examined (**Figure 8**). As 3AIC and 2ZID are both proteins involved in EPS synthesis, genes associated with EPS synthesis (*gtfB*, *gtfC*, *ftf*, *dexA*, *dexB*, and *scrB*) were selected. For 3M7V, its encoding gene (*deoB*) and two related genes involved in the pentose phosphate pathway (*gapN* and *rpiA*) were selected. The heatmap shows that most genes involved in EPS synthesis, including encoding genes of 3AIC and 2ZID (*gtfC* and *dexB*), were upregulated. The encoding gene of 3M7V (*deoB*) was not found differentially expressed. Its related genes showed different regulatory directions (*gapN* was upregulated and *rpiA* was downregulated).

DISCUSSION

Small molecule compounds have been extensively explored as potent anti-caries agents targeting caries-associated bacteria. In this study, we described the antimicrobial and antibiofilm effects

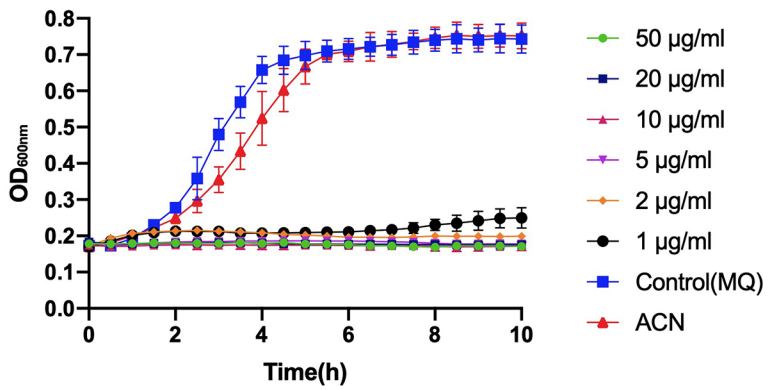

FIGURE 2 | Growth curve of planktonic *Streptococcus mutans* UA159 incubated with 1, 2, 5, 10, 20, and 50 μg/ml of 1,3-bis[3,5-bis(trifluoromethyl)phenyl]urea (BPU). The same volumes of deionized water (MQ) and acetonitrile (ACN) were added to control groups. Values indicate means ± SDs from three independent experiments.

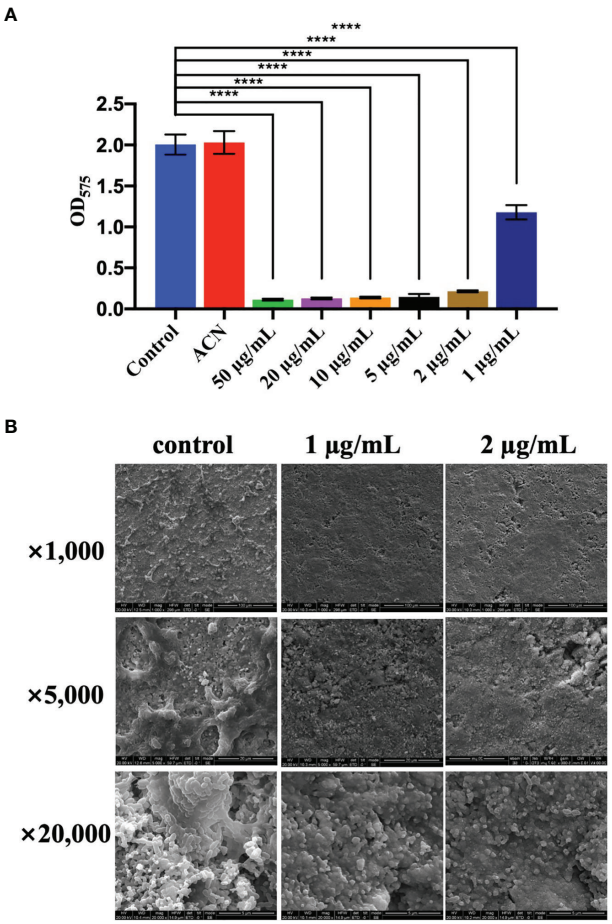

FIGURE 3 | Effect of different levels of 1,3-bis[3,5-bis(trifluoromethyl)phenyl]urea (BPU) on biofilm formation of *Streptococcus mutans* UA159. **(A)** Biomass of biofilms quantified with crystal violet staining assay. **(B)** Representative SEM images of biofilms treated with 1 and 2 μg/ml of BPU or acetonitrile (control). Means ± SDs from three independent experiments are shown. **** indicates $p < 0.0001$.

of a novel diaryl urea derivative, BPU. *In silico* simulation indicated that the small molecule compound had the potential to bind the key enzymes involved in EPS biosynthesis and the pentose phosphate pathway. The transcriptomic study suggested that except for EPS synthesis, nitrogen metabolism and stress-responsive pathway were also affected by the small molecule.

Diaryl rings have previously been suggested to be able to bind specific bacterial proteins (Limban et al., 2020; Sroor et al., 2021) and act as enzyme inhibitors. Our *in silico* molecular docking also found strong binding potential between BPU and several enzymes involved in the biological processes of *S. mutans*. Interestingly, 2 of the top 3 hits (2ZID and 3AIC) are involved in the biosynthesis of EPS. EPS is the main component of the extracellular matrix of bacterial biofilms, and the ability to synthesize EPS is a vital virulence factor of *S. mutans* (Koo et al., 2013; Krzysciak et al., 2014; Klein et al., 2015). Protein 2ZID is a dextran glucosidase hydrolyzing the α-1,6-glucosidic linkage of α-1,6-D-glucans and derived oligosaccharides (Hondoh et al., 2008). Protein 3AIC is a glucosyltransferase responsible for water-insoluble and water-soluble glucan syntheses in *S. mutans* (Ito et al., 2011). The binding mode prediction shows that the diaryl urea derivative molecule binds to either substrate binding pocket or catalytic domains of the two proteins. This indicates that the binding of the molecule can competitively inhibit the activity of 3AIC and 2ZID. A review of the literature shows that a number of 3AIC inhibitors have been proved effective in inhibiting biofilm formation of *S. mutans* and thus caries development (Ren et al., 2016; Zhang et al., 2017; Lin et al., 2021). In this study, we noticed significantly less biofilm formation after BPU treatment with crystal violet assay and SEM observation. CLSM examination and EPS quantification further confirmed that production of EPS was severely impaired by the treatment of BPU. Further transcriptomic analysis revealed that both genes encoding 3AIC and 2ZID (*gtfC* and *dexB*) were upregulated in *S. mutans* treated with BPU. The expression of several genes with associated functions, including *gtfB*, *ftf*, and *dexA* (Li and Burne, 2001; Koo et al., 2013; Yang et al., 2019), was also upregulated. This could be a result of negative feedback of the inhibited activity of corresponding proteins. Accordingly, genes encoding related transcription repressors (*sacR* and *scrR*)

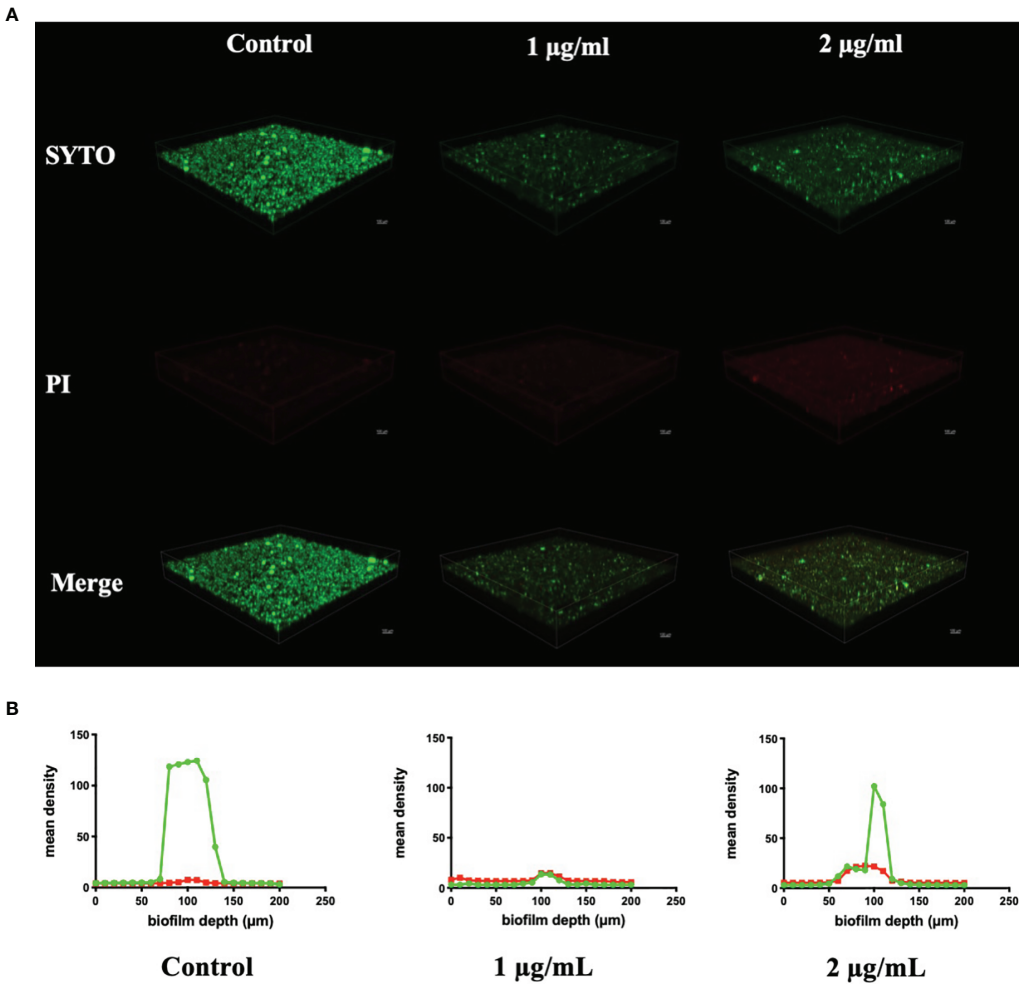

FIGURE 4 | Live/dead staining of *Streptococcus mutans* UA159 biofilms treated with 1 and 2 μg/ml of 1,3-bis[3,5-bis(trifluoromethyl)phenyl]urea (BPU). **(A)** Representative three-dimensional visualization of live (green) and dead (red) cells in *S. mutans* biofilms formed on saliva-coated hydroxyapatite (sHA) discs. **(B)** Mean density of green and red fluorescence throughout *S. mutans* biofilms quantified using ImageJ software.

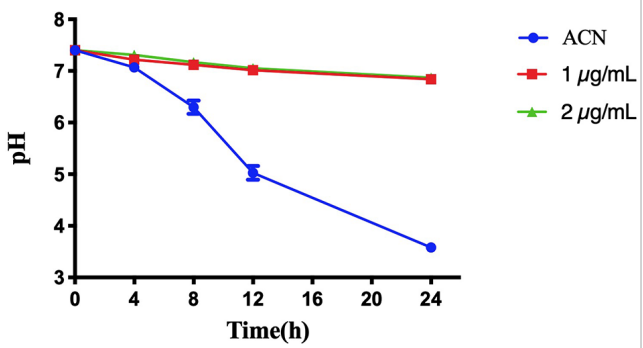

FIGURE 5 | pH change of the supernatant of *Streptococcus mutans* UA159 biofilms treated with or without 1,3-bis[3,5-bis(trifluoromethyl)phenyl]urea (BPU). Values are presented as means ± SDs from three independent experiments. ACN, acetonitrile.

were downregulated (**Supplementary Table 1**) (Siegers and Entian, 1995; Hiratsuka et al., 1998), further confirming that bacterial cells were combating the inhibitive effect of BPU on EPS synthesis.

Our results suggest that the treatment of BPU not only inhibits biofilm formation but also affects planktonic growth. An examination of the transcriptomic profile revealed that, except for the EPS synthesis pathway, multiple genes involved in stress response were differentially expressed. Previous studies have found that the function of stress response proteins is important for bacterial physiology. Deficiency of oxidative stress response regulator Rex has been found to lead to an extended lag phase of planktonic growth of *S. mutans* (Bitoun et al., 2011). Moreover, expression of *gtfC* was also found significantly differentially expressed due to deficiency of Rex, leading to decreased biofilm formation and altered biofilm morphology (Bitoun et al., 2011). In our study, the downregulation of *rex* could be associated with decreased

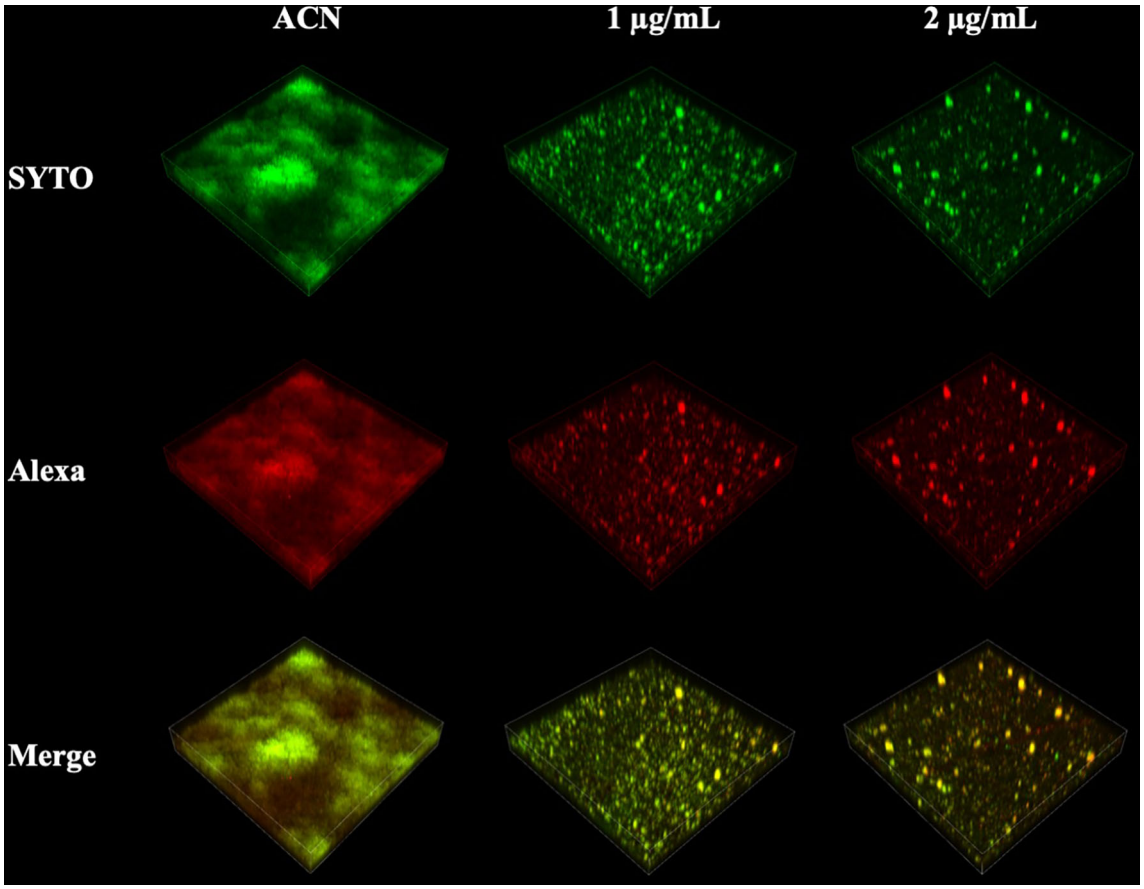

FIGURE 6 | Confocal laser scanning microscopy (CLSM) images of *Streptococcus mutans* biofilm exopolysaccharide (EPS) synthesis affected by 1,3-bis[3,5-bis (trifluoromethyl) phenyl]urea (BPU). Green, bacterial cells (stained with SYTO 9); red, EPS (stained with Alexa 647). Representative three-dimensional images are exhibited.

planktonic growth and biofilm formation. The regulatory effect of SpxA has been implicated in oxidative stress response, antibiotic response, and biofilm formation (Pamp et al., 2006; Kajfasz et al., 2015; Nilsson et al., 2019). Similarly, two genes involved in oxidative and thermal stress responses, *clpE* and *ciaR*, have the ability to affect the biofilm formation of *S. mutans* (Zhu et al., 2017; Biswas et al., 2021). All three abovementioned genes involved in stress response were found to be downregulated in the current study after BPU treatment (**Supplementary Table 2**). The involvement of stress response indicates new targets for novel anti-caries agents.

Additionally, relatively abundant changes in nitrogen metabolism in the BPU-treated group were observed in the transcriptomic profile. By metabolizing nitrogen-containing compounds, mainly amino sugars such as glucosamine and *N*-acetylglucosamine, bacteria are provided with essential materials for macromolecule synthesis (Ardin et al., 2014). The ability to utilize amino sugars is also closely associated with the competitiveness of bacteria to thrive in the oral cavity (Chen et al., 2020). The current study reports the downregulation of genes encoding a membrane ammonium transporter (*glnB*) (Ardin et al., 2014) and a glutamine synthetase regulator (*glnR*) (Chen et al., 2010). Results of *in silico* molecular docking suggest that a key factor affecting cellular entrance of amino acid, NagB (2RI0), has a relatively high binding potential with BPU molecule (−9 kcal/mol, **Table 2**) (Kawada-Matsuo et al., 2012). The potential inhibition of NagB together with the downregulation of associated genes supports that nitrogen metabolism may be inhibited by the diaryl urea derivative. The resulting decreased synthesis of virulence-related factors, including cell surface protein antigen and glucosyltransferase, can lead to less bacterial aggregation and thus less biofilm formation (Kawada-Matsuo et al., 2012).

The molecular docking analysis suggests that the BPU molecule has the potential to bind to an enzyme involved in the pentose phosphate pathway (3M7V, DeoB). According to previous studies, DeoB acts as a vital role in the pentose phosphate pathway, providing a precursor for phosphoribosyl pyrophosphate, which is involved in histidine and purine biosynthesis (Tozzi et al., 2006; Xue et al., 2012). However, we did not notice significant changes in expression of the encoding gene *deoB* in groups treated with BPU in the transcriptional profile. Nor did we find an obvious change in the pentose phosphate pathway according to GO enrichment analysis. One

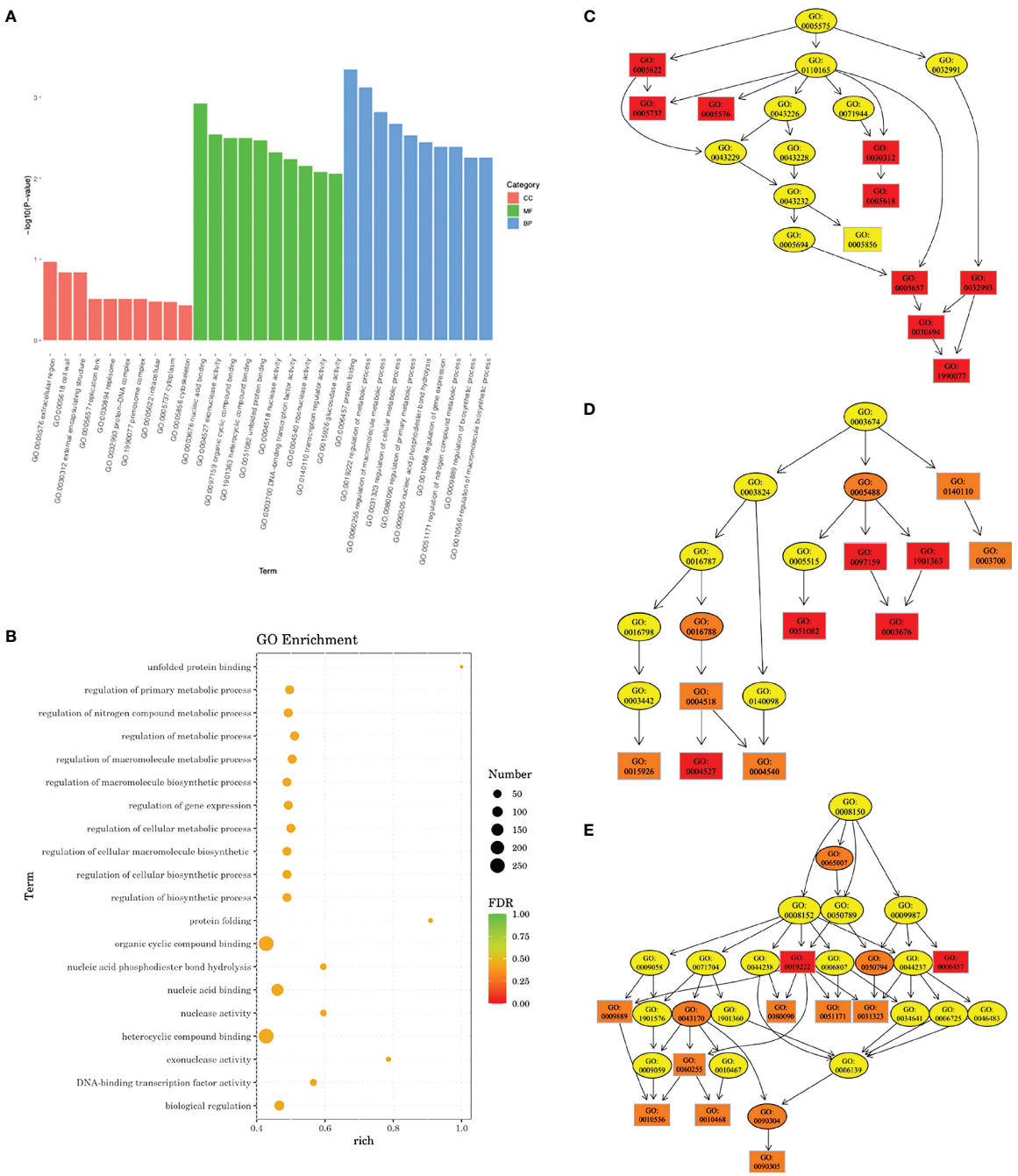

FIGURE 7 | Gene Ontology (GO) enrichment analysis of transcriptomic profile. **(A)** Bar plot showing the most significantly enriched GO terms. CC, cellular component; MF, molecular function; BP, biological process. **(B)** Rich factors of 20 GO terms with the smallest false discovery rate (FDR) values. Directed acyclic graph (DAG) in cellular component **(C)**, molecular function **(D)**, and biological process **(E)**. Deeper color indicates a higher level of enrichment. GO accession number is shown.

explanation is that while a strong binding potential exists between the molecule and the protein, the binding site may not be close to the essential substrate or metal ion binding site. Therefore, the activity of 3M7V and the pentose phosphate pathway may not be significantly affected. Till now, very little information on the functional groups of 3M7V is available, and the effect of the diaryl urea derivative on the protein and its associated pathway requires further validation.

Based on the structure of BPU, previous literature predicted that it may affect cell wall biosynthesis and membrane permeability (Nelson et al., 2015). We were expecting to find changes in GO terms involved in cellular component using GO

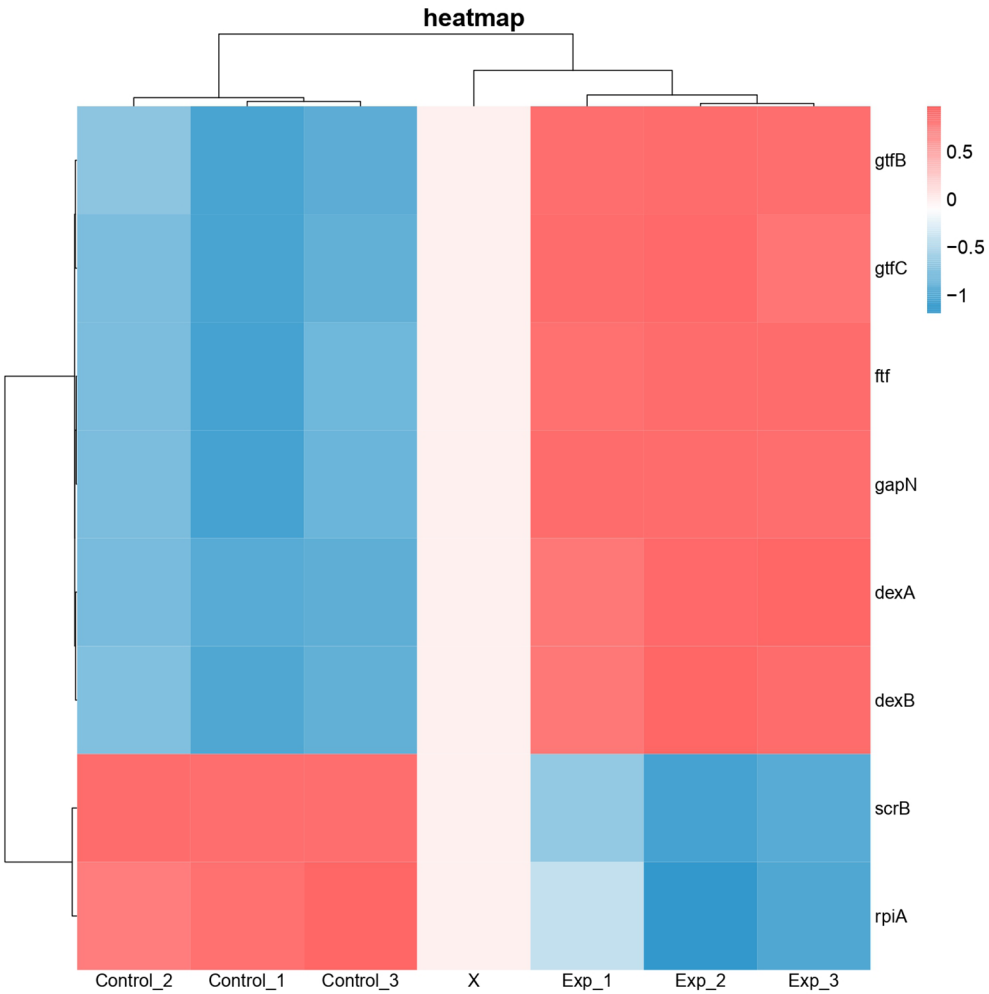

FIGURE 8 | Heatmap of differentially expressed genes associated with protein functions of 3AIC, 2ZID, and 3M7V. Control groups were treated with acetonitrile. Experimental groups were treated with 2 μg/ml of 1,3-bis[3,5-bis(trifluoromethyl)phenyl]urea (BPU). Genes *gtfB*, *gtfC*, *ftf*, *dexA*, *dexB*, and *scrB* are involved in exopolysaccharide biosynthesis. Genes *gapN* and *rplA* are involved in pentose phosphate pathway. Blue indicates lower expression, and red indicates higher expression.

enrichment analysis. However, no significant alteration was found. We looked specifically into genes involved in the GO term "cell wall" and found 3 DEGs (**Supplementary Table 3**). What may be of interest is that 2 upregulated genes, *spaP* and *dexA*, encode cell surface proteins, which are important for the adherence of *S. mutans* to the tooth surface (SpaP) and dextran-dependent aggregation (DexA) (Goldschmidt et al., 1990; Yang et al., 2019). This is again in accordance with the upregulation of other EPS synthesis-related genes. The results suggest that multiple steps and factors involved in or associated with EPS synthesis are influenced by the diaryl urea derivative.

In the present study, we noticed a strong inhibitive effect of BPU on growth, biofilm formation, and acidogenesis of *S. mutans*. Instead of being dosage-dependent, the inhibition seemed to be similar among groups treated with different concentrations of BPU. In other words, the inhibitory effect seemed to be an "ON/OFF" mode. In fact, this is not the first time that we found this kind of inhibition mode in *S. mutans*. One possible explanation is that the small molecule affects essential factor(s) involved in bacterial growth and/or metabolism. For example, our previous study confirmed that different concentrations of fluoride led to similar levels of inhibition of enolase activity, a key enzyme in glycolysis, in an *S. mutans* strain (Liao et al., 2018). As we found alterations in several biological signs of progress including sugar metabolism, nitrogen metabolism, and stress response, it is difficult to identify the major switch for the "ON/OFF" inhibition. Further knockout studies could help disclose the inhibitory "switch" of BPU.

In conclusion, our current study has confirmed the strong antimicrobial and antibiofilm effects of a novel urea derivative molecule, BPU, against caries-associated *S. mutans*. Structure-based *in silico* prediction together with the transcriptomic study has suggested the involvement of several biological processes affected by the small molecule. It is predicted that the treatment

of BPU could alter the expression of genes involved in EPS synthesis, stress response, and nitrogen metabolism, leading to immediate and strong inhibition of bacterial growth, acid production, and biofilm formation. Our work illustrates that BPU is a promising agent to be used in caries prevention.

DATA AVAILABILITY STATEMENT

The transcriptomic data presented in the study are deposited in NCBI SRA database with accession number PRJNA819867.

AUTHOR CONTRIBUTIONS

YL and FY contributed to the conception and design of the study. YL and MZ conducted the experiments. YL performed the transcriptomic analysis. All authors contributed to the interpretation of the data. YL wrote the first draft of the manuscript. All authors contributed to the manuscript revision and approved the submitted version.

FUNDING

This work was supported by the National Natural Science Funds (grant number 82001035), the Jiangsu Natural Science Funds (grant number SBK2020041847), the Nanjing Clinical Research Center for Oral Diseases (grant number 2019060009), and the "3456" Cultivation Program for Junior Talents of Nanjing Stomatological School, Medical School of Nanjing University (grant number).

SUPPLEMENTARY MATERIAL

The Supplementary Material for this article can be found online at: https://www.frontiersin.org/articles/10.3389/fcimb.2022.904488/full#supplementary-material

REFERENCES

Ardin, A. C., Fujita, K., Nagayama, K., Takashima, Y., Nomura, R., Nakano, K., et al. (2014). Identification and Functional Analysis of an Ammonium Transporter in Streptococcus Mutans. *PloS One* 9 (9), e107569. doi: 10.1371/journal.pone.0107569

Biswas, S., Dhaked, H. P. S., Keightley, A., and Biswas, I. (2021). Involvement of ClpE ATPase in Physiology of Streptococcus Mutans. *Microbiol. Spectr.* 9 (3), e0163021. doi: 10.1128/Spectrum.01630-21

Bitoun, J. P., Nguyen, A. H., Fan, Y., Burne, R. A., and Wen, Z. T. (2011). Transcriptional Repressor Rex Is Involved in Regulation of Oxidative Stress Response and Biofilm Formation by Streptococcus Mutans. *FEMS Microbiol. Lett.* 320 (2), 110–117. doi: 10.1111/j.1574-6968.2011.02293.x

Busschaert, N., Kirby, I. L., Young, S., Coles, S. J., Horton, P. N., Light, M. E., et al. (2012). Squaramides as Potent Transmembrane Anion Transporters. *Angew Chem. Int. Ed Engl.* 51 (18), 4426–4430. doi: 10.1002/anie.201200729

Chen, P. M., Chen, Y. Y., Yu, S. L., Sher, S., Lai, C. H., and Chia, J. S. (2010). Role of GlnR in Acid-Mediated Repression of Genes Encoding Proteins Involved in Glutamine and Glutamate Metabolism in Streptococcus Mutans. *Appl. Environ. Microbiol.* 76 (8), 2478–2486. doi: 10.1128/AEM.02622-09

Chen, L., Walker, A. R., Burne, R. A., and Zeng, L. (2020). Amino Sugars Reshape Interactions Between Streptococcus Mutans and Streptococcus Gordonii. *Appl. Environ. Microbiol.* 87 (1), e01459–20. doi: 10.1128/AEM.01459-20

Cui, T., Luo, W., Xu, L., Yang, B., Zhao, W., and Cang, H. (2019). Progress of Antimicrobial Discovery Against the Major Cariogenic Pathogen Streptococcus Mutans. *Curr. Issues Mol. Biol.* 32, 601–644. doi: 10.21775/cimb.032.601

Goldschmidt, R. M., Thoren-Gordon, M., and Curtiss, R. (1990). Regions of the Streptococcus Sobrinus spaA Gene Encoding Major Determinants of Antigen I. *J. Bacteriol* 172 (7), 3988–4001. doi: 10.1128/jb.172.7.3988-4001.1990

Gunduz, M. G., Ugur, S. B., Guney, F., Ozkul, C., Krishna, V. S., Kaya, S., et al. (2020). 1,3-Disubstituted Urea Derivatives: Synthesis, Antimicrobial Activity Evaluation and *In Silico* Studies. *Bioorg Chem.* 102, 104104. doi: 10.1016/j.bioorg.2020.104104

Hiratsuka, K., Wang, B., Sato, Y., and Kuramitsu, H. (1998). Regulation of Sucrose-6-Phosphate Hydrolase Activity in Streptococcus Mutans: Characterization of the scrR Gene. *Infect. Immun.* 66 (8), 3736–3743. doi: 10.1128/IAI.66.8.3736-3743.1998

Hondoh, H., Saburi, W., Mori, H., Okuyama, M., Nakada, T., Matsuura, Y., et al. (2008). Substrate Recognition Mechanism of Alpha-1,6-Glucosidic Linkage Hydrolyzing Enzyme, Dextran Glucosidase From Streptococcus Mutans. *J. Mol. Biol.* 378 (4), 913–922. doi: 10.1016/j.jmb.2008.03.016

Ito, K., Ito, S., Shimamura, T., Weyand, S., Kawarasaki, Y., Misaka, T., et al. (2011). Crystal Structure of Glucansucrase From the Dental Caries Pathogen Streptococcus Mutans. *J. Mol. Biol.* 408 (2), 177–186. doi: 10.1016/j.jmb.2011.02.028

Kajfasz, J. K., Rivera-Ramos, I., Scott-Anne, K., Gregoire, S., Abranches, J., and Lemos, J. A. (2015). Transcription of Oxidative Stress Genes Is Directly Activated by SpxA1 and, to a Lesser Extent, by SpxA2 in Streptococcus Mutans. *J. Bacteriol* 197 (13), 2160–2170. doi: 10.1128/JB.00118-15

Kawada-Matsuo, M., Mazda, Y., Oogai, Y., Kajiya, M., Kawai, T., Yamada, S., et al. (2012). GlmS and NagB Regulate Amino Sugar Metabolism in Opposing Directions and Affect Streptococcus Mutans Virulence. *PloS One* 7 (3), e33382. doi: 10.1371/journal.pone.0033382

Klein, M. I., Hwang, G., Santos, P. H., Campanella, O. H., and Koo, H. (2015). Streptococcus Mutans-Derived Extracellular Matrix in Cariogenic Oral Biofilms. *Front. Cell Infect. Microbiol.* 5. doi: 10.3389/fcimb.2015.00010

Koo, H., Falsetta, M. L., and Klein, M. I. (2013). The Exopolysaccharide Matrix: A Virulence Determinant of Cariogenic Biofilm. *J. Dent. Res.* 92 (12), 1065–1073. doi: 10.1177/0022034513504218

Koo, H., Xiao, J., Klein, M. I., and Jeon, J. G. (2010). Exopolysaccharides Produced by Streptococcus Mutans Glucosyltransferases Modulate the Establishment of Microcolonies Within Multispecies Biofilms. *J. Bacteriol* 192 (12), 3024–3032. doi: 10.1128/JB.01649-09

Krzysciak, W., Jurczak, A., Koscielniak, D., Bystrowska, B., and Skalniak, A. (2014). The Virulence of Streptococcus Mutans and the Ability to Form Biofilms. *Eur. J. Clin. Microbiol. Infect. Dis.* 33 (4), 499–515. doi: 10.1007/s10096-013-1993-7

Liao, Y., Brandt, B. W., Li, J., Crielaard, W., Van Loveren, C., and Deng, D. M. (2017). Fluoride Resistance in Streptococcus Mutans: A Mini Review. *J. Oral. Microbiol.* 9 (1), 1344509. doi: 10.1080/20002297.2017.1344509

Liao, Y., Yang, J., Brandt, B. W., Li, J., Crielaard, W., van Loveren, C., et al. (2018). Genetic Loci Associated With Fluoride Resistance in Streptococcus Mutans. *Front. Microbiol.* 9. doi: 10.3389/fmicb.2018.03093

Li, Y., and Burne, R. A. (2001). Regulation of the gtfBC and Ftf Genes of Streptococcus Mutans in Biofilms in Response to pH and Carbohydrate. *Microbiol. (Reading)* 147 (Pt 10), 2841–2848. doi: 10.1099/00221287-147-10-2841

Limban, C., Chifiriuc, M. C., Caproiu, M. T., Dumitrascu, F., Ferbinteanu, M., Pintilie, L., et al. (2020). New Substituted Benzoylthiourea Derivatives: From Design to Antimicrobial Applications. *Molecules* 25 (7), 1478. doi: 10.3390/molecules25071478

Lin, Y., Chen, J., Zhou, X., and Li, Y. (2021). Inhibition of Streptococcus Mutans Biofilm Formation by Strategies Targeting the Metabolism of

Exopolysaccharides. *Crit. Rev. Microbiol.* 47 (5), 667–677. doi: 10.1080/1040841X.2021.1915959

Nelson, J. W., Plummer, M. S., Blount, K. F., Ames, T. D., and Breaker, R. R. (2015). Small Molecule Fluoride Toxicity Agonists. *Chem. Biol.* 22 (4), 527–534. doi: 10.1016/j.chembiol.2015.03.016

Nijampatnam, B., Ahirwar, P., Pukkanasut, P., Womack, H., Casals, L., Zhang, H., et al. (2021). Discovery of Potent Inhibitors of Streptococcus Mutans Biofilm With Antivirulence Activity. *ACS Med. Chem. Lett.* 12 (1), 48–55. doi: 10.1021/acsmedchemlett.0c00373

Nijampatnam, B., Casals, L., Zheng, R., Wu, H., and Velu, S. E. (2016). Hydroxychalcone Inhibitors of Streptococcus Mutans Glucosyl Transferases and Biofilms as Potential Anticaries Agents. *Bioorg Med. Chem. Lett.* 26 (15), 3508–3513. doi: 10.1016/j.bmcl.2016.06.033

Nilsson, M., Jakobsen, T. H., Givskov, M., Twetman, S., and Tolker-Nielsen, T. (2019). Oxidative Stress Response Plays a Role in Antibiotic Tolerance of Streptococcus Mutans Biofilms. *Microbiol. (Reading)* 165 (3), 334–342. doi: 10.1099/mic.0.000773

Pamp, S. J., Frees, D., Engelmann, S., Hecker, M., and Ingmer, H. (2006). Spx Is a Global Effector Impacting Stress Tolerance and Biofilm Formation in Staphylococcus Aureus. *J. Bacteriol.* 188 (13), 4861–4870. doi: 10.1128/JB.00194-06

Qiu, W., Zhou, Y., Li, Z., Huang, T., Xiao, Y., Cheng, L., et al. (2020). Application of Antibiotics/Antimicrobial Agents on Dental Caries. *BioMed. Res. Int.* 2020, 5658212. doi: 10.1155/2020/5658212

Ren, Z., Cui, T., Zeng, J., Chen, L., Zhang, W., Xu, X., et al. (2016). Molecule Targeting Glucosyltransferase Inhibits Streptococcus Mutans Biofilm Formation and Virulence. *Antimicrob. Agents Chemother.* 60 (1), 126–135. doi: 10.1128/AAC.00919-15

Siegers, K., and Entian, K. D. (1995). Genes Involved in Immunity to the Lantibiotic Nisin Produced by Lactococcus Lactis 6F3. *Appl. Environ. Microbiol.* 61 (3), 1082–1089. doi: 10.1128/aem.61.3.1082-1089.1995

Sroor, F. M., Othman, A. M., Tantawy, M. A., Mahrous, K. F., and El-Naggar, M. E. (2021). Synthesis, Antimicrobial, Anti-Cancer and *In Silico* Studies of New Urea Derivatives. *Bioorg Chem.* 112, 104953. doi: 10.1016/j.bioorg.2021.104953

Tang, B., Gong, T., Zhou, X., Lu, M., Zeng, J., Peng, X., et al. (2019). Deletion of Cas3 Gene in Streptococcus Mutans Affects Biofilm Formation and Increases Fluoride Sensitivity. *Arch. Oral. Biol.* 99, 190–197. doi: 10.1016/j.archoralbio.2019.01.016

Tozzi, M. G., Camici, M., Mascia, L., Sgarrella, F., and Ipata, P. L. (2006). Pentose Phosphates in Nucleoside Interconversion and Catabolism. *FEBS J.* 273 (6), 1089–1101. doi: 10.1111/j.1742-4658.2006.05155.x

Wang, X., Liu, L., Zhou, X., Huo, Y., Gao, J., and Gu, H. (2020). Casein Phosphopeptide Combined With Fluoride Enhances the Inhibitory Effect on Initial Adhesion of Streptococcus Mutans to the Saliva-Coated Hydroxyapatite Disc. *BMC Oral. Health* 20 (1), 169. doi: 10.1186/s12903-020-01158-8

Wu, Y. (1965). [Synthesis of Subtitute Urea Derivative and Its *In Vitro* Antimicrobial Effect.]. *Yao Xue Xue Bao* 08), 523–532. doi: 10.16438/j.0513-4870.1965.08.007%WCNKI

Xue, X., Li, J., Wang, W., Sztajer, H., and Wagner-Dobler, I. (2012). The Global Impact of the Delta Subunit RpoE of the RNA Polymerase on the Proteome of Streptococcus Mutans. *Microbiol. (Reading)* 158 (Pt 1), 191–206. doi: 10.1099/mic.0.047936-0

Yang, Y., Mao, M., Lei, L., Li, M., Yin, J., Ma, X., et al. (2019). Regulation of Water-Soluble Glucan Synthesis by the Streptococcus Mutans dexA Gene Effects Biofilm Aggregation and Cariogenic Pathogenicity. *Mol. Oral. Microbiol.* 34 (2), 51–63. doi: 10.1111/omi.12253

Yang, S., Zhang, J., Yang, R., and Xu, X. (2021). Small Molecule Compounds, A Novel Strategy Against Streptococcus Mutans. *Pathogens* 10 (12), 1540. doi: 10.3390/pathogens10121540

Younson, J., and Kelly, C. (2004). The Rational Design of an Anti-Caries Peptide Against Streptococcus Mutans. *Mol. Divers.* 8 (2), 121–126. doi: 10.1023/b:modi.0000025655.93643.fa

Zhang, Q., Nguyen, T., McMichael, M., Velu, S. E., Zou, J., Zhou, X., et al. (2015). New Small-Molecule Inhibitors of Dihydrofolate Reductase Inhibit Streptococcus Mutans. *Int. J. Antimicrob. Agents* 46 (2), 174–182. doi: 10.1016/j.ijantimicag.2015.03.015

Zhang, Q., Nijampatnam, B., Hua, Z., Nguyen, T., Zou, J., Cai, X., et al. (2017). Structure-Based Discovery of Small Molecule Inhibitors of Cariogenic Virulence. *Sci. Rep.* 7 (1), 5974. doi: 10.1038/s41598-017-06168-1

Zhu, B., Ge, X., Stone, V., Kong, X., El-Rami, F., Liu, Y., et al. (2017). ciaR Impacts Biofilm Formation by Regulating an Arginine Biosynthesis Pathway in Streptococcus Sanguinis SK36. *Sci. Rep.* 7 (1), 17183. doi: 10.1038/s41598-017-17383-1

Conflict of Interest: The authors declare that the research was conducted in the absence of any commercial or financial relationships that could be construed as a potential conflict of interest.

Publisher's Note: All claims expressed in this article are solely those of the authors and do not necessarily represent those of their affiliated organizations, or those of the publisher, the editors and the reviewers. Any product that may be evaluated in this article, or claim that may be made by its manufacturer, is not guaranteed or endorsed by the publisher.

frontiers | Frontiers in Cellular and Infection Microbiology

ORIGINAL RESEARCH
published: 23 May 2022
doi: 10.3389/fcimb.2022.881899

Multimodal Data Integration Reveals Mode of Delivery and Snack Consumption Outrank Salivary Microbiome in Association With Caries Outcome in Thai Children

Tong Tong Wu[1], Jin Xiao[2], Samantha Manning[1], Prakaimuk Saraithong[3], Komkham Pattanaporn[4], Bruce J. Paster[5], Tsute Chen[5], Shruti Vasani[2], Christie Gilbert[6], Yan Zeng[2] and Yihong Li[7]**

[1] Department of Biostatistics and Computational Biology, University of Rochester Medical Center, Rochester, NY, United States, [2] Eastman Institute for Oral Health, University of Rochester Medical Center, Rochester, NY, United States, [3] Department of Internal Medicine, Division of Infectious Diseases, Medical School University of Michigan, Ann Arbor, MI, United States, [4] Mae Fah Luang University School of Dentistry, Chiang Rai, Thailand, [5] Department of Microbiology, Forsyth Institute, Cambridge, MA, United States, [6] Department of Microbiology and Immunology, University of Rochester Medical Center, Rochester, NY, United States, [7] Department of Public and Ecosystem Health, Cornell University Master of Public Health Program, Ithaca, NY, United States

OPEN ACCESS

Edited by:
Yuan Liu,
University of Pennsylvania,
United States

Reviewed by:
Jiyao Li,
Sichuan University, China
Ruijie Huang,
Sichuan University, China

***Correspondence:**
Yihong Li
yihong.li@cornell.edu
Jin Xiao
jin_xiao@urmc.rochester.edu

Specialty section:
This article was submitted to Microbiome in Health and Disease, a section of the journal Frontiers in Cellular and Infection Microbiology

Received: 23 February 2022
Accepted: 20 April 2022
Published: 23 May 2022

Citation:
Wu TT, Xiao J, Manning S, Saraithong P, Pattanaporn K, Paster BJ, Chen T, Vasani S, Gilbert C, Zeng Y and Li Y (2022) Multimodal Data Integration Reveals Mode of Delivery and Snack Consumption Outrank Salivary Microbiome in Association With Caries Outcome in Thai Children. Front. Cell. Infect. Microbiol. 12:881899. doi: 10.3389/fcimb.2022.881899

Early childhood caries (ECC) is not only the most common chronic childhood disease but also disproportionately affects underserved populations. Of those, children living in Thailand have been found to have high rates of ECC and severe ECC. Frequently, the cause of ECC is blamed on a handful of cariogenic organisms, such as *Streptococcus mutans* and *Streptococcus sobrinus*. However, ECC is a multifactorial disease that results from an ecological shift in the oral cavity from a neutral pH (~7.5) to an acidic pH (<5.5) environment influenced by the host individual's biological, socio-behavioral, and lifestyle factors. Currently, there is a lack of understanding of how risk factors at various levels influence the oral health of children at risk. We applied a statistical machine learning approach for multimodal data integration (parallel and hierarchical) to identify caries-related multiplatform factors in a large cohort of mother-child dyads living in Chiang Mai, Thailand (N=177). Whole saliva (1 mL) was collected from each individual for DNA extraction and 16S rRNA sequencing. A set of maternal and early childhood factors were included in the data analysis. Significantly, vaginal delivery, preterm birth, and frequent sugary snacking were found to increase the risk for ECC. The salivary microbial diversity was significantly different in children with ECC or without ECC. Results of linear discriminant analysis effect size (LEfSe) analysis of the microbial community demonstrated that *S. mutans*, *Prevotella histicola*, and *Leptotrichia hongkongensis* were significantly enriched in ECC children. Whereas *Fusobacterium periodonticum* was less abundant among caries-free children, suggesting its potential to be a candidate biomarker for good oral health. Based on the multimodal data

integration and statistical machine learning models, the study revealed that the mode of delivery and snack consumption outrank salivary microbiome in predicting ECC in Thai children. The biological and behavioral factors may play significant roles in the microbial pathobiology of ECC and warrant further investigation.

Keywords: oral microbiome, saliva, multimodal analysis, early childhood caries, machine learning, diet

INTRODUCTION

Early childhood caries (ECC) is the single most common chronic childhood disease, known to disproportionately afflict more than 73% of underprivileged preschool children worldwide (Dye et al., 2007; Dye et al., 2012).

More than 50% of 3-year-old Thai children experienced ECC (Bureau of Dental Health, 2018). Chronically persistent ECC can progress to severe-ECC (S-ECC) impacting the primary dentition and adding a significant financial burden to the involved families. Several studies have depicted a higher prevalence of ECC in Thailand, with as high as 44.5% non-cavitated initial lesions and 24.5% cavitated advanced lesions being reported among 15–19-month-old children in Central Thailand (Ledder et al., 2018). In addition, a prospective study demonstrated ECC progressed rapidly among 9-18-month-old children in Southern Thailand (reported incidence of 2% at nine months, 22.8% at 12 months, and 68.1% at 18 months of age) (Thitasomakul et al., 2006). Nationwide, the ECC prevalence among 3-year-olds and 5-year-olds was 52.9% and 75.6%, respectively; 98% of them had untreated caries (Bureau of Dental Health, 2018). This highlights the urgent need to raise awareness among Thai parents/caregivers and healthcare providers to implement more effective preventive strategies for ECC control.

While ECC is an infectious disease initiated by cariogenic pathogens, it is now understood as a multifactorial and ecology-based disease (Simon-Soro and Mira, 2015), with the interplay between host, environment, and oral microbiota affecting the onset and severity of the disease (Pitts et al., 2017; Bowen et al., 2018). Factors such as environmental (exposure to water fluoridation and fluoride toothpaste, oral hygiene), biological (dental plaque accumulation, cariogenic microbial composition), lifestyle (breastfeeding pattern, frequent sugar consumption, obesity), and socio-cultural (low socio-economic status, marital status, maternal oral health perception, utilization of dental care) have been linked to ECC (Chanpum et al., 2020). A longitudinal cohort study among 3-year-old children in Northern Thailand reported that suboptimal water fluoridation, low socioeconomic status, frequent sugar consumption, and dental plaque accumulation contributed to high ECC prevalence (44.1%) (Peltzer and Mongkolchati, 2015). Additionally, studies have reported inconclusive results for the association between ECC and prolonged breastfeeding habits. However, one cross-sectional study indicated that ECC's higher prevalence and severity among breastfed Thai children was significantly associated with factors such as age, children's oral health status, and breastfeeding pattern/duration (Chanpum et al., 2020). Furthermore, our previous study among 182 3-year-old and 166 5-year-old Thailand preschool children revealed that mode of birth delivery was significantly correlated with *Streptococcus mutans* colonization and caries outcomes in young Thai children (Pattanaporn et al., 2013; Saraithong et al., 2015). Taken together, findings from these studies confirm that ECC is a public health concern in Thailand owing to the rising disease burden. With a thorough understanding of the underlying risk factors and effective prevention strategies, it is hoped that this knowledge will help reduce the ECC disease burden among Thai children as well as children worldwide.

Due to the multifactorial etiology of ECC, a valid prediction model that utilizes sensitive microbial markers from oral microbiota (including but not limited to *S. mutans*) at early life, together with medical-socio-behavior and environmental factors, would offer a substantial opportunity to predict ECC and help generate a personalized preventive regimen. A few recent studies have demonstrated machine learning predictive modeling using 16S rRNA sequencing of oral samples, but they lack consideration for multifactorial nature of tooth decay (Teng et al., 2015; Grier et al., 2020). Our team has recently developed a multivariate ECC prediction model that uses a machine learning approach incorporating microorganism composition and demographic-environmental factors among a small group of US mother-child dyads (Wu et al., 2021). Here, we further developed stepwise, parallel integrative, statistical machine learning (ML) models to identify caries-related multiplatform factors [environment, biomedical (child and maternal), socio-behavior-feeding, and oral microorganisms) in a large Thai mother-child dyad.

METHODS

Study Population

This cross-sectionally-designed study is a subset of a parent study detailed previously (Pattanaporn et al., 2013). The current study enrolled 177 3-year-old children and their biological mothers during the children's immunization visit at the Health Promoting Hospital in Chiang Mai, Thailand, from July to December of 2009. Children who had significant congenital anomalies, chronic illness, or had taken any antibiotics within six weeks prior to examinations were excluded. A structured questionnaire was used to obtain data on family socio-demographics (age, sex, primary care provider, and maternal/family background), maternal pregnancy and past medical history (mode of delivery, gestational age, birth weight), as well as child's feeding practice (breastfeeding, bottle feeding, and

mother pre-chewing food), dietary habits (consumption of fruit juice, snacks, gum, lollipop candy, dried fruit, soft drink, child sleeping with bottle), and oral health practices. Information about delivery methods, gestational age, and child's birth weight were further verified from accessing the hospital medical records. Chi-squared statistics were used to examine the differences between categorical variables. The Ethical Committee approved the protocol for this study of the Faculty of Dentistry, Chiang Mai University, Thailand (No. 12/2008). Written informed consent was obtained from all mothers or responsible caregivers at the time of children's hospital visits.

Dental Examination and Saliva Collection

Two calibrated dentists performed a comprehensive dental examination for all children and their mothers using the WHO criteria of decayed, missing, and filled teeth (DMFT for the mothers and *dmft* for the children) (Organization. WH, 1997). The presence of ECC was also recorded as a detectable white-spot lesion or cavity following American Academy of Pediatric Dentistry criteria (American Academy of Pediatric Dentistry, 2022). Approximately 1 ml whole saliva was collected from the mothers and their children after chewing a piece of paraffin wax for 1 min under the close supervision of a medical professional. The saliva samples were stored in centrifuge tubes and immediately transferred to a -20°C freezer in the microbiology laboratory at the Chiang Mai University Faculty of Dentistry until further microbiome analysis.

DNA Extraction and 16S rRNA Sequencing

The microbial DNA extractions were performed at the microbiology laboratory at New York University College of Dentistry using a standard procedure (Saraithong et al., 2015). Briefly, 500μl of each saliva sample was used for whole-genome DNA extraction using Epicentre MasterPure™ DNA Purification kit. The 16S rRNA sequencing was conducted at the Forsyth Institute, Cambridge, MA. A total of 129 genus-specific probes and 638 species-level probes were used for bacterial identification. QIIME 1.9.1 (Caporaso et al., 2010) was used to quantify the composition and diversity of each community based on its open-reference OTU picking facility. Sequencing data that passed quality controls were included in this study to develop a caries prediction model and were assigned to operational taxonomic units (OTUs). OTUs having zero counts across all the samples or only appearing in one sample were removed from further analysis.

Alpha diversity analysis was performed using the phyloseq package (McMurdie and Holmes, 2013). The results were plotted across samples and reviewed as box plots for each group or experimental factor. Further, the statistical significance of grouping based on experimental factor was also estimated using a t-test. Beta-diversity similarity or distance between sample was measured using non-phylogenetic Bray-Curtis distance. Ordination-based methods Principal Coordinate Analysis (PCoA) was used to visualize these matrices in the 2D plot where each point represents the entire microbiome of a single sample. The statistical significance of the clustering pattern in ordination plots for beta diversity was evaluated using anyone among Permutational MANOVA (PERMANOVA). A *P* value less than 0.05 was considered statistically significant.

The Core microbiome analysis was adopted from the core function in the R package microbiome. The result of this analysis was represented in the form of a heatmap of core taxa or features where Y-axis represents the prevalence level of core features across the detection threshold (Relative abundance) range on the X-axis. A heat tree map depicting the OTU classifications and differential abundance comparison between salivary microbiome of children with ECC and caries-free children was employed. Taxa that have a significant abundance difference between ECC children vs. caries-free children was measured by the Wilcoxon Rank Sum test. Linear discriminant analysis (LDA) coupled with effect size (LEfSe) analysis (Segata et al., 2011) and non-parametric factorial Kruskal-Wallis sum-rank test were used to identify differentially abundant bacterial taxa regarding ECC status. Bacterial features were considered to be significant based on the logarithmic LDA score threshold >2.0 and false discovery rate <0.1.

Development of Machine Learning Prediction Models

The primary outcome was the caries status (Y/N) of children. The independent variables were grouped into three platforms based on the distal to proximal relationship to ECC: 1) Maternal socio-demographic-behavior-environmental factors (seven variables); 2) Children's socio-demographic-behavior-environmental factors (20 variables); 3) Children's oral microbial factors (386 variables). The characteristics of the two groups (ECC and Caries-free children) were compared using t-test for continuous data and Chi-square or Fisher's exact tests for categorical data.

OTUs with fewer than 10 reads were removed from the dataset to ensure the sufficient depths. The centered log-ratio (CLR) transformation was applied to the relative abundance of taxa, where for each subject, the sample vector undergoes a transformation based on the logarithm of the ratio between the individual elements and the geometric mean of the vector. CLR removes the value-range restriction of percentages (relative abundance is a percentage) but keeps the sum constraint of compositional data.

First, we took the parallel integration approach to integrate data from different platforms. Data collected on the three platforms were put together and fitted in penalized logistic regression model using least absolute shrinkage and selection operator (LASSO) with the response variable being the binary indicator of whether the subject has caries or not (1 = caries present, 0 = no caries present). The LASSO tuning parameter was chosen using k-fold (k = 10) cross-validation. The solution path was created to show the order of the variables entering the model.

Then, the hierarchical integration approach, a two-step procedure, was used to integrate data collected on the three platforms listed above. First, a LASSO penalized logistic regression model was fit for each of the four platforms, with the same response variable of having caries or not. Next, the LASSO tuning parameter was chosen using k-fold (k = 10) cross-validation for each model. The set of variables selected for each of

the four platforms were then collected together and used as candidate variables to fit the final LASSO-penalized logistic regression model. Again, 10-fold cross-validation was used to determine the optimal number of variables in the final model. Finally, the solution paths for the four models and the final model were created.

RESULTS

The demographic characteristics of the children with or without ECC are shown in **Table 1**. No significant differences were found between the ECC and caries-free children regarding maternal age and antibiotic use. There was an increase of ECC in mothers who prechewed food for their children, although the difference was marginally significant (p=0.051). In terms of children's factors, significantly more ECC children than caries-free children were born vaginally [63.27% vs. 43.04%, p=0.007; Odd's ratio = 2.28, 95% CI (1.19, 4.37)] or preterm (45.95% vs. 30.38%, p=0.035). More than 83% ECC children were colonized with high levels of *S. mutans* compared to 20% in caries-free children (p<0.001). More caries-free children were found to use fluoridated toothpaste (p=0.009); were bottle fed (p=0.040); and less frequently consumed soft drinks (p=0.003), snacks (p=0.003), lollipop (p=0.017), and other candies (p=0.015).

Salivary Microbiome Diversity

The microbiome data include 79,001 OTUs [excluding OTUs with fewer than two sequences and sequences that fail to align with PyNAST (Caporaso et al., 2010)] for 354 samples. The sequence reads of all samples in the study are deposited in the NCBI Sequence Read Archive (SRA) as a study under the accession number of PRJNA824062. For the rarefaction curves, see **Figure S1**. Microbial community variation measured by alpha diversity was seen among children from different age groups, the mode of delivery, mother chew food practice, and children's ECC status (**Figure 1**). For instance, the salivary microbiome of 2-year-old children and born vaginally had a higher alpha diversity (Observed and Fischer index) than 3-year-old children and born with C-section (**Figures 1A, B**) . The alpha diversity was significantly higher in children who frequently consumed snacks (**Figure 1D**).

Principle coordinate analysis (PCOA) plot was generated using OTU metrics based on beta diversity (Bray-Curtis index). The study demonstrated the beta diversity of the salivary microbiome of children differs depending on sex (p<0.01), age (p=0.02), mode of delivery (p<0.001), whether mother chews food for the child (p=0.02), and children's caries severity measured by *dmft* (p<0.01) (**Figure 2**). However, the overall beta diversity was not significantly different among ECC and caries-free children (when ECC is defined using AAPD criteria) (**Figure 2F**).

Salivary Microbiome Core

Taxa at the genus and species level with more than 20% prevalence and more than 0.01% relative abundance are depicted. Interestingly, most of the genera and species were the same among the ECC and the caries-free children. However, several core taxa relative abundance and prevalence differed between the two groups. For instance, *Rothia aeria, Prevotella melaninogenica, Streptococcus sanguinis*, and *Corynebacterium durum* were more prevalent and enriched in caries-free children, while *Leptotrichia shahii* and *Corynebacterium matruchotii* were more prevalent and enriched in ECC children (**Figure 3**).

Discriminate Features Between ECC and Caries-Free Children

To identify discriminate taxa between the ECC and caries-free children, heat trees depicted the OTU classifications and differential abundance comparison at the genus level (**Figure 4A**) and at the species level (**Figure 4B**) between the salivary microbiome of children with and without ECC. In the heat trees, size and color of nodes and edges are correlated with the abundance ratio of organisms in ECC children vs. caries-free children. Taxa colored in red are enriched in ECC Children (e.g., *S. mutans*, *P. histicola*, *L. hongkongesis*, and *L. shahii*, etc.). Taxa colored in blue are enriched in caries-free children (e.g., *F. periodonticum*, *Actinomyces gerensceriae*, *Oribacterium sinus*, and *Veillonella rogosae*, etc.). Taxa with labels had a significant differential abundance between ECC children and caries-free children measured by the Wilcoxon Rank Sum test, p<0.05. The significant differential abundances were further verified in the linear discriminant analysis effect size (LEfSe) analysis and random forest at the species level (**Figure 5A**). The ECC group had an increased abundance in *S. mutans*, *P. histicola*, and *L. hongkongesis* compared to an increased abundance in *F. periodonticum, Leptotrichia* sp., *V. rogosae, O. sinus*, and *P. nigrescens* in caries-free groups (**Figure 5B**).

ECC Caries Prediction Models

All children had more than 100 OTU reads per subject. Ninety OTUs with fewer than 10 reads were removed from the dataset to ensure sufficient depths. The final dataset included 177 children with 416 variables in total, in which seven were maternal socio-demographic-behavior-environmental factors (platform 1), 20 were children's socio-demographic-behavior-environmental factors (platform 2), and 386 were children's oral microbial factors (platform 3). In the two-step model building approach, three separate LASSO penalized logistic regression models were fitted for the three platforms in step 1. Two maternal socio-demographic-behavior-environmental factors from the platform 1 (**Figure 6A**), 11 children's socio-demographic-behavior-environmental factors from the platform 2 (**Figure 6B**), and 11 children's oral microbial factors from the platform 3 (**Figure 6C**) were selected based on 10-fold cross-validation.

In step 2, the 24 variables from the previous step were used as the candidate variables and the final model selects nine. Nine variables entered the final logistic regression model, they were, in order, *F. periodonticum*, *S. mutans*, *O. sinus*, *P. histicola*, snack, *Treponema amylovorum*, *F. nucleatum* subsp. a*nimalis*, vaginal delivery, and *L. hongkongensis* (**Figure 6D**). In particular, vaginal delivery, snack, *L. hongkongensis*, *P. histicola*, and *S. mutans* had a positive effect on ECC with an increased risk of having caries. *F. nucleatum* subsp.

TABLE 1 | Characteristics of Thai children with and without ECC.

Independent covariates	ECC children (n = 98)	Caries-free children (n = 79)	P value
Maternal factors			
Mothers biomedical			
Age group			
20 year old	41.84% (41)	27.85% (22)	0.053
30 year old	58.16% (57)	72.15% (57)	
Antibiotic use (Y)	88.78% (87)	84.81% (67)	0.435
Maternal behavior			
Caregiver			
Mother (Full time)	53.06% (52)	43.04% (34)	0.406
Mother (Not full time)	36.73% (36)	45.57% (36)	
Other than mother	10.20% (10)	11.39% (9)	
Mother prechewing food	37.76% (37)	24.05% (19)	0.051
Smoking	2.04% (2)	1.27% (1)	0.581
Maternal oral health			
Caries (Y)	94.90% (93)	92.41% (73)	0.495
S. mutans level			
SM Strip score 0 - CFU $<10^4$	32.65% (32)	35.44% (28)	0.408
SM strip score 1 – CFU 10^4 - 10^5	31.63% (31)	37.97% (30)	
SM strip score 2 – CFU 10^5 - 10^6	25.51% (25)	15.19% (12)	
SM strip score 3 – CFU $>10^6$	10.20% (10)	11.39% (9)	
Children's factors			
Child biomedical			
Age group			
2 years old	34.69% (34)	29.11% (23)	0.430
3 years old	65.31% (64)	70.89% (56)	
Sex (Male)	62.24% (61)	56.96% (45)	0.476
Delivery mode			
Vaginal	63.27% (62)	43.04% (34)	0.007*
C-section	36.73% (36)	56.96% (45)	
Preterm birth (Y)	45.92% (45)	30.38% (24)	0.035*
Low birth weight (Y)	3.06% (3)	5.06% (4)	0.382
Antibiotic use (Y)	88.78% (87)	94.94% (75)	0.116
Child oral health behavior			
Brush teeth daily (Y)	87.76% (86)	93.67% (74)	0.184
Uses fluoridated toothpaste (Y)	57.14% (56)	75.95% (60)	0.009*
Child eating habits			
Soft drink			
Never/Rarely	21.43% (21)	44.30% (35)	0.003*
Sometimes	21.43% (21)	10.13% (8)	
≥1 per day	57.14% (56)	45.57% (36)	
Fruit Juice			
Never/rare	10.20% (10)	13.92% (11)	0.447
≥1 time per day	89.80% (88)	86.08% (68)	
Snack			
Never/rare	7.14% (7)	22.78% (18)	0.003*
≥1 time per day	92.86% (91)	77.22% (61)	
Lollipop candy			
Never/rare	47.96% (47)	65.82% (52)	0.017*
≥1 time per day	52.04% (51)	34.18% (27)	
Other candy			
Never/rare	33.67% (33)	51.90% (41)	0.015*
≥1 time per day	66.33% (65)	48.10% (38)	
Cakes			
Never/rare	21.43% (21)	11.39% (9)	0.077
≥1 time per day	78.57% (77)	88.61% (70)	
Child environment			
Water type			
Bottle water	66.33% (65)	73.42% (58)	0.752
Tap water	14.29% (14)	12.66% (10)	
Well underground water	8.16% (8)	6.33% (5)	
Mixed sources	11.22% (11)	7.59% (6)	
Child feeding			

(Continued)

TABLE 1 | Continued

Independent covariates	ECC children (n = 98)	Caries-free children (n = 79)	P value
Breast feeding (Y)	97.96% (96)	98.73% (78)	0.581
Bottle feeding (Y)	73.47% (72)	86.08% (68)	0.040*
Bottle fed with sweet milk (Y)	9.18% (9)	2.53% (2)	0.062
Child oral health status			
S. mutans level			
SM Strip score 0 - CFU $<10^4$	9.18% (9)	63.29% (50)	<0.001*
SM strip score 1 – CFU 10^4 - 10^5	7.14% (7)	16.46% (13)	<0.001*
SM strip score 2 – CFU 10^5 - 10^6	25.51% (25)	12.66% (10)	
SM strip score 3 – CFU $>10^6$	58.16% (57)	7.59% (6)	
Smooth surface caries (number of surfaces, mean ± SD)	4.42 ± 5.6	0	

Statistical significance level <0.05; Chi-squared test.

animalis, *F. periodonticum*, *O. sinus*, and *T. amylovorum* showed decreased risk for having ECC in our cohort. As a comparison, the one-step model with the same nine variables resulted in the same regression coefficients (**Figure S2**). The area under the curve (AUC) value for the two-step predictive model was 0.85.

$$logit(p) = X\beta = 0.283 + 0.117 \text{ vagianl delivery} + 0.241 \text{ snack} - 0.104\ F.\ nucleatum\ subsp\ animalis - 0.019\ F.\ periodonticum + 0.040\ L.\ hongkongensis - 0.110\ O.\ sinus + 0.058\ P.\ histicola + 0.040\ S.\ mutans - 0.130\ T.\ amylovorum$$

DISCUSSION

Caries occurrence in preschool-age children depends on several host and environmental factors, which can ultimately disturb the oral microbiome equilibrium. Studies of caries risk assessment and prediction at an individual level are consequential for a clinical decision-making at a patient-care level and design appropriate evidence-based caries preventive interventions at a community level (Chanpum et al., 2020). The highlight of this study is the interdisciplinary approach incorporating data platforms from multiple sources, which include 1) the carefully acquired mother-child dyads dataset containing information of socio-demographic, medical, and delivery information; caries examination, oral health behavior, and dietary practice; 2) the salivary microbiome 16S rRNA gene sequencing dataset; 3) the use of linear discriminant analysis coupled with effect size (LEfSe) analysis (Segata et al., 2011) to determine differentially abundant bacterial taxa associated with ECC or caries-free children; and 4) the application of a novel machine learning approach to develop a multi-platform caries prediction model with quantifiable coefficients.

The initial objective of this study sought to examine the caries-associated risk factors among the 177 mother-child dyads. The significant risk factors for ECC included preterm birth, high levels of *S. mutans*, increased consumption of soft drinks, snacks, and candies, and used less fluoride toothpaste. Vaginal-born children are 2.27 times more likely to experience ECC compared to their counterparts. These findings are consistent with those evidenced in earlier studies (Pattanaporn et al., 2013; Twetman et al., 2020). What is not yet clear is how those plausible caries-associated risk factors impact on oral microbial composition in 2- to 3-year-old children. In addition to microbes, our predictive model was successful at identifying behavioral and environmental risk factors for developing caries; the conceptual inference is drawn in **Figure 7**. Interestingly, our model revealed that vaginal delivery predicted the onset of caries in these Thai children. While there is limited knowledge on how the delivery route impacts the oral ecology of overall oral health, several studies have demonstrated a relationship between the delivery route and oral microbiome development (Xiao et al., 2020). For example, a birth cohort study among Irish infants revealed a higher oral microbial community diversity in children born by cesarean. However, the impact of birth mode on the oral microbiome was only observed up to the first week of age. This influence diminished after the first week of life. Another study examined the oral microbiome of very low birth weight infants and found a higher relative abundance of *Ureaplasma* and *Pantoea* in the vaginal-born infants, but a higher colonization prevalence of *Corynebacterium*, *Methylobacterium*, and *Variovorax* in cesarean-born infants (Li et al., 2020). Other studies indicated that the bacterial profile colonized in infants born vaginally resembles mothers' vaginal bacterial communities, whereas the microbial community of infants born by cesarean section resembles those present on mothers' skin (Dominguez-Bello et al., 2010; Lif Holgerson et al., 2011; Drell et al., 2017). Worth noting that research on infants' gut microbiome development and delivery mode revealed similar findings to the oral microbiome. These findings included an increased similarity to their mother's gut microbiome when born vaginally (Bäckhed et al., 2015), delayed colonization of prominent commensals in cesarean born infants (Dogra et al., 2015), and lower diversity in cesarean born infants when compared to vaginally-born infants (Hesla et al., 2014). Due to the importance of understanding the impact of the maternal oral microbiome on children's caries outcome, our future study will further analyze the relatedness of the maternal and children's salivary bacteriome and their impact on ECC. Importantly, we also found a lower diversity in the cesarean-born children in our study (**Figure 1A**). Further, 3-year-old children had a lower alpha diversity than the children at 2 years of age in our study (**Figure 1B**). This could be reflective of the stabilization of the oral microbiome that occurs after 2 years of age; at this point, children become stably colonized by resident

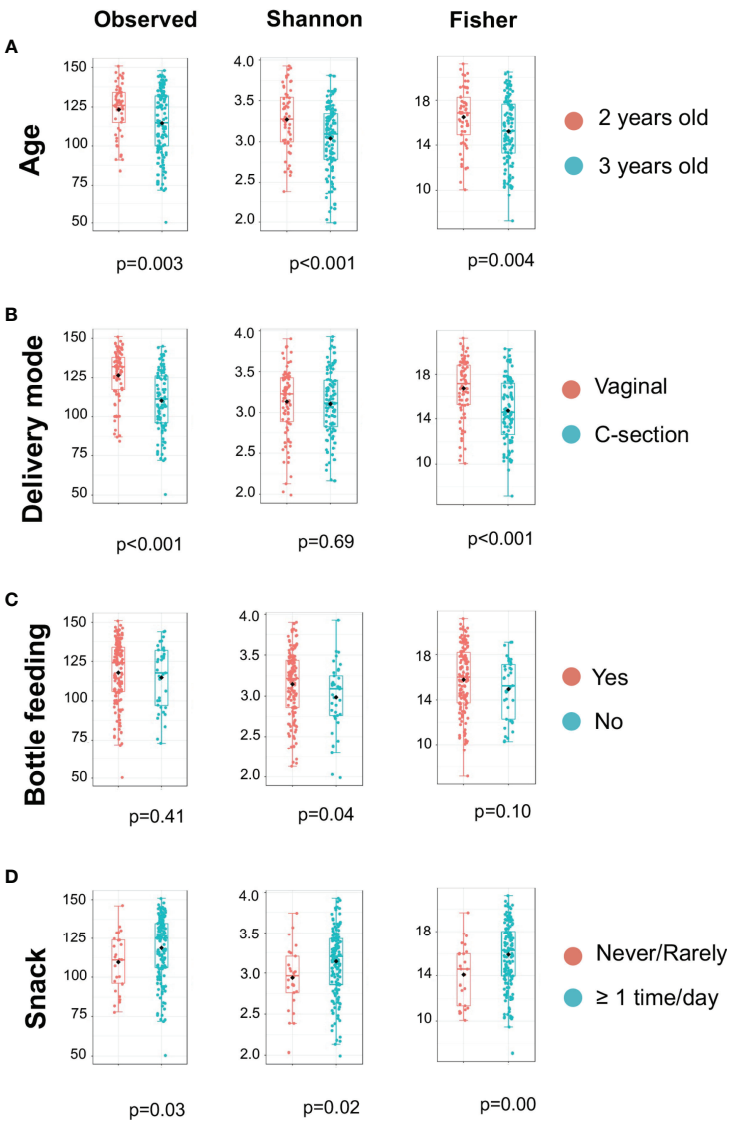

FIGURE 1 | Alpha Diversity of salivary microbiome among children. Microbial variation measured by alpha diversity index among children from different age group **(A)**, mode of delivery **(B)**, Bottle feeding **(C)**, and Consumption of snacks **(D)**. T-test was used for the statistical comparisons.

bacteria of the oral cavity and have fewer bacteria that are from environmental exposures (Dashper et al., 2019).

Sugary snacks are known to serve as the substrate for oral microbial metabolism, leading to acidification of the oral environment, favoring aciduric and cariogenic microorganisms, and causing tooth hard tissue demineralization and, ultimately, caries (Marsh, 2018). More than two-thirds (68%) of US 2-year-olds and roughly three-quarters (74%) of 3-year-olds consumed some type of dessert or candy in a day (Fox et al., 2010). Our findings that frequent snacking is a risk factor for caries is supported by previous studies that have emphasized the importance of limiting cariogenic or sugary snack consumption as part of a good oral health routine to prevent caries onset (Hong et al., 2014; Moimaz et al., 2014).

To build the caries-predictive model, the study first identified commonly recognized caries risk microbial factors, such as children's age, model of delivery, preterm birth, frequency of snack consumption, and presence of *S. mutans* and other potential caries-associated bacteria. Additionally, we detected several other microbial species, either caries-associated or protective that traditionally have received less attention.

For the penalized regression models, both the variables selected into the model and the order they enter the model were important. A variable entering a model sooner (i.e., at a higher lambda value, the tuning parameter) indicates that it is deemed significant under harsher penalties. In our final logistic regression model, the coefficients of vaginal delivery, snack, presence of *S. mutans, L. hongkongensis*, and *P. histicola*, were

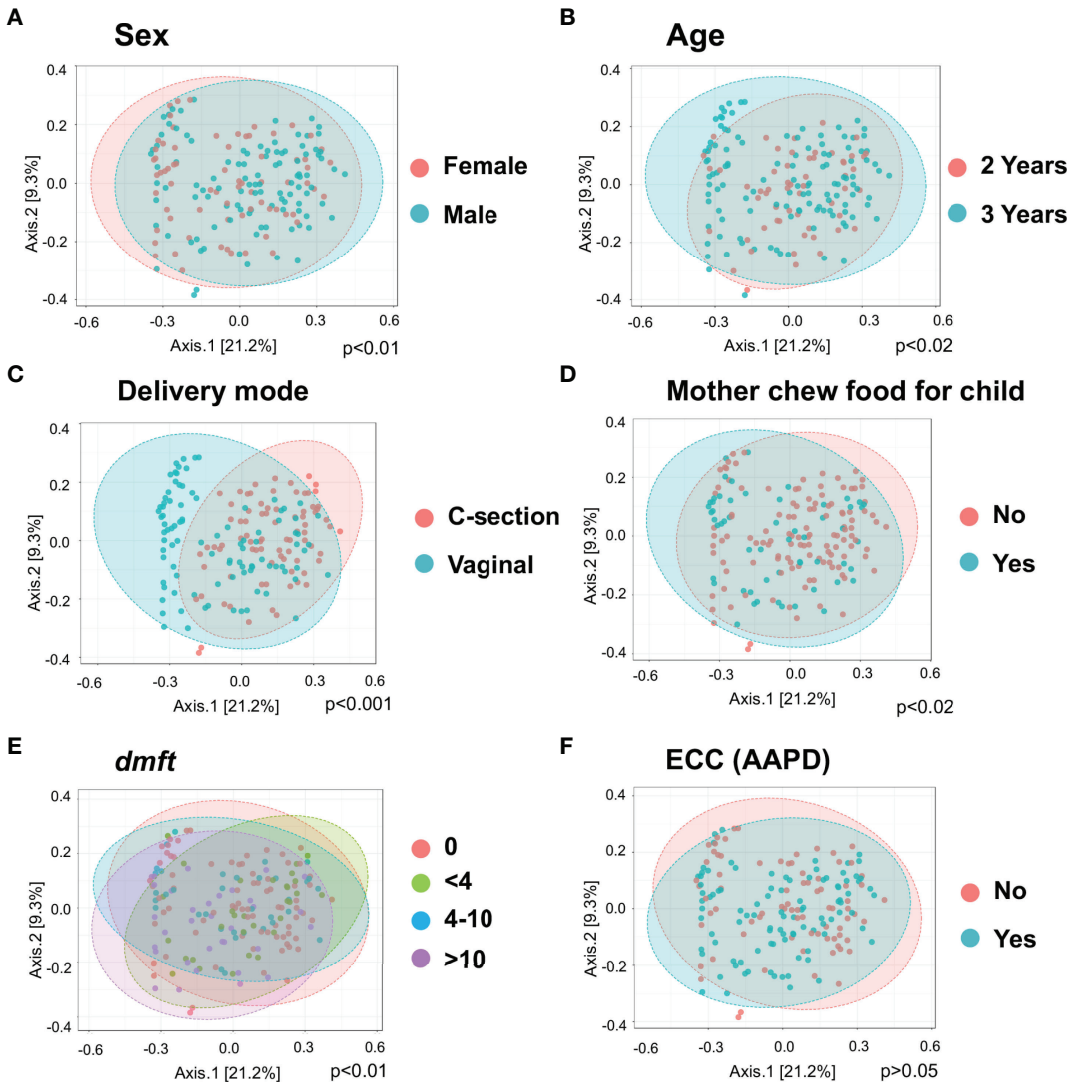

FIGURE 2 | Diversity of salivary microbiome among children. Principle coordinate analysis (PCOA) plot is generated using OTU metrics based on beta diversity (Bray-Curtis index) for different sex groups **(A)**, Age **(B)**, Mode of delivery **(C)**, Mother chew food for child **(D)**, Child caries severity *dmft* **(E)**, and ECC status **(F)**. Permutational MANOVA (PERMANOVA) was used for these statistical comparisons between or among the categorical groups.

positive, indicating the change in log-odds of an individual having caries due to a one-unit increase in those variables. More specifically, the coefficient for vaginal delivery in the 2-step model was 0.1174. The odds ratio of having caries for a child who was delivered by vaginal, compared with a child who was c-sectionally delivered, could be 12% higher. Likewise, having snacks increases the odds of having caries by 27%.

Meanwhile, the coefficients of presence of *F. periodonticum, F. nucleatum* subsp. *animalis*, *O. sinus*, and *T. amylovorum* were negative, indicating a decrease in the log-odds of an individual having caries, which means that for a negative coefficient, the subject is less likely to have caries as those variable increase. The results suggest that the enriched levels of those four bacterial species in the saliva present a reduced risk for ECC.

Predictors Identified in Machine Learning Model

This study identified the plausible caries-promoting microbial species, which were enriched in ECC samples, were *S. mutans, P. histicola*, and *L. hongkongensis.*

Streptococcus mutans

ECC children are known to have a higher relative abundance of salivary and plaque *S. mutans*, well-known for its acidogenicity, aciduricity, and capability of synthesizing extracellular matrix using carbohydrates (Banas, 2004) (Tanner et al., 2011; Gross et al., 2012; Yang et al., 2012; Ma et al., 2015; Johansson et al., 2016; Richards et al., 2017; Xiao et al., 2018). Not surprisingly, this species was firstly found as caries promoting species in our model.

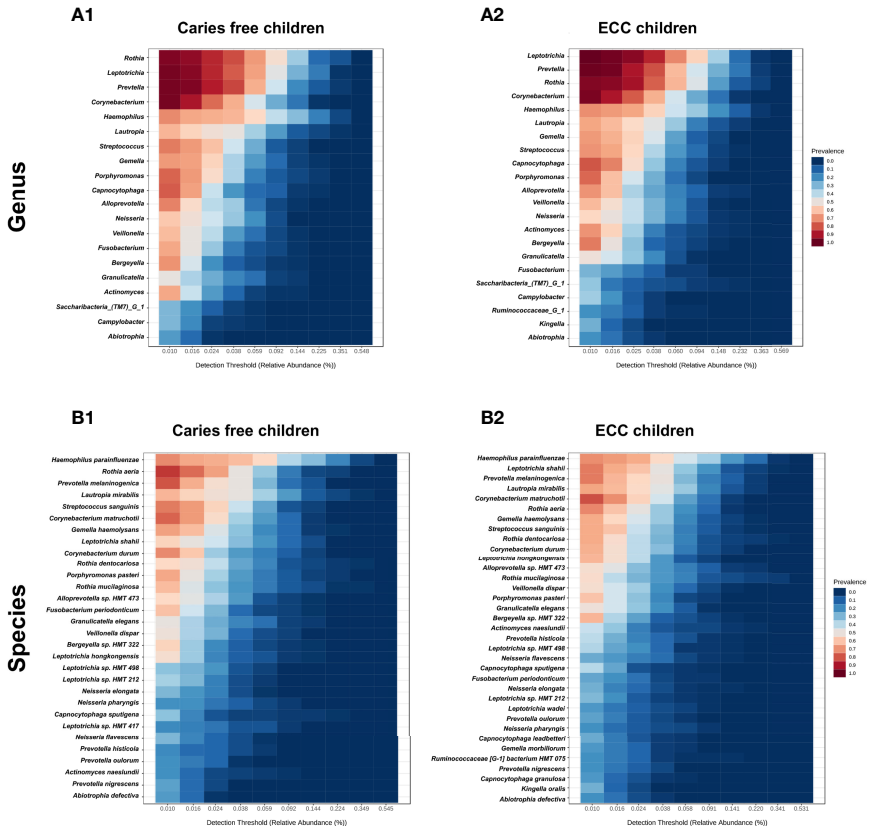

FIGURE 3 | Core salivary microbiome of ECC and carries-free children. Taxa at the genus and species level with more than 20% prevalence and more than 0.01% relative abundance are depicted. in caries free children **(A1, B1)** and ECC children **(A2, B2)**.

Prevotella histicola

Prevotella histicola was found in two independent studies (Teng et al., 2015; Wu et al., 2021) that used a machine learning approach to identify discriminative species in caries-active and caries-free children. Despite previously reported association between *P. histicola* and increased caries risk in children (Hurley et al., 2019), it remains unclear about the potential cariogenicity of *P. histocola* and its interaction with other oral microorganisms in leading to a caries-prone condition in the oral cavity.

Leptotrichia hongkongensis

Leptotrichia species normally reside in the oral cavity, gastrointestinal system, and urogenital system. They are typically not considered pathogenic, but may cause opportunistic infections in an immune-suppressed host (Eribe and Olsen, 2017). Xu et al. characterized microbial composition in supragingival plaque samples from children younger than 30 months old and observed that *L. hongkongensis* was identified in caries-affected subjects (Xu et al., 2014). *L. hongkongensis* was also more predominant in adults with active caries (Johansson et al., 2016). Interestingly, *L. hongkongensis* co-occurred with other *Leptotrichia* and *Fusobacterium* species that contributed to black stains of dental caries in primary dentition. Despite the observed associations of *Leptotrichia* species with caries, there remains a gap in understanding their role in the progression of caries.

This study further identified several potentially protective microbial species enriched in caries-free children: *F. periodonticum*, *F. nucleatum* subsp. *animalis, Treponema amylovorum, O. sinus.* Interestingly, three of these species (*F. periodonticum*, *F. nucleatum*, *T. amylovorum*) are commonly known periodontal pathogens.

Fusobacterium periodonticum

F. periodonticum, although without clear evidence on its role in the etiopathogenesis of periodontal disease, is considered to be an opportunistic pathogen residing in deep periodontal pockets and gingival sulcus (Park et al., 2010). Jiang and colleagues observed that *F. periodonticum* was significantly predominant in the saliva of caries-free children compared to caries-affected, which could be suggestive of a caries protective role (Jiang et al., 2016). These findings were also consistent with a similar case-control cohort study examining bacterial profiles of adults with caries (Belstrøm et al., 2014). A more recent study analyzed the variation of the tongue microbiota and its association with dental caries among 6-7-year-old and 11-12-year-old children. The study results demonstrated a more frequent presentation of *F. periodonticum* in children without history of dental

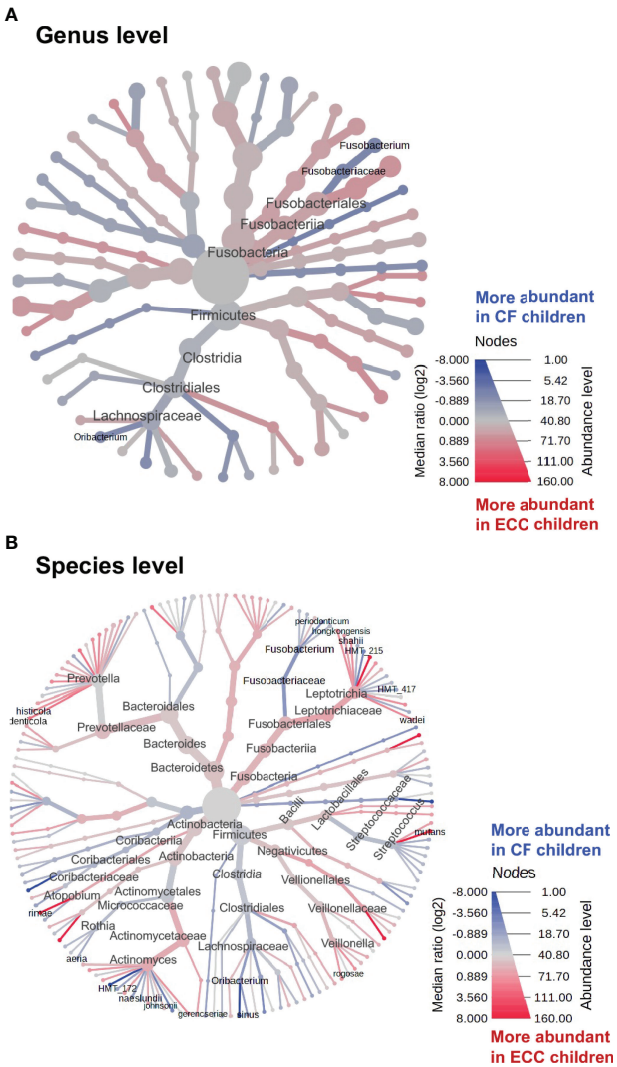

FIGURE 4 | Heat trees of salivary microbiome abundance among ECC and caries-free children. The heat trees depict the OTU classifications and differential abundance comparison at the genus level **(A)** and at the species level **(B)** between salivary microbiome of children with ECC and without ECC. In the heat trees, size and color of nodes and edges are correlated with the abundance ratio of organisms in ECC children vs. caries-free children. Taxa colored in red are enriched in ECC Children, whereas taxa colored in blue are enriched in caries-free children. Taxa with labels indicate a significant abundance difference between ECC children vs. caries-free children measured by the Wilcoxon Rank Sum test ($p<0.05$).

caries (Zhang et al., 2021). Thus, salivary counts of *F. periodonticum* can be used as a biomarker and may help caries risk screening (Belstrøm et al., 2014; Jiang et al., 2016).

Fusobacterium nucleatum

F. nucleatum is a commonly recognized periodontal pathogen and regarded as a bridging colonizer that adheres to the early colonizers of dental plaque, followed by adhesion from late plaque colonizers (Aruni et al., 2015). Its FadA adhesin has been identified as a virulence factor for both *F. nucleatum and F. periodonticum*, which is absent in other fusobacterium species and are considered to assist them in binding to host cells (Han, 2015). Studies have reportedly detected *Fusobacterium* species including *F. nucleatum* in abundance in the healthy oral microbiota among children (Teng et al., 2015). Tanner et al. reported *F. nucleatum* as more frequently detected in caries-free children (Tanner et al., 2011). Heinrich-Weltzien et al., indicated that *F. nucleatum* was found more frequently in non-discolored plaque samples (Tanner et al., 2011).

Treponema amylovorum

T. amylovorum species are highly motile, fastidious, saccharolytic gram-negative spirochetes majorly associated with subgingival plaque in periodontal disease (Wyss et al., 1997; Siqueira and Rôças, 2004). Although the majority of the scientific evidence

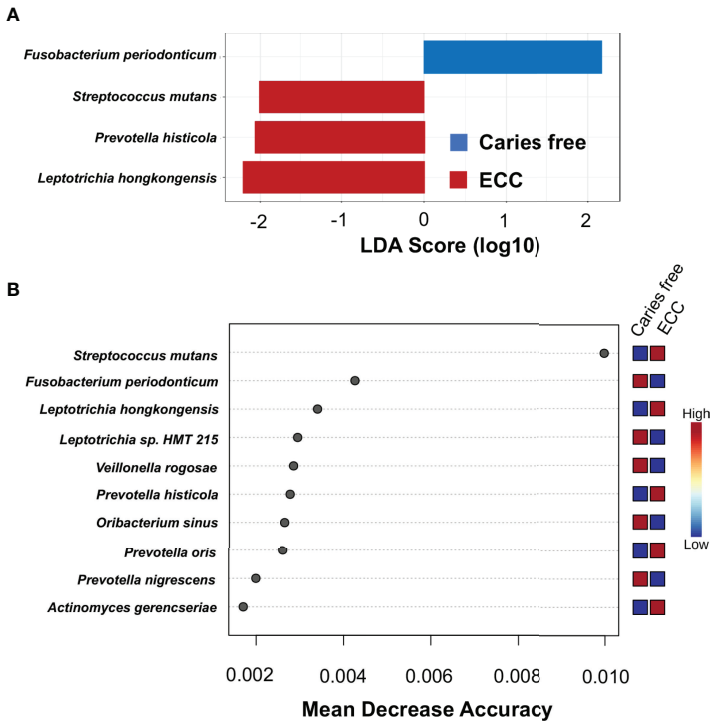

FIGURE 5 | Taxa at genus level differently enriched in ECC and caries-free children. **(A)** Linear discriminant analysis (LDA) effect size (LEfSe) method was performed to compare taxa between ECC and caries-free children. The bar plot lists the significantly differential taxa based on effect size (LDA score $\log_{10}$ >2.0 and FDR <0.1). **(B)** Random forest identified important features at the species level that were differently enriched among ECC and caries-free children. Red indicates a higher abundance in ECC, whereas blue indicates a higher abundance in caries-free children.

links *T. amylovorum* with periodontal and endodontic diseases, our study results indicated that the presence and higher abundance of *T. amylovorum* in Thai children are associated with a lower risk for ECC, which is a novel finding.

Oribacterium sinus

O. sinus was initially isolated from purulent discharge of a 6-year-old-child with bilateral maxillary sinusitis (Carlier et al., 2004). A longitudinal cohort study examined the oral microbiome development during the first four years of life and subsequent development of ECC (Dashper et al., 2019). Although *O. sinus* had a higher (≥90%) prevalence when children are between 1-4 years of age, making its way to the 'core oral microbiome' of young children, the relative abundance of *O. sinus* was not suggested to be significantly associated with caries status (Dashper et al., 2019).

Veillonella rogosae

V. rogosae has been identified as a species associated with caries-free condition from other discriminate methods. *Veillonella* species, including *V. rogosae*, are early plaque colonizers with metabolic requirements that are dependent upon organic acids, including lactic acid, produced by *Streptococcus*. Thus, together these species are considered to co-aggregate and contribute to biofilm formation and maturation in early stages (Mashima and Nakazawa, 2014). Studies have reported that age, geographic location, diet, and oral health behaviors influence the proportion of oral *Veillonella* species. One such study (Djais et al., 2019) examined the proportion of oral *Veillonella* species in the saliva samples of Japanese children 4- to 14-years-old as a measure of their oral health status. Interestingly, the detection of *V. rogosae* declined with deteriorating oral hygiene status (49.1% in good hygiene vs. 44.4% in moderate hygiene vs. 34.1% in poor oral hygiene). A study in Thai children with different oral hygiene status (good, moderate, and poor) revealed similar findings. *V. rogosae* prevalence was significantly lower in the poor oral hygiene group than in the good oral hygiene groups, whereas, *Veillonella parvula* and *Veillonella tobetsuensis* were significantly more prevalent in the poor oral hygiene group (Mashima et al., 2016; Theodorea et al., 2017). These findings, together with ours, suggest that the abundance of *V. rogosae* may be a predictor of good oral hygiene status and potentially a caries protective factor among children.

We took two data integration approaches in this paper. The first parallel integration approach treats factors on different platforms equally and assumes no specific correlation structures among factors. The second hierarchical integration approach is indeed an integration with pre-selection on each platform first. It can be considered to take into account the correlation structure within each platform. The two approaches usually produce different outcomes since the pools of candidate predictor

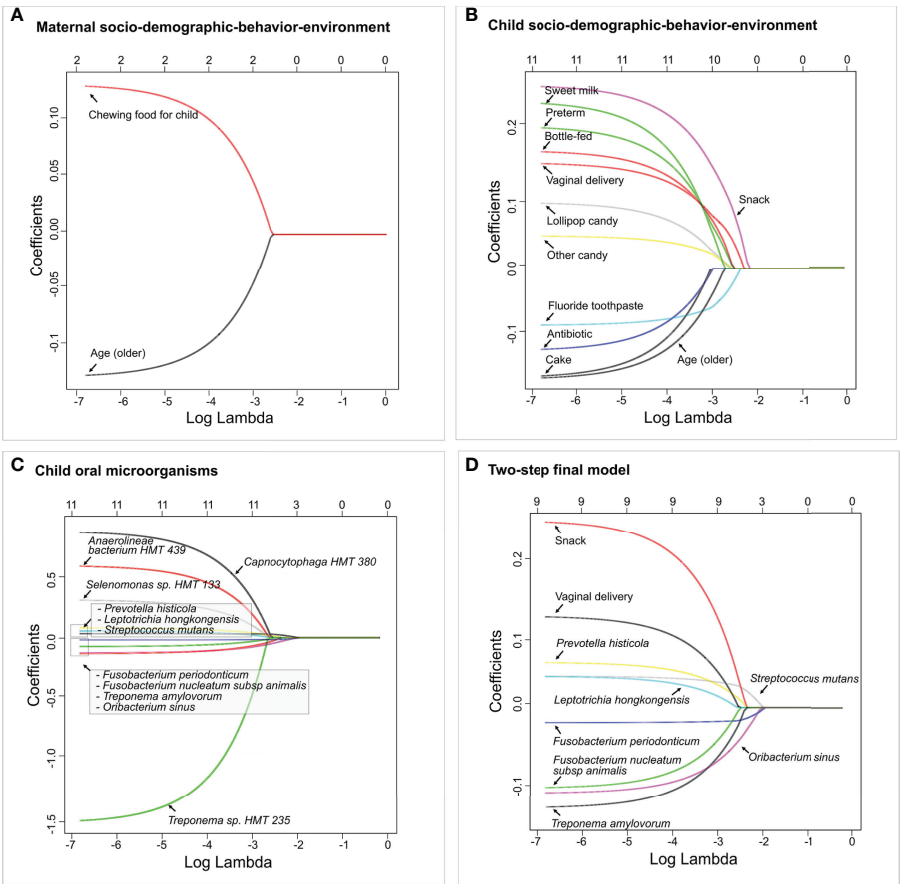

FIGURE 6 | Identified factors associated with child's caries risk using factors *via* two-step model. LASSO penalized logistic regression modeling was used for caries predictor selection based on 413 variables, including children's saliva samples. Specifically, variables from three separate platforms were identified shown in **(A)** Maternal socio-demographic-behavior-environmental factors, **(B)** Children's socio-demographic-behavior-environmental factors, and **(C)** Children's salivary microorganisms. The final two-step model using variables identified from **(A–C)** is shown in **(D)**. The LASSO solution path above shows how the model is built sequentially by adding one variable at a time to the active set. The 2-step predictive model is the following (area under the curve: 0.85).

FIGURE 7 | Conceptual causal inference from multiplatform variables assessed in the study.

variables are different but are expected to have a great overlap. It is a coincidence that the two models in this paper are exactly the same, which also indicates good reproducibility and reliability.

The following limitations need to be considered when interpreting the study results: 1) The study was conducted in one Thailand city. Thus, generalization to other populations is unreliable due to the difference in racial, ethnical, cultural, and dietary background; 2) With the dataset being cross-sectional, the models are built upon the existing caries status, not through the longitudinal onset of caries. Future validations of our models are warranted using longitudinal dataset. There is an additional need for a more mechanistic understanding of how bacteria, such as *V. rogosae* and *L. hongkongensis*, are involved in protecting the oral cavity from caries progression.

CONCLUSIONS

Multimodal data integration using statistical machine learning models revealed that the mode of delivery and sugary snack consumption outranks salivary microbiome in predicting dental caries in a large cohort of mother-child dyads living in Thailand. Future machine learning approaches that include microbial and environmental risk factors are needed to comprehensively assess the dynamic changes of children's caries risk factors in a longitudinal cohort.

DATA AVAILABILITY STATEMENT

The datasets presented in this study can be found in online repositories. The name of the repository and accession number can be found below: NCBI; PRJNA824062.

ETHICS STATEMENT

The Ethical Committee approved the protocol for this study of the Faculty of Dentistry, Chiang Mai University, Thailand (No. 12/2008). Written informed consent to participate in this study was provided by the participants' legal guardian/next of kin.

AUTHOR CONTRIBUTIONS

TTW, JX, and YL contributed to the conception, design, data acquisition, analysis, and interpretation, drafting and critically revising the manuscript. PS and KP contributed to the clinical data collection. PS was responsible for microbial DNA extraction. BP and CG were responsible for DNA sequencing. SM, SV, and YZ contributed to data acquisition, analysis, and critically revising the manuscript. All authors have read and approved the final version of the manuscript and agree to be accountable for all aspects of the work.

FUNDING

Dr. JX research was supported by the National Institute of Dental and Craniofacial Research grant K23DE027412.

SUPPLEMENTARY MATERIAL

The Supplementary Material for this article can be found online at: https://www.frontiersin.org/articles/10.3389/fcimb.2022.881899/full#supplementary-material

REFERENCES

American Academy of Pediatric Dentistry. (2020). Policy on Early Childhood Caries (ECC): Classifications, Consequences, and Preventive Strategies. *The Reference Manual of Pediatric Dentistry*. (Chicago, Ill.: American Academy of Pediatric Dentistry), 79–81. Available at: https://www.aapd.org/media/policies_guidelines/p_eccclassifications.pdf.

Aruni, A. W., Dou, Y., Mishra, A., and Fletcher, H. M. (2015). The Biofilm Community-Rebels With a Cause. *Curr. Oral. Health Rep.* 2 (1), 48–56. doi: 10.1007/s40496-014-0044-5

Bäckhed, F., Roswall, J., Peng, Y., Feng, Q., Jia, H., Kovatcheva-Datchary, P., et al. (2015). Dynamics and Stabilization of the Human Gut Microbiome During the First Year of Life. *Cell Host Microbe* 17 (5), 690–703. doi: 10.1016/j.chom.2015.04.004

Banas, J. A. (2004). Virulence Properties of Streptococcus Mutans. *Front. Biosci.* 9, 1267–1277. doi: 10.2741/1305

Belstrøm, D., Fiehn, N. E., Nielsen, C. H., Holmstrup, P., Kirkby, N., Klepac-Ceraj, V., et al. (2014). Altered Bacterial Profiles in Saliva From Adults With Caries Lesions: A Case-Cohort Study. *Caries Res.* 48 (5), 368–375. doi: 10.1159/000357502

Bowen, W. H., Burne, R. A., Wu, H., and Koo, H. (2018). Oral Biofilms: Pathogens, Matrix, and Polymicrobial Interactions in Microenvironments. *Trends Microbiol.* 26 (3), 229–242. doi: 10.1016/j.tim.2017.09.008

Bureau of Dental Health (2018). *The 8th Thailand National Oral Health Survey Report 2017* (Nonthaburi: Ministry of Public Health, Thailand), 1–330.

Caporaso, J. G., Bittinger, K., Bushman, F. D., DeSantis, T. Z., Andersen, G. L., and Knight, R. (2010). PyNAST: A Flexible Tool for Aligning Sequences to a Template Alignment. *Bioinformatics* 26 (2), 266–267. doi: 10.1093/bioinformatics/btp636

Caporaso, J. G., Kuczynski, J., Stombaugh, J., Bittinger, K., Bushman, F. D., Costello, E. K., et al. (2010). QIIME Allows Analysis of High-Throughput Community Sequencing Data. *Nat. Methods* 7 (5), 335–336. doi: 10.1038/nmeth.f.303

Carlier, J. P., K'Ouas, G., Bonne, I., Lozniewski, A., and Mory, F. (2004). Oribacterium Sinus Gen. Nov., Sp. Nov., Within the Family 'Lachnospiraceae' (Phylum Firmicutes). *Int. J. Syst. Evol. Microbiol.* 54 (Pt 5), 1611–1615. doi: 10.1099/ijs.0.63060-0

Chanpum, P., Duangthip, D., Trairatvorakul, C., and Songsiripradubboon, S. (2020). Early Childhood Caries and Its Associated Factors Among 9- to 18-Month Old Exclusively Breastfed Children in Thailand: A Cross-Sectional Study. *Int. J. Environ. Res. Public Health* 17 (9), 3194–3204. doi: 10.3390/ijerph17093194

Dashper, S. G., Mitchell, H. L., Lê Cao, K. A, Carpenter, L., Gussy, M. G., Calache, H., et al. (2019). Temporal Development of the Oral Microbiome and Prediction of Early Childhood Caries. *Sci. Rep.* 9 (1), 19732. doi: 10.1038/s41598-019-56233-0

Djais, A. A., Theodorea, C. F., Mashima, I., Otomo, M., Saitoh, M., and Nakazawa, F. (2019). Identification and Phylogenetic Analysis of Oral Veillonella Species Isolated From the Saliva of Japanese Children. *F1000Res* 8, 616. doi: 10.12688/f1000research.18506.5

Dogra, S., Sakwinska, O., Soh, S. E., Ngom-Bru, C., Brück, W. M., Berger, B., et al. (2015). Dynamics of Infant Gut Microbiota Are Influenced by Delivery Mode

and Gestational Duration and Are Associated With Subsequent Adiposity. *mBio* 6 (1), e02419-14. doi: 10.1128/mBio.02419-14

Dominguez-Bello, M. G., Costello, E. K., Contreras, M., Magris, M., Hidalgo, G., Fierer, N., et al. (2010). Delivery Mode Shapes the Acquisition and Structure of the Initial Microbiota Across Multiple Body Habitats in Newborns. *Proc. Natl. Acad. Sci. U. S. A.* 107 (26), 11971–11975. doi: 10.1073/pnas.1002601107

Drell, T., Stsepetova, J., Simm, J., Rull, K., Aleksejeva, A., Antson, A., et al. (2017). The Influence of Different Maternal Microbial Communities on the Development of Infant Gut and Oral Microbiota. *Sci. Rep.* 7 (1), 9940. doi: 10.1038/s41598-017-09278-y

Dye, B. A., Li, X., and Thorton-Evans, G. (2012). Oral Health Disparities as Determined by Selected Healthy People 2020 Oral Health Objectives for the United States, 2009-2010. *NCHS Data Brief* 104, 1–8.

Dye, B. A., Tan, S., Smith, V., Lewis, B. G., Barker, L. K., Thornton-Evans, G., et al. (2007). Trends in Oral Health Status: United States, 1988-1994 and 1999-2004. *Vital Health Stat Ser. 11 Data Natl. Health Survey* 248), 1–92.

Eribe, E. R. K., and Olsen, I. (2017). Leptotrichia Species in Human Infections II. *J. Oral. Microbiol.* 9 (1), 1368848. doi: 10.1080/20002297.2017.1368848

Fox, M. K., Condon, E., Briefel, R. R., Reidy, K. C., and Deming, D. M. (2010). Food Consumption Patterns of Young Preschoolers: Are They Starting Off on the Right Path? *J. Am. Diet Assoc.* 110 (12 Suppl), S52–S59. doi: 10.1016/j.jada.2010.09.002

Grier, A., Myers, J. A., O'Connor, T. G., Quivey, R. G., Gill, S. R., and Kopycka-Kedzierawski, D. T. (2020). Oral Microbiota Composition Predicts Early Childhood Caries Onset. *J. Dent. Res.* 100 (6), 599–607. doi: 10.1177/0022034520979926

Gross, E. L., Beall, C. J., Kutsch, S. R., Firestone, N. D., Leys, E. J., and Griffen, A. L. (2012). Beyond *Streptococcus Mutans*: Dental Caries Onset Linked to Multiple Species by 16S rRNA Community Analysis. *PLoS One* 7 (10), e47722. doi: 10.1371/journal.pone.0047722

Han, Y. W. (2015). Fusobacterium Nucleatum: A Commensal-Turned Pathogen. *Curr. Opin. Microbiol.* 23, 141–147. doi: 10.1016/j.mib.2014.11.013

Hesla, H. M., Stenius, F., Jäderlund, L., Nelson, R., Engstrand, L., Alm, J., et al. (2014). Impact of Lifestyle on the Gut Microbiota of Healthy Infants and Their Mothers—the ALADDIN Birth Cohort. *FEMS Microbiol. Ecol.* 90 (3), 791–801. doi: 10.1111/1574-6941.12434

Hong, C. H., Bagramian, R. A., Hashim Nainar, S. M., Straffon, L. H., Shen, L., and Hsu, C. Y. (2014). High Caries Prevalence and Risk Factors Among Young Preschool Children in an Urban Community With Water Fluoridation. *Int. J. Paediatric Dentis.* 24 (1), 32–42. doi: 10.1111/ipd.12023

Hurley, E., Barrett, M. P. J., Kinirons, M., Whelton, H., Ryan, C. A., Stanton, C., et al. (2019). Comparison of the Salivary and Dentinal Microbiome of Children With Severe-Early Childhood Caries to the Salivary Microbiome of Caries-Free Children. *BMC Oral. Health* 19 (1), 13. doi: 10.1186/s12903-018-0693-1

Jiang, S., Gao, X., Jin, L., and Lo, E. C. (2016). Salivary Microbiome Diversity in Caries-Free and Caries-Affected Children. *Int. J. Mol. Sci.* 17 (12), 1978–1991. doi: 10.3390/ijms17121978

Johansson, I., Witkowska, E., Kaveh, B., Lif Holgerson, P., and Tanner, A. C. (2016). The Microbiome in Populations With a Low and High Prevalence of Caries. *J. Dent. Res.* 95 (1), 80–86. doi: 10.1177/0022034515609554

Ledder, R. G., Kampoo, K., Teanpaisan, R., and McBain, A. J. (2018). Oral Microbiota in Severe Early Childhood Caries in Thai Children and Their Families: A Pilot Study. *Front. Microbiol.* 9, 2420. doi: 10.3389/fmicb.2018.02420

Lif Holgerson, P., Harnevik, L., Hernell, O., Tanner, A. C., and Johansson, I. (2011). Mode of Birth Delivery Affects Oral Microbiota in Infants. *J. Dent. Res.* 90 (10), 1183–1188. doi: 10.1177/0022034511418973

Li, H., Zhang, Y., Xiao, B., Xiao, S., Wu, J., and Huang, W. (2020). Impacts of Delivery Mode on Very Low Birth Weight Infants' Oral Microbiome. *Pediatr. Neonatol.* 61 (2), 201–209. doi: 10.1016/j.pedneo.2019.10.004

Ma, C., Chen, F., Zhang, Y., Sun, X., Tong, P., Si, Y., et al. (2015). Comparison of Oral Microbial Profiles Between Children With Severe Early Childhood Caries and Caries-Free Children Using the Human Oral Microbe Identification Microarray. *PLoS One* 10 (3), e0122075. doi: 10.1371/journal.pone.0122075

Marsh, P. D. (2018). In Sickness and in Health-What Does the Oral Microbiome Mean to Us? An Ecological Perspective. *Adv. Dental Res.* 29 (1), 60–65. doi: 10.1177/0022034517735295

Mashima, I., and Nakazawa, F. (2014). The Influence of Oral Veillonella Species on Biofilms Formed by Streptococcus Species. *Anaerobe* 28, 54–61. doi: 10.1016/j.anaerobe.2014.05.003

Mashima, I., Theodorea, C. F., Thaweboon, B., Thaweboon, S., and Nakazawa, F. (2016). Identification of Veillonella Species in the Tongue Biofilm by Using a Novel One-Step Polymerase Chain Reaction Method. *PloS One* 11 (6), e0157516. doi: 10.1371/journal.pone.0157516

McMurdie, P. J., and Holmes, S. (2013). Phyloseq: An R Package for Reproducible Interactive Analysis and Graphics of Microbiome Census Data. *PLoS One* 8 (4), e61217. doi: 10.1371/journal.pone.0061217

Moimaz, S. A., Garbin, A. J., Lima, A. M., Lolli, L. F., Saliba, O., and Garbin, C. A. (2014). Risk Factors in the Mother-Child Relationship That Predispose to the Development of Early Childhood Caries. *Eur. Arch. Paediatric Dentistry Off. J. Eur. Acad. Paediatric Dentistry.* 15 (4), 245–250. doi: 10.1007/s40368-014-0108-1

Organization. WH (1997). *Oral Health Surveys - Basic Methods. 4th ed* (Geneva: World Health Organization).

Park, S. N., Park, J. Y., and Kook, J. K. (2010). Development of Species-Specific Polymerase Chain Reaction Primers for Detection of Fusobacterium Periodonticum. *Microbiol. Immunol.* 54 (12), 750–753. doi: 10.1111/j.1348-0421.2010.00279.x

Pattanaporn, K., Saraithong, P., Khongkhunthian, S., Aleksejuniene, J., Laohapensang, P., Chhun, N., et al. (2013). Mode of Delivery, Mutans Streptococci Colonization, and Early Childhood Caries in Three- to Five-Year-Old Thai Children. *Commun. Dent. Oral. Epidemiol.* 41 (3), 212–223. doi: 10.1111/cdoe.12013

Peltzer, K., and Mongkolchati, A. (2015). Severe Early Childhood Caries and Social Determinants in Three-Year-Old Children From Northern Thailand: A Birth Cohort Study. *BMC Oral. Health* 15, 108. doi: 10.1186/s12903-015-0093-8

Pitts, N. B., Zero, D. T., Marsh, P. D., Ekstrand, K., Weintraub, J. A., Ramos-Gomez, F., et al. (2017). Dental Caries. *Nat. Rev. Dis. Primers.* 3, 17030. doi: 10.1038/nrdp.2017.30

Richards, V. P., Alvarez, A. J., Luce, A. R., Bedenbaugh, M., Mitchell, M. L., Burne, R. A., et al. (2017). Microbiomes of Site-Specific Dental Plaques From Children With Different Caries Status. *Infect. Immun.* 85 (8), e00106–17. doi: 10.1128/IAI.00106-17

Saraithong, P., Pattanaporn, K., Chen, Z., Khongkhunthian, S., Laohapensang, P., Chhun, N., et al. (2015). Streptococcus Mutans and Streptococcus Sobrinus Colonization and Caries Experience in 3- and 5-Year-Old Thai Children. *Clin. Oral. Investigat.* 19 (8), 1955–1964. doi: 10.1007/s00784-015-1437-0

Segata, N., Izard, J., Waldron, L., Gevers, D., Miropolsky, L., Garrett, W. S., et al. (2011). Metagenomic Biomarker Discovery and Explanation. *Genome Biol.* 12 (6), R60. doi: 10.1186/gb-2011-12-6-r60

Simon-Soro, A., and Mira, A. (2015). Solving the Etiology of Dental Caries. *Trends Microbiol.* 23 (2), 76–82. doi: 10.1016/j.tim.2014.10.010

Siqueira, J. F. Jr., and Rôças, I. N. (2004). Treponema Species Associated With Abscesses of Endodontic Origin. *Oral. Microbiol. Immunol.* 19 (5), 336–339. doi: 10.1111/j.1399-302x.2004.00156.x

Tanner, A. C., Kent, R. L.Jr., Holgerson, P. L., Hughes, C. V., Loo, C. Y., Kanasi, E., et al. (2011). Microbiota of Severe Early Childhood Caries Before and After Therapy. *J. Dent. Res.* 90 (11), 1298–1305. doi: 10.1177/0022034511421201

Tanner, A. C., Mathney, J. M., Kent, R. L., Chalmers, N. I., Hughes, C. V., Loo, C. Y., et al. (2011). Cultivable Anaerobic Microbiota of Severe Early Childhood Caries. *J. Clin. Microbiol.* 49 (4), 1464–1474. doi: 10.1128/JCM.02427-10

Teng, F., Yang, F., Huang, S., Bo, C., Xu, Z. Z., Amir, A., et al. (2015). Prediction of Early Childhood Caries *via* Spatial-Temporal Variations of Oral Microbiota. *Cell Host Microbe* 18 (3), 296–306. doi: 10.1016/j.chom.2015.08.005

Theodorea, C. F., Mashima, I., Thaweboon, B., Thaweboon, S., and Nakazawa, F. (2017). Molecular Detection of Oral Veillonella Species in the Saliva of Children With Different Oral Hygiene Statuses. *Int. J. Curr. Microbiol. Appl. Sci.* 6 (7), 449–461. doi: 10.20546/ijcmas.2017.607.054

Thitasomakul, S., Thearmontree, A., Piwat, S., Chankanka, O., Pithpornchaiyakul, W., Teanpaisan, R., et al. (2006). A Longitudinal Study of Early Childhood Caries in 9- to 18-Month-Old Thai Infants. *Commun. Dent. Oral. Epidemiol.* 34 (6), 429–436. doi: 10.1111/j.1600-0528.2006.00292.x

Twetman, S., Boustedt, K., Roswall, J., and Dahlgren, J. (2020). Systematic Review Suggests a Relationship Between Moderate to Late Preterm Birth and Early Childhood Caries. *Acta Paediatr.* 109 (12), 2472–2478. doi: 10.1111/apa.15424

Wu, T. T., Xiao, J., Sohn, M. B., Fiscella, K. A., Gilbert, C., Grier, A., et al. (2021). Machine Learning Approach Identified Multi-Platform Factors for Caries

Prediction in Child-Mother Dyads. *Front. Cell Infect. Microbiol.* 11, 727630. doi: 10.3389/fcimb.2021.727630

Wyss, C., Choi, B. K., Schüpbach, P., Guggenheim, B., and Göbel, U. B. (1997). Treponema Amylovorum Sp. Nov., A Saccharolytic Spirochete of Medium Size Isolated From an Advanced Human Periodontal Lesion. *Int. J. Syst. Bacteriol.* 47 (3), 842–845. doi: 10.1099/00207713-47-3-842

Xiao, J., Fiscella, K. A., and Gill, S. R. (2020). Oral Microbiome: Possible Harbinger for Children's Health. *Int. J. Oral. Sci.* 12 (1), 12. doi: 10.1038/s41368-020-0082-x

Xiao, J., Grier, A., Faustoferri, R. C., Alzoubi, S., Gill, A. L., Feng, C., et al. (2018). Association Between Oral Candida and Bacteriome in Children With Severe ECC. *J. Dent. Res.* 97 (13), 1468–1476. doi: 10.1177/0022034518790941

Xu, H., Hao, W., Zhou, Q., Wang, W., Xia, Z., Liu, C., et al. (2014). Plaque Bacterial Microbiome Diversity in Children Younger Than 30 Months With or Without Caries Prior to Eruption of Second Primary Molars. *PLoS One* 9 (2), e89269. doi: 10.1371/journal.pone.0089269

Yang, F., Zeng, X., Ning, K., Liu, K. L., Lo, C. C., Wang, W., et al. (2012). Saliva Microbiomes Distinguish Caries-Active From Healthy Human Populations. *ISME J.* 6 (1), 1–10. doi: 10.1038/ismej.2011.71

Zhang, D., Takeshita, T., Furuta, M., Kageyama, S., Asakawa, M., Nambu, K., et al. (2021). Tongue Microbiota Composition and Dental Caries Experience in Primary School Children. *mSphere* 6 (2), e01252–20. doi: 10.1128/mSphere.01252-20

Conflict of Interest: The authors declare that the research was conducted in the absence of any commercial or financial relationships that could be construed as a potential conflict of interest.

Publisher's Note: All claims expressed in this article are solely those of the authors and do not necessarily represent those of their affiliated organizations, or those of the publisher, the editors and the reviewers. Any product that may be evaluated in this article, or claim that may be made by its manufacturer, is not guaranteed or endorsed by the publisher.

frontiers | Frontiers in Cellular and Infection Microbiology

REVIEW
published: 30 June 2022
doi: 10.3389/fcimb.2022.900918

Dental Materials for Oral Microbiota Dysbiosis: An Update

Jieyu Zhu[1†], Wenlin Chu[1,2†], Jun Luo[2], Jiaojiao Yang[1], Libang He[1*] and Jiyao Li[1]*

[1] State Key Laboratory of Oral Diseases, Department of Cariology and Endodontics, National Clinical Research Center for Oral Diseases, West China Hospital of Stomatology, Sichuan University, Chengdu, China, [2] College of Polymer Science and Engineering, State Key Laboratory of Polymer Materials Engineering, Sichuan University, Chengdu, China

The balance or dysbiosis of the microbial community is a major factor in maintaining human health or causing disease. The unique microenvironment of the oral cavity provides optimal conditions for colonization and proliferation of microbiota, regulated through complex biological signaling systems and interactions with the host. Once the oral microbiota is out of balance, microorganisms produce virulence factors and metabolites, which will cause dental caries, periodontal disease, etc. Microbial metabolism and host immune response change the local microenvironment in turn and further promote the excessive proliferation of dominant microbes in dysbiosis. As the product of interdisciplinary development of materials science, stomatology, and biomedical engineering, oral biomaterials are playing an increasingly important role in regulating the balance of the oral microbiome and treating oral diseases. In this perspective, we discuss the mechanisms underlying the pathogenesis of oral microbiota dysbiosis and introduce emerging materials focusing on oral microbiota dysbiosis in recent years, including inorganic materials, organic materials, and some biomolecules. In addition, the limitations of the current study and possible research trends are also summarized. It is hoped that this review can provide reference and enlightenment for subsequent research on effective treatment strategies for diseases related to oral microbiota dysbiosis.

Keywords: oral microbiota, dysbiosis, oral biofilms, anti-fouling, antimicrobial biomaterials, dental applications

OPEN ACCESS

Edited by:
Jin Xiao,
University of Rochester, United States

Reviewed by:
Yuan Liu,
University of Pennsylvania, United States
Fuhua Yan,
Nanjing Stomatological Hospital (NSH), China

***Correspondence:**
Jiaojiao Yang
jiaojiao.yang@scu.edu.cn
Libang He
helibang@163.com

†These authors have contributed equally to this work and share first authorship

Specialty section:
This article was submitted to Microbiome in Health and Disease, a section of the journal Frontiers in Cellular and Infection Microbiology

Received: *21 March 2022*
Accepted: *07 June 2022*
Published: *30 June 2022*

Citation:
Zhu J, Chu W, Luo J, Yang J, He L and Li J (2022) Dental Materials for Oral Microbiota Dysbiosis: An Update. Front. Cell. Infect. Microbiol. 12:900918. doi: 10.3389/fcimb.2022.900918

Abbreviations: EPS, extracellular polymeric substances; ADS, arginine deiminase system; IPS, intracellular polysaccharides; PRRs, pattern recognition receptors; PAMP, pathogen-associated molecular patterns; IL-1, interleukin-1; IL-6, interleukin-6, TNF, tumor necrosis factor; TLRs, toll-like receptors; IL-8, interleukin-8; Th17, T helper 17 cells; IL-17, interleukin-17; IL-23, interleukin-23; TGF-β, transforming growth factor-β; MMP, matrix metalloproteinases; PEG, polyethylene glycol; MPC, 2-methacryloyloxyethyl phosphorylcholine; Ti, titanium; PEG-PAsp, polyethylene glycol-poly (aspartic acid); LBL, layer by layer; TiO_2, titanium dioxide; UV, ultraviolet; ROS, reactive oxygen species; PTT, Photothermal therapy; NIR, near-infrared light; PDA, polydopamine; GOx, glucose oxidase; MOF, metal-organic frameworks; TiO_{2-x}, oxygen-deficient titania; GO, graphene oxide; NO, nitric oxide; MSNs, mesoporous silica nanoparticles; QAS, quaternary ammonium salts; DMAHDM, dimethylaminohexadecyl methacrylate; ACP, amorphous calcium phosphate; N-X, nitrogen-halogen; PAA, polyacrylic acid; PDT, photodynamic therapy; TBO, toluidine blue O; PP, protoporphyrin IX; Ce 6, Chlorin e6; PEI, polyethyleneimine; SF, silk fibroin; NH_3^+, positively charged ammonium groups AMPs, antimicrobial peptides; MIC, minimum inhibitory concentration; GTR, guided tissue regeneration.

1 INTRODUCTION

The microbiota is involved in the maintenance of host health through multiple pathways. It promotes the maturation of immune cells and the normal development of immune function for immune regulation, acts as a physical barrier to protect the body from foreign pathogens, participates in energy extraction from food, and affects appetite (Wang et al., 2017).

The oral microbiota is an important part of the human microbiota, encompassing over 700 bacterial species, as well as a variety of viruses, fungi, protozoa, and archaea (Deo and Deshmukh, 2019). A healthy individual has 100 to 200+ species of resident bacteria colonized in the oral cavity (Rosier et al., 2018). Fungi are also involved in constituting healthy oral microbiota, while their loads are orders of magnitude lower than bacteria, their size and morphology and synergy with bacteria are crucial in the construction of dental plaque (Diaz et al., 2017). Mark Welch et al. combined sequencing data with spectral fluorescence imaging and revealed that 13 genera are abundant and highly prevalent both in supragingival and subgingival plaque: *Corynebacterium*, *Capnocytophaga*, *Fusobacterium*, *Lepidium*, *Actinomyces*, *Streptococcus*, *Neisseria*, *Haemophilus/Aggregobacteria*, *Porphyromonas*, *Rothella*, *Lautropia*, *Veillonella* and *Prevotella* (Mark Welch et al., 2016).

One of the unique features of the oral cavity compared to the anatomy of other parts of the human body is the presence of teeth. Due to its unique anatomy, the oral cavity contains several distinct ecological niches such as saliva, soft tissue surfaces of the mucosa and hard tissue surfaces of teeth, with different microbial communities (Schwiertz, 2016). The mucous has a constantly renewed physiological process, and the shedding of its aging epithelium is not conducive to the long-term colonization of bacteria (Costalonga and Herzberg, 2014). The salivary microbiota is mainly derived from the shedding of biofilms on the surface of oral tissues, covering 3621 bacterial taxa, of which *Bacteroidetes* (genus *Prevotella*) and *Firmicutes* (genus *Streptococcus* and *Veillonella*) are the main phyla (Keijser et al., 2008). The cheek and palate surfaces have only a single layer of bacteria due to the continuous sloughing of the superficial epithelial layers. However, the tongue surface has multiple layers of biofilm-like bacteria, mainly including *Streptococcus salivarius* (*S. salivarius*), *Rothia mucilaginosa*, and an uncharacterized species of *Eubacterium* (strain FTB41) (Kazor et al., 2003). Significantly, teeth protrude from the mucosal tissue that covers the oral cavity, providing a stable surface for bacterial biofilm formation (Tuominen and Rautava, 2021). According to the location, microbiota on the teeth surface can be divided into two parts: supragingival microbiota (above the gum) and subgingival microbiota (below the gum), which will be described in detail below.

As the most common form of oral microbiota, oral biofilms constitute dynamic, interrelated metabolic networks, whose composition and activity are mainly determined by environment and host (Mclean, 2014). Oral Biofilms are organized communities containing large varieties of microbes embedded in a matrix of extracellular polymeric substances (EPS), whose scaffold is composed of biological macromolecules such as protein, carbohydrate, and nucleic acid (Kuang et al., 2018). The complex microbial network exists interspecies cross-feeding and obtains nutrients, sugars, and amino acids from mucin-containing saliva through the function of glycosidases (Mosaddad et al., 2019). The oral microbiota maintains a healthy state of the microenvironment through multiple pathways. *Veillonella* spp., as one of the main anaerobic bacteria in the oral cavity, is considered beneficial attributes to their abilities that metabolize lactic acid to weaker acids and transfer nitrate (NO_3^-) to nitrite (NO_2^-) (Wicaksono et al., 2020). In addition, there are two main pathways for oral microbiota to generate alkali. Some species like *S. salivarius* and *Actinomyces naeslundii* (*A. naeslundii*) metabolize urea by urease enzymes to produce alkali. The other route is the arginine deiminase system (ADS), from which ADS-positive bacteria like *Streptococcus sanguinis* (*S. sanguinis*) metabolize arginine and yield ornithine, ammonia, ATP, and CO_2 (Liu et al., 2012; Huang et al., 2018). The metabolism of urea and arginine increases local pH, prevents demineralization and promotes remineralization, and also establishes ecological advantages for commensal bacteria and inhibits the growth of various pathogens, thereby maintaining a healthy oral environment (Bowen et al., 2018).

This review addresses the mechanisms underlying the role of the oral microbiota in health and disease states, with a focus on oral diseases caused by microbiota disturbances, including caries, periodontal diseases and peri-implant diseases. On this basis, the emerging materials developed in recent years are reviewed, which are mainly divided into two categories: antifouling materials (covering polymeric agents, biomolecules and metal oxides) and antibacterial materials (covering metals and metal oxides, inorganic nonmetallic materials, organic small molecules, polymers and antimicrobial peptides).

2 ORAL MICROBIOTA-RELATED DISEASES

2.1 Dental Caries

Dental caries, also known as tooth decay, is one of the most prevalent chronic diseases in the world, which can damage both crown and root surface throughout the life cycle, whether in primary or permanent dentition (Selwitz et al., 2007). It is the leading cause of pain and tooth loss in the mouth. As a biofilm-mediated, sugar-driven and multifactorial disease, caries brings about dynamic demineralization and remineralization of dental hard tissue (Pitts et al., 2017). The etiology of dental caries has developed over the centuries, and the involvement of microbes has been acknowledged as early as the late 1800s (Russell, 2009). What can be determined is that the dynamics of carious lesions depend on the availability of fermentable sugars, microbiota, host, and other environmental conditions. However, the specific role of microorganisms in the development and progression of dental caries remains to be further understood.

2.1.1 Supragingival Microbiota

The anatomy of the oral cavity is exceptional compared to that of other human body sites. A unique feature is hard tissue, i.e., teeth that protrude through the mucosa covering a major part of the oral cavity. Teeth provide non-shedding surfaces for distinct bacterial biofilm formation, whereas mucosal surfaces are continuously renewing and older epithelial layers are shedding from the surface, presenting challenges to permanent bacterial colonization (Sedghi et al., 2021). Peculiarly, there is an acquired pellicle covering the teeth surface, which is composed of lipids, proteins, glycolipids, and glycoproteins (Chawhuaveang et al., 2021). Acquired pellicle can protect teeth enamel from acid attack, but also regulates the further attachment of bacteria and promotes the development of biofilm (Thomas et al., 2021).

The structured microbiota is embedded in the EPS matrix consisting of proteins, polysaccharides, lipids, nucleic acids, and other biomolecules and firmly attached to the substrate surface to form biofilms. The physicochemical properties of EPS are critical for the biochemical action of biofilms, including mechanical stability, signal transmission, gene swapping, and antimicrobial tolerance (Karygianni et al., 2020). The initially formed EPS matrix promotes microbial colonization and aggregation, and as the matrix further expands, the EPS wraps around bacterial cells, providing a supportive framework for the development of microscopic colonies (Flemming et al., 2016). The extracellular matrix protects biofilms from mechanical removal and antibacterial agent and creates localized regions of low pH by inhibiting the buffering capacity of saliva, which can facilitate intensive localized acidification and teeth demineralization (Valm, 2019).

The primary initial colonizing bacteria are *Streptococcus*, followed closely by gram-positive bacilli, particularly *Actinomyces* spp. Subsequently, other cocci and bacilli gradually attached to the foregoing gram-positive biofilm (Larsen and Fiehn, 2017). Among them, *Fusobacterium nucleatum* (*F. nucleatum*) plays an essential role in the maturation of biofilms by co-aggregating with the initial bacteria and succeeding gram-negative and motile bacteria, such as *Bacteroidetes* and *Spirochaetes* (Benitez-Paez et al., 2014). Eventually, the cariogenic microbiota is dominated by thriving acidogenic and aciduric microorganisms, including mutans and non-mutans *Streptococcus*, *Actinomyces*, *Bifidobacterium*, *Lactobacillus*, and *Scardovia* spp., whose further synergistic effect will promote EPS generate and microenvironment acidification (Lamont et al., 2018).

Recent advances based on DNA and RNA techniques have further shed light on the microbiota associated with caries. In carious lesions whether in enamel or dentin, the supragingival microbiota dramatically decreased from 500-700 species to 100-200 species-level phylotypes (Simon-Soro and Mira, 2015). The bacteria involved in enamel caries were mainly *Veillonella*, *Rothia*, and *Leptotrichia*, while the bacteria involved in dentin caries were mainly *S. sanguinis*, *Atopobium*, *Schlegelella*, *Pseudoromibacter*, and *Lactobacilli* (Vanaki, 2020). *Streptococcus mutans* (*S. mutans*) and *Lactobacillus* are closely related to dental caries, which can ferment sucrose to polysaccharides and produce lactic and ATP (Zeng and Burne, 2016; Tanner et al., 2018). Some other common cariogenic bacteria exhibit the high potential of sugar decomposition and acid production, including *Corynebacterium*, *Granulicatella*, *Propionibacterium*, and certain strains of *Leptotrichia* (Lamont et al., 2018). And the lactic can be utilized as a carbon source for *Veillonellae*, one of the aciduric species (Chalmers et al., 2008). Besides, *Candida albicans* (*C. albicans*) interact with glucosyltransferases produced by *S. mutans*, enhancing the virulence of the biofilm matrix, which plays a crucial role in early childhood caries (Koo et al., 2018).

2.1.2 Diet and Microbiota

Frequent intake of carbohydrates plays an important role in altering the oral microbiota. Tanner et al. suggested that caries is the result of an imbalance between acid-producing and acid-tolerant bacteria, which is closely related to a frequent diet containing sugar or carbohydrates (Tanner et al., 2018). When sugar intake is low and infrequent, the microbiota on the teeth can remain stable and the small amount of acid production can be easily neutralized by saliva, protecting the teeth from acid erosion and demineralization (Takahashi and Nyvad, 2011). Overexposure to fermentable carbohydrates facilitates the production of EPS and acidic metabolites, as well as the collection of acidogenic and aciduric microorganisms, thus driving the conversion to pathogenic microbiota (Bowen et al., 2018). Microbes will be embedded in the biofilm matrix when carbohydrates are ingested frequently. As a result, local pH is lowered by continuous acid production that avoids saliva buffer, thereby inducing the mineral balance towards demineralization (Takahashi and Nyvad, 2011).

Ecological perspectives for microbiota dysbiosis in dental caries contain 3 reversible stages (Takahashi and Nyvad, 2011). The healthy state's microbiota on the enamel surface consists mainly of non-mutans *Streptococci* and *Actinomyces*, with mild and uncommon acid production. When demineralization/remineralization is in equilibrium or the balance is tilted towards mineral gain, it is in a dynamic stability stage. When frequent carbohydrate supplies lead to a prolonged acidic environment, acid production and acidity of non-mutans bacteria are adaptively enhanced, and more aciduric strains selectively increase. Therefore, the demineralization/remineralization balance is induced to shift towards mineral loss and promotes caries development, which is in an acidogenic stage. The prolonged acidic condition further induces acidic selection of aciduric and acidogenic bacteria to become dominant bacteria, including *mutans Streptococci* and *Lactobacilli* as well as aciduric strains of non-mutans *Streptococci*, *Actinomyces*, Bifidobacteria, and yeasts, which is called an aciduric stage.

Compared with glucose, fructose, and starch, sucrose has strong cariogenic potential due to its fermentability and can be used as a substrate for glucosyltransferase of *S. mutans* to synthesize EPS and intracellular polysaccharides (IPS) (Paes Leme et al., 2006). EPS boost bacterial adhesion on tooth surfaces, causing structural and chemical changes of the biofilm matrix, which makes it more difficult to remove

biofilm (Liu et al., 2018b). In addition, IPS reduces pH during nutrient deprivation, leading to the selective proliferation of cariogenic microbiota (Costa Oliveira et al., 2021).

Dental caries is an event of microbiota dysbiosis, and diet plays a key role by providing a highly structured and localized acidic microenvironment, promoting caries development through demineralization that conversely shapes the constitution and bioactivity of microbiota. Apparently, challenges existing in controlling cariogenic biofilms mainly include the following aspects. First, the cariogenic microorganisms entangled in the EPS-rich biofilm matrix are protected by the matrix, making it hard to combat or eliminate. Second, EPS generate an extremely acidic microenvironment, promoting the proliferation of cariogenic microbiota and reducing the therapeutic efficacy of drugs. Lastly, because of the rapid refresh effect caused by oral activity and saliva scouring, topical medications barely sustained on biofilms.

2.2 Periodontitis

Unlike infections caused by a single microbial pathogen, periodontitis is triggered by the synergy of multiple microbial communities rather than by specific microorganisms. Arguably, periodontitis is not an infectious disease, but a dysbiosis disease, relating to changes in species abundance in the microbiota and the impact of such changes on health (Lamont et al., 2018). In addition, periodontal dysbiosis is in connection with the disruption of tissue homeostasis, largely due to microbial subversion of local immune response (Hajishengallis, 2015). As the disease progresses, further periodontal tissue destruction will eventually lead to loosening and even loss of teeth, directly affecting chewing or speaking function as well as aesthetics, reducing the patient's quality of life (Pihlstrom et al., 2005).

2.2.1 Subgingival Microbiota

Characteristics of the local environment determine the properties of relevant microbiota. Matching the constant renewal of gingival epithelial cells, the corresponding microbiota develops more rapidly and is less complex than that on the tooth surface (Hajishengallis and Lamont, 2021). Furthermore, to cope with loss upon host cell death, plenty of colonizing bacteria in the junctional epithelium invade tissue and internalize within the epithelium, where they are protected from host immune molecules (Yilmaz et al., 2006; Lee et al., 2020). The subgingival microbiota in health includes gram-positive bacteria and a few numerically abundant gram-negative bacteria, spatially arranged in organized associations and interacting in a physical and metabolic way (Curtis et al., 2020). Among them, gram-positive cocci and rod cells predominated in number during early colonization (Listgarten, 1976). *Actinomyces* spp. can co-aggregate with other bacteria such as *Streptococcus* in initiate colonization stage to construct the skeleton of dental plaque biofilms (Kolenbrander et al., 2006). Notably, there are still health-related species in periodontitis and vice versa, further confirming that periodontal disease is caused by a dysbiosis rather than a single pathogen (Curtis et al., 2020).

Compared with healthy individuals, the total bacterial count of the subgingival microbiota in periodontitis individuals was similar. However, the predominant bacterial species in the subgingival microbiota of the two subjects have a significant difference. The subgingival microbiota in health has higher proportions of *Streptococcus* species, suggesting it is the main component of the health subgingival microbial community. Nevertheless, periodontitis had a higher proportion of obligate anaerobic bacteria in the subgingival microbiota, especially Porphyromonas *gingivalis* (*P. gingivalis*), *Tannerella forsythia* (*T. forsythia*), and *Eubacterium saphenum* (*E. saphenum*) (Abiko et al., 2010). Socransky and his team utilized whole genomic DNA probes and checkerboard DNA-DNA hybridization to distinguish the periodontal microbiotas and create a color-coded system to characterize them. Among them, the "red complex" group consisting of *P. gingivalis*, *T. forsythia*, and *Treponema denticola* (*T. denticola*) is the most closely related to periodontal disease, increasing in number with the depth of periodontal pocket (Socransky et al., 1998; Mineoka et al., 2008). The bridging orange-complex species, i.e., *F. nucleatum* and *Prevotella* spp., and late red-complex colonizers, take longer to mature than fast thriving yellow-complex species in the early colonization such as *Streptococcus* spp. (Teles et al., 2013).

It is obvious that the dysbiosis of the microbiota causes differences in metabolic pathways and functions. Elevated levels of bacterial motility proteins and flagellar assembly may imply an increased invasive capacity of pathogenic bacteria in periodontitis (Cai et al., 2021). Studies have shown that bacterial phenolic acid metabolites, especially phenylacetate and volatile sulfur compounds were positively associated with periodontal exploration depth (Liebsch et al., 2019; Abdullah et al., 2020). In addition, valine, phenylalanine, isoleucine, tyrosine, and butyrate were significantly upregulated in periodontitis subjects, while lactate, pyruvate, and N-acetyl were the most strongly expressed in healthy subjects (Romano et al., 2018).

Co-infection can enhance adhesion and invasion of the red complex to gingival epithelial cells (Li et al., 2015). Synergistic community interaction provides a platform for comprehensive regulation of actions, including obtaining nutrient acquisition, expressing genes, and swapping DNA. It is now well established that, the pathogenicity of periodontal pathogens only becomes meaningful under the interaction of synergistic microbial communities, determining the nature and function of the whole microbiota (Hajishengallis and Lamont, 2012).

2.2.2 Host Immune Defense

Although the predominant colonization of certain bacteria is considered to be closely associated with periodontal disease, they have also been detected in a healthy state. Therefore, it cannot be arbitrarily assumed that these bacteria are the sole cause of periodontal disease, as their pathogenic process requires the evolution from a healthy, organized microbiota to a dysbiotic microbiota, which ultimately promotes inflammation and tissue destruction of the periodontal tissue. It is now widely accepted that periodontitis is an inflammatory disease destructing periodontal soft and hard tissues. Microbiota dysbiosis is an initiating factor of local inflammation, while hyperactivation of the host immune

system is the direct factor that stimulates osteoclast activity and causes alveolar bone resorption (Pan et al., 2019).

Under physiological conditions, the immune system does not mount a severe inflammatory response during immune monitoring and tolerance of the microbiota (Graves et al., 2019). However, the immune system will overreact in the context of microbiota dysbiosis, contributing to localized inflammatory infiltration. As the dysregulated microbiota continuously stimulates and hurts periodontal tissue, immune cells such as specific T cell subsets, antigen presenting cells, and mononuclear phagocytes are recruited locally. During this process, the interaction of pattern recognition receptors (PRRs) with pathogen-associated molecular patterns (PAMP) expressed by the pathogen microorganisms leads to the secretion of pro-inflammatory cytokines, including interleukin-1 (IL-1), interleukin-6 (IL-6), and tumor necrosis factor (TNF), which has the function of activating lymphocyte and destroying tissue (Graves, 2008; Gu and Han, 2020). Additionally, immune cells secret a cluster of particular cytokines, activating relevant signaling pathways and promoting the differentiation of specific lymphocyte subsets with the participation of IL-1 and IL-6. These lymphocyte subsets in turn secrete specific patterns of cytokines that serve as positive-feedback factors or direct effectors to regulate the immune response as well as osteoclast activity (Pan et al., 2019).

P. gingivalis can secret toxic factors like LPS, gingipains, and pili to directly destroy periodontal tissues, and also activate host immune cells to trigger local immune responses and motivate the release of inflammatory mediators, resulting in secondary tissue damage (Jia et al., 2019). As PAMP recognition receptors, toll-like receptors (TLRs) can mediate the host's innate immune response to *P. gingivalis*, the foundation of acquired immunity, playing a crucial role in the occurrence and development of periodontitis (Nakayama and Ohara, 2017).

As an important factor in periodontal tissue destruction, matrix metalloproteinases have the ability to decompose the extracellular matrix and basement membrane, representing a group of structurally related but genetically distinct enzymes. The expression of matrix metalloproteinases is low in healthy periodontal tissues. However, when interleukin-8 (IL-8) is secreted in response to bacterial biofilms, neutrophils are recruited to sites containing biofilms and secrete matrix metalloproteinases 8, which mainly degrades interstitial collagen (Sorsa et al., 2006). It has been found that *F. nucleatum* may induce the production of matrix metalloproteinase-13, which can degrade collagens of types I, III and IV, as well as fibronectin (Uitto et al., 2003). The activation of matrix metalloproteinases is a combined result of tissue, plasma and bacterial proteinases, combined with the effects of oxidative stress (Cekici et al., 2014).

Recently, some studies have identified T helper 17 (Th17) cells and correlative cytokines such as interleukin-17 (IL-17) have been implicated in the pathogenesis of periodontitis because of the ability to induce osteoclastogenesis (Cheng et al., 2014; Bunte and Beikler, 2019). The study by Cheng et al. showed that *P. gingivalis* and *Actinobacillus actinomycetemcomitans* enhance Th17/IL-17 responses through activating human CD14(+) monocytes (Cheng et al., 2016).

2.3 Peri-Implant Diseases

Over the past 50 years, the application of dental implants to improve chewing efficiency and living quality of patients with loss of teeth has become more and more prevalent due to its remarkable biological advantages (Buser et al., 2017). But in the last 30 years, peri-implant infective diseases have emerged, including peri-implant mucositis only involving peri-implant soft tissue and peri-implantitis that also involves peri-implant bone loss (Zitzmann and Berglundh, 2008; Berglundh et al., 2018). Peri-implant diseases cause implant loosening or eventual removal in most cases, placing a huge financial burden on the patient and severely impairing quality of life (Greenstein and Cavallaro, 2014).

Peri-implant diseases and periodontal diseases share similar risk factors, making their clinical outcomes similar. However, recent proteomic and molecular studies have shown a significant difference between peri-implant diseases and periodontal diseases.

2.3.1 Peri-Implant Microbiota

Dental implants provide a colonized surface for microbiota that differs teeth in roughness, surface energy, morphology, and material. In detail, dental implants are made of titanium and/or ceramics, in the shape of a conical screw, have a higher surface roughness and lower surface energy than teeth, so they are more susceptible to bacterial adhesion, and have greater bacterial abundance (Robitaille et al., 2016).

Surface irregular bacterial colonization begins about 30 minutes after the dental implant is placed in the oral tissue (Van winkelhoff et al., 2000). Driven by van der Waals forces, electrostatic and hydrophobic interactions, bacteria approach and finally adhere to the acquired pellicle, thereby establishing irreversible adhesion, followed by up-regulation of bacterial metabolic activity and extensive bacterial colonization of the implant surface (Wassmann et al., 2017). At the whole-microbiome level, the peri-implant microbiota has comparatively low diversity and less variability, which was characterized by 71 species (Ghensi et al., 2020). The healthy peri-implant oral microenvironment is predominantly colonized by *Streptococcus*, which accounts for 45% to 86% of supragingival and subgingival peri-implant microbiota. Besides, *Actinomyces* as well as *Rothia* and *Neisseria* species have also been continually isolated (Quirynen et al., 2005).

Whereas 12 species were enriched in peri-implantitis: *Fretibacterium fastidiosum* (*F. fastidiosum*), *T. forsythia*, *Desulfobulbus* spp. oral taxon 041, *Treponema socranskii*, *Filifactor alocis*, *T. denticola*, *Porphyromonas endodontalis* (*P. endodontalis*), *Treponema maltophilum*, *Pseudoramibacter alactolyticus*, *Treponema lecithinolyticum*, *P. gingivalis*, *F. nucleatum* (Ghensi et al., 2020). Using 16S rRNA sequencing, Schaumann et al investigated the microbial composition of biofilms at different oral sites in individuals with peri-implantitis (Schaumann et al., 2014). The study found that the most abundant submucosal species on implants were *Rothia*, *Streptococcaceae*, and *Porphyromonas*, while the most abundant subgingival bacteria on teeth were *Prevotella*, *Streptococcaceae*, and *TG5*.

A recent study by Shi et al. determined that the richness, diversity, and distribution of microbiota were very similar between peri-implant mucositis and peri-implantitis, both having the core microbiota: *Porphyromonas*, *Fusobacterium*, *Treponema*, *Prevotella*, and *Campylobacter* (Shi et al., 2022). Compared with periodontal diseases, peri-implant diseases are related to higher levels of *Peptococcus*, *Mycoplasma*, *Eubacterium*, *Campylobacter*, *Butyrivibrio*, *S. mutans*, and *Treponema*, and lower levels of *Prevotella*, non-mutans *Streptococcus*, *Lactobacillus*, *Selenomonas*, *Leptotrichia*, *Actinomyces* (Robitaille et al., 2016). Another study showed some interesting results, such as *Selenomonas artemidis*, *Eikenella corrodens*, *Ottowia* sp. HOT894 and *Neisseria meningitidis* appeared to uniquely be relevant to peri-implants inflammation (Schincaglia et al., 2017). Ghensi et al. suggested defining the "peri-implantitis-related complex" of 7 species strongly characterizing peri-implantitis sites: the red complex triad (*P. gingivalis*, *T. forsythia*, *T. denticola*), the *P. endodontalis* and *F. fastidiosum* species, the *Prevotella intermedia*, and *F. nucleatum* species (Ghensi et al., 2020). Among them, *F. nucleatum* is closely associated with peri-implant diseases, especially peri-implant mucositis, and is also a key bacterium in the microbiota associated with periodontal disease.

In addition, observational studies suggested that peri-implantitis was an intricate and multifactorial infection, associated with opportunistic pathogens such as *Staphylococcus aureus* (*S. aureus*) and *Pseudomonas aeruginosa* (*P. aeruginosa*), fungal organisms (*C. albicans*, *Candida boidinii*, *Paelicomyces* spp., *Penicillum* spp., *Rhadotorula laryngis*), and viruses (human cytomegalovirus, Epstein-Barr virus) (Schwarz et al., 2018).

In a word, the peri-implant disease is associated with dysbiosis in the microbiota, some of which may take part in the initiation of disease while others contribute to disease progression.

2.3.2 Host Immune Defense

Peri-implant mucositis is characterized by changes in the composition of the microbiota with an increase in gram-negative microorganisms and activation of local host responses. Microbiota dysbiosis causes the release of chemotactic peptides and cytokines that recruit leukocytes such as neutrophils to peri-implant pockets, thus engulfing and digesting bacteria. However, if the neutrophils degranulate by excessive bacteria, they will release toxic enzymes and damage peri-implant tissue (Petkovic et al., 2010).

Health-associated bacterial biomarkers include chaperonin, iron uptake protein A2, and phosphoenolpyruvate carboxylase. Some biomarkers like ribulose biphosphate carboxylase, succinyl-CoA:3-ketoacid-coenzyme A transferase, and DNA-directed RNA polymerase subunit beta are specific in periodontitis and are also important in peri-implantitis (Baliban et al., 2012). Chemokines (IL-8 and MIP-1α) and proinflammatory cytokines (IL-1β and TNF-α) may serve as markers for monitoring the condition of peri-implant tissues (Petkovic et al., 2010). Immunohistochemical staining showed that IL-1α expression was more prevalent in peri-implant tissues, whereas TNF-α expression was more prevalent in periodontitis tissues (Konittinen et al., 2006).

The pro-inflammatory molecule IL-17, produced by Th17 cells, modulates multiple biological inflammatory effects, including recruiting neutrophils and macrophages and stimulating other pro-inflammatory mechanisms (Ouyang et al., 2008). Mardegan et al. investigated the Th17 (IL-17 and interleukin-23, IL-23) and Treg (transforming growth factor-β, TGF-β) cytokine gene expression levels in healthy and peri-implantitis tissues (Mardegan et al., 2017). A predominant Th17 response and a reduction of Treg response was observed in peri-implantitis tissue compared to healthy tissue, especially arising from up-regulation of IL-23 and down-regulation of TGF-β around the implant.

Mikolai et al investigated early host-microbe interaction based on a peri-implant oral mucosa-biofilm model and obtained profound knowledge (Mikolai et al., 2020). The study showed *P. gingivalis* is capable of attenuating the PI3K-Akt signaling pathway and disrupting cell-cell junctions at gene and protein levels, thereby enhancing bacterial colonization and damaging the epithelial barrier. Furthermore, the release of antimicrobial peptides or mucosa breakdown products and/or the presence of *P. gingivalis* may lead to altered bacterial distribution with an increased proportion of *Veillonella dispar*, deriving lipopolysaccharides to induce TLR4-dependent host cell responses, which can lead to inflammation. Intriguingly, compared to periodontitis, fibroblasts isolated from peri-implantitis had greater production of matrix metalloproteinases (MMP), vascularizing factors, and complement receptor C1q, and less production of metalloproteinase inhibitors and growth factors, which promote collagen synthesis, which may explain the faster and more extensive tissue destruction in peri-implantitis (Belibasakis, 2014).

Duarte et al. used quantitative polymerase chain reaction to assess the gene expression of different inflammatory factors in gingiva from healthy implants and various degrees of peri-implant diseases (Duarte et al., 2009). The study revealed that, concerning inflammatory factors, IL-12 and TNF-α were higher in severe peri-implantitis, followed by initial peri-implantitis and mucositis, while IL-4 was higher in healthy projects, followed by mucositis, severe, and initial peri-implantitis. In consideration of osteoclastogenesis-related factors, RANKL increased with peri-implantitis severity, while OPG mRNA levels were higher in healthy implants, followed by initial, severe peri-implantitis, and mucositis.

3 MATERIALS STRATEGIES

3.1 Antifouling Materials

Building an early biofilm asks for the absorption of protein to the solid surfaces to construct the salivary acquired pellicles, along with the adherence of initial colonizers to them. Then the subsequent adhering of other oral pathogens to immobilized bacteria, also known as cohesion or coaggregation, leads to maturation of the biofilm (Kolenbrander et al., 2010). The antifouling property of biomaterials, including protein

repulsion and bacteria anti-adhesion, can protect surfaces from invasion of early biofilm. In addition, the accumulation of dead pathogens and bio-foulants on oral surfaces or dental materials can be prevented by introducing the antifouling property, which unblocks other biofunctions (Duan et al., 2022). Current antifouling materials are usually polymeric antifouling agents, besides, some biomolecules and special metals also show the antifouling property.

3.1.1 Polymeric Agents

An effective intervention for inhibiting the absorption of bacteria and protein on the material surfaces is to reduce the contact area among them. For this purpose, the water barrier effect of hydrophilic materials can play a certain role. In theory, a hydrophilic material usually has strong hydrogen bond interactions with water molecules, which can induce water molecules to bind intensively with material surfaces, leading to the formation of a hydration layer with the shielding effect. The existence of a hydration layer can make it difficult for bacteria and protein to get close to material surfaces, thus achieving a good anti-fouling property (Jin et al., 2022). Currently, polyethylene glycol (PEG) and zwitterionic polymer are the two most widely used hydrophilic anti-fouling materials (Venault et al., 2014; Lee et al., 2019). PEG is a flexible polymer with -CH_2-CH_2-O- as the repeated unit, which make it not only has hydrogen bonding with water molecules, but also equip with the steric repulsion effect to prevent the invasion of bacteria and protein. Benefitting from the ion's solvent effect, zwitterionics has a stronger interaction to form a denser hydration layer. Among all, 2-methacryloyloxyethyl phosphorylcholine (MPC) has been used in the antifouling application due to its optimizable molecular structure (Baggerman et al., 2019). The surface charge can be adjusted by controlling the positive to negative groups ratio. Consequently, the antiadhesion propertied can be tuned. However, materials with the hydrophilic property are not stable to bind with the matrix, which is also the main limitation to develop them as the antifouling coating. Buxadera-Palomero et al. once prepared PEG coatings on the titanium (Ti, still contemplated to be the first choice in dental implant therapy) surface by plasma polymerization (Hwang et al., 2012). Subsequently, they took advantage of the pulsed electrodeposition technology to construct the PEG coating on Ti surfaces (Buxadera-Palomero et al., 2020). Both two means can achieve expected bacteria antiadhesion. But the successful coating by plasma polymerization and electrodeposition depends on extra devices, complicating the whole process. To solve it, the method that PEG or zwitterionics are fixed on the substrate surfaces by chemical grafting has come into view. Choi et al. grafted MPC brushes on the PMMA resins with different grafting efficiencies by the free radical polymerization (Choi et al., 2020). Meanwhile, the hydration and MPC dynamics were evaluated logically and quantitatively by molecular simulation and Raman spectroscope to optimize the antifouling property. The resulting resins proved a nonspecific bacteria antiadhesion behavior aiming at *A. naeslundii*, *S. aureus* and *P. aeruginosa* (**Figure 1A**). Silane chemistry is another available method to graft organic polymers to inorganic substrates. Alkoxysilane of silane coupling agents is reactive to inorganic matter, while organo-functional groups can be compatible with organic matter. Peng et al. prepared silane-ended PEG chain with varied molecular weight and coated it on the tooth stainless steel archwire (Peng et al., 2017). The PEG-coated archwire showed excellent long-term bacteria antiadhesion properties (**Figure 1B**). Coating materials with chemical grafting is only applicable to the modification of dental materials such as implants or resins rather than oral tissue. In view of the abundant existence of Ca^{2+} ions on the tooth surfaces, modifying polymers with groups that can interact with these ions has been an alternative. For example, Hou et al. synthesized a highly hydrophilic diblock copolymer polyethylene glycol-poly (aspartic acid) (PEG-PAsp), where carboxyl groups in the PAsp segments provide binding sites with Ca^{2+} on the enamel surfaces, so that PEG segments on the other side can inhibit *S. mutans* and Stoeptococcus *sanguis* (*S. sanguis*) adhesion on the enamel (Hou et al., 2020). Compared with carboxyl groups, PO_4^{3-} groups are equipped with stronger ability to bind with Ca^{2+}. Inspired by this, Kang et al. modified MPC polymers with PO_4^{3-} to immobilize them on the tooth surfaces (Kang et al., 2016). Researches demonstrated that the introduction of PO_4^{3-} ensured sufficient MPC coatings, resulting in increasing hydrophilicity and decreasing the adhesion of protein and *S. mutans*.

When the solution of bacteria or protein contacts the solid surface of materials, the new interaction between foulants and materials needs to be supplied to support the disruption of original liquid-liquid and solid-solid intermolecular force and to form the intermolecular force between the liquid and the solid surface. During this process, the former reflects the surface energy of liquid and solid materials respectively, and the latter represents the wettability of materials. So hydrophobic materials, or rather materials with lower surface energy, can weaken the interaction between foulants and materials, further improving the antiadhesion capability (Cazzaniga et al., 2015). The silicon-based materials are one of the most widely used polymeric antifouling agents for their low surface energy. Polysiloxane and its derivatives are typical silicone materials and have been demonstrated to serve as coatings for resistance to protein sorption (Yilgör and Yilgör, 2014; Santiago et al., 2016). Recently, Yu et al. synthesized a branched silicone methacrylate and incorporated it into the resin composites aiming at inhibiting the bacterial adhesion by decreasing the resin surface energy (Yu et al., 2020). Fluoropolymers are another option to serve as the low-surface-energy coatings for oral care. Churchley et al. synthesized a series of fluoropolymers and investigated their effectiveness as dental-care coatings (Churchley et al., 2008). These coatings behaved good resistance to several oral bacteria including *S. sanguinis*, *A. naeslundii* and cariogenic *S. mutans* and showed the potential of inhibiting acid demineralization. But it is regrettable that a correlation between anti-adhesion capability of fluoropolymers and their fluorine content or surface energy has not been established.

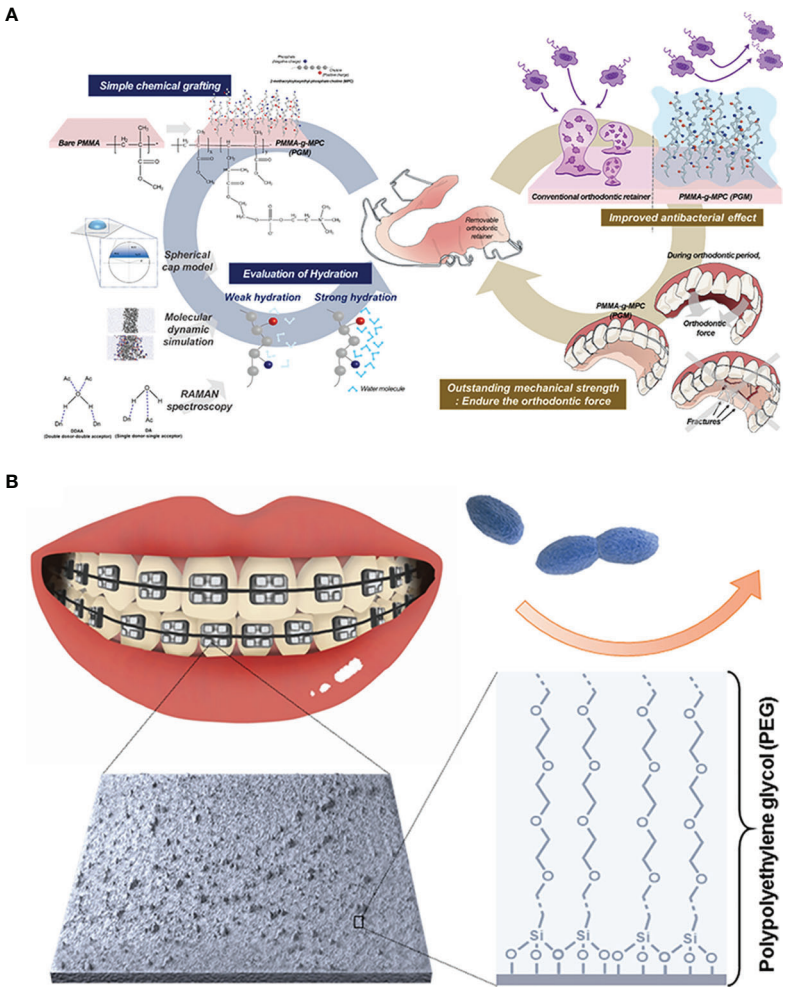

FIGURE 1 | Polymeric anti-fouling strategies: **(A)** zwitterionic antifouling coating grafted onto the PMMA resin for bacterial anti-adhesion; **(B)** hydrophilic PEG-coated stainless steel archwire to achieve antiadhesive property.

3.1.2 Biomolecules

DNA is an emerging highly stable biopolymer in the biomedical field due to its unique and predictable properties. Attributed to the fact that some bacteria are known to deposit DNA to prevent the colonization of other bacteria around them, recent research has hypothesized that DNA coatings possess antifouling properties against bacteria (Berne et al., 2010). Subbiahdoss et al. coated DNA on the matrix by the layer by layer (LBL) technique to determine whether DNA coatings can inhibit microbial fouling (Subbiahdoss et al., 2019). Reduced number of several adherent bacteria on the DNA-coated matrix showed the potential in antifouling applications. Later, this team used a multilayer coating composed of DNA and chitosan by the LbL deposition on PMMA resins and Ti implants and demonstrated that these modified surfaces can prevent bacteria adhesion and biofilm formation (Ouni et al., 2021).

3.1.3 Metal Oxide

The light-induced hydrophobic and hydrophilic transformation property of metal oxides enable them to be used for surface self-cleaning. Under the illumination of ultraviolet (UV) light with energy greater than the band gap, the valence band electrons of the metal oxides are excited to the conduction band, resulting in the formation of holes in the valence band. The holes "randomly walk" to the surface of the metal oxides and react with surface oxygen ions to form oxygen vacancies. At this time, oxygen vacancies can promote the dissociation and absorption of water molecules in the air to form a chemical adsorption surface (surface hydroxyl groups). Hydroxyl groups can further adsorb water molecules, thereby improving the hydrophilicity of the surface (Caputo et al., 2008; Sahoo et al., 2013). Since the viewpoint that the hydrophilicity and wettability of titanium dioxide (TiO_2) polycrystalline films can be transformed by UV irradiation was proposed by Fujishima in 1997 (Wang et al., 1997),

several metal oxides including ZnO, α-Fe_2O_3, WO_3, V_2O_5 and SnO_2 have been found successively to possess the photo-induced hydrophilicity (Feng et al., 2004; Lim et al., 2007; Papadopoulou et al., 2009; Gu et al., 2010; Talinungsang et al., 2019). For example, Papadopoulou et al. prepared ZnO nanograins by pulsed laser deposition and proved the light-induced superhydrophilicity in the hydrophobic structures (Papadopoulou et al., 2009). Yan et al. observed that the hydrophilic transformation behavior can also occur in α-Fe_2O_3 nanoflake films, whose contact angles can be switched from 160 to 0° upon stimulation brought from UV irradiation (Feng et al., 2004).

However, the light-induced hydrophobic and hydrophilic transformation property of metal oxides is reversible (Caputo et al., 2008). That is to say, the absorbed hydroxyl groups on the surface would be replaced again with oxygen in the air and hydrophilic materials return to their hydrophobic state once UV irradiation was stopped. The inevitable reversibility limits the application of metal oxides as light-induced antifouling materials in the treatment of oral diseases.

From the application point of view, the major disadvantage of metal oxides lies in its roughness and wettability, which is closely related to the surface topological structures (Packham, 2003; Chen et al., 2021). Hence, it is important to achieve their structure adjustable, especially at the micro/nanoscale. TiO_2 nanomaterials are representative of nano-topological surfaces with the bacterial anti-adhesion property. Nowadays, nanostructured TiO_2 materials with good wettability were extensively investigated in antifouling applications. Hu et al. constructed a composite nanostructure of TiO_2 nanotubes on the substrates, which exhibited *S. sanguinis* and *S. mutans* antiadhesion behaviors (Hu et al., 2018). In addition to nanotubes, nanostructure surfaces such as nanopores, nanorods and nanogrooves have been indicated to possess good bacteria antiadhesion properties (Ferraris et al., 2017; Valdez-Salas et al., 2019). Besides, changing parameters of nanopatterns can lead to the changes of roughness and hydrophilicity on the surfaces, affecting the antiadhesion ability (Chen et al., 2021). For example, Krunal et al. studied the effects of different diameters of TiO_2 nanotubes on the adherence of two oral bacteria S. *sanguinis* and *S. mutans* (Narendrakumar et al., 2015). In this study, they showed that the amount of attached bacteria can be adjusted as changing the nanotube diameters and demonstrated the possibility of tailoring nanostructure.

3.2 Antibacterial Materials

Antifouling agents have surely come into play in preventing microbial attachment and biofilm formation. Once bacteria are attached on the surfaces of teeth and dental materials to form the biofilm, antifouling agents are of no effect. While materials with antimicrobial properties are capable of killing those attached bacteria or destroying EPS according to several mechanisms and have become a strong candidate to regulate microbial environments.

3.2.1 Metal and Metal Oxide

Many metal elements such as Ag, Cu, Zn and so on perform broad-spectrum antibacterial ability as positively charged metal ions (Ag^+, Cu^{2+}, Zn^{2+}) can cause membrane destabilization and pore formation, leading to cytoplasmic metabolites leakage (Kędziora et al., 2018). However, releasing large amounts of metal ions in a short period of time will cause local excessive concentrations, producing a toxic effect on cells. To solve the problem, metal and metal oxide nanoparticles are used to achieve the ions' slow release by the oxidative dissolution of ions from the nanoparticle surface. Besides, nanoparticles themselves have the ability of physical damage and membrane destabilization, which can reduce the number of needed metal ions (Gold et al., 2018). Dutra-Correa et al. functioned Ag nanoparticles with stabilizers to control the nanoparticle sizes and prevent aggregation (Dutra-Correa et al., 2018). These functioned nanoparticles can be incorporated into the dental adhesive at a lower concentration than that of previous studies. The antibacterial experiment and mechanical analysis demonstrated that Ag nanoparticles at a low concentration can still have the antibacterial effect on *S. mutans* without increasing the influence on mechanical properties of adhesive.

In addition to the contact-killing mechanism of metal nanoparticles, they can also lead to the change of surrounding environment such as elevating temperature or generating reactive oxygen species (ROS) to kill bacteria by response to external stimulus. Photothermal therapy (PTT) is a kind of emerging antibacterial means and has been achieved by the absorption of near-infrared light (NIR) of metal nanoparticles, especially Ag nanoparticles to generate heat, thus causing high temperature in the local to denature proteins of bacteria and kill them. Xu et al. developed a removable multilevel photothermal antibacterial nanoagent in which Fe_3O_4 was used as the core and polydopamine (PDA), Ag and glycol chitosan were coated in sequence (Xu et al., 2022). The existence of PDA slowed down the release of Ag^+ so as to avoid tissue damage while the photothermal conversion property of Ag nanoparticles can realize effective sterilization within a short time when they were irradiated by NIR. The antibacterial experiment revealed the excellent bacterial and biofilm inhibition ratio (over 95% and 50% respectively) aiming at oral cariogenic bacteria.

In 2007, paramagnetic Fe_3O_4 nanoparticles with the peroxidase-like activity were discovered by Yan's team for the first time (Gao et al., 2007). The finding led to rapid development in the research for nanoparticles with similar property. So far, several kinds of metal and metal oxide nanoparticles including Fe_3O_4, Pt, Pd, Au, CeO_2, CuO and so on have been confirmed to have the peroxidase-like activity (Fang et al., 2018; Xiang et al., 2020). Such nanoparticles with enzyme-like catalytic activity are also known as nanoenzyme, which can break down H_2O_2 to generate ROS at acidic pH values for degrading the biofilm EPS and simultaneously killing embedded bacteria. Gao et al. synthesized catalytic nanoparticles containing biocompatible Fe_3O_4 with peroxidase-like activity in a solvothermal system (Gao et al., 2016). These catalytic nanoparticles have been shown to activate exogenous H_2O_2 *in situ* to generate ROS that can achieve not only rapid bacteria killing but glucan degradation in biofilm EPS. Furthermore, the nanoparticles also exhibited an additional property of preventing hydroxyapatite demineralization, which was beneficial from the caries treatment.

Likewise, Liu et al. designed a nanoparticles Ferumoxytol, which was comprised of iron oxide cores coated with carboxymethyl-dextran (Liu et al., 2018a). The nanoparticles also displayed biofilm disruption capability by activating H_2O_2 to cause *S. mutans* death and EPS matrix degradation (**Figure 2A**). The subsequent research revealed the antibacterial specificity of Ferumoxytol against *S. mutans*. They analyzed that the targeting property could be attributed to the interactions between carboxymethyl-dextran of Ferumoxytol and specific glucan-binding proteins of *S. mutans* (**Figure 2B**) (Liu et al., 2021b). Although these catalytic nanoparticles exhibited excellent antibacterial properties, the inappropriate additive amount of exogenous H_2O_2 can induce excess ROS causing cell damage. Considering that, glucose oxidase (GOx), an endogenous oxidoreductase that can catalyze the oxidation of β-D glucose into H_2O_2, has come into view (Chaichi and Ehsani, 2016; Laothanachareon et al., 2018). Ji et al. prepared Fe_3O_4 nanoparticles and modified them with GOx (Ji et al., 2021). GOx can catalyze glucose in the biofilm matrix to generate H_2O_2, which can be further catalyzed by Fe_3O_4 nanoparticles to produce ROS. In addition, the oxidation of GOx depleted the oxygen and glucan, helping to starve bacteria to death. Inspired by the specific binding of glucan and oxidation capability of GOx, Huang et al. coated iron oxide nanoparticles with both glucan and GOx (Huang et al., 2021). The resulting nanohybrid had significant *S. mutans* killing efficacy without affecting commensal *S. oralis*. To reduce the used amount of nanoparticles, these metals can be fixed in other materials such as carbon nitride and metal-organic frameworks (MOF) (Wang et al., 2020; Wu et al., 2021b). Yu et al. reported single-atom dopped MOF catalytic systems with several metal atoms including Pt, Au, Cu, and Ru for the treatment of periodontitis (Yu et al., 2022). Due to its three-dimensional and porous structure, the MOF-based catalytic system had plentiful catalytic sites so as to improve catalytic activity and reduce metal consumption (Liu et al., 2020).

In addition to being a light-responsive antifouling agent, TiO_2 is a commonly used photocatalyst, which could respond to UV to

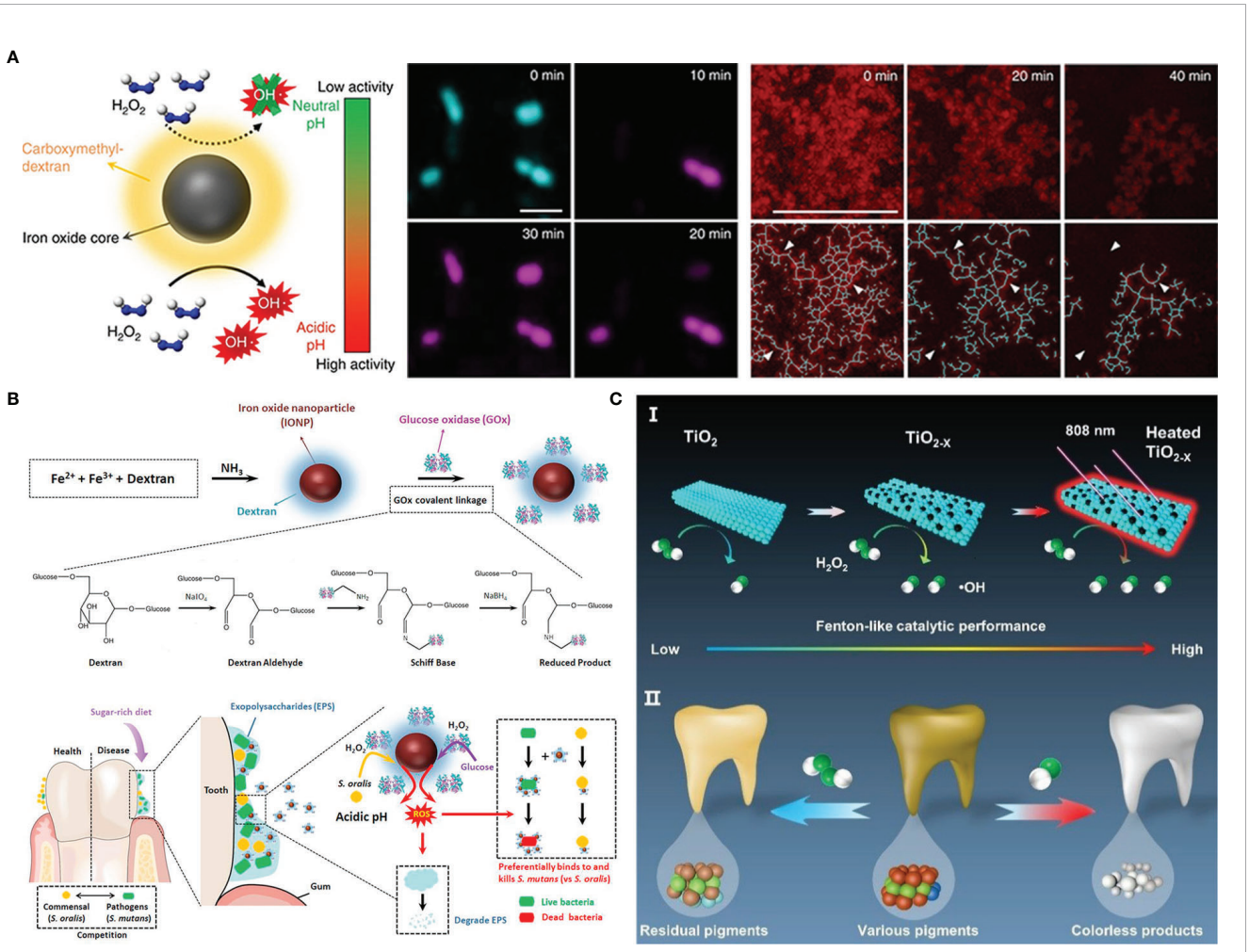

FIGURE 2 | Metal nanoparticles antibacterial strategies: **(A)** combining Dex-IONP nanoparticles and additional H_2O_2 to generate ROS for disturbing biofilms; **(B)** Dex-IONP-GOx nanoparticles as nanoenzyme to release ROS for precision targeting of bacteria; **(C)** Oxygen-deficient nanotitania with enhanced photothermal Fenton-like reaction for destroying biofilms.

generate ROS for destroying microbes. However, exposure to UV light is harmful to cells and tissues restricts the application of TiO_2 (Musk et al., 1989). So, the current advancements mainly focus on facilitating visible light adsorption by narrowing the TiO_2 band gap (Asahi et al., 2001). Previous literature found that doping with nitrogen endowed TiO_2 with superior visible light-catalytic activity (Livraghi et al., 2006). Inspired by this, Florez et al. synthesized nitrogen-dopped TiO_2 nanoparticles and immobilized them in the dental adhesive resins (Esteban Florez et al., 2018). There was a higher antibacterial level when exposed to blue light than in the dark, which demonstrated the contribution of nitrogen to band-gap narrows. In addition to nonmetal atoms doping, oxygen-deficient titania (TiO_{2-x}) can exhibit better photo-catalytic performance than TiO_2 due to its improved separation of electron-hole pairs and extended visible light absorbance regions (Chen et al., 2011; Naldoni et al., 2012). Hu et al. prepared TiO_{2-x} nanoparticles from TiO_2 based on the solid-state chemical reduction method (Hu et al., 2021). The presence of oxygen vacancy improved the catalytic activity under NIR irradiation and meanwhile, elevated temperature brought from photo-thermal conversion can also kill bacteria (**Figure 2C**).

3.2.2 Inorganic Nonmetallic Materials

As the two main inorganic nonmetal materials, carbon nanotube and graphene oxide (GO) have a similar antibacterial mechanism. The penetration of the sharp and narrow structure of two materials onto the surface of bacteria can cause damage in the integrity of cell walls (Teh and Lai, 2019). F. Al-Thani et al. have studied the antibacterial efficiency of GO and concluded that GO can work against several microbiomes including eukaryotic fungus, Gram-negative and positive bacteria (Al-thani et al., 2014).

Nitric oxide (NO) is an endogenous diatomic radical whose antibacterial activity origin from its reaction with superoxide and oxygen. In the process, peroxynitrite and dinitrogen trioxide were formed to kill bacteria through lipid peroxidation and DNA cleavage (Bogdan, 2001; Hetrick et al., 2008). Compared with direct delivery of NO, a NO-releasing system will be applicable to oral surgery. J. Backlund et al. loaded NO into PAMAM dendrimers and discussed the influence of different pH and the alkyl chains length of dendrimers on NO-release kinetics (Backlund et al., 2016). Improved antibacterial actions can be observed at lower pH values and when NO was loaded into longer alkyl chain-modified dendrimers. Similarly, NO-releasing hyperbranched polykanamycins and hyperbranched polyamidoamines systems designed by Yang et al. can not only reduce the metabolic activity of biofilm, but also kill embed bacteria. The greater efficacy was observed under aerobic versus anaerobic conditions (Ma et al., 2020).

3.2.3 Organic Small Molecules

The gold standard aiming at oral bacteria in the clinical treatment is the use of antibacterial agent chlorhexidine (Balagopal and Arjunkumar, 2013). Recent advances about the delivery of chlorhexidine in different carrier systems can achieve a slow release or controlled release of chlorhexidine for prolonging the releasing time and reducing drugs usage. Akram et al. reported a strategy that mesoporous silica nanoparticles (MSNs) were grafted with poly (L-glycolic acid) to load chlorhexidine and studied the release behaviors under the oral acid-producing environment (Akram et al., 2021). Equipped with exceptional surface area and porous structures, MSNs can load drugs for improving efficacy. PGA is a kind of synthesized polypeptide with the pH-responsive property, which guaranteed a significant effect on chlorhexidine release behaviors and nanoparticles degradation.

Quaternary ammonium salts (QAS) have been one of the most widely studied antibacterial agents on account of their chemical structure with ease of design and modification. The antibacterial capability originates from the interactions between cationic QAS molecules and the bacterial cell membranes with negative charges (Ramburrun et al., 2021). The antibacterial property of QAS can be optimized by changing the length of alkyl chains of QAS molecules. For example, QAS molecules with longer alkyl chains (C6-C18) are more applicable to kill bacteria because long alkyl chains can disrupt the phospholipid molecules on the cell membranes (Jiao et al., 2017). While relating to the antifungal therapy, it's necessary to expose more quaternary ammonium groups with positive charge, thus shorter alkyl chains are rather needed (De Prijck et al., 2010; Duan et al., 2022). Dimethylaminohexadecyl methacrylate (DMAHDM) is a kind of QAS antibacterial monomer with an alkyl length of 16, showing strong antibacterial activity and antibacterial efficacy (Zhou et al., 2013). Bhadila et al. developed a bioactive antibacterial composite with DMAHDM and amorphous calcium phosphate (ACP) (Bhadila et al., 2020). The composite can not only protect dentin at the restoration margins from invading of *S. mutans* biofilm, but also promote dentin remineralization. As a small molecular antibacterial agent, QAS can also be grafted onto polymer chains with biological functions to play an antibacterial role. Fanfoni et al. designed and synthesized a series of di-methacrylate bis-QAS that bear two quaternary ammonium groups in a monomer (Fanfoni et al., 2021). These synthesized monomers had the potential of stabilizing polymer networks as crosslinkers, and the existence of two quaternary ammonium groups increased the antibacterial activity.

N-halamines are a class of small molecular compounds with one or several nitrogen-halogen (N-X) bonds, in which X could be Cl, Br or I. Among them, Cl is the most widely used element because of the most advantageous stability of N-Cl bonds. The antibacterial property of N-halamines originates from the release of Cl^+. Releasing Cl^+ first chlorinates the external protein matrix of the bacteria to form a protective layer around the bacteria, which helps it penetrate into the bacterial cells. Cl^+ going into the bacteria further oxidizes the key cellular components containing mercaptan and sulfide, and finally denatures the proteins by counter-chlorination (Dong et al., 2017). It can be seen from the structure of N-halamines that the dissociation constant of Cl element in aqueous solution decreases in the order of imide > amide > amine, which means that the Cl^+ releasing capability decreases in the same

order (Akdag et al., 2006). Contrarily, the durable stability of N-halamines can get improved in order. Wu et al. grafted polyacrylic acid (PAA) onto Ti implants for N-Cl functionalization to acquire porous renewable antibacterial coatings (Wu et al., 2021a). In the research, they utilize excess ethanediamine to react with PAA to ensure that the resulting coatings can contain not only amide but also amine. Such molecular design can provide a synergistic antibacterial effect of rapid and long-lasting functions (**Figure 3A**).

Antibacterial photodynamic therapy (PDT) enjoys a tough interest in current oral and dental applications. Photosensitizers around tissues are activated by the light irradiation of a specific wavelength, and the excited photosensitizers transfer the energy to the surrounding oxygen to generate the highly active ROS, which can oxidize the adjacent biological macromolecules for killing bacteria (Stájer et al., 2020). Current photosensitizers used for PDT are porphyrin, chlorophyll, toluidine blue O (TBO), phthalocyanine compounds and these derivatives (Li et al., 2021). Zhang et al. designed a zwitterion-modified porphyrin by the conjugation of protoporphyrin IX (PP) and a zwitterion moiety (Zhang et al., 2021). PP segments can improve the generation of ROS by purple light irradiation for tooth whitening and *S. mutans* biofilm eradication, while the superhydrophilic zwitterion can increase the solubility of modified porphyrin and ROS yields. Chlorin e6 (Ce 6), a class

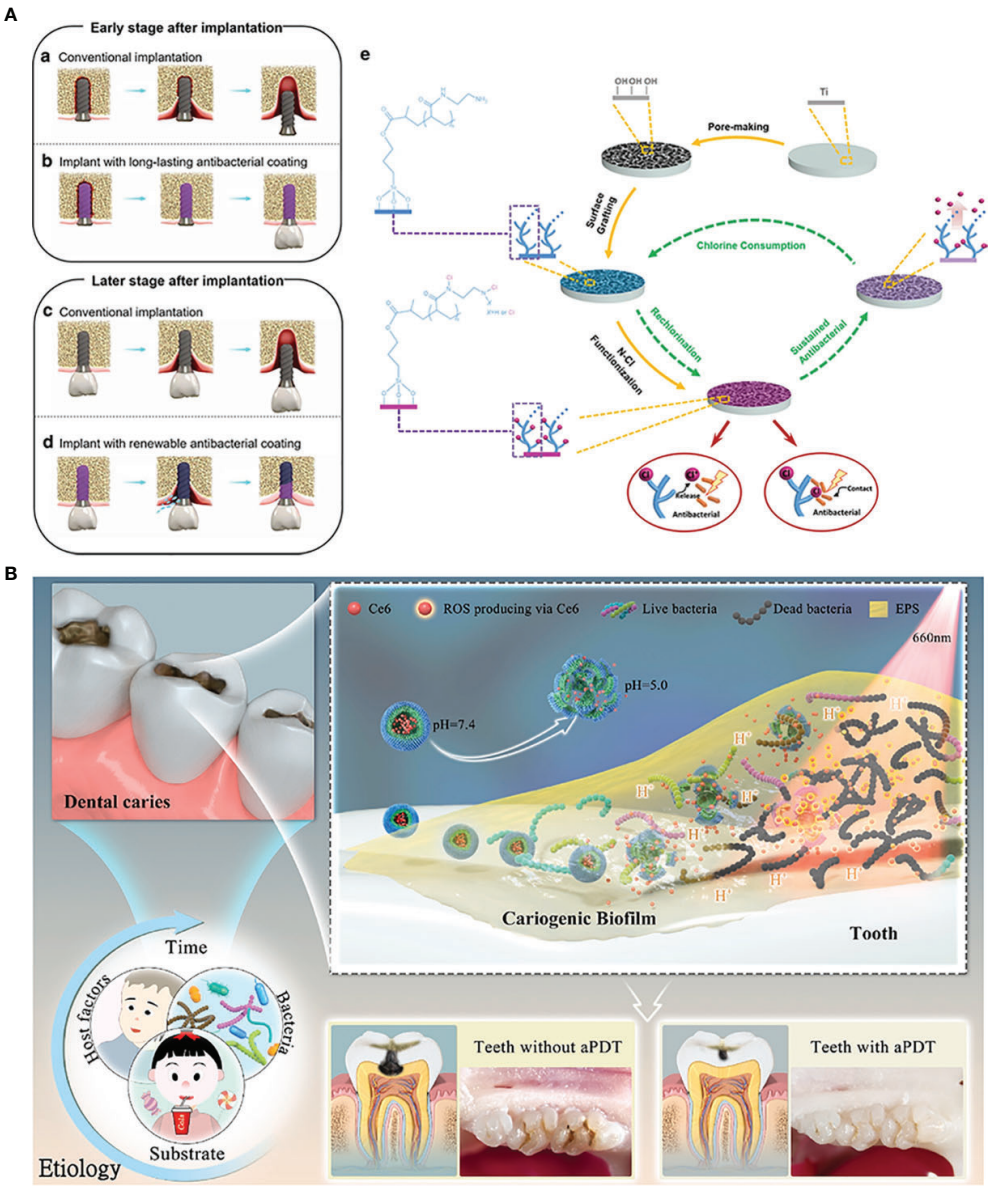

FIGURE 3 | Organic micromolecules antibacterial strategies: **(A)** the renewal of active chlorine from N-halamines coating to achieve long-lasting antibacterial property; **(B)** chlorin e6-mediated PDT therapy for bioresponsive bacterial resistance.

of small molecular photosensitizer extracted from natural chlorophyll, has been revealed to have a brilliant ROS generation efficacy and absorption of visible red light (Ding et al., 2018). Liu et al. once designed an amphiphilic and pH-responsive polymer, which can self-assemble into spherical structure in a neutral condition and disassemble under an acidic environment. Considering the lower pH in the caries environment, they encapsulated Ce 6 with the polymer for PDT on demand (**Figure 3B**) (Liu et al., 2021a). A. Balhaddad et al. constructed a nanoplatform by assembling TBO and magnetic Fe_3O_4. In addition to the photodynamic antibacterial property of Ce 6, Fe_3O_4 equipped the nanoplatform with the capability to penetrate deep sites under external magnetic forces, resulting in an improved disinfection effect (Balhaddad et al., 2021).

3.2.4 Polymers

Compared to inorganic and organic small molecular antimicrobial agents, polymer with antibacterial activity is a hot topic of current research due to its high density of effective functional groups. Usual polymers can be divided into synthetic polymers and natural polymers. Among them, Polyethyleneimine (PEI) is a typical synthetic cationic antibacterial polymer, which can interact with the polar acid groups on the bacteria to destroy cell membranes (Pietrokovski et al., 2016). Karatepe et al. incorporated PEI and silk fibroin (SF) into dental resins. In addition to reinforced mechanical strength brought from SF, PEI endowed resins with the resistance to bacterial erosion of *P. aeruginosa* (Karatepe and Ozdemir, 2020).

As extracted from matters in nature, natural polymers often exhibit low toxicity, good biocompatibility and biodegradation. For example, chitosan is extracted by the deacetylation of chitin and the positively charged ammonium groups (NH_3^+) can be generated upon protonation of amino groups. NH_3^+ can interact with negatively charged bacterial cell membranes to cause leakage (Benhabiles et al., 2012). Peng et al. reported an antimicrobial coating by incorporating PEG and chitosan to combat bacterial infection (Peng et al., 2020). Herein, the coating showed a long-lasting colony-suppression activity against *S. mutans*. Similar to QAS, the length of hydrophobic groups can also influence the antibacterial activity. Phuangkaew et al. introduced hydrophobic entities and quaternary ammonium groups to improve the antibacterial capability (Phuangkaew et al., 2022).

3.2.5 Antimicrobial Peptides

Natural AMPs are a class of polypeptides with broad antibacterial activity extracted from plants, amphibians or human bodies, which are usually composed of hydrophobic regions and positively charged hydrophilic regions (Parhi et al., 2021). The hydrophobic regions, such as tryptophan and leucine, can be in combination with the phospholipid bilayer membrane, while the presence of hydrophilic positively charged arginine and lysine can play an antibacterial role. Even though human oral saliva contains different kinds of AMPs, when acting on oral microorganisms, the minimum inhibitory concentration (MIC) should be reached. It is worth noting that the concentration of natural AMPs in the gingival crevicular fluid is much lower than MIC of most microorganisms. Although oral endogenous AMPs are not enough to produce antibacterial effect on pathogenic bacteria, the wide range of sources provides a new idea for the treatment of oral diseases with additional AMPs. A variety of AMPs, including α-defensin, β-defensin, histatin, and histoprotestatin (such as LL-37), are normally present in oral saliva and have been shown to have antibacterial effects against multiple oral bacteria (Gorr, 2009).

The antibacterial activities of natural AMPs have been extensively studied, but their sources are limited and polypeptide chains are too long and complex to be flexible. On the contrary, *de novo* designed AMPs and the antibacterial units extracted from natural AMPs can solve these problems without impairing the antibacterial activity. For example, $G(IIKK)_3I\text{-}NH_2$ (called as G3) is a man-made helical peptide, and has been proven to have antibacterial activity against *S. mutans* biofilms (Zhang et al., 2020). P-113 ($AKRHHGYKRKFH\text{-}NH_2$) is a histidine-rich 12-amino acid polypeptide from saliva protein histatin 5. In light of previous research, P-113 has bactericidal effects on oral important pathogenic microorganisms (Rothstein et al., 2001; Sajjan et al., 2001). Wang et al. provided a novel and stable Nal-P-113 by replacing tryptophan and histidine residues with the bulky amino acids β-naphthylalanine and β-(4,4'-biphenyl) alanine to increase salt resistance. The variant AMP retained high antibacterial activity against *Stoeptococcus gordonii*, *F. nucleatum* and *P. gingivalis* even at high salt concentrations (Wang et al., 2015).

3.3 Materials for the Disease Treatment

The emergence of antifouling and bactericidal materials provides a new means for the treatment of oral diseases caused by dysbiosis of bacteria. However, the actual oral environment determines the diversity of causes and complexity of results of oral diseases, so single anti-fouling or bactericidal performance is not enough to meet the needs of disease treatment. For example, the overgrowth of oral caries-causing bacteria *S. mutans* is the direct cause of dental caries. In this process, the local pH of oral cavity is also decreased, which further leads to tooth hard tissue demineralization in acidic environment. Consequently, the treatment for dental caries is usually involving a combination of antifouling/antibacterial property and promoting tooth remineralization. Zhou et al. grafted P-113 (the smallest fragment of AMP H5) with different end moieties in order to achieve binding to tooth enamel, killing *S. mutans*, resisting demineralization and promoting remineralization (Zhou et al., 2021). The study suggested the potential of modified P-113 as the functional agent for preventing dental caries (**Figure 4A**). To inhibit the failure of resin-based dental materials brought from recurrent caries, Melo et al. filled resin with Ag nanoparticles, DMAHDM and ACP. In addition to the antibacterial activity of Ag and DMADHM, ACP can release Ca^{2+} and PO_4^{3-} for remineralization and acid neutralization (Melo et al., 2016).

As one of the most common chronic infections, periodontitis will result in the destruction of periodontal tissue including alveolar bone, periodontal ligament and cementum root. The ultimate goal of periodontal therapy is the regeneration of all

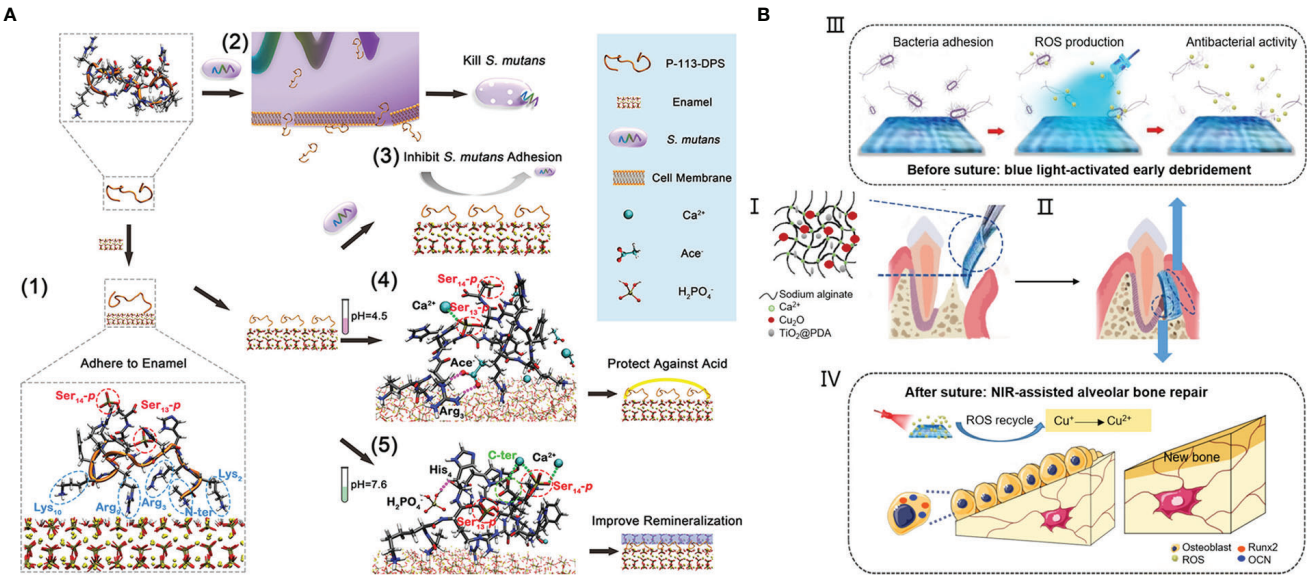

FIGURE 4 | The combined treatment of oral diseases: **(A)** a multifunctional antibacterial peptide coating with modified end groups for adhering to enamel, bacterial anti-adherence and enamel remineralization to achieve caries management; **(B)** an injectable dual light-responsive GTR membrane with the antibacterial property and osteogenic capability to address requirements of periodontitis therapy.

periodontal components, while the therapy usually combines conventional anti-infective measures with guided tissue regeneration (GTR) or the application of cytokines, growth factors, or bioactive molecules (Bottino and Thomas, 2015). Nasajpour et al. developed a biodegradable GTR membrane made with a mixed solution of poly(caprolactone) and ZnO by electrospinning for treating periodontitis (Nasajpour et al., 2018). The incorporation of ZnO improved the antibacterial activity and osteoconductivity simultaneously. Xu et al. proposed an injectable sodium alginate hydrogel containing Cu_2O and PDA-coated TiO_2 (Xu et al., 2020). The liquid to solid phase transition during the gelation process can make the hydrogel match the irregular defect sites. The blue light-responsive property of TiO_2 can generate ROS that can not only kill bacteria but also oxide Cu^+ to Cu^{2+} for stimulating osteogenesis (**Figure 4B**). Zhang et al. developed a microneedle patch for drug delivery of antibiotics and cytokines IL-4 and TGF-β to achieve immunoregulation and tissue regeneration (Zhang et al., 2022).

Like periodontal infection, peri-implantitis is a multimicrobial disease that causes bone absorption and ultimately implant failure. In view of the fact that bacterial infection is the main cause of peri-implantitis, the common treatment method is still to improve the antibacterial performance of implants through bacterial adhesion prevention and sterilization (De Avila et al., 2020). At present, most implants are made of pure titanium and titanium alloy materials. However, titanium implants widely used in clinical practice do not have outstanding anti-infection ability (Chen et al., 2021). More recently, researchers have tried to kill bacteria by mixing pure titanium or its alloys with other metals such as Ag, Cu, and Zn that have inherent antibacterial properties (Chen et al., 2016; Wang et al., 2019). Another way to improve the antibacterial ability of implants is the usage of an antifouling or bactericidal material as the coating of the implant surface. Hoyos-Nogués et al. presented a three-in-one trifunctional strategy by preparing a coating with PEG, AMP and RGD tripeptide. The strategy can promote the attachment and spreading of osteoblasts on implant surfaces and inhibit bacterial colonization on them (Hoyos-Nogues et al., 2018).

4 CONCLUSIONS AND PERSPECTIVES

The oral ecosystem contains several distinct niches, which support the colonization of complex and heterogeneous microbial communities. There are dynamic interactions between oral environments and the compositions of oral microbiota and between oral microorganisms. These interactions can prevent humans from invasion and attack. The oral microbiome is individual and relatively stable as time goes on as long as the oral health is maintained. However, the significant change of key parameters influencing microbial growth will disturb the balanced interactions and lead to the development of pathogenic microorganisms. Once the oral microbial dysbiosis occurs, people are susceptible to being attacked by oral diseases such as dental caries, periodontitis, and peri-implantitis.

There is a close relationship between the occurrence of oral diseases and the overgrowth of pathogenic bacteria and the formation of their biofilms. In the past few decades, the development of materials science, chemistry and biomedical

engineering as well as their intersection promote the blooming research aiming at antibacterial materials. The methods of resisting microbial invasion involve antiadhesion, sterilization and even their combination. In addition to hydrophilic and hydrophobic materials that have been studied extensively, bioinspired DNA is an optional antifouling agent. The photoinduced hydrophobic-hydrophilic transformation property of TiO_2 and its modification of surface morphology can achieve controllable bacterial adhesion, showing potential in preventing peri-implantitis. There is a wider range of bactericidal materials, ranging from inorganic materials such as metals and carbides to organic small molecules, synthetic polymers and some natural molecules. the development of distinct categories of materials enriches antibacterial means: metal ions, chlorhexidine and QAS are still mainstreams, while the application of NO, Cl^+ and AMP is also increasingly emerging. Moreover, mature nanotechnology makes it possible for nanoenzyme, PTT and PDT to be used in the treatment of oral diseases, which further expands the application of some metal and organic molecules. These antibacterial materials have been combined with other methods for the research of treating oral diseases such as dental caries, periodontitis and peri-implantitis based on the characteristics of different oral diseases, showing excellent results.

Although the research on oral antibacterial materials is thriving, these materials are not widely used in clinic. The antibacterial experiment *in vitro* only focuses on one or several pathogenic bacteria. Considering the complexity of microorganisms in the oral environment, it is difficult to predict the effect of antibacterial materials applied to oral cavity. Materials possessing bactericidal effects usually have cytotoxicity as well. In order to achieve good antibacterial properties, it is usually necessary to increase the concentration of materials with low antibacterial activity, which may cause worse biocompatibility. Therefore, a balance between the antibacterial activity and biocompatibility of materials needs to be found in the future. Finally, the results of basic research should be effectively translated into real and affordable products, which requires the joint cooperation and efforts of researchers, doctors and patients.

AUTHOR CONTRIBUTIONS

JZ and WC drafted the manuscript. JLuo and JLi provided valuable insights for the manuscript. JY and LH reviewed and edited the manuscript. All authors have approved the final version of the manuscript.

FUNDING

This work was supported by National Natural Science Foundation of China (51903169, 81991500, 81991501 and 82170949); Key Research and Development Program of Sichuan Province (2021YFS0057 and 2020YFS0180).

REFERENCES

Abdullah, M. A., Alasqah, M., SANAA, M. S., and Gufran, K. (2020). The Relationship Between Volatile Sulfur Compounds and the Severity of Chronic Periodontitis: A Cross-Sectional Study. *J. Pharm. Bioallied. Sci.* 12, S268–S273. doi: 10.4103/jpbs.JPBS_81_20

Abiko, Y., Sato, T., Mayanagi, G., and Takahashi, N. (2010). Profiling of Subgingival Plaque Biofilm Microflora From Periodontally Healthy Subjects and From Subjects With Periodontitis Using Quantitative Real-Time PCR. *J. Periodontal. Res.* 45, 389–395. doi: 10.1111/j.1600-0765.2009.01250.x

Akdag, A., Okur, S., Mckee, M. L., and Worley, S. D. (2006). The Stabilities of N– Cl Bonds in Biocidal Materials. *J. Chem. Theory Comput.* 2, 879–884. doi: 10.1021/ct060007s

Akram, Z., Aati, S., Ngo, H., and Fawzy, A. (2021). pH-Dependent Delivery of Chlorhexidine From PGA Grafted Mesoporous Silica Nanoparticles at Resin-Dentin Interface. *J. Nanobiotechnol.* 19, 43. doi: 10.1186/s12951-021-00788-6

Al-thani, R. F., Patan, N. K., and Al-Maadeed, M. A. (2014). Graphene Oxide as Antimicrobial Against Two Gram-Positive and Two Gram-Negative Bacteria in Addition to One Fungus. *Online J. Biol. Sci.* 14, 230–239. doi: 10.3844/ojbsci.2014.230.239

Asahi, R., Morikawa, T., Ohwaki, T., Aoki, K., and Taga, Y. (2001). Visible-Light Photocatalysis in Nitrogen-Doped Titanium Oxides. *Science* 293, 269–271. doi: 10.1126/science.1061051

Backlund, C. J., Worley, B. V., and Schoenfisch, M. H. (2016). Anti-Biofilm Action of Nitric Oxide-Releasing Alkyl-Modified Poly(Amidoamine) Dendrimers Against Streptococcus Mutans. *Acta Biomat.* 29, 198–205. doi: 10.1016/j.actbio.2015.10.021

Baggerman, J., Smulders, M. M., and Zuilhof, H. (2019). Romantic Surfaces: A Systematic Overview of Stable, Biospecific, and Antifouling Zwitterionic Surfaces. *Langmuir* 35, 1072–1084. doi: 10.1021/acs.langmuir.8b03360

Balagopal, S., and Arjunkumar, R. (2013). Chlorhexidine: The Gold Standard Antiplaque Agent. *J. Pharm. Sci. Res.* 5, 270.

Balhaddad, A. A., Xia, Y., LAN, Y., Mokeem, L., Ibrahim, M. S., Weir, M. D., et al. (2021). Magnetic-Responsive Photosensitizer Nanoplatform for Optimized Inactivation of Dental Caries-Related Biofilms: Technology Development and Proof of Principle. *ACS Nano.* 15, 19888–19904. doi: 10.1021/acsnano.1c07397

Baliban, R. C., Sakellari, D., Li, Z., Dimaggio, P. A., Garcia, B. A., and Floudas, C. A. (2012). Novel Protein Identification Methods for Biomarker Discovery *via* a Proteomic Analysis of Periodontally Healthy and Diseased Gingival Crevicular Fluid Samples. *J. Clin. Periodontol.* 39, 203–212. doi: 10.1111/j.1600-051X.2011.01805.x

Belibasakis, G. N. (2014). Microbiological and Immuno-Pathological Aspects of Peri-Implant Diseases. *Arch. Oral. Biol.* 59, 66–72. doi: 10.1016/j.archoralbio.2013.09.013

Benhabiles, M. S., Salah, R., Lounici, H., Drouiche, N., Goosen, M. F. A., and Mameri, N. (2012). Antibacterial Activity of Chitin, Chitosan and its Oligomers Prepared From Shrimp Shell Waste. *Food Hydrocol.* 29, 48–56. doi: 10.1016/j.foodhyd.2012.02.013

Benitez-Paez, A., Belda-Ferre, P., Simon-Soro, A., and Mira, A. (2014). Microbiota Diversity and Gene Expression Dynamics in Human Oral Biofilms. *BMC Genomics* 15, 311. doi: 10.1186/1471-2164-15-311

Berglundh, T., Armitage, G., Araujo, M. G., Avila-ORTIZ, G., Blanco, J., Camargo, P. M., et al. (2018). Peri-Implant Diseases and Conditions: Consensus Report of Workgroup 4 of the 2017 World Workshop on the Classification of Periodontal and Peri-Implant Diseases and Conditions. *J. Periodontol.* 89 Suppl 1, S313–S318. doi: 10.1002/JPER.17-0739

Berne, C., Kysela, D. T., and Brun, Y. V. (2010). A Bacterial Extracellular DNA Inhibits Settling of Motile Progeny Cells Within a Biofilm. *Mol. Microbiol.* 77, 815–829. doi: 10.1111/j.1365-2958.2010.07267.x

Bhadila, G., Filemban, H., Wang, X., Melo, M. A. S., Arola, D. D., Tay, F. R., et al. (2020). Bioactive Low-Shrinkage-Stress Nanocomposite Suppresses S. Mutans Biofilm and Preserves Tooth Dentin Hardness. *Acta Biomat.* 114, 146–157. doi: 10.1016/j.actbio.2020.07.057

Bogdan, C. (2001). Nitric Oxide and the Immune Response. *Nat. Immunol.* 2, 907–916. doi: 10.1038/ni1001-907

Bottino, M. C., and Thomas, V. (2015). Membranes for Periodontal Regeneration-a Materials Perspective. *Biomat. Oral. Craniomaxillofacial. Appl.* 17, 90–100. doi: 10.1159/000381699

Bowen, W. H., Burne, R. A., Wu, H., and Koo, H. (2018). Oral Biofilms: Pathogens, Matrix, and Polymicrobial Interactions in Microenvironments. *Trends Microbiol.* 26, 229–242. doi: 10.1016/j.tim.2017.09.008

Bunte, K., and Beikler, T. (2019). Th17 Cells and the IL-23/IL-17 Axis in the Pathogenesis of Periodontitis and Immune-Mediated Inflammatory Diseases. *Int. J. Mol. Sci.* 20, 3394. doi: 10.3390/ijms20143394

Buser, D., Sennerby, L., and De Bruyn, H. (2017). Modern Implant Dentistry Based on Osseointegration: 50 Years of Progress, Current Trends and Open Questions. *Periodontol. 2000.* 73, 7–21. doi: 10.1111/prd.12185

Buxadera-Palomero, J., Albó, K., Gil, F. J., Mas-Moruno, C., and Rodríguez, D. (2020). Polyethylene Glycol Pulsed Electrodeposition for the Development of Antifouling Coatings on Titanium. *Coatings* 10, 456. doi: 10.3390/coatings10050456

Cai, Z., Lin, S., Hu, S., and Zhao, L. (2021). Structure and Function of Oral Microbial Community in Periodontitis Based on Integrated Data. *Front. Cell Infect. Microbiol.* 11, 663756. doi: 10.3389/fcimb.2021.663756

Caputo, G., Nobile, C., Kipp, T., Blasi, L., Grillo, V., Carlino, E., et al. (2008). Reversible Wettability Changes in Colloidal TiO_2 Nanorod Thin-Film Coatings Under Selective UV Laser Irradiation. *J. Phys. Chem. C.* 112, 701–714. doi: 10.1021/jp0777061

Cazzaniga, G., Ottobelli, M., Ionescu, A., Garcia-Godoy, F., and Brambilla, E. (2015). Surface Properties of Resin-Based Composite Materials and Biofilm Formation: A Review of the Current Literature. *Am. J. Dent.* 28, 311–320.

Cekici, A., Kantarci, A., Hasturk, H., and Van Dyke, T. E. (2014). Inflammatory and Immune Pathways in the Pathogenesis of Periodontal Disease. *Periodontol* 64, 57–80. doi: 10.1111/prd.12002

Chaichi, M. J., and Ehsani, M. (2016). A Novel Glucose Sensor Based on Immobilization of Glucose Oxidase on the Chitosan-Coated Fe_3O_4 Nanoparticles and the Luminol–H2O2–gold Nanoparticle Chemiluminescence Detection System. *Sens. Actuat. B. Chem.* 223, 713–722. doi: 10.1016/j.snb.2015.09.125

Chalmers, N. I., Palmer, R. J.Jr., Cisar, J. O., and Kolenbrander, P. E. (2008). Characterization of a Streptococcus Sp.-Veillonella Sp. Community Micromanipulated From Dental Plaque. *J. Bacteriol.* 190, 8145–8154. doi: 10.1128/JB.00983-08

Chawhuaveang, D. D., Yu, O. Y., Yin, I. X., Lam, W. Y., Mei, M. L., and Chu, C. H. (2021). Acquired Salivary Pellicle and Oral Diseases: A Literature Review. *J. Dent. Sci.* 16, 523–529. doi: 10.1016/j.jds.2020.10.007

Cheng, W. C., Hughes, F. J., and Taams, L. S. (2014). The Presence, Function and Regulation of IL-17 and Th17 Cells in Periodontitis. *J. Clin. Periodontol.* 41, 541–549. doi: 10.1111/jcpe.12238

Cheng, W. C., Van Asten, S. D., Burns, L. A., Evans, H. G., Walter, G. J., Hashim, A., et al. (2016). Periodontitis-Associated Pathogens P. Gingivalis and A. Actinomycetemcomitans Activate Human CD14(+) Monocytes Leading to Enhanced Th17/IL-17 Responses. *Eur. J. Immunol.* 46, 2211–2221. doi: 10.1002/eji.201545871

Chen, X., Liu, L., Yu, P. Y., and Mao, S. S. J. S. (2011). Increasing Solar Absorption for Photocatalysis With Black Hydrogenated Titanium Dioxide Nanocrystals. *Mat. Sci. Eng. C.* 331, 746–750. doi: 10.1126/science.1200448

Chen, Z., Wang, Z., Qiu, W., and Fang, F. (2021). Overview of Antibacterial Strategies of Dental Implant Materials for the Prevention of Peri-Implantitis. *Bioconjug. Chem.* 32, 627–638. doi: 10.1021/acs.bioconjchem.1c00129

Chen, M., Zhang, E., and Zhang, L. (2016). Microstructure, Mechanical Properties, Bio-Corrosion Properties and Antibacterial Properties of Ti–Ag Sintered Alloys. *Mat. Sci. Eng. C.* 62, 350–360. doi: 10.1016/j.msec.2016.01.081

Choi, W., Jin, J., Park, S., Kim, J. Y., Lee, M. J., Sun, H., et al. (2020). Quantitative Interpretation of Hydration Dynamics Enabled the Fabrication of a Zwitterionic Antifouling Surface. *ACS Appl. Mat. Interfaces.* 12, 7951–7965. doi: 10.1021/acsami.9b21566

Churchley, D., Rees, G. D., Barbu, E., Nevell, T. G., and Tsibouklis, J. (2008). Fluoropolymers as Low-Surface-Energy Tooth Coatings for Oral Care. *Int. J. Pharm.* 352, 44–49. doi: 10.1016/j.ijpharm.2007.10.024

Costalonga, M., and Herzberg, M. C. (2014). The Oral Microbiome and the Immunobiology of Periodontal Disease and Caries. *Immunol. Lett.* 162, 22–38. doi: 10.1016/j.imlet.2014.08.017

Costa Oliveira, B. E., Ricomini Filho, A. P., Burne, R. A., and Zeng, L. (2021). The Route of Sucrose Utilization by Streptococcus Mutans Affects Intracellular Polysaccharide Metabolism. *Front. Microbiol.* 12, 636684. doi: 10.3389/fmicb.2021.636684

Curtis, M. A., Diaz, P. I., and Van Dyke, T. E. (2020). The Role of the Microbiota in Periodontal Disease. *Periodontol. 2000.* 83, 14–25. doi: 10.1111/prd.12296

De Avila, E. D., Van Oirschot, B. A., and Van Den Beucken, J. J. (2020). Biomaterial-Based Possibilities for Managing Peri-Implantitis. *J. Periodont. Res.* 55, 165–173. doi: 10.1111/jre.12707

Deo, P. N., and Deshmukh, R. (2019). Oral Microbiome: Unveiling the Fundamentals. *J. Oral. Maxillofac. Pathol.* 23, 122–128. doi: 10.4103/jomfp.JOMFP-304-18

De Prijck, K., De Smet, N., Coenye, T., Schacht, E., and Nelis, H. J. (2010). Prevention of Candida Albicans Biofilm Formation by Covalently Bound Dimethylaminoethylmethacrylate and Polyethylenimine. *Mycopathologia* 170, 213–221. doi: 10.1007/s11046-010-9316-3

Diaz, P. I., Hong, B. Y., Dupuy, A. K., and Strausbaugh, L. D. (2017). Mining the Oral Mycobiome: Methods, Components, and Meaning. *Virulence* 8, 313–323. doi: 10.1080/21505594.2016.1252015

Ding, Y.-F., Li, S., Liang, L., Huang, Q., Yuwen, L., Yang, W., et al. (2018). Highly Biocompatible Chlorin E6-Loaded Chitosan Nanoparticles for Improved Photodynamic Cancer Therapy. *ACS Appl. Mat. Interfaces.* 10, 9980–9987. doi: 10.1021/acsami.8b01522

Dong, A., Wang, Y.-J., Gao, Y., Gao, T., and Gao, G. (2017). Chemical Insights Into Antibacterial N-Halamines. *Chem. Rev.* 117, 4806–4862. doi: 10.1021/acs.chemrev.6b00687

Duan, S., Wu, R., Xiong, Y.-H., Ren, H.-M., Lei, C., Zhao, Y.-Q., et al. (2022). Multifunctional Antimicrobial Materials: From Rational Design to Biomedical Applications. *Prog. Mat. Sci.* 125, 100887. doi: 10.1016/j.pmatsci.2021.100887

Duarte, P. M., De Mendonca, A. C., Maximo, M. B., Santos, V. R., Bastos, M. F., and Nociti Junior, F. H. (2009). Differential Cytokine Expressions Affect the Severity of Peri-Implant Disease. *Clin. Oral. Implants. Res.* 20, 514–520. doi: 10.1111/j.1600-0501.2008.01680.x

Dutra-Correa, M., Leite, A., De Cara, S., Diniz, I. M. A., Marques, M. M., Suffredini, I. B., et al. (2018). Antibacterial Effects and Cytotoxicity of an Adhesive Containing Low Concentration of Silver Nanoparticles. *J. Dent.* 77, 66–71. doi: 10.1016/j.jdent.2018.07.010

Esteban Florez, F. L., Hiers, R. D., Larson, P., Johnson, M., O'rear, E., Rondinone, A. J., et al. (2018). Antibacterial Dental Adhesive Resins Containing Nitrogen-Doped Titanium Dioxide Nanoparticles. *Mat. Sci. Eng. C.* 93, 931–943. doi: 10.1016/j.msec.2018.08.060

Fanfoni, L., Marsich, E., Turco, G., Breschi, L., and Cadenaro, M. (2021). Development of Di-Methacrylate Quaternary Ammonium Monomers With Antibacterial Activity. *Acta Biomat.* 129, 138–147. doi: 10.1016/j.actbio.2021.05.012

Fang, G., Li, W., Shen, X., Perez-Aguilar, J. M., Chong, Y., Gao, X., et al. (2018). Differential Pd-Nanocrystal Facets Demonstrate Distinct Antibacterial Activity Against Gram-Positive and Gram-Negative Bacteria. *Nat. Commun.* 9, 1–9. doi: 10.1038/s41467-017-02502-3

Feng, X. J., Feng, L., Jin, M. H., Zhai, J., Jiang, L., and Zhu, D. B. (2004). Reversible Super-Hydrophobicity to Super-Hydrophilicity Transition of Aligned ZnO Nanorod Films. *J. Am. Chem. Soc.* 126, 62. doi: 10.1021/ja0386360

Ferraris, S., Giachet, F. T., Miola, M., Bertone, E., Varesano, A., Vineis, C., et al. (2017). Nanogrooves and Keratin Nanofibers on Titanium Surfaces Aimed at Driving Gingival Fibroblasts Alignment and Proliferation Without Increasing Bacterial Adhesion. *Mat. Sci. Eng. C.* 76, 1–12. doi: 10.1016/j.msec.2017.02.152

Flemming, H. C., Wingender, J., Szewzyk, U., Steinberg, P., Rice, S. A., and Kjelleberg, S. (2016). Biofilms: An Emergent Form of Bacterial Life. *Nat. Rev. Microbiol.* 14, 563–575. doi: 10.1038/nrmicro.2016.94

Gao, L., Liu, Y., Kim, D., LI, Y., Hwang, G., Naha, P. C., et al. (2016). Nanocatalysts Promote Streptococcus Mutans Biofilm Matrix Degradation and Enhance Bacterial Killing to Suppress Dental Caries *In Vivo*. *Biomaterials* 101, 272–284. doi: 10.1016/j.biomaterials.2016.05.051

Gao, L., Zhuang, J., Nie, L., Zhang, J., Zhang, Y., Gu, N., et al. (2007). Intrinsic Peroxidase-Like Activity of Ferromagnetic Nanoparticles. *Nat. Nanotechnol.* 2, 577–583. doi: 10.1038/nnano.2007.260

Ghensi, P., Manghi, P., Zolfo, M., Armanini, F., Pasolli, E., Bolzan, M., et al. (2020). Strong Oral Plaque Microbiome Signatures for Dental Implant Diseases Identified by Strain-Resolution Metagenomics. *NPJ Biofilms. Microbiom.* 6, 47. doi: 10.1038/s41522-020-00155-7

Gold, K., Slay, B., Knackstedt, M., and Gaharwar, A. K. (2018). Antimicrobial Activity of Metal and Metal-Oxide Based Nanoparticles. *Adv. Ther.* 1, 1700033. doi: 10.1002/adtp.201700033

Gorr, S. U. (2009). Antimicrobial Peptides of the Oral Cavity. *Periodontology* 51, 152–180. doi: 10.1111/j.1600-0757.2009.00310.x

Graves, D. (2008). Cytokines That Promote Periodontal Tissue Destruction. *J. Periodontol.* 79, 1585–1591. doi: 10.1902/jop.2008.080183

Graves, D. T., Correa, J. D., and Silva, T. A. (2019). The Oral Microbiota Is Modified by Systemic Diseases. *J. Dent. Res.* 98, 148–156. doi: 10.1177/0022034518805739

Greenstein, G., and Cavallaro, J. (2014). Failed Dental Implants: Diagnosis, Removal and Survival of Reimplantations. *J. Am. Dent. Assoc.* 145, 835–842. doi: 10.14219/jada.2014.28

Gu, Y., and Han, X. (2020). Toll-Like Receptor Signaling and Immune Regulatory Lymphocytes in Periodontal Disease. *Int. J. Mol. Sci.* 21, 3329. doi: 10.3390/ijms21093329

Gu, C., Zhang, J., and Tu, J. (2010). A Strategy of Fast Reversible Wettability Changes of WO3 Surfaces Between Superhydrophilicity and Superhydrophobicity. *J. Colloid. Interface Sci.* 352, 573–579. doi: 10.1016/j.jcis.2010.08.064

Hajishengallis, G. (2015). Periodontitis: From Microbial Immune Subversion to Systemic Inflammation. *Nat. Rev. Immunol.* 15, 30–44. doi: 10.1038/nri3785

Hajishengallis, G., and Lamont, R. J. (2012). Beyond the Red Complex and Into More Complexity: The Polymicrobial Synergy and Dysbiosis (PSD) Model of Periodontal Disease Etiology. *Mol. Oral. Microbiol.* 27, 409–419. doi: 10.1111/j.2041-1014.2012.00663.x

Hajishengallis, G., and Lamont, R. J. (2021). Polymicrobial Communities in Periodontal Disease: Their Quasi-Organismal Nature and Dialogue With the Host. *Periodontol. 2000.* 86, 210–230. doi: 10.1111/prd.12371

Hetrick, E. M., Shin, J. H., Stasko, N. A., Johnson, C. B., Wespe, D. A., Holmuhamedov, E., et al. (2008). Bactericidal Efficacy of Nitric Oxide-Releasing Silica Nanoparticles. *ACS Nano.* 2, 235–246. doi: 10.1021/nn700191f

Hou, A., Luo, J., Zhang, M., Li, J., Chu, W., Liang, K., et al. (2020). Two-In-One Strategy: A Remineralizing and Anti-Adhesive Coating Against Demineralized Enamel. *Int. J. Oral. Sci.* 12, 27. doi: 10.1038/s41368-020-00097-y

Hoyos-Nogues, M., Buxadera-Palomero, J., Ginebra, M. P., Manero, J. M., Gil, F. J., and Mas-Moruno, C. (2018). All-In-One Trifunctional Strategy: A Cell Adhesive, Bacteriostatic and Bactericidal Coating for Titanium Implants. *Colloids. Surf. B. Biointerface.* 169, 30–40. doi: 10.1016/j.colsurfb.2018.04.050

Huang, X., Browngardt, C. M., Jiang, M., Ahn, S. J., Burne, R. A., and Nascimento, M. M. (2018). Diversity in Antagonistic Interactions Between Commensal Oral Streptococci and Streptococcus Mutans. *Caries. Res.* 52, 88–101. doi: 10.1159/000479091

Huang, Y., Liu, Y., Shah, S., Kim, D., Simon-Soro, A., Ito, T., et al. (2021). Precision Targeting of Bacterial Pathogen *via* Bi-Functional Nanozyme Activated by Biofilm Microenvironment. *Biomaterials* 268, 120581. doi: 10.1016/j.biomaterials.2020.120581

Hu, X., Xie, L., Xu, Z., Liu, S., Tan, X., Qian, R., et al. (2021). Photothermal-Enhanced Fenton-Like Catalytic Activity of Oxygen-Deficient Nanotitania for Efficient and Safe Tooth Whitening. *ACS Appl. Mat. Interfaces.* 13, 35315–35327. doi: 10.1021/acsami.1c06774

Hu, X., Xu, R., Yu, X., Chen, J., Wan, S., Ouyang, J., et al. (2018). Enhanced Antibacterial Efficacy of Selective Laser Melting Titanium Surface With Nanophase Calcium Phosphate Embedded to TiO2 Nanotubes. *BioMed. Mat.* 13, 045015. doi: 10.1088/1748-605X/aac1a3

Hwang, D. S., Zeng, H., Lu, Q., Israelachvili, J., and Waite, J. H. (2012). Adhesion Mechanism in a DOPA-Deficient Foot Protein From Green Mussels. *Soft. Mat.* 8, 5640–5648. doi: 10.1039/c2sm25173f

Jia, L., Han, N., Du, J., Guo, L., Luo, Z., and Liu, Y. (2019). Pathogenesis of Important Virulence Factors of Porphyromonas Gingivalis *via* Toll-Like Receptors. *Front. Cell Infect. Microbiol.* 9, 262. doi: 10.3389/fcimb.2019.00262

Jiao, Y., Niu, L.-N., Ma, S., Li, J., tay, F. R., and Chen, J. H. (2017). Quaternary Ammonium-Based Biomedical Materials: State-Of-the-Art, Toxicological Aspects and Antimicrobial Resistance. *Prog. Polym. Sci.* 71, 53–90. doi: 10.1016/j.progpolymsci.2017.03.001

Ji, Y., Han, Z., Ding, H., Xu, X., Wang, D., Zhu, Y., et al. (2021). Enhanced Eradication of Bacterial/Fungi Biofilms by Glucose Oxidase-Modified Magnetic Nanoparticles as a Potential Treatment for Persistent Endodontic Infections. *ACS Appl. Mat. Interfaces.* 13, 17289–17299. doi: 10.1021/acsami.1c01748

Jin, H., Tian, L., Bing, W., Zhao, J., and Ren, L. (2022). Bioinspired Marine Antifouling Coatings: Status, Prospects, and Future. *Prog. Mat. Sci.* 124, 100889. doi: 10.1016/j.pmatsci.2021.100889

Kędziora, A., Speruda, M., Krzyżewska, E., Rybka, J., Łukowiak, A., and Bugla-Płoskońska, G. (2018). Similarities and Differences Between Silver Ions and Silver in Nanoforms as Antibacterial Agents. *Int. J. Mol. Sci.* 19, 444. doi: 10.3390/ijms19020444

Kang, S., Lee, M., Kang, M., Noh, M., Jeon, J., Lee, Y., et al. (2016). Development of Anti-Biofouling Interface on Hydroxyapatite Surface by Coating Zwitterionic MPC Polymer Containing Calcium-Binding Moieties to Prevent Oral Bacterial Adhesion. *Acta Biomat.* 40, 70–77. doi: 10.1016/j.actbio.2016.03.006

Karatepe, U. Y., and Ozdemir, T. (2020). Improving Mechanical and Antibacterial Properties of PMMA *via* Polyblend Electrospinning With Silk Fibroin and Polyethyleneimine Towards Dental Applications. *Bioact. Mat.* 5, 510–515. doi: 10.1016/j.bioactmat.2020.04.005

Karygianni, L., Ren, Z., KOO, H., and Thurnheer, T. (2020). Biofilm Matrixome: Extracellular Components in Structured Microbial Communities. *Trends Microbiol.* 28, 668–681. doi: 10.1016/j.tim.2020.03.016

Kazor, C. E., Mitchell, P. M., Lee, A. M., Stokes, L. N., Loesche, W. J., Dewhirst, F. E., et al. (2003). Diversity of Bacterial Populations on the Tongue Dorsa of Patients With Halitosis and Healthy Patients. *J. Clin. Microbiol.* 41, 558–563. doi: 10.1128/JCM.41.2.558-563.2003

Keijser, B. J., Zaura, E., Huse, S. M., van der Vossen, J. M., Schuren, F. H., Montijn, R. C., et al. (2008). Pyrosequencing Analysis of the Oral Microflora of Healthy Adults. *J. Dent. Res.* 87, 1016–1020. doi: 10.1177/154405910808701104

Kolenbrander, P. E., Palmer, R. J., JR., Periasamy, S., and Jakubovics, N. S. (2010). Oral Multispecies Biofilm Development and the Key Role of Cell-Cell Distance. *Nat. Rev. Microbiol.* 8, 471–480. doi: 10.1038/nrmicro2381

Kolenbrander, P. E., Palmer, R. J., JR., Rickard, A. H., Jakubovics, N. S., Chalmers, N. I., and Diaz, P. I. (2006). Bacterial Interactions and Successions During Plaque Development. *Periodontol* 42, 47–79. doi: 10.1111/j.1600-0757.2006.00187.x

Konittinen, Y. T., Ma, J., Lappalainen, R., Laine, P., Kitti, U., Santavirta, S., et al. (2006). Immunohistochemical Evaluation of Inflammatory Mediators in Failing Implants. *Internat. J. Periodont. Rest* 26, 135–141.

Koo, H., Andes, D. R., and Krysan, D. J. (2018). Candida-Streptococcal Interactions in Biofilm-Associated Oral Diseases. *PloS Pathog.* 14, e1007342. doi: 10.1371/journal.ppat.1007342

Kuang, X., Chen, V., and Xu, X. (2018). Novel Approaches to the Control of Oral Microbial Biofilms. *BioMed. Res. Int.* 2018, 6498932. doi: 10.1155/2018/6498932

Lamont, R. J., Koo, H., and Hajishengallis, G. (2018). The Oral Microbiota: Dynamic Communities and Host Interactions. *Nat. Rev. Microbiol.* 16, 745–759. doi: 10.1038/s41579-018-0089-x

Laothanachareon, T., Tamayo-Ramos, J. A., Nijsse, B., and Schaap, P. J. (2018). Forward Genetics by Genome Sequencing Uncovers the Central Role of the Aspergillus Niger goxB Locus in Hydrogen Peroxide Induced Glucose Oxidase Expression. *Front. Microbiol.* 9, 2269. doi: 10.3389/fmicb.2018.02269

Larsen, T., and Fiehn, N. E. (2017). Dental Biofilm Infections - an Update. *APMIS* 125, 376–384. doi: 10.1111/apm.12688

Lee, M. J., Kwon, J. S., Kim, J. Y., Ryu, J. H., Seo, J. Y., Jang, S., et al. (2019). Bioactive Resin-Based Composite With Surface Pre-Reacted Glass-Ionomer Filler and Zwitterionic Material to Prevent the Formation of Multi-Species Biofilm. *Dent. Mat.* 35, 1331–1341. doi: 10.1016/j.dental.2019.06.004

Lee, J. S., Spooner, R., Chowdhury, N., Pandey, V., wellslager, B., Atanasova, K. R., et al. (2020). *In Situ* Intraepithelial Localizations of Opportunistic Pathogens, Porphyromonas Gingivalis and Filifactor Alocis, in Human Gingiva. *Curr. Res. Microb. Sci.* 1, 7–17. doi: 10.1016/j.crmicr.2020.05.001

Liebsch, C., Pitchika, V., Pink, C., Samietz, S., kastenmuller, G., Artati, A., et al. (2019). The Saliva Metabolome in Association to Oral Health Status. *J. Dent. Res.* 98, 642–651. doi: 10.1177/0022034519842853

Li, Y., Guo, H. M., Wang, X. J., Lu, Y., Yang, C. Y., and Yang, P. S. (2015). Coinfection With Fusobacterium Nucleatum can Enhance the Attachment and Invasion of Porphyromonas Gingivalis or Aggregatibacter Actinomycetemcomitans to Human Gingival Epithelial Cells. *Arch. Oral. Biol.* 60, 1387–1393. doi: 10.1016/j.archoralbio.2015.06.017

Lim, H. S., Kwak, D., Lee, D. Y., Lee, S. G., and Cho, K. (2007). UV-Driven Reversible Switching of a Roselike Vanadium Oxide Film Between Superhydrophobicity and Superhydrophilicity. *J. Am. Chem. Soc.* 129, 4128–4129. doi: 10.1021/ja0692579

Li, Z., Pan, W., Shi, E., Bai, L., Liu, H., Li, C., et al. (2021). A Multifunctional Nanosystem Based on Bacterial Cell-Penetrating Photosensitizer for Fighting Periodontitis *via* Combining Photodynamic and Antibiotic Therapies. *ACS Biomat. Sci. Eng.* 7, 772–786. doi: 10.1021/acsbiomaterials.0c01638

Listgarten, M. A. (1976). Structure of the Microbial Flora Associated With Periodontal Health and Disease in Man. A Light and Electron Microscopic Study. *J. Periodontol.* 47, 1–18. doi: 10.1902/jop.1976.47.1.1

Liu, Y., Huang, Y., kim, D., Ren, Z., Oh, M. J., cormode, D. P., et al. (2021b). Ferumoxytol Nanoparticles Target Biofilms Causing Tooth Decay in the Human Mouth. *Nano. Lett.* 21, 9442–9449. doi: 10.1021/acs.nanolett.1c02702

Liu, D., Ma, X., Ji, Y., Chen, R., Zhou, S., Yao, H., et al. (2021a). Bioresponsive Nanotherapy for Preventing Dental Caries by Inhibiting Multispecies Cariogenic Biofilms. *Bioact. Mat.* 14, 1–14. doi: 10.1016/j.bioactmat.2021.12.016

Liu, Y., Naha, P. C., Hwang, G., Kim, D., Huang, Y., Simon-Soro, A., et al. (2018a). Topical Ferumoxytol Nanoparticles Disrupt Biofilms and Prevent Tooth Decay *In Vivo via* Intrinsic Catalytic Activity. *Nat. Commun.* 9, 2920. doi: 10.1038/s41467-018-05342-x

Liu, Y. L., Nascimento, M., and Burne, R. A. (2012). Progress Toward Understanding the Contribution of Alkali Generation in Dental Biofilms to Inhibition of Dental Caries. *Int. J. Oral. Sci.* 4, 135–140. doi: 10.1038/ijos.2012.54

Liu, Y., Ren, Z., Hwang, G., and Koo, H. (2018b). Therapeutic Strategies Targeting Cariogenic Biofilm Microenvironment. *Adv. Dent. Res.* 29, 86–92. doi: 10.1177/0022034517736497

Liu, C., Yao, J., Hu, J., Akakuru, O. U., Sun, S., Chen, T., et al. (2020). Navigating nMOF-Mediated Enzymatic Reactions for Catalytic Tumor-Specific Therapy. *Mat. Horiz.* 7, 3176–3186. doi: 10.1039/D0MH01225D

Livraghi, S., Paganini, M. C., Giamello, E., Selloni, A., DI Valentin, C., and Pacchioni, G. (2006). Origin of Photoactivity of Nitrogen-Doped Titanium Dioxide Under Visible Light. *J. Am. Chem. Soc.* 128, 15666–15671. doi: 10.1021/ja064164c

Mardegan, G. P., Shibli, J. A., Roth, L. A., Faveri, M., Giro, G., and Bastos, M. F. (2017). Transforming Growth Factor-Beta, Interleukin-17, and IL-23 Gene Expression Profiles Associated With Human Peri-Implantitis. *Clin. Oral. Implants. Res.* 28, e10–e15. doi: 10.1111/clr.12846

Mark Welch, J. L., Rossetti, B. J., Rieken, C. W., dewhirst, F. E., and Borisy, G. G. (2016). Biogeography of a Human Oral Microbiome at the Micron Scale. *Proc. Natl. Acad. Sci. U.S.A.* 113, E791–E800. doi: 10.1073/pnas.1522149113

Ma, S., Wu, Y., and Zhou, F. (2020). Bioinspired Synthetic Wet Adhesives: From Permanent Bonding to Reversible Regulation. *Curr. Opin. Colloid. Interface Sci.* 47, 84–98. doi: 10.1016/j.cocis.2019.11.010

Mclean, J. S. (2014). Advancements Toward a Systems Level Understanding of the Human Oral Microbiome. *Front. Cell Infect. Microbiol.* 4, 98. doi: 10.3389/fcimb.2014.00098

Melo, M. A., Orrego, S., Weir, M. D., Xu, H. H., and Arola, D. D. (2016). Designing Multiagent Dental Materials for Enhanced Resistance to Biofilm Damage at the Bonded Interface. *ACS Appl. Mat. Interfaces.* 8, 11779–11787. doi: 10.1021/acsami.6b01923

Mikolai, C., Kommerein, N., Ingendoh-Tsakmakidis, A., Winkel, A., Falk, C. S., and Stiesch, M. (2020). Early Host-Microbe Interaction in a Peri-Implant Oral Mucosa-Biofilm Model. *Cell Microbiol.* 22, e13209. doi: 10.1111/cmi.13209

Mineoka, T., Awano, S., Rikimaru, T., Kurata, H., Yoshida, A., Ansai, T., et al. (2008). Site-Specific Development of Periodontal Disease is Associated With Increased Levels of Porphyromonas Gingivalis, Treponema Denticola, and Tannerella Forsythia in Subgingival Plaque. *J. Periodontol.* 79, 670–676. doi: 10.1902/jop.2008.070398

Mosaddad, S. A., Tahmasebi, E., Yazdanian, A., Rezvani, M. B., Seifalian, A., Yazdanian, M., et al. (2019). Oral Microbial Biofilms: An Update. *Eur. J. Clin. Microbiol. Infect. Dis.* 38, 2005–2019. doi: 10.1007/s10096-019-03641-9

Musk, P., Campbell, R., Staples, J., Moss, D., and Parsons, P. J. (1989). Solar and UVC-Induced Mutation in Human Cells and Inhibition by Deoxynucleosides. *Mutat. Res. Lett.* 227, 25–30. doi: 10.1016/0165-7992(89)90064-X

Nakayama, M., and Ohara, N. (2017). Molecular Mechanisms of Porphyromonas Gingivalis-Host Cell Interaction on Periodontal Diseases. *Jpn. Dent. Sci. Rev.* 53, 134–140. doi: 10.1016/j.jdsr.2017.06.001

Naldoni, A., Allieta, M., Santangelo, S., Marelli, M., Fabbri, F., Cappelli, S., et al. (2012). Effect of Nature and Location of Defects on Bandgap Narrowing in Black TiO2 Nanoparticles. *J. Am. Chem. Soc.* 134, 7600–7603. doi: 10.1021/ja3012676

Narendrakumar, K., Kulkarni, M., Addison, O., Mazare, A., Junkar, I., Schmuki, P., et al. (2015). Adherence of Oral Streptococci to Nanostructured Titanium Surfaces. *Dent. Mat.* 31, 1460–1468. doi: 10.1016/j.dental.2015.09.011

Nasajpour, A., Ansari, S., Rinoldi, C., Rad, A. S., Aghaloo, T., Shin, S. R., et al. (2018). A Multifunctional Polymeric Periodontal Membrane With Osteogenic and Antibacterial Characteristics. *Adv. Funct. Mat.* 28, 1703437. doi: 10.1002/adfm.201703437

Ouni, O. A., Subbiahdoss, G., Scheberl, A., and Reimhult, E. (2021). DNA Polyelectrolyte Multilayer Coatings Are Antifouling and Promote Mammalian Cell Adhesion. *Materials* 14, 4596. doi: 10.3390/ma14164596

Ouyang, W., Kolls, J. K., and Zheng, Y. (2008). The Biological Functions of T Helper 17 Cell Effector Cytokines in Inflammation. *Immunity* 28, 454–467. doi: 10.1016/j.immuni.2008.03.004

Packham, D. E. (2003). Surface Energy, Surface Topography and Adhesion. *Int. J. Adhes. Adhes.* 23, 437–448. doi: 10.1016/S0143-7496(03)00068-X

Paes Leme, A. F., Koo, H., Bellato, C. M., Bedi, G., and Cury, J. A. (2006). The Role of Sucrose in Cariogenic Dental Biofilm Formation–New Insight. *J. Dent. Res.* 85, 878–887. doi: 10.1177/154405910608501002

Pan, W., Wang, Q., and Chen, Q. (2019). The Cytokine Network Involved in the Host Immune Response to Periodontitis. *Int. J. Oral. Sci.* 11, 30. doi: 10.1038/s41368-019-0064-z

Papadopoulou, E. L., Barberoglou, M., Zorba, V., Manousaki, A., Pagkozidis, A., Stratakis, E., et al. (2009). Reversible Photoinduced Wettability Transition of Hierarchical ZnO Structures. *J. Phys. Chem. C.* 113, 2891–2895. doi: 10.1021/jp8085057

Parhi, S., Pal, S., Das, S. K., and Ghosh, P. (2021). Strategies Toward Development of Antimicrobial Biomaterials for Dental Healthcare Applications. *Biotechnol. Bioeng.* 118, 4590–4622. doi: 10.1002/bit.27948

Peng, L., Chang, L., Liu, X., Lin, J., Liu, H., Han, B., et al. (2017). Antibacterial Property of a Polyethylene Glycol-Grafted Dental Material. *ACS Appl. Mat. Interfaces.* 9, 17688–17692. doi: 10.1021/acsami.7b05284

Peng, L., Chang, L., Si, M., Lin, J., Wei, Y., Wang, S., et al. (2020). Hydrogel-Coated Dental Device With Adhesion-Inhibiting and Colony-Suppressing Properties. *ACS Appl. Mat. Interfaces.* 12, 9718–9725. doi: 10.1021/acsami.9b19873

Petkovic, A. B., Matic, S. M., Stamatovic, N. V., Vojvodic, D. V., Todorovic, T. M., Lazic, Z. R., et al. (2010). Proinflammatory Cytokines (IL-1beta and TNF-Alpha) and Chemokines (IL-8 and MIP-1alpha) as Markers of Peri-Implant Tissue Condition. *Int. J. Oral. Maxillofac. Surg.* 39, 478–485. doi: 10.1016/j.ijom.2010.01.014

Phuangkaew, T., Booranabunyat, N., Kiatkamjornwong, S., Thanyasrisung, P., and Hoven, V. P. (2022). Amphiphilic Quaternized Chitosan: Synthesis, Characterization, and Anti-Cariogenic Biofilm Property. *Carbohydr. Polym.* 277, 118882. doi: 10.1016/j.carbpol.2021.118882

Pietrokovski, Y., Nisimov, I., Kesler-SHVERO, D., Zaltsman, N., and Beyth, N. (2016). Antibacterial Effect of Composite Resin Foundation Material Incorporating Quaternary Ammonium Polyethyleneimine Nanoparticles. *J. Prosthet. Dent.* 116, 603–609. doi: 10.1016/j.prosdent.2016.02.022

Pihlstrom, B. L., Michalowicz, B. S., and Johnson, N. W. (2005). Periodontal Diseases. *Lancet* 366, 1809–1820. doi: 10.1016/S0140-6736(05)67728-8

Pitts, N. B., Zero, D. T., Marsh, P. D., Ekstrand, K., Weintraub, J. A., Ramos-Gomez, F., et al. (2017). Dental Caries. *Nat. Rev. Dis. Primers* 3, 17030. doi: 10.1038/nrdp.2017.30

Quirynen, M., Vogels, R., Pauwels, M., Haffajee, A. D., Socransky, S. S., Uzel, N. G., et al. (2005). Initial Subgingival Colonization of 'Pristine' Pockets. *J. Dent. Res.* 84, 340–344. doi: 10.1177/154405910508400409

Ramburrun, P., Pringle, N. A., Dube, A., Adam, R. Z., D'souza, S., and aucamp, M. (2021). Recent Advances in the Development of Antimicrobial and Antifouling Biocompatible Materials for Dental Applications. *Materials* 14, 3167. doi: 10.3390/ma14123167

Robitaille, N., Reed, D. N., Walters, J. D., and Kumar, P. S. (2016). Periodontal and Peri-Implant Diseases: Identical or Fraternal Infections? *Mol. Oral. Microbiol.* 31, 285–301. doi: 10.1111/omi.12124

Romano, F., Meoni, G., Manavella, V., Baima, G., Tenori, L., Cacciatore, S., et al. (2018). Analysis of Salivary Phenotypes of Generalized Aggressive and Chronic

Periodontitis Through Nuclear Magnetic Resonance-Based Metabolomics. *J. Periodontol.* 89, 1452–1460. doi: 10.1002/JPER.18-0097

Rosier, B. T., Marsh, P. D., and Mira, A. (2018). Resilience of the Oral Microbiota in Health: Mechanisms That Prevent Dysbiosis. *J. Dent. Res.* 97, 371–380. doi: 10.1177/0022034517742139

Rothstein, D. M., Spacciapoli, P., Tran, L. T., Xu, T., Roberts, F. D., Dalla Serra, M., et al. (2001). Anticandida Activity is Retained in P-113, a 12-Amino-Acid Fragment of Histatin 5. *Antimicrob. Agents Chemother.* 45, 1367–1373. doi: 10.1128/AAC.45.5.1367-1373.2001

Russell, R. R. (2009). Changing Concepts in Caries Microbiology. *Am. J. Dent.* 22, 304–310.

Sahoo, M., Mathews, T., Antony, R. P., Krishna, D. N., Dash, S., and Tyagi, A. K. (2013). Physico-Chemical Processes and Kinetics of Sunlight-Induced Hydrophobic <–> Superhydrophilic Switching of Transparent N-Doped TiO2 Thin Films. *ACS Appl. Mat. Interfaces.* 5, 3967–3974. doi: 10.1021/am400785x

Sajjan, U. S., Tran, L. T., Sole, N., Rovaldi, C., Akiyama, A., Friden, P. M., et al. (2001). P-113D, an Antimicrobial Peptide Active Against Pseudomonas Aeruginosa, Retains Activity in the Presence of Sputum From Cystic Fibrosis Patients. *Antimicrob. Agents Chemother.* 45, 3437–3444. doi: 10.1128/AAC.45.12.3437-3444.2001

Santiago, A., Irusta, L., Schäfer, T., Corres, A., Martin, L., and González, A. (2016). Resistance to Protein Sorption as a Model of Antifouling Performance of Poly (siloxane-Urethane) Coatings Exhibiting Phase Separated Morphologies. *Prog. Org. Coat.* 99, 110–116. doi: 10.1016/j.porgcoat.2016.05.011

Schaumann, S., Staufenbiel, I., Scherer, R., Schilhabel, M., Winkel, A., Stumpp, S. N., et al. (2014). Pyrosequencing of Supra- and Subgingival Biofilms From Inflamed Peri-Implant and Periodontal Sites. *BMC Oral. Health* 14, 157. doi: 10.1186/1472-6831-14-157

Schincaglia, G. P., Hong, B. Y., Rosania, A., Barasz, J., Thompson, A., Sobue, T., et al. (2017). Clinical, Immune, and Microbiome Traits of Gingivitis and Peri-Implant Mucositis. *J. Dent. Res.* 96, 47–55. doi: 10.1177/0022034516668847

Schwarz, F., Derks, J., Monje, A., and Wang, H. L. (2018). Peri-Implantitis. *J. Periodontol.* 89 Suppl 1, S267–S290. doi: 10.1002/JPER.16-0350

Schwiertz, A. (2016). Microbiota of the Human Body: Implications in Health and Disease. Preface. *Adv. Exp. Med. Biol.* 902. doi: 10.1007/978-3-319-31248-4

Sedghi, L., Dimassa, V., Harrington, A., Lynch, S. V., and Kapila, Y. L. (2021). The Oral Microbiome: Role of Key Organisms and Complex Networks in Oral Health and Disease. *Periodontol. 2000.* 87, 107–131. doi: 10.1111/prd.12393

Selwitz, R. H., Ismail, A. I., and Pitts, N. B. (2007). Dental Caries. *Lancet* 369, 51–59. doi: 10.1016/S0140-6736(07)60031-2

Shi, Y., Tong, Z., Zhang, Y., Si, M., and He, F. (2022). Microbial Profiles of Peri-Implant Mucositis and Peri-Implantitis: Submucosal Microbial Dysbiosis Correlates With Disease Severity. *Clin. Oral. Implants. Res.* 33, 172–183. doi: 10.1111/clr.13880

Simon-Soro, A., and Mira, A. (2015). Solving the Etiology of Dental Caries. *Trends Microbiol.* 23, 76–82. doi: 10.1016/j.tim.2014.10.010

Socransky, S. S., Haffajee, A. D., Cugini, M. A., Smith, C., and Kent, R. L., JR. (1998). Microbial Complexes in Subgingival Plaque. *J. Clin. Periodontol.* 25, 134–144. doi: 10.1111/j.1600-051X.1998.tb02419.x

Sorsa, T., Tjaderhane, L., Konttinen, Y. T., Lauhio, A., Salo, T., Lee, H. M., et al. (2006). Matrix Metalloproteinases: Contribution to Pathogenesis, Diagnosis and Treatment of Periodontal Inflammation. *Ann. Med.* 38, 306–321. doi: 10.1080/07853890600800103

Stájer, A., Kajári, S., Gajdács, M., Musah-Eroje, A., and Baráth, Z. (2020). Utility of Photodynamic Therapy in Dentistry: Current Concepts. *Dent. J.* 8, 43. doi: 10.3390/dj8020043

Subbiahdoss, G., Zeng, G., Aslan, H., Ege Friis, J., Iruthayaraj, J., Zelikin, A. N., et al. (2019). Antifouling Properties of Layer by Layer DNA Coatings. *Biofouling* 35, 75–88. doi: 10.1080/08927014.2019.1568417

Takahashi, N., and Nyvad, B. (2011). The Role of Bacteria in the Caries Process: Ecological Perspectives. *J. Dent. Res.* 90, 294–303. doi: 10.1177/0022034510379602

Talinungsang, Upadhaya, D., Kumar, P., Purkayastha, D. D. (2019). Superhydrophilicity of Photocatalytic ZnO/SnO2 Heterostructure for Self-Cleaning Applications. *J. Sol-Gel. Sci. Technol.* 92, 575–584. doi: 10.1007/s10971-019-05127-8

Tanner, A. C. R., Kressirer, C. A., Rothmiller, S., Johansson, I., and Chalmers, N. I. (2018). The Caries Microbiome: Implications for Reversing Dysbiosis. *Adv. Dent. Res.* 29, 78–85. doi: 10.1177/0022034517736496

Teh, S. J., and Lai, C. W. (2019). "Carbon Nanotubes for Dental Implants," in *Applications of Nanocomposite Materials in Dentistry*. doi: 10.1016/B978-0-12-813742-0.00005-5

Teles, R., Teles, F., Frias-Lopez, J., Paster, B., and Haffajee, A. (2013). Lessons Learned and Unlearned in Periodontal Microbiology. *Periodontol* 62, 95–162. doi: 10.1111/prd.12010

Thomas, C., Minty, M., Vinel, A., Canceill, T., Loubières, P., Burcelin, R., et al. (2021). Oral Microbiota: A Major Player in the Diagnosis of Systemic Diseases. *Diagnostics* 11, 1376. doi: 10.3390/diagnostics11081376

Tuominen, H., and Rautava, J. (2021). Oral Microbiota and Cancer Development. *Pathobiology* 88, 116–126. doi: 10.1159/000510979

Uitto, V. J., Overall, C. M., and Mcculloch, C. (2003). Proteolytic Host Cell Enzymes in Gingival Crevice Fluid. *Periodontol. 2000.* 31, 77–104. doi: 10.1034/j.1600-0757.2003.03106.x

Valdez-Salas, B., Beltrán-Partida, E., Nedev, N., Ibarra-wiley, R., Salinas, R., Curiel-Álvarez, M., et al. (2019). Controlled Antifungal Behavior on Ti6Al4V Nanostructured by Chemical Nanopatterning. *Mat. Sci. Eng. C.* 96, 677–683. doi: 10.1016/j.msec.2018.11.086

Valm, A. M. (2019). The Structure of Dental Plaque Microbial Communities in the Transition From Health to Dental Caries and Periodontal Disease. *J. Mol. Biol.* 431, 2957–2969. doi: 10.1016/j.jmb.2019.05.016

Vanaki, S. S. (2020). Targeting Actual Dental Caries-Associated Bacteria. *Contemp. Clin. Dent.* 11, 209–210. doi: 10.4103/ccd.ccd_855_20

Van winkelhoff, A. J., Goene, R. J., Benschop, C., and Folmer, T. (2000). Early Colonization of Dental Implants by Putative Periodontal Pathogens in Partially Edentulous Patients. *Clin. Oral. Implants. Res.* 11, 511–520. doi: 10.1034/j.1600-0501.2000.011006511.x

Venault, A., Yang, H. S., Chiang, Y. C., Lee, B. S., Ruaan, R. C., and Chang, Y. (2014). Bacterial Resistance Control on Mineral Surfaces of Hydroxyapatite and Human Teeth *via* Surface Charge-Driven Antifouling Coatings. *ACS Appl. Mat. Interfaces.* 6, 3201–3210. doi: 10.1021/am404780w

Wang, H. Y., Cheng, J. W., Yu, H. Y., Lin, L., Chih, Y. H., and Pan, Y. P. (2015). Efficacy of a Novel Antimicrobial Peptide Against Periodontal Pathogens in Both Planktonic and Polymicrobial Biofilm States. *Acta Biomat.* 25, 150–161. doi: 10.1016/j.actbio.2015.07.031

Wang, X., Dong, H., Liu, J., Qin, G., Chen, D., and Zhang, E. (2019). *In Vivo* Antibacterial Property of Ti-Cu Sintered Alloy Implant. *Mat. Sci. Eng. C.* 100, 38–47. doi: 10.1016/j.msec.2019.02.084

Wang, R., Hashimoto, K., Fujishima, A., Chikuni, M., Kojima, E., Kitamura, A., et al. (1997). Light-Induced Amphiphilic Surfaces. *Nature* 388, 431–432. doi: 10.1038/41233

Wang, B., Yao, M., Lv, L., Ling, Z., and Li, L. (2017). The Human Microbiota in Health and Disease. *Engineering* 3, 71–82. doi: 10.1016/J.ENG.2017.01.008

Wang, Z., Zhang, R., Yan, X., and Fan, K. (2020). Structure and Activity of Nanozymes: Inspirations for *De Novo* Design of Nanozymes. *Mat. Today* 41, 81–119. doi: 10.1016/j.mattod.2020.08.020

Wassmann, T., Kreis, S., Behr, M., and Buergers, R. (2017). The Influence of Surface Texture and Wettability on Initial Bacterial Adhesion on Titanium and Zirconium Oxide Dental Implants. *Int. J. Implant. Dent.* 3, 32. doi: 10.1186/s40729-017-0093-3

Wicaksono, D. P., Washio, J., Abiko, Y., Domon, H., and Takahashi, N. (2020). Nitrite Production From Nitrate and Its Link With Lactate Metabolism in Oral Veillonella Spp. *Appl. Environ. Microbiol.* 86, e01255–e01220. doi: 10.1128/AEM.01255-20

Wu, T., Sun, J., Lei, J., Fan, Q., Tang, X., Zhu, G., et al. (2021b). An Efficient Treatment of Biofilm-Induced Periodontitis Using Pt Nanocluster Catalysis. *Nanoscale* 13, 17912–17919. doi: 10.1039/D1NR05198A

Wu, S., Xu, J., Zou, L., Luo, S., Yao, R., Zheng, B., et al. (2021a). Long-Lasting Renewable Antibacterial Porous Polymeric Coatings Enable Titanium Biomaterials to Prevent and Treat Peri-Implant Infection. *Nat. Commun.* 12, 3303. doi: 10.1038/s41467-021-23069-0

Xiang, M., Zhu, M., Yang, Z., He, P., Wei, J., Gao, X., et al. (2020). Dual-Functionalized Apatite Nanocomposites With Enhanced Cytocompatibility and Osteogenesis for Periodontal Bone Regeneration. *ACS Biomat. Sci. Eng.* 6, 1704–1714. doi: 10.1021/acsbiomaterials.9b01893

Xu, X., Fan, M., Yu, Z., Zhao, Y., Zhang, H., Wang, J., et al. (2022). A Removable Photothermal Antibacterial "Warm Paste" Target for Cariogenic Bacteria.. *Chem. Eng. J.* 429, 132491. doi: 10.1016/j.cej.2021.132491

Xu, Y., Zhao, S., Weng, Z., Zhang, W., Wan, X., Cui, T., et al. (2020). Jelly-Inspired Injectable Guided Tissue Regeneration Strategy With Shape Auto-Matched and Dual-Light-Defined Antibacterial/Osteogenic Pattern Switch Properties. *ACS Appl. Mat. Interfaces.* 12, 54497–54506. doi: 10.1021/acsami.0c18070

Yilgör, E., and Yilgör, I. (2014). Silicone Containing Copolymers: Synthesis, Properties and Applications. *Prog. Polym. Sci.* 39, 1165–1195. doi: 10.1016/j.progpolymsci.2013.11.003

Yilmaz, O., Verbeke, P., Lamont, R. J., and Ojcius, D. M. (2006). Intercellular Spreading of Porphyromonas Gingivalis Infection in Primary Gingival Epithelial Cells. *Infect. Immun.* 74, 703–710. doi: 10.1128/IAI.74.1.703-710.2006

Yu, Y., Cheng, Y., Tan, L., Liu, X., Li, Z., Zheng, Y., et al. (2022). Theory-Screened MOF-Based Single-Atom Catalysts for Facile and Effective Therapy of Biofilm-Induced Periodontitis. *Chem. Eng. J.* 431, 133279. doi: 10.1016/j.cej.2021.133279

Yu, X., He, J., Li, S., Liu, F., Yang, J., and Deng, F. (2020). Preparation of Experimental Resin Composites With an Anti-Adhesion Effect Against S. Mutans Using Branched Silicone Methacrylate. *J. Mech. Behav. BioMed. Mat.* 101, 103414. doi: 10.1016/j.jmbbm.2019.103414

Zeng, L., and Burne, R. A. (2016). Sucrose- and Fructose-Specific Effects on the Transcriptome of Streptococcus Mutans, as Determined by RNA Sequencing. *Appl. Environ. Microbiol.* 82, 146–156. doi: 10.1128/AEM.02681-15

Zhang, J., Chen, C., Chen, J., Zhou, S., Zhao, Y., Xu, M., et al. (2020). Dual Mode of Anti-Biofilm Action of G3 Against Streptococcus Mutans. *ACS Appl. Mat. Interfaces.* 12, 27866–27875. doi: 10.1021/acsami.0c00771

Zhang, X., Hasani-Sadrabadi, M. M., Zarubova, J., Dashtimighadam, E., Haghniaz, R., Khademhosseini, A., et al. (2022). Immunomodulatory Microneedle Patch for Periodontal Tissue Regeneration. *Matter* 5, 666–682. doi: 10.1016/j.matt.2021.11.017

Zhang, H., Zhu, Y., Li, Y., Qi, X., Yang, J., Qi, H., et al. (2021). A Bifunctional Zwitterion-Modified Porphyrin for Photodynamic Nondestructive Tooth Whitening and Biofilm Eradication. *Adv. Funct. Mat.* 31, 2104799. doi: 10.1002/adfm.202104799

Zhou, H., Li, F., Weir, M. D., and Xu, H. H. (2013). Dental Plaque Microcosm Response to Bonding Agents Containing Quaternary Ammonium Methacrylates With Different Chain Lengths and Charge Densities. *J. Dent.* 41, 1122–1131. doi: 10.1016/j.jdent.2013.08.003

Zhou, L., Li, Q. L., and Wong, H. M. (2021). A Novel Strategy for Caries Management: Constructing an Antibiofouling and Mineralizing Dual-Bioactive Tooth Surface. *ACS Appl. Mat. Interfaces.* 13, 31140–31152. doi: 10.1021/acsami.1c06989

Zitzmann, N. U., and Berglundh, T. (2008). Definition and Prevalence of Peri-Implant Diseases. *J. Clin. Periodontol.* 35, 286–291. doi: 10.1111/j.1600-051X.2008.01274.x

Conflict of Interest: The authors declare that the research was conducted in the absence of any commercial or financial relationships that could be construed as a potential conflict of interest.

Publisher's Note: All claims expressed in this article are solely those of the authors and do not necessarily represent those of their affiliated organizations, or those of the publisher, the editors and the reviewers. Any product that may be evaluated in this article, or claim that may be made by its manufacturer, is not guaranteed or endorsed by the publisher.

frontiers | Frontiers in Cellular and Infection Microbiology

ORIGINAL RESEARCH
published: 13 July 2022
doi: 10.3389/fcimb.2022.931011

Evolutionary Relationships Between Dysregulated Genes in Oral Squamous Cell Carcinoma and Oral Microbiota

Yang Fang[1], *Yi Yang*[2] *and Chengcheng Liu*[2]*

[1] Department of Laboratory Medicine, Third Affiliated Hospital of Zhengzhou University, Zhengzhou, China, [2] State Key Laboratory of Oral Diseases, National Clinical Research Center for Oral Diseases, Department of Periodontics, West China School and Hospital of Stomatology, Sichuan University, Chengdu, China

Oral squamous cell carcinoma (OSCC) is one of the most prevalent cancers in the world. Changes in the composition and abundance of oral microbiota are associated with the development and metastasis of OSCC. To elucidate the exact roles of the oral microbiota in OSCC, it is essential to reveal the evolutionary relationships between the dysregulated genes in OSCC progression and the oral microbiota. Thus, we interrogated the microarray and high-throughput sequencing datasets to obtain the transcriptional landscape of OSCC. After identifying differentially expressed genes (DEGs) with three different methods, pathway and functional analyses were also performed. A total of 127 genes were identified as common DEGs, which were enriched in extracellular matrix organization and cytokine related pathways. Furthermore, we established a predictive pipeline for detecting the coevolutionary of dysregulated host genes and microbial proteomes based on the homology method, and this pipeline was employed to analyze the evolutionary relations between the seven most dysregulated genes (MMP13, MMP7, MMP1, CXCL13, CRISPO3, CYP3A4, and CRNN) and microbiota obtained from the eHOMD database. We found that cytochrome P450 3A4 (CYP3A4), a member of the cytochrome P450 family of oxidizing enzymes, was associated with 45 microbes from the eHOMD database and involved in the oral habitat of *Comamonas testosteroni* and *Arachnia rubra*. The peptidase M10 family of matrix metalloproteinases (MMP13, MMP7, and MMP1) was associated with *Lacticaseibacillus paracasei*, *Lacticaseibacillus rhamnosus*, *Streptococcus salivarius*, *Tannerella* sp._HMT_286, and *Streptococcus infantis* in the oral cavity. Overall, this study revealed the dysregulated genes in OSCC and explored their evolutionary relationship with oral microbiota, which provides new insight for exploring the microbiota–host interactions in diseases.

Keywords: OSCC, oral microbiota, evolutionary relationships, matrix metalloproteinases, DEGs1

OPEN ACCESS

Edited by:
Jin Xiao,
University of Rochester, United States

Reviewed by:
Xian Xia,
Hubei Normal University, China
Aruni Wilson,
Loma Linda University, United States

***Correspondence:**
Chengcheng Liu
liuchengcheng519@163.com

Specialty section:
This article was submitted to Microbiome in Health and Disease, a section of the journal Frontiers in Cellular and Infection Microbiology

Received: *28 April 2022*
Accepted: *20 June 2022*
Published: *13 July 2022*

Citation:
Fang Y, Yang Y and Liu C (2022) Evolutionary Relationships Between Dysregulated Genes in Oral Squamous Cell Carcinoma and Oral Microbiota. Front. Cell. Infect. Microbiol. 12:931011. doi: 10.3389/fcimb.2022.931011

Abbreviations: DEGs, differentially expressed genes; MMPs, peptidase M10 family of matrix metalloproteinases; OSCC, oral squamous cell carcinoma; GEO, Gene Expression Omnibus; GO, The Gene Ontology; MF, Molecular Function; CC, Cellular Component; BP, Biological Process; FDR, adjusted P-value; FC: fold change; KEGG, Kyoto Encyclopedia of Genes and Genomes.

INTRODUCTION

Head and neck squamous cell carcinoma (HNSCC) is the seventh most common malignancy in the world, accounting for more than 90% of head and neck malignancies (Mody et al., 2021). HNSCC originates from the squamous epithelium of the upper respiratory tract and digestive tract of the oral cavity, pharynx, and larynx, among which pharyngeal squamous cell carcinoma, laryngeal squamous cell carcinoma, and OSCC are the most common. OSCC often has a great impact on patients' chewing, swallowing, language, breathing, and other functions and even threatens their lives (Johnson et al., 2020). In recent years, the incidence of OSCC has been on the rise, becoming a world public health problem with high morbidity and mortality (Ferlay et al., 2019). Studies have shown that, in addition to major risk factors such as tobacco and alcohol abuse, exposure to environmental pollutants and viruses, specific oral bacteria, or oral microbial communities may play an important role in the occurrence and progression of OSCC (Fitzsimonds et al., 2020; Irfan et al., 2020). The human microbiome coevolved and coexisted, and OSCC that also grows in the oral cavity may themselves be the hosts of oral microbiota. The oral cavity harbors over 700 microbial species and both pathogenic and commensal strains are involved in the development of OSCC. Evidence has indicated a correlation of some specific species with OSCC, including *Porphyromonas gingivalis*, *Fusobacterium nucleatum*, *Treponema denticola*, *Streptococcus gordonii*, and human papilloma virus 16 (Fitzsimonds et al., 2020).

The current strategies to investigate the role of the oral microbiota in OSCC have predominantly focused on detecting oral microbial communities present or populational shifts in OSCC samples and studying the effect and mechanism of specific oral microbial challenges on biological processes (BPs) related to OSCC occurrences, such as cell proliferation, cell apoptosis, and the epithelial to mesenchymal transition. Perspective studies should focus on exploring the oral microbiota potentially related to OSCC. However, oral microbes are abundant and approximately 30% of them cannot be cultured. Thus, determining oral microbial–host interactions between species experimentally is a challenging task (Fritz et al., 2013). Computational approaches are an ideal approach to aid in screening for microbial–host interactions, with time-saving and economic advantages (Dix et al., 2016; Fitzsimonds et al., 2020). From an evolutionary perspective, if there is significant similarity between two protein sequences, they may originate from a common ancestor and have the same or similar functions (Pearson, 2013). Therefore, the most common method to explore protein function is pair-wise protein sequence comparison to "transfer" or prediction of function based on sequence similarity between proteins of known and unknown function (Rost, 1999; Bork, 2000; Devos and Valencia, 2000). And BLAST is a classic pairwise approach that can search protein sequence similarities all against all (Camacho et al., 2009). Based on this principle, several approaches have been established to determine pathogen–host protein–protein interactions (PHIs), including protein homology prediction, structural domain–based methods, and machine learning–based methods (English and Albersheim, 1969; Wojcik and Schächter, 2001; Pagel et al., 2004; Qi et al., 2010; Dyer et al., 2011).

Increasing evidence has shown that shared evolutionary history matters to both microbiota and hosts (Davenport et al., 2017). Microorganisms include bacteria, viruses, fungi, and some small protists. These organisms typically have smaller proteomes, based on which they can be analyzed for community heterogeneity, activity, and function. If the entire proteome of a microorganism is regarded as a protein that is evolutionarily conserved, the entire microbiome is a living organism composed of a large number of such proteins. Based on the principle of protein–protein interaction (PPI), the interaction relationship between the entire proteome of microorganisms and the host can be predicted. Oral microbiota colonize the oral mucosa, and they have a coevolutionary relationship; therefore, based on the principle of coevolutionary association inferring functional interactions, this study established a predictive pipeline for the evolutionarily interconnected evolution of dysregulated host genes and microbial proteomes (Devos and Valencia, 2000). We identified dysregulated genes in OSCC tissues by analyzing gene expression datasets from the GEO database and explored their evolutionary relations with oral microbiota with this pipeline. The results are expected to provide new insights into the interactions between oral microbiota and OSCC.

MATERIALS AND METHODS

Data Collection

The Gene Expression Omnibus (GEO) database contains a large number of gene expression profiling (high-throughput sequencing and microarray datasets) and RNA methylation profiles that are submitted by different research laboratories in the world (Edgar et al., 2002). We retrieved the related gene expression datasets by OSCC and oral keywords. The criteria for the retrieved datasets must contain different sequencing platforms. Finally, the microarray datasets (GSE138206) and high-throughput sequencing datasets (GSE140707) were downloaded from the GEO database. The GSE138206 dataset contains six OSCC tissues (Ca), tissues adjacent to cancer (P), and contralateral normal tissues (N), and the GSE140707 contains three tumorous and adjacent tissues from OSCC sufferers.

DEGs Identification

All analyses of differentially expressed genes (DEGs) were performed by R language. The GEO query package (Sean and Meltzer, 2007) was used to obtain collected datasets from the GEO database. For microarray datasets, the statistically significant DEGs were acquired by utilizing the limma package (Ritchie et al., 2015) with adjusted P-value (FDR) < 0.05 and |log2 (fold change (FC))| > 1. The Deseq2 (Love et al., 2014) and EdgeR (Robinson et al., 2010) packages were utilized to analyze RNA sequencing data and filter significant DEGs between OSCC and adjacent normal tissues.

Enrichment Analyses

The Gene Ontology (GO) describes our knowledge of the biological function in three aspects: molecular function (MF), cellular component (CC), and BP (The Gene Ontology, Consortium 2019). The Kyoto Encyclopedia of Genes and Genomes (KEGG) pathway is a database utilized for genomic and biological pathway and other omics studies (Kanehisa and Goto, 2000). We used the ClusterProfile package (Yu et al., 2012) to identify the potential functions of the significant DEGs with the GO and KEGG databases, and the results were displayed by the ggplot2 package (Wickham, 2011) with a cutoff of $p < 0.05$.

Evolutionary Relation With the Oral Microbiome

The microbe data (1,903 microbiome genomes with 4,665,857 proteins) were downloaded from the expanded Human Oral Microbiome Database (eHOMD) (Escapa et al., 2018). The eHOMD provides comprehensive curated information on bacteria in the human mouth and aerodigestive tract, including the pharynx, nasal passages, sinuses, and esophagus. The DEG homologous proteins were searched by BLAST+ software (Camacho et al., 2009) with an e-value < 0.001. We used the MEGA11 software to identify the evolutionary relationship between DEGs and oral microbiomes by MEGA11 software (Tamura et al., 2021). Multiple sequence alignment was performed by MUSCLE (Edgar, 2004) (Gap Open:-2.9, Hydrophobicity Multiplier:1.2, Max Iterations:16, Min Diag Length:24), using the maximum likelihood method (JTT model and NNI ML heuristic method) to reconstruct the phylogenetic tree. The iTOL is used to illustrate the phylogenetic tree (Letunic and Bork, 2006).

RESULTS

Transcriptional Landscapes of OSCC

This study was performed according to the workflow (**Figure 1A**). A total of 280 DEGs in microarray dataset GSE138206 were identified by the limma package with 162 upregulated genes and 118 downregulated genes (**Figure 1C**, **Table S1**). Analysis of the high-throughput sequencing datasets GSE140707 by Deseq2 packages obtained 1,699 DEGs of OSCC, and, of these, 652 genes and 1,047 genes were upregulated and downregulated, respectively (**Figure 1D**, **Table S2**). In addition, 1,215 DEGs were identified by EdgeR with 666 upregulated genes and 549 downregulated genes (**Table S3**). Taking the intersection of three different package analyses of two OSCC datasets and plotting the Venn diagram, 127 common DEGs were obtained (**Figure 1B**, **Table S4**). Additionally, there were five significant DEGs (MMP10, MUCL1, TGM3, WIF1, and TMPRSSS11B) that were identified only in GSE138206 (**Figure 1C**). In addition to the intersection, seven high fold change expression genes (CST1, IGHV1-3, IGHV1-18, MAGEA6, HMGCS2, KRT84, and KRTAP13-2) were identified in GSE140707 (**Figure 1D**).

Dysregulation of Genes Related to Extracellular Matrixes and Cytokines in OSCC

Seven genes belonged to the intersection of DEGs identified by three different methods were dysregulated genes in OSCC. Among them, MMP13, MMP7, MMP1, and CXCL13 genes were upregulated in OSCC tissues, and CRISP3, CYP3A4, and CRNN genes were downregulated (**Figure 2A**). To gain insight into the pathways and function of common DEGs of OSCC, the

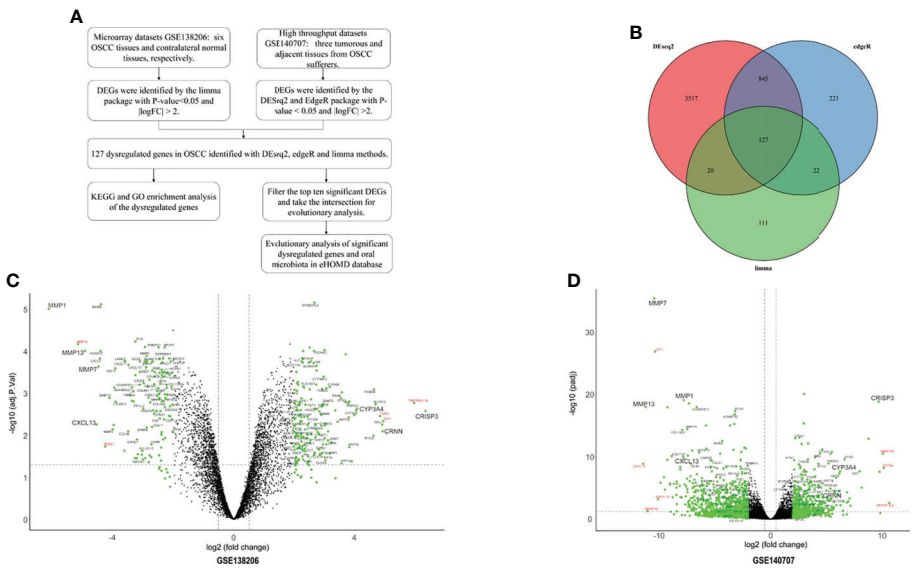

FIGURE 1 | The identified of DEGs. **(A)** The flowchart of research design. **(B)** The two datasets showed an overlap of 127 differentially expressed genes (DEGs) which were identified by three different methods. **(C)** The volcano map of microarray dataset GSE138206. **(D)** The volcano map of high-throughput sequencing dataset GSE140707. The DEGs are marked in light blue; the 127 common DEGs are labeled with black, and red labels are DEGs in each dataset.

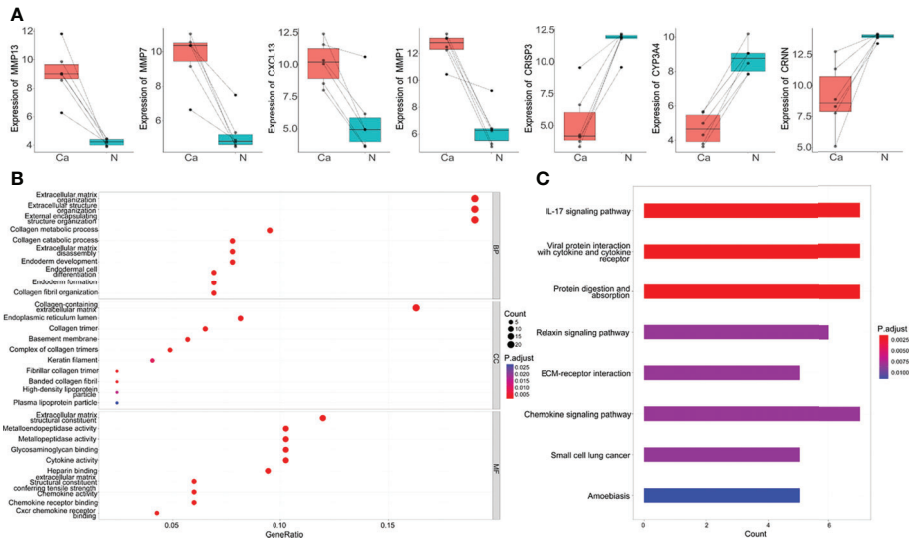

FIGURE 2 | The top DEGs and common DEGs enrichment analysis results. **(A)** The expression of seven DEGs in microarray dataset GSE138206. Ca, cancer; N, Normal. **(B)** The enrichment analysis results of GO database with BP, CC and MF. **(C)** The enrichment analysis results of KEGG Pathway. Adjusted P-value < 0.05 was considered significant.

GO enrichment analysis and KEGG enrichment analysis were performed. It was observed that DEGs were enriched in categories associated with extracellular matrix (ECM) organization, collagen metabolic process, metallopeptidase activity, glycosaminoglycan binding, and cytokine activity (**Figure 2B**). KEGG analysis showed that the 127 DEGs were significantly enriched in 10 pathways, such as cytokine-cytokine receptor interaction, IL-17 signaling pathway, viral protein interaction with cytokine and cytokine receptor, and protein digestion and absorption. Notably, COL4A1, COL4A2, COL4A6, FN1, and LAMC2 genes were also enriched in the ECM receptor interaction pathway (**Figure 2C**).

Evolutionary Relationship Between the Dysregulated Genes and Oral Microbiota

To explore the evolutionary relationships of the seven DEGs and oral microbiota. We used the BLAST method to align 1,903 microbiome genomes (total 4,665,857 proteins) in human microbiome which retrieved from the eHOMD database. We set the BLAST cutoff with e-value < 10^{-3} against the microbiome genome search for the homologous proteins (**Table 1**). We searched 350 homologous proteins within 45 species of microorganisms with the CYP3A4 gene by BLAST software. Among these microorganisms, *Comamonas testosteroni KF-1*, *Comamonas testosteroni CNB-2*, *Comamonas testosteroni S44*, and *Arachnia rubra DSMZ* 10012 inhabit in the oral cavity (**Table S5**). Oral colonizers with an evolutionary relationship to MMP1 include *Streptococcus infantis ATCC* 700779, *Streptococcus infantis SPAR10*, and *Tannerella* sp.*_HMT_286 W11667* (**Table S6**). Interestingly, *Tannerella* sp.*_HMT_286 W11667* and MMP5 as well as MM13 also have a coevolutionary relationship (**Tables S7**, **S8**). In addition, MMP13 also has a coevolutionary relationship with *Lacticaseibacillus paracasei*, *Lacticaseibacillus rhamnosus*, and

TABLE 1 | The homologous proteins searched of seven DEGs.

Gene name	Gene annotation	Species	Strain	Oral	Uassigned	Protein	Species name
CRISP3	cysteine-rich secretory protein (CRISP) family	1	1	0	1	1	NA
CYP3A4	cytochrome P450 superfamily of enzymes	45	119	2	43	350	*Comamonas testosteroni, rubra*
MMP1	peptidase M10 family of matrix metalloproteinases	7	39	4	3	40	*Lacticaseibacillus rhamnosus, Lacticaseibacillus paracasei*, *Streptococcus salivarius, Tannerella* sp.*_HMT_286*
MMP7	peptidase M10 family of matrix metalloproteinases	9	16	1	8	16	*Tannerella* sp.*_HMT_286*
MMP13	peptidase M10 family of matrix metalloproteinases	5	11	2	3	13	*Streptococcus infantis*, *Tannerella* sp.*_HMT_286*
CXCL13	C-X-C Motif Chemokine Ligand 13	0	0	0	0	0	NA
CRNN	The "fused gene" family of proteins	0	0	0	0	0	eNA

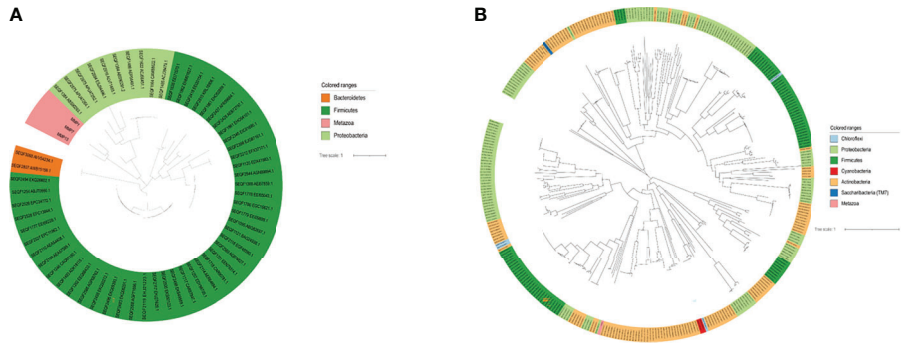

FIGURE 3 | The evolutionary relation analysis of Top DEGs. **(A)** The evolutionary relation between MMP13, MMP7, and MMP1 with the microbiome. **(B)** The evolutionary relation between CYP3A4 with the microbiome.

Streptococcus salivarius, which live in the oral cavity (**Table S8**). **Figure 3A** shows the evolutionary relations among the MMP13, MMP7, and MMP1 genes of oral genomes. As can be seen from the results of the analysis of the evolutionary relationship, three upregulated genes have homologs with the phyla of *Bacteroidetes*, *Firmicutes*, and *Proteobacteria*. The most significant aspect of this relationship is Proteobacteria, which contains 8 oral species and 10 proteins. The evolutionary relations of CYP3A4 genes are shown in **Figure 3B**.

DISCUSSION

OSCC is the most common malignancy, accounting for 80%–90% of oral malignancies. Oral microbiota is a major risk factor for OSCC. Associated interactions between oral microorganisms and host can promote the progression of OSCC (Bai et al., 2022). In this study, we identified 652 upregulated and 1,047 downregulated genes in the OSCC tissues based on the GSE140707 dataset, as well as 162 upregulated and 118 downregulated genes in the GSE138216 dataset. The unique significance of 127 DEGs by three methods was based on the analyzed metadata. DEGs were identified in both datasets associated with the IL-17 signaling pathway, viral protein interaction with cytokines and cytokine receptors, and protein digestion and absorption. Seven significant dysregulated genes in OSCC tissues were further identified, including four upregulated genes MMP13, MMP7, MMP1, and CXCL13 and three downregulated genes CRSP3, CYP3A4, and CRNN. In the present study, we established a predictive pipeline for exploring the evolutionary relationship between the oral microbiota in the eHOMD database and the dysregulated genes in OSCC based on the principle of coevolution.

Matrix metalloproteinases (MMPs) are involved in normal physiological processes of decomposing ECM, such as tissue remodeling, embryonic development, and reproduction, as well as in disease processes of arthritis and metastasis (Snoek-van Beurden and Von den Hoff, 2005). The MMP13, MMP7, and MMP1 genes encode members of the peptidase M10 family of MMPs. Consistent with our findings, previous studies have reported the dysregulated expression of them in OSCC progression. For instance, overexpression of both transcriptional and translational levels of MMP13 was found in OSCC tissues (Johansson et al., 1997; Culhaci et al., 2004; Luukkaa et al., 2006). Highly expressed MMP13 protein also showed a significant correlation with tumor staging and lymph node metastasis (Vincent-Chong et al., 2014). The expression of MMP7 and MMP1 was also upregulated in OSCC tissues. The expression of MMP7 and MMP1 were also upregulated in OSCC tissues. The MMP1 gene was activated in aggressive OSCC (Impola et al., 2004; Jordan et al., 2004; Chuang et al., 2008; Makinen et al., 2014).

Moreover, the MMP1 gene might be used as a potential target to improve diagnosis and as an oral cancer marker for OSCC (Hashimoto et al., 2004; Yen et al., 2009; Yang et al., 2020). Functional enrichment analysis revealed that MMP13, MMP7, and MMP1 were related to ECM organization, ECM disassembly, extracellular structure organization, and endoderm development. Tumors can utilize ECM remodeling to create a microenvironment that promotes tumorigenesis and metastasis. Therefore, we speculate that the overexpression of MMP13, MMP7, and MMP1 might involve invasiveness and metastasis of OSCC by modulating ECM remodeling.

The homology search method identified an evolutionary relationship with the oral microbiota for the MMP13, MMP7, and MMP1 genes. We chose MMP family genes to explore their evolutionary relationship with microbial species because MMP family differential expression was significant when differentially expressed genes were analyzed. The *Lacticaseibacillus paracasei*, *Lactobacillus rhamnosus*, *Streptococcus salivarius*, *Tannerella* sp. *HMT 286*, and *Streptococcus infantis five* species were hit homologous. In the previous study, Pushalkar et al. assessed the microbial diversity in OSCC tissues and non-tumor tissues. The results showed that the microbial load of *Lacticaseibacillus* paracasei has a significant variation (Pushalkar et al., 2012). It has been reported that the administration of *Lactobacillus rhamnosus* was able to increase the effect of anticancer molecules tested on human OSCC (Cheng et al., 2017). These results

demonstrated the potential of *Lactobacillus rhamnosus* as a beneficial effect adjuvant treatment for OSCC. In OSCC patients undergoing tumor resection, the percentage of saliva-reactive cytotoxic T cells was positively correlated with recurrence-free survival (Wang et al., 2018). Another study (Pavlova et al., 2013) showed that *Streptococcus salivarius* is involved in alcohol metabolism to acetaldehyde, which has a carcinogenic potential (Vogelmann and Amieva, 2007; Marttila et al., 2013). Consistent with our findings, evidence has also shown a significant difference of *Streptococcus infantis* between OSCC patients and healthy individuals (Hsiao et al., 2018). These all support the reliability of our predictive pipeline for exploring the interaction between dysregulated genes in OSCC and oral microbiota.

The CYP3A4 gene encodes a member of the cytochrome P450 superfamily of enzymes and is involved in the metabolism of sterols, steroid hormones, retinoids, and fatty acids (Chen et al., 2000; Marill et al., 2000; Badawi et al., 2001). Cytoscape software by the Matthews correlation coefficient (MCC) algorithm was used to predict CYP3A4 at the core position in the network and highlight the first 10 types of OSCC DEGs (Li et al., 2022). It is worth noting that there found 350 homologous proteins including 45 microbes were found by evolutionary analysis in this study. Among them, *Comamonas testosteroni* and *Arachnia rubra* can inhabit in the oral cavity. Up to 348 microorganisms were unassigned information on their location in the human body. Extracts of *Arachnia rubra* are associated with human OSCC production and modulation of tumor-specificity values (Suzuki et al., 2014). However, we noticed that the two previously reported bacteria associated with OSCC, *Porphyromonas gingivalis* and *Clostridium perfringens*, were not found when using this method to explore the relationship between dysregulated genes and oral microbiota. We speculate that the possible reason is that, although these bacteria play an important role in OSCC, there is no homologous evolutionary relationship with the genes that we screened. CXCL13, CRISPO3, and CRNN have newly identified dysregulated genes by this study, and their effects on the OSCC need to be further investigated for experimental validation.

Microorganisms, including bacteria, viruses, and archaea, inhabit a wide range of hosts in different ecological niches and ecosystems (Braga et al., 2016). Deciphering microbial–host interactions can provide new therapeutic strategies for maintaining health or improving disease states. However, determining microbial–host interactions between species experimentally is a challenging task due to many other limitations related to the size, scope, feasibility of studies, and sample availability of microbial populations (Fritz et al., 2013). Computational approaches can overcome some of these limitations and thus enhance our understanding of microbial–host interactions (Dix et al., 2016). Molecular ecological networks are used to study the interactions between molecules (from different species or even kingdoms) in a larger ecosystem (Yang et al., 2017; Meyer et al., 2020). From a mechanistic perspective, the most widely studied types of interactions among species interactions include microbial networks, PPIs, and RNA-mediated interactions. Therefore, many computational methods developed to study microbe–host interactions have focused on the three types of interactions mentioned above. However, all of these inference methods have the feature of studying microbe–host interactions based on the characteristics of the sequence structure. In this study, we propose the use of coevolutionary principles to infer microbial–host interactions based on sequence structure. The use of the coevolutionary principle better reflects the conserved protein structure of the species than the direct use of sequence structure. Therefore, we established a predictive pipeline to study the interaction between DEGs and oral microbiota in OSCC based on sequence-structure conservativeness and coevolutionary principles. Of course, the method has its shortcomings, that is, the method is based on the inference that species have the same protein conserved modules during the evolutionary process, and if the studied DEGs and microbial proteins do not have the same evolutionary conserved modules, they cannot be studied by this method. However, this method provides a novelty way and new ideas for exploring the relationship between host genes and host symbiotic microorganism.

DATA AVAILABILITY STATEMENT

The original contributions presented in the study are included in the article/**Supplementary Material**. Further inquiries can be directed to the corresponding author.

AUTHOR CONTRIBUTIONS

YF contributed to the study conception and design, data acquisition, analysis, and interpretation, and in the drafting the of the manuscript. YF and YY contributed to data acquisition, analysis, and interpretation. CL contributed to the study conception and design and the drafting and critical revision of the manuscript. All the authors approved the final version of the manuscript and agreed to be accountable for all aspects of the work.

FUNDING

This work is supported by PhD research startup foundation of the Third Affiliated Hospital of Zhengzhou University (2021080).

SUPPLEMENTARY MATERIAL

The Supplementary Material for this article can be found online at: https://www.frontiersin.org/articles/10.3389/fcimb.2022.931011/full#supplementary-material

Supplementary Table 1 | The DEGs in GSE138206 dataset were identified by limma packages.

Supplementary Table 2 | The DEGs in GSE140707 dataset were identified by the Deseq2 package.

Supplementary Table 3 | The DEGs in GSE140707 dataset were identified by the EdgeR package.

Supplementary Table 4 | The 127 common DEGs.

Supplementary Table 5 | The homolog searched results of CYP3A4 genes.

Supplementary Table 6 | The homolog searched results of MMP13 genes.

Supplementary Table 7 | The homolog searched results of MMP7 genes.

Supplementary Table 8 | The homolog searched results of MMP1 genes.

REFERENCES

Badawi, A. F., Cavalieri, E. L., and Rogan, E. G. (2001). "Role of Human Cytochrome P450 1a1, IA2, 1B1, and 3A4 in the 2-, 4-, and 16 Alpha-Hydroxylation of 17 Beta-Estradiol." *Metab. Clin. Exp.* 50 (9), 1001–1003. doi: 10.1053/meta.2001.25592

Bai, H., Yang, J., Meng, S., and Liu, X. X. X. C. (2022). "Oral Microbiota-Driven Cell Migration in Carcinogenesis and Metastasis." *Front. Cell Infect. Microbiol.* 12. doi: 10.3389/fcimb.2022.864479

Bork, P. (2000). "Powers and Pitfalls in Sequence Analysis: The 70% Hurdle." *Genome Res.* 10 (4), 398–400. doi: 10.1101/gr.10.4.398

Braga, R. M., Dourado, M. N., and Araujo, W. L. (2016). "Microbial Interactions: Ecology in a Molecular Perspective." *Braz. J. Microbiol.* 47 (Suppl 1), 86–98. doi: 10.1016/j.bjm.2016.10.005

Camacho, C., Coulouris, G., Avagyan, V., Ma, N., Papadopoulos, J., Bealer, K., et al. (2009). "BLAST+: Architecture and Applications." *BMC Bioinf.* 10, 421. doi: 10.1186/1471-2105-10-421

Cheng, Z., Xu, H., Wang, X., and Liu, Z. (2017). "Lactobacillus Raises *In Vitro* Anticancer Effect of Geniposide in HSC-3 Human Oral Squamous Cell Carcinoma Cells." *Exp. Ther. Med.* 14 (5), 4586–4594. doi: 10.3892/etm.2017.5105

Chen, H., Howald, W. N., and Juchau, M. R. (2000). "Biosynthesis of All-Trans-Retinoic Acid From All-Trans-Retinol: Catalysis of All-Trans-Retinol Oxidation by Human P-450 Cytochromes." *Drug Metab. Disposition* 28 (3), 315–322.

Chuang, H. C., Su, C. Y., Huang, H. Y., Huang, C. C., Chien, C. Y., Du, Y. Y., et al. (2008). "Active Matrix Metalloproteinase-7 is Associated With Invasion in Buccal Squamous Cell Carcinoma." *Modern Pathol.* 21 (12), 1444–1450. doi: 10.1038/modpathol.2008.99

Culhaci, N., Metin, K., Copcu, E., and Dikicioglu, E. (2004). "Elevated Expression of MMP-13 and TIMP-1 in Head and Neck Squamous Cell Carcinomas may Reflect Increased Tumor Invasiveness." *BMC Cancer* 4, 42. doi: 10.1186/1471-2407-4-42

Davenport, E. R., Sanders, J. G., Song, S. J., Amato, K. R., Clark, A. G., and Knight, R. (2017). "The Human Microbiome in Evolution." *BMC Biol.* 15 (1), 127. doi: 10.1186/s12915-017-0454-7

Devos, D., and Valencia, A. (2000). "Practical Limits of Function Prediction." *Proteins Struct. Funct. Bioinf.* 41 (1), 98–107. doi: 10.1002/1097-0134(20001001)41:1<98::AID-PROT120>3.0.CO;2-S

Dix, A., Vlaic, S., Guthke, R., and Linde, J. (2016). "Use of Systems Biology to Decipher Host-Pathogen Interaction Networks and Predict Biomarkers." *Clin. Microbiol. Infect.* 22 (7), 600–606. doi: 10.1016/j.cmi.2016.04.014

Dyer, M. D., Murali, T. M., and Sobral, B. W. (2011). "Supervised Learning and Prediction of Physical Interactions Between Human and HIV Proteins." *Infect. Genet. Evol.* 11 (5), 917–923. doi: 10.1016/j.meegid.2011.02.022

Edgar, R. C. (2004). "MUSCLE: Multiple Sequence Alignment With High Accuracy and High Throughput." *Nucleic Acids Res.* 32 (5), 1792–1797. doi: 10.1093/nar/gkh340

Edgar, R., Domrachev, M., and Lash, A. E. (2002). "Gene Expression Omnibus: NCBI Gene Expression and Hybridization Array Data Repository." *Nucleic Acids Res.* 30 (1), 207–210. doi: 10.1093/nar/30.1.207

English, P. D., and Albersheim, P. (1969). Host-Pathogen Interactions: I. A Correlation Between α-Galactosidase Production and Virulence 1. *Plant Physiol.* 44 (2), 217–224. doi: 10.1104/pp.44.2.217

Escapa, I. F., Chen, T., Huang, Y., Gajare, P., Dewhirst, F. E., and Lemon, K. P. (2018). "New Insights Into Human Nostril Microbiome From the Expanded Human Oral Microbiome Database (eHOMD): A Resource for the Microbiome of the Human Aerodigestive Tract." *Msystems* 3 (6), e00187–18. doi: 10.1128/mSystems.00187-18

Ferlay, J., Colombet, M., Soerjomataram, I., Mathers, C., Parkin, D. M., Pineros, M., et al. (2019). "Estimating the Global Cancer Incidence and Mortality in 2018: GLOBOCAN Sources and Methods." *Int. J. Cancer* 144 (8), 1941–1953. doi: 10.1002/ijc.31937

Fitzsimonds, Z. R., Rodriguez-Hernandez, C. J., Bagaitkar, J., and Lamont, R. J. (2020). "From Beyond the Pale to the Pale Riders: The Emerging Association of Bacteria With Oral Cancer." *J. Dental Res.* 99 (6), 604–612. doi: 10.1177/0022034520907341

Fritz, J. V., Desai, M. S., Shah, P., Schneider, J. G., and Wilmes, P. (2013). "From Meta-Omics to Causality: Experimental Models for Human Microbiome Research." *Microbiome* 1 (1), 14. doi: 10.1186/2049-2618-1-14

Hashimoto, T., Uchida, K., Okayama, N., Imate, Y., Suehiro, Y., Hamanaka, Y., et al. (2004). "Association of Matrix Metalloproteinase (MMP)-1 Promoter Polymorphism With Head and Neck Squamous Cell Carcinoma." *Cancer Lett.* 211 (1), 19–24. doi: 10.1016/j.canlet.2004.01.032

Hsiao, J. R., Chang, C. C., Lee, W. T., Huang, C. C., Ou, C. Y., Tsai, S. T., et al. (2018). "The Interplay Between Oral Microbiome, Lifestyle Factors and Genetic Polymorphisms in the Risk of Oral Squamous Cell Carcinoma." *Carcinogenesis* 39 (6), 778–787. doi: 10.1093/carcin/bgy053

Impola, U., Uitto, V. J., Hietanen, J., Hakkinen, L., Zhang, L., Larjava, H., et al. (2004). "Differential Expression of Matrilysin-1 (MMP-7), 92 kD Gelatinase (MMP-9), and Metalloelastase (MMP-12) in Oral Verrucous and Squamous Cell Cancer." *J. Pathol.* 202 (1), 14–22. doi: 10.1002/path.1479

Irfan, M., Delgado, R. Z. R., and Frias-Lopez, J. (2020). "The Oral Microbiome and Cancer." *Front. Immunol.* 11. doi: 10.3389/fimmu.2020.591088

Johansson, N., Airola, K., Grénman, R., Kariniemi, A. L., Saarialho-Kere, U., and Kähäri, V. M. (1997). "Expression of Collagenase-3 (Matrix Metalloproteinase-13) in Squamous Cell Carcinomas of the Head and Neck." *Am. J. Pathol.* 151 (2), 499–508.

Johnson, D. E., Burtness, B., René Leemans, C., Lui, V. W. Y., Bauman, J. E., and Grandis, J. R. (2020). Head and Neck Squamous Cell Carcinoma. *Nat. Rev. Dis. Primers* 6 (1), 92. doi: 10.1038/s41572-020-00224-3

Jordan, R. C. K., Macabeo-Ong, M., Shiboski, C. H., Dekker, N., Ginzinger, D. G., Wong, D. T. W., et al. (2004). "Overexpression of Matrix Metalloproteinase-1 and-9 mRNA is Associated With Progression of Oral Dysplasia to Cancer." *Clin. Cancer Res.* 10 (19), 6460–6465. doi: 10.1158/1078-0432.Ccr-04-0656

Kanehisa, M., and Goto, S. (2000). KEGG: Kyoto Encyclopedia of Genes and Genomes. *Nucleic Acids Res.* 28 (1), 27–30. doi: 10.1093/nar/28.1.27

Letunic, I., and Bork, P. (2006). Interactive Tree Of Life (iTOL): An Online Tool for Phylogenetic Tree Display and Annotation. *Bioinformatics* 23 (1), 127–128. doi: 10.1093/bioinformatics/btl529

Li, C. S., Shi, Y. Y., Zuo, L. H., Xin, M. Z., Guo, X. M., Sun, J. L., et al. (2022). "Identification of Biomarkers Associated With Cancerous Change in Oral Leukoplakia Based on Integrated Transcriptome Analysis." *J. Oncol.* 2022, 4599305. doi: 10.1155/2022/4599305

Love, M. I., Huber, W., and Anders, S. (2014). "Moderated Estimation of Fold Change and Dispersion for RNA-Seq Data With Deseq2." *Genome Biol.* 15 (12), 550. doi: 10.1186/s13059-014-0550-8

Luukkaa, M., Vihinen, P., Kronqvist, P., Vahlberg, T., Pyrhönen, S., Kähäri, V. M., et al. (2006). "Association Between High Collagenase-3 Expression Levels and Poor Prognosis in Patients With Head and Neck Cancer." *Head Neck* 28 (3), 225–234. doi: 10.1002/hed.20322

Makinen, L. K., Hayry, V., Hagstrom, J., Sorsa, T., Passador-Santos, F., Keski-Santti, H., et al. (2014). "Matrix Metalloproteinase-7 and Matrix Metalloproteinase-25 in Oral Tongue Squamous Cell Carcinoma." *Head Neck J. Sci. Specialties Head Neck* 36 (12), 1783–1788. doi: 10.1002/hed.23539

Marill, J., Cresteil, T., Lanotte, M., and Chabot, G. G. (2000). "Identification of Human Cytochrome P450s Involved in the Formation of All-Trans-Retinoic

Acid Principal Metabolites." *Mol. Pharmacol.* 58 (6), 1341–1348. doi: 10.1124/mol.58.6.1341

Marttila, E., Bowyer, P., Sanglard, D., Uittamo, J., Kaihovaara, P., Salaspuro, M., et al. (2013). "Fermentative 2-Carbon Metabolism Produces Carcinogenic Levels of Acetaldehyde in Candida Albicans." *Mol. Oral. Microbiol.* 28 (4), 281–291. doi: 10.1111/omi.12024

Meyer, J. M., Leempoel, K., Losapio, G., and Hadly, E. A. (2020). "Molecular Ecological Network Analyses: An Effective Conservation Tool for the Assessment of Biodiversity, Trophic Interactions, and Community Structure." *Front. Ecol. Evol.* 8. doi: 10.3389/fevo.2020.588430

Mody, M. D., Rocco, J. W., Yom, S. S., Haddad, R. I., and Saba, N. F. (2021). "Head and Neck Cancer." *Lancet* 398 (10318), 2289–2299. doi: 10.1016/s0140-6736(21)01550-6

Pagel, P., Wong, P., and Frishman, D. (2004). "A Domain Interaction Map Based on Phylogenetic Profiling." *J. Mol. Biol.* 344 (5), 1331–1346. doi: 10.1016/j.jmb.2004.10.019

Pavlova, S. I., Jin, L., Gasparovich, S. R., and Tao, L. (2013). "Multiple Alcohol Dehydrogenases But No Functional Acetaldehyde Dehydrogenase Causing Excessive Acetaldehyde Production From Ethanol by Oral Streptococci." *Microbiol. (Reading)* 159 (Pt 7), 1437–1446. doi: 10.1099/mic.0.066258-0

Pearson, W. R. (2013). An Introduction to Sequence Similarity ("Homology") Searching. *Curr. Protoc. Bioinf. Chapter 3:Unit3.1.* doi: 10.1002/0471250953.bi0301s42

Pushalkar, S., Ji, X., Li, Y., Estilo, C., Yegnanarayana, R., Singh, B., et al. (2012). "Comparison of Oral Microbiota in Tumor and Non-Tumor Tissues of Patients With Oral Squamous Cell Carcinoma." *BMC Microbiol.* 12, 144. doi: 10.1186/1471-2180-12-144

Qi, Y., Tastan, O., Carbonell, J. G., Klein-Seetharaman, J., and Weston, J. (2010). "Semi-Supervised Multi-Task Learning for Predicting Interactions Between HIV-1 and Human Proteins." *Bioinformatics* 26 (18), i645–i652. doi: 10.1093/bioinformatics/btq394

Ritchie, M. E., Phipson, B., Wu, D., Hu, Y., Law, C. W., Shi, W., et al. (2015). "Limma Powers Differential Expression Analyses for RNA-Sequencing and Microarray Studies." *Nucleic Acids Res.* 43 (7), e47. doi: 10.1093/nar/gkv007

Robinson, M. D., McCarthy, D. J., and Smyth, G. K. (2010). "Edger: A Bioconductor Package for Differential Expression Analysis of Digital Gene Expression Data." *Bioinformatics* 26 (1), 139–140. doi: 10.1093/bioinformatics/btp616

Rost, B. (1999). "Twilight Zone of Protein Sequence Alignments." *Protein Eng.* 12 (2), 85–94. doi: 10.1093/protein/12.2.85

Sean, D., and Meltzer, P. S. (2007). "GEOquery: A Bridge Between the Gene Expression Omnibus (GEO) and BioConductor." *Bioinformatics* 23 (14), 1846–1847. doi: 10.1093/bioinformatics/btm254

Snoek-van Beurden, P. A., and Von den Hoff, J. W. (2005). "Zymographic Techniques for the Analysis of Matrix Metalloproteinases and Their Inhibitors." *Biotechniques* 38 (1), 73–83. doi: 10.2144/05381rv01

Suzuki, R., Matsuno, S., Sakagami, H., Okada, Y., and Shirataki, Y. (2014). "Search of New Cytotoxic Crude Materials Against Human Oral Squamous Cell Carcinoma Using 1H NMR-Based Metabolomics." *Anticancer Res.* 34 (8), 4117–4120.

Tamura, K., Stecher, G., and Kumar, S. (2021). "MEGA11: Molecular Evolutionary Genetics Analysis Version 11." *Mol. Biol. Evol.* 38 (7), 3022–3027. doi: 10.1093/molbev/msab120

The Gene Ontology, Consortium (2019). The Gene Ontology Resource: 20 Years and Still GOing Strong. *Nucleic Acids Res.* 47 (D1), D330–D338. doi: 10.1093/nar/gky1055

Vincent-Chong, V. K., Salahshourifar, I., Karen-Ng, L. P., Siow, M. Y., Kallarakkal, T. G., Ramanathan, A., et al. (2014). "Overexpression of MMP13 Is Associated With Clinical Outcomes and Poor Prognosis in Oral Squamous Cell Carcinoma." *ScientificWorldJournal* 2014, 897523. doi: 10.1155/2014/897523

Vogelmann, R., and Amieva, M. R. (2007). "The Role of Bacterial Pathogens in Cancer." *Curr. Opin. Microbiol.* 10 (1), 76–81. doi: 10.1016/j.mib.2006.12.004

Wang, J., Sun, F., Lin, X., Li, Z., Mao, X., and Jiang, C. (2018). "Cytotoxic T Cell Responses to Streptococcus are Associated With Improved Prognosis of Oral Squamous Cell Carcinoma." *Exp. Cell Res.* 362 (1), 203–208. doi: 10.1016/j.yexcr.2017.11.018

Wickham, H. (2011). "Ggplot2." *Wiley Interdiscip. Rev.: Comput. Stat* 3 (2), 180–185. doi: 10.1002/wics.147

Wojcik, J., and Schächter, V. (2001). "Protein-Protein Interaction Map Inference Using Interacting Domain Profile Pairs." *Bioinformatics* 17 (Suppl 1), S296–S305. doi: 10.1093/bioinformatics/17.suppl_1.s296

Yang, B., Dong, K., Guo, P., Guo, P., Jie, G., Zhang, G., et al. (2020). "Identification of Key Biomarkers and Potential Molecular Mechanisms in Oral Squamous Cell Carcinoma by Bioinformatics Analysis." *J. Comput. Biol.* 27 (1), 40–54. doi: 10.1089/cmb.2019.0211

Yang, G., Peng, M., Tian, X., and Dong, S. (2017). "Molecular Ecological Network Analysis Reveals the Effects of Probiotics and Florfenicol on Intestinal Microbiota Homeostasis: An Example of Sea Cucumber." *Sci. Rep.* 7 (1), 4778. doi: 10.1038/s41598-017-05312-1

Yen, C. Y., Chen, C. H., Chang, C. H., Tseng, H. F., Liu, S. Y., Chuang, L. Y., et al. (2009). "Matrix Metalloproteinases (MMP) 1 and MMP10 But Not MMP12 are Potential Oral Cancer Markers." *Biomarkers* 14 (4), 244–249. doi: 10.1080/13547500902829375

Yu, G., Wang, L. G., Han, Y., and He, Q. Y. (2012). "Clusterprofiler: An R Package for Comparing Biological Themes Among Gene Clusters." *Omics* 16 (5), 284–287. doi: 10.1089/omi.2011.0118

Conflict of Interest: The authors declare that the research was conducted in the absence of any commercial or financial relationships that could be construed as a potential conflict of interest.

Publisher's Note: All claims expressed in this article are solely those of the authors and do not necessarily represent those of their affiliated organizations, or those of the publisher, the editors and the reviewers. Any product that may be evaluated in this article, or claim that may be made by its manufacturer, is not guaranteed or endorsed by the publisher.

frontiers | Frontiers in Cellular and Infection Microbiology

TYPE Original Research
PUBLISHED 02 August 2022
DOI 10.3389/fcimb.2022.931072

OPEN ACCESS

EDITED BY
Jin Xiao,
University of Rochester, United States

REVIEWED BY
Aruni Wilson,
Loma Linda University, United States
Shishang Qin,
Peking University, China

*CORRESPONDENCE
Chengcheng Liu
liuchengcheng519@163.com
Yi Yang
yangyi528@scu.edu.cn

SPECIALTY SECTION
This article was submitted to Microbiome in Health and Disease, a section of the journal Frontiers in Cellular and Infection Microbiology

RECEIVED 28 April 2022
ACCEPTED 11 July 2022
PUBLISHED 02 August 2022

CITATION
Fang Y, Yang Y and Liu C (2022) New feature extraction from phylogenetic profiles improved the performance of pathogen-host interactions. *Front. Cell. Infect. Microbiol.* 12:931072. doi: 10.3389/fcimb.2022.931072

New feature extraction from phylogenetic profiles improved the performance of pathogen-host interactions

Yang Fang[1,2], Yi Yang[1]* and Chengcheng Liu[3]*

[1]Key Laboratory of Bio-Resources and Eco-Environment of Ministry of Education, College of Life Sciences, Sichuan University, Chengdu, China, [2]Department of Laboratory Medicine, Third Affiliated Hospital of Zhengzhou University, Zhengzhou, China, [3]State Key Laboratory of Oral Diseases, Department of Periodontics, National Clinical Research Center for Oral Diseases, West China School & Hospital of Stomatology, Sichuan University, Chengdu, China

Motivation: The understanding of pathogen-host interactions (PHIs) is essential and challenging research because this potentially provides the mechanism of molecular interactions between different organisms. The experimental exploration of PHI is time-consuming and labor-intensive, and computational approaches are playing a crucial role in discovering new unknown PHIs between different organisms. Although it has been proposed that most machine learning (ML)–based methods predict PHI, these methods are all based on the structure-based information extracted from the sequence for prediction. The selection of feature values is critical to improving the performance of predicting PHI using ML.

Results: This work proposed a new method to extract features from phylogenetic profiles as evolutionary information for predicting PHI. The performance of our approach is better than that of structure-based and ML-based PHI prediction methods. The five different extract models proposed by our approach combined with structure-based information significantly improved the performance of PHI, suggesting that combining phylogenetic profile features and structure-based methods could be applied to the exploration of PHI and discover new unknown biological relativity.

Availability and implementation: The KPP method is implemented in the Java language and is available at https://github.com/yangfangs/KPP.

KEYWORDS

pathogen-host interaction, machine learning, phylogenetic profile, virus, bacteria

Abbreviations: PHI, pathogen-host interactions; ML, machine learning; KPP, kmer phylogenetic profile; Gor, Golovinomyces orontii; Hpa, Hyaloperonospora arabidopsidis; Psy, Pseudomonas syringae; Ara, Arabidopsis thaliana RF; Random Forest; AA, amino acid; auPRC, area under the precision-recall curve.

Introduction

Pathogen-host interactions (PHIs) are crucial for understanding the interactions between different organisms. Most diseases in humans are caused by the virus (Brass et al., 2008; McDermott et al., 2012), and knowing the mechanisms of human PHI is important for developing effective therapeutics. In the study of plants, pathogen infections reduce crop yields (Bernardes-de-Assis et al., 2009; Savary et al., 2012). Understanding the PHI in plants is essential for the defense against plant diseases. The early analyses were built on yeast by the yeast two-hybrid approach (Uetz et al., 2000; Ito et al., 2001). This method provided an experimental way to explore protein-protein interactions in yeast cells. However, exploring PHI based on experimental methods is time-consuming and expensive, and computational methods play an important role in complementing the experimental methods. Over the past decade, various methods have been proposed for deciphering PHI. These include structure-based methods (Shen et al., 2007; Guo et al., 2008; Zhou et al., 2012), homology-based methods (Krishnadev and Srinivasan, 2011; Wuchty, 2011), domain-motif approaches (Dyer et al., 2007; Evans et al., 2009), and machine learning–based (ML-based) methods (Qi et al., 2010; Dyer et al., 2011).

With an increasing number of experimental PHI data being published, many databases have been developed to collect and store these PHI data (Ako-Adjei et al., 2015; Calderone et al., 2015; Guirimand et al., 2015; Urban et al., 2017). Because a large number of experimental PHIs are available, it is possible to use experimental data to drive supervised ML-based methods to predict PHI. For example, Yang et al. used four structure-based feature methods and one network-based feature vector trained by the random forest (RF) method to increase the prediction accuracy of plant PHIs (Yang et al., 2019). Abbsali et al. encoded human and hepatitis C virus proteins as feature vectors by six different descriptors trained by four different ML-based methods that achieved high accuracy and specificity (Emamjomeh et al., 2014). Xianyi et al. extracted five structure-based features with the ML method to predict human and bacterial interactions (Lian et al., 2019). Therefore, extracting protein information features from different methods can significantly improve the prediction results of PHI. Although features can be extracted from various information or evidence for predicting PHI by ML-based methods, most ML-based methods generate features from protein sequence information.

For the first time, the phylogenetic profile was used to predict gene function based on homologies of a reference genome across organisms (Pellegrini et al., 1999). The phylogenetic profile plays a critical role in exploring gene functions (Eisen and Wu, 2002; Jiang, 2008; Li et al., 2014). In addition, the phylogenetic profile has been widely explored in the protein-protein interactions (Pellegrini et al., 1999; Date and Marcotte, 2003; Wu et al., 2003). We first combined the phylogenetic profile and the ML method to explore the PHI. The features extracted from the phylogeny can better reflect the homology relationship in the evolution of the various organisms.

We provide a new method named KPP (kmer phylogenetic profile) that extracts features from the phylogenetic profile for the ML-based method–predicted plant PHI. Our methods construct phylogenetic profiles by contig information and extend phylogenetic profiles by five various models [based on properties of amino acids (AAs)]. We concatenate the phylogenetic feature, and structure-based features significantly improved the prediction results suggesting that the descriptor features extracted from the phylogenetic profile are very important information for predicting plant PHI. In addition, the test results showed that the KPP method can also be applied to the PHI prediction of human bacteria and human viruses. The KPP method is implemented in the Java language (which supports Linux, Windows, and Mac OS platforms) and is freely accessible from the Github repository (https://github.com/yangfangs/KPP).

Results

Extracting phylogenetic profile features for predicting plant PHI

Here, we design a method named KPP that extracts features from phylogenetic profile to predict the interaction of plant pathogens and hosts (Figure 1). First, we build the contig index by kmer. We split each AA sequence into a kmer set and searched the consensus region of this kmer as contig index (Gregory, 2001). Using contigs as an index can effectively compress data compared to kmer while reducing the number of retrievals when extracting features and improving computational efficiency (Supplementary Figure 1). Second, we constructed the phylogenetic profile by the contig index; in this step, the rows and columns of the phylogenetic profile are represented by contigs and species, respectively (Figure 1A). Moreover, there were five different models used to build the phylogenetic profile. The AA profile is constructed by amino acids. The HY profile is constructed based on the hydrophilic and hydrophobic properties of AAs. The PO profile is driven by the polar properties of AAs, and the CH profile is built by the charged properties of AAs. The HY&PO&CH(CHP) profile concatenates three different properties of AAs to build a phylogenetic profile. The classification of various models based on the 20 common AAs has their specific chemical characteristics and their different roles in protein structure and function (Scheiner et al., 2002) are summarized in Supplementary Table 1. As shown in Figure 1B, we extracted features from binary phylogenetic profiles that combine or concatenate various method features to predict plant PHI. We trained this feature by the ML-based method; here, we use RF as

a classifier to predict the interaction of PHI. Additionally, the area under the precision-recall curve (auPRC) is used as an indicator to evaluate the quality of the model.

The phylogenetic profile feature is significant for ML

The phylogenetic profile provided significant data features for the ML training. In this study, we chose three different pathogens *Golovinomyces orontii* (Gor), *Hyaloperonospora arabidopsidis* (Hpa), and *Pseudomonas syringae* (Psy), and also *Arabidopsis thaliana* (Ara) as the host plant (Mukhtar et al., 2011; Wessling et al., 2014). These three pathogen species and one plant species comprised the Gor-Ara, Hpa-Ara, and Psy-Ara test datasets, respectively. Gor and Hpa are eukaryotic pathogens that contain 122 and 104 positive pairs, respectively. Psy is a prokaryotic pathogen that contains 233 positive pairs. The negative pairs are 10 times as large as the positive pairs generated from random pairs in each species (Yang et al., 2019). We used the KPP algorithm to generate the kmer set to construct the contig index and phylogenetic profile. We extracted the feature from the phylogenetic profile and normalized this feature by the z-score method. The mean of these positive and negative feature data is presented in Figure 2 (taxonomy by phylum). As shown in Figure 2, all the test data show that the mean value of the feature of the negative data is stable at 0, and the positive data will fluctuate up and down the negative data and have significant differences (Mann–Whitney two-tailed test p-value< 10^{-8}). This difference is most obvious in the interaction between eukaryotic pathogens and Ara. (Figures 2A, C). The results suggest that the extract profile from the phylogenetic profile can be used to distinguish the positive and negative pairs of each pathogen to Ara. A strong predicted true pair sample by phylogenetic profile feature was observed (Supplementary Figure 2). The predicted probability shows that negative test samples appear in the probability interval of 0 to 0.5. In the probability interval greater than 0.7, only the predicted results of the positive test samples are available. This indicates that the feature values extracted from the phylogenetic profile can better separate the positive and negative test results and have higher precision.

The performance of the KPP algorithm

The performance of the five models

Here, we test five different models by 10-fold cross-validation and the PR curves illustrated in Figure 3. From PR curves, we can see that the auPRC of all predicted models greater than 0.5 indicates that the feature extracted from the phylogenetic profile can distinguish positive and negative data well. The performance of the three plant PHI test datasets showed that Psy-Ara (aucPRC = 0.685 for AA model) performed better than the Hpa-Ara (aucPRC = 0.574 for AA model) and Gor-Ara (aucPRC = 0.618 for AA model) species in the test. What is interesting about the test sample in Figure 3D is that, as the test sample set increases (All-Ara), the performance

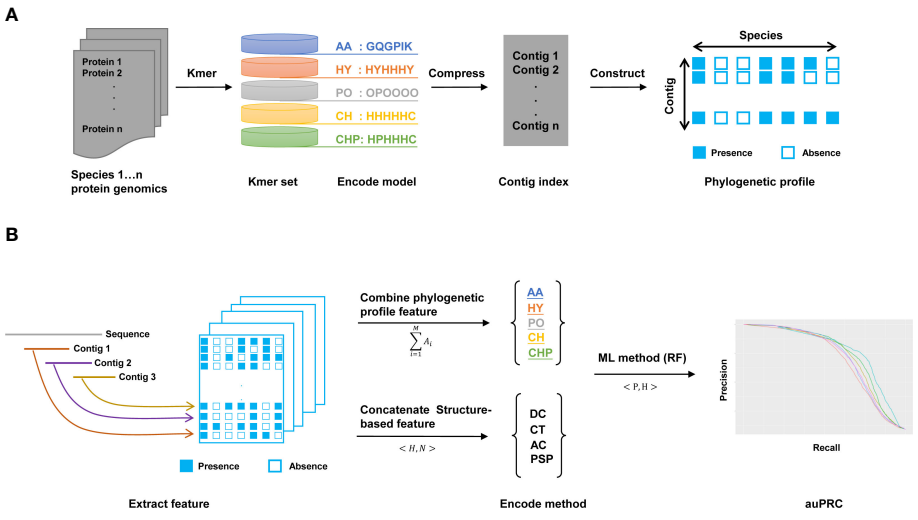

FIGURE 1
The workflow of this work. **(A)** Construction of the kmer phylogenetic profile. Each protein sequence was cut to the kmer set and compressed to the contig index to construct the phylogenetic profile. There are AA, HY, PO, CH, and CHP models for building kmer phylogenetic profiles. **(B)** Extracting features and predicting by the ML method. There are two ways to merge features. One is the "combine method" for merging five models to extract features from phylogenetic profiles. Another is the "concatenate method" for the structure-based method. In this work, we use the RF method to predict plant PHI.

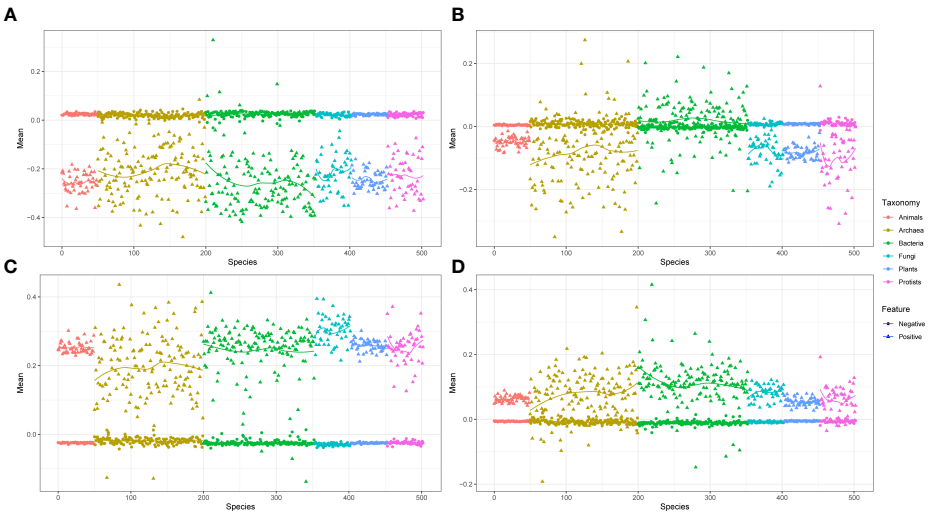

FIGURE 2
The distribution of positive and negative train feature data based on phylogenetic profile. **(A)** The feature data distribution of Gor-Ara. **(B)** The feature data distribution of Psy-Ara. **(C)** The feature data distribution of Hpa-Ara. **(D)** All-Ara feature data. All of these features were extracted from the AA model with 503 species and the kmers setting with 6. The red and blue dots represent negative and positive data, respectively.

results of the five models have improved. The auPRC values all exceeded 0.7 except for the PO model (Figure 3D). These results suggest that the phylogenetic profile features are a powerful indicator that can distinguish whether there is an interaction between pathogens and hosts in plant PHI.

Parameter optimization for performance

We used contigs and species to construct phylogenetic profiles and extract features for ML to predict plant PHI. The length of the kmer and the selection of the species number are critical to the performance of the prediction results. We use

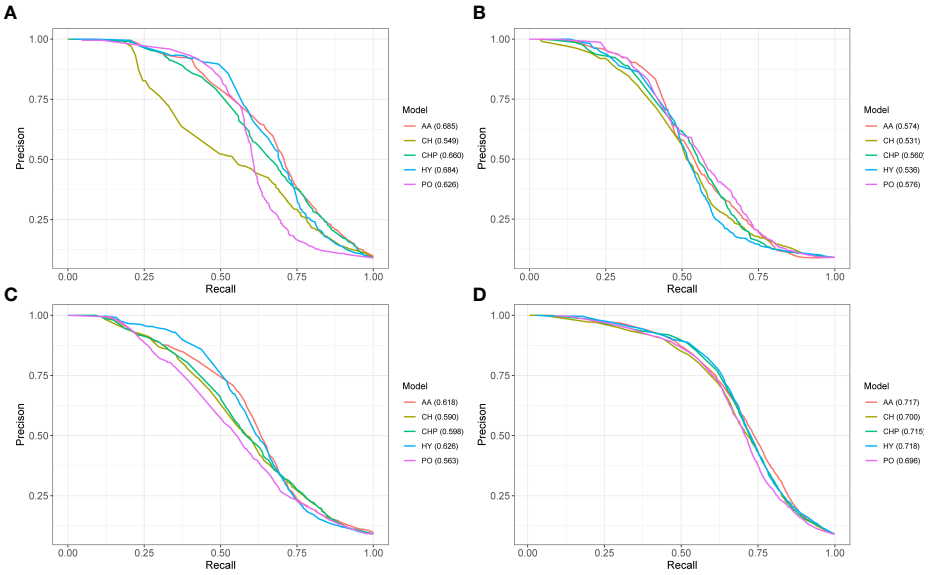

FIGURE 3
The performance of phylogenetic profile features predicted pathogen-host interactions. PR curves show the performance of five different models on the 10-fold cross-validation test. Panels **(A–D)** represent the results from the Ara-Psy, Ara- Hpa, Ara-Gor, and All-Ara training samples, respectively.

different numbers of species to construct a phylogenetic profile (test with AA model, k = 6 and randomly chose the species with 72, 503, and 1,000) (Supplementary Table 2). The results show that the performance of the predicted results increased as the number of species increased. Too many species chosen will reduce the speed of contigs searches, so based on the balance of calculation time and accuracy, we chose 503 species as the optimal species selection for constructing phylogenetic profiles (Supplementary Figure 3 and Supplementary Table 3). Due to the different properties of AAs, we encode AA characters into four different models, which will lead to the optimal length of kmer for each model being various. We tested kmer length against different models to select the optimal kmer value with 503 species (Supplementary Table 4). The result clearly shows that for the AA, HY, PO, CH, and CHP models, the optimal kmer values are 6, 22, 27, 19, 15, respectively. The following tests on the algorithm are based on these optimal parameters.

The phylogenetic profile feature significantly improved the performance of ML prediction

We concatenate novel phylogenetic profile features (CHP model) with sequence features to improve the performance of prediction in the plant PHI. To compare the influence of phylogenetic profile features on the performance, we compared the structure-based + CHP with the structure-based descriptions (CT, AC, DC, and PSP descriptions in the Methods section) based on the RF algorithm. As shown in Figure 4, the aucPRC values of the structure-based + CHP method in the 10-fold cross-validation test were 0.766, 0.705, 0.755, and 0.775 for the Gor-Ara, Psy-Ara, Hpa-Ara, and All-Ara test data, respectively, whereas the corresponding values of the structure-based method were 0.745, 0.662, 0.690, and 0.765, respectively. In addition, the performance of the other models (AA, CH, PO, and HY) + the structure-based model is shown in Supplementary Table 5. The results show that by concatenating the feature extracted from the phylogenetic profile with the structure-based feature to predict plant PHI, five different models can improve the performance of the prediction results. It also shows that the phylogenetic profile is a significant feature for the prediction of plant PHI based on the ML method. In general, the structure-based + CHP feature was reported significantly more often than the structure-based descriptor only. The results of cross-validation clearly show that phylogenetic profile features can substantially improve the predicted performance of plant PHI. The traditional method uses the concatenate method to connect different features to improve the dimensionality of the training feature value and improve the accuracy (Emamjomeh et al., 2014; Yang et al., 2019; Yang et al., 2020). Strikingly, because the features extracted from the phylogenetic profile by five models have the same dimensions (503), we proposed a "combine" method to merge feature values for ML. The merged value dimension has not increased, and the length of the feature is still 503, which greatly reduces the calculation pressure and improves the prediction speed. At the same time, the performance of our "combine" method (combine AA, HY, PO, CH, and CHP features) is

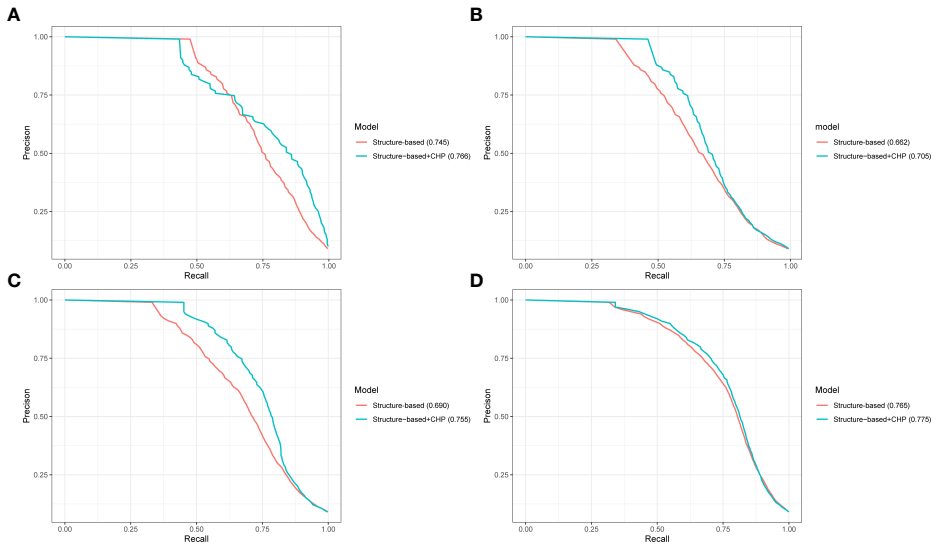

FIGURE 4
The performance of merging different features predicted pathogen-host interactions. PR curves showing the performance based only on the structure-based and structure-based + CHP models on the 10-fold cross-validation test. Panels **(A–D)** represent the results from the Ara-Psy, Ara- Hpa, Ara-Gor, and All-Ara training samples, respectively.

better than that of the traditional concatenate method (Supplementary Figure 4).

Here, we use the RF method as the main ML algorithm to predict plant PHI because it performed better than the other ML methods. We also compared corresponding results with different ML algorithms, including support vector classifier (SVC), gradient boosting classifier (GBC), K-neighbors classifier (KNC), AdaBoost classifier (ADB), and Naive Bayes (NB) (Supplementary Figure 5). These algorithms were implemented by the Python-based library Scikit-learn (Pedregosa et al., 2011). We found that RF (auPRC = 0.715) obtained the best performance in the All-Ara test dataset, followed by ADB (auPRC = 0.609) and GBC (auPRC = 0.560). However, the SVC (auPRC = 0.450), KNC (auPRC = 0.368), and NB (auPRC = 0.167) methods obtained the worst performance and were not applicable to plant PHI prediction (Supplementary Figure 5D). There was a similar performance ranking in the other three test datasets (Supplementary Figures 5A–C). This result suggested that the RF method was the best appropriate ML algorithm for predicting plant PHI, and we used this method to train phylogenetic profile features for predicting plant PHI.

The performance of the KPP feature in human PHI

We validate the performance of the KPP method in human PHI by human bacteria (13,413 positive pairs) and human virus (14,789 positive pairs). The human-bacteria PHI and human-virus–positive were collected from HPIDB 3.0 database (Ammari et al., 2016). The human-virus PHI contains six virus species (*influenza A virus*, *human papillomavirus type 16*, *measles virus*, *Zika virus*, *HIV-1 M:B_HXB2R*, and *human herpesvirus*). In this test dataset, *influenza A virus* was the most positive pair among these six species including 6,070 positive pairs. The species with the least number of positive pairs was the *measles virus*, which contained a total of 906 positive pairs (Supplementary Table 6). The human-bacteria PHI contains five bacterial species (*Yersinia pestis*, *Bacillus anthracis*, *Francisella tularensis*, *Saccharomyces cerevisiae*, and *Streptococcus pyogenes*). Because there is no database of PHI for the oral cavity, we collected experimental human–oral bacteria PHI (Rosa et al., 2020). We extracted 485 bacteria that inhabited in the human oral cavity from the eHOMD database (Chen et al., 2010). We checked these oral bacteria to human interactions from the DIOGRID database (Stark et al., 2006), IntAct database (Kerrien et al., 2012), and HPIDB3.0 database (Ammari et al., 2016). However, we only identified 13 positive pairs in *Streptococcus pyogenes* bacteria as human oral bacteria (Supplementary Table 6). We test the performance of KPP features in human bacteria and various by 10-fold cross-validation and the auPRC shown in Figure 5. As shown in Figure 5, the auPRC of human bacteria is 0.880, and the auPRC of human viruses is 0.896. Strikingly, the performance of the KPP method in animal PHI tests is better than that in plant PHI tests. This result suggested that the KPP feature improves not only the performance of plant PHI but also that of human-bacteria and human-virus PHI.

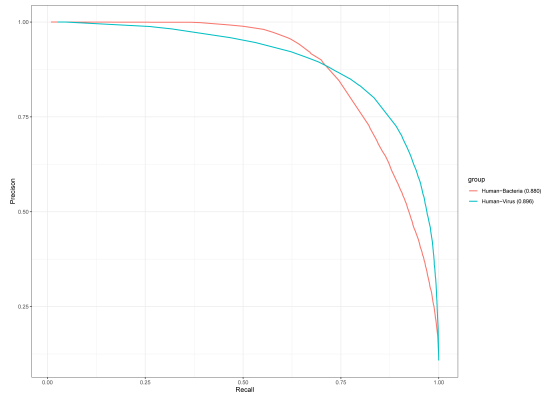

FIGURE 5
The performance of the KPP method predicted human bacteria and human viruses. Ten-fold cross-validation constructs auPRC for human bacteria and human viruses.

Prediction of PHI between humans with viruses and bacteria by the KPP method

We used the KPP method extract feature to predict human-virus and human-bacteria PHIs with the RF method. As shown in Table 1, the three viruses (*human herpesvirus 4 strain B95-8*, *Zika virus*, and *influenza A virus*) and bacteria (*Bacillus anthracis*, *Yersinia pestis*, and *Glossosomatidae)* reported significantly predicted results. However, *HIV-1 M:B_HXB2R*, *measles virus strain Schwarz*, *and Saccharomyces cerevisiae* S288C did not obtain significant prediction results with the 0.6 predicted cutoff. *Human herpesvirus 4 strain B95-8*, *Zika virus*, and *influenza A virus* predicted significant pairs of PHIs of 19, 2, and 19, respectively, with a cutoff of 0.6 (Supplementary Table 7). The predicted pairs of PHIs for *Bacillus anthracis*, *Yersinia pestis*, and *Glossosomatidae* were 24, 295, and 144, respectively (Supplementary Table 8). Because human-bacteria PHI obtained a lower AUC performance in the training dataset, we chose a higher threshold value at the time of prediction.

Discussion

In this work, we developed a KPP method to extract phylogenetic profile features for predicting plant PHI. The KPP method provides five models to construct a phylogenetic profile based on the properties of AAs. Because the feature

TABLE 1 Prediction of the PHIs between humans with viruses and bacteria by the KPP method.

Species	Taxonomy ID	Train AUC	Predicted pairs	Cutoff
Human herpesvirus 4 strain B95-8	10377	0.874	19	0.600
Zika virus	64320	0.770	2	0.600
Influenza A virus	381518	0.842	19	0.600
HIV-1 M:B_HXB2R	11706	0.932	NA	0.600
Measles virus strain Schwarz	132487	0.970	NA	0.600
Bacillus anthracis	1392	0.730	24	0.700
Yersinia pestis	632	0.700	295	0.850
Glossosomatidae	177416	0.653	144	0.700
Saccharomyces cerevisiae S288C	559292	0.994	NA	0.600

dimensions extracted from five various phylogenetic profiles are the same, we first proposed a method of longitudinally merging features to keep the feature dimensions unchanged, instead of concatenating the feature values to increase the dimension of the feature values. The results show that combining the extracted features from five different models was better than the concatenated features in predicting performance. The feature extract from the phylogenetic profile reflecting the biological significance of PHI in evolution was adopted. The results show that the feature values extracted by KPP can significantly improve the predictive performance of plant PHI. The KPP method extraction feature can be extended to predict the PHI of other organisms.

The performance of three plant PHI test datasets showed that the prokaryote organism of Psy (Figure 3A aucPRC = 0.685 for AA model) species performed better than the prokaryotes of Hpa (Figure 3B aucPRC = 0.574 for AA model) and Gor (Figure 3C aucPRC =0.618 for AA model) species in the test. It can be seen that the algorithm performed better for prokaryotes and less well for eukaryotes. About the human PHI test, the performance of human-bacteria PHI (aucPRC = 0.880) and human viruses (auPRC = 0.896) was better than the performance in the plant PHI test dataset (auPRC = 0.717 with AA model). auPRC of human bacteria is 0.880, and the auPRC of human viruses is 0.896. This also shows that the KPP algorithm that we developed can be applied to the prediction of PHI among different species and performs better for human PHI prediction.

We used the Gor-Ara, Psy-Ara, and Hpa-Ara training datasets for predicting the plant PHI. In the training dataset, the PPIN-1 proteins displayed high connectivity in AI-1MAIN and the PPIN-1 proteins as effector targets, in particular, are highly connected nodes within the overall plant network (Mukhtar et al., 2011). The protein TCP14 in plants interacted with 23 distinct Gor effector candidates, 25 Hpa effectors, and 4 Psy effectors that were the most targeted host protein (Wessling et al., 2014). Furthermore, TCP13, TCP15, and TCP19 were also targeted multiple times by effectors from at least two pathogens and exhibited altered infection phenotypes in the plant test dataset (Wessling et al., 2014). We identified SYNE1 (hsa:23345) and TTN (hsa:7273) genes as the hub genes in the host organism by predicting human-virus PHI (Supplementary Table 7). The SYNE1 genes encode a spectrin repeat-containing protein expressed in skeletal and smooth muscle, and peripheral blood lymphocytes; related pathways are meiosis and cell cycle, mitotic. The TTN gene encodes a large abundant protein of striated muscle. The diseases associated with TTN include myopathy and Salih myopathy. The SYNE1 mediates the docking of the capsid protein of human herpesviruses to nuclear pore complex proteins (Hong et al., 2021).

In the future, we hope that this approach will not only contribute as a useful predictor to accelerate the exploration of plant PHIs but also extend to the prediction of the PHI of more organisms.

Methods

KPP algorithm

Building the contig index and constructing the phylogenetic profile

Before creating a contig index, we needed to obtain a kmer set from n species proteomics. Here, the parameter $k \in (1,2,3,\ldots, n)$ and the kmer set are generated from the five different methods AA, HY, PO, CH, and CHP. A contig is composed of one or more consecutive kmers that are connected end to end. Building a contig index in advance can effectively compress the number of kmer and reduce the number of kmer backtracking queries, thereby improving the computational efficiency of feature extraction. We used the contig index to trace back whether the contig index existed in n species and generated a 0-1 (absence-presence) matrix as the binary phylogenetic profile.

Extract feature from phylogenetic profile

KPP cuts each pathogen and host sequence S to a kmer set and searches contigs C. For each C , we extract feature array A from the binary PHI phylogenetic profile. The extracted feature function is defined as $f(C,A) = \sum_{i=1}^{C} A_i$.

Combined method

Five model features extracted from the PHI phylogenetic profile have the same length. We propose a "combine" method to integrate the features for ML. The combined function is defined as $f(M,A)=\sum_{i=1}^{M}A_i$, where M is the feature extracted by the five different models. A is the feature array extracted from the PHI phylogenetic profile by various models.

Concatenate method

The feature extract from the phylogenetic profile concatenated with other methods to integrate features was defined as $\langle H,N\rangle$. Here, H is the feature array extracted from the phylogenetic profile. N is the feature extracted from other methods, for example, the structure-based method in this study.

The structure-based method

DC method

DC represents the descriptor of two AAs in the protein sequence (Zhou et al., 2012). Dipeptide composition gives a 400-dimensional descriptor defined as $f(r,s)=\frac{N_{r,s}}{N-1}\ r,s=1,2,\ldots,20$, where $N_{r,s}$ is the number of dipeptides represented by AA type r and type s .

CT method

The CT method is based on the percentage of three AAs in the sequence (Shen et al., 2007). Tripeptide composition gives a 343-dimensional descriptor defined as $f(r,s,t)=\frac{N_{r,s,t}}{N-2}\ r,s,t=1,2,\ldots,7$,where $N_{r,s,t}$ is the number of tripeptides represented by AA type r , s , and t.

AC method

The AC descriptor extracts features by accounting for the effects of the interaction of residues with a certain distance (Guo et al., 2008). The 210-dimensional calculation function was defined as $f(lag,j)=\frac{1}{N-lag}\sum_{i=1}^{N-lag}(X_{i,j}-\frac{1}{L}\sum_{i=1}^{N}X_{i,j})\times(X_{(i+lag),j}-\frac{1}{N}\sum_{i=1}^{N}R_{i,j})\ j=1,2,\ldots,7$,where N is the length of sequence X , j denotes one descriptor, and i is the position in the sequence X . Here, *lag* ranges from 1 to 30 in this work.

PSP method

The PSP feature is based on protein secondary structure composition (Hoskins et al., 2006) and protein disorder information (Hsu et al., 2012; Meng et al., 2017) that was first proposed by Yang et al. (Yang et al., 2019). They calculated the fraction of three different secondary structure elements (a helix, b strand, and coil) and the percentage of disordered residues in three regions of the N terminus, C terminus, and the full sequence (Yang et al., 2019). Here, we calculate secondary structure and disorder information by PSSpred (Yan et al., 2013) and IUPred (Dosztanyi et al., 2005), respectively.

Test data

The three different pathogens Gor (122 positive pairs), Hpa (104 positive pairs), and Psy (233 positive pairs) and also the negative pairs were downloaded from http://systbio.cau.edu.cn/intersppi/index.php (Yang et al., 2019). The criteria for choosing these three pathogens and Ara are that these interactions have been experimentally verified as real physical interactions. The experimentally verified human-bacteria (13,413 positive pairs) and human-virus interactions (14,789) were collected from HPIDB 3.0 database (Ammari et al., 2016). The positive interactions were filtered by "physical association" items in the PSI-MITAB(2.5) file while excluding the interactions betweenproteins with less than 30 AAs or nonstandard AAs. The sequences of the human bacterial and viral proteins were retrieved from the UniPort database (Consortium U 2014). Specifically, the ratio of negative pairs to positive pairs was 10:1. The proteomic data of species (503 species) for constructing the phylogenetic profile were downloaded from the KEGG database (Kanehisa and Goto, 2000).

Performance evaluation

To conduct a stringent performance assessment, 10-fold cross-validation tests were carried out. We chose the precision-recall curve (PR curve) and the auPRC to assess the performance of our models. The formulas to calculate precision and recall are as follows:

$$Precision = PPV = \frac{TP}{TP+FP}$$

$$Recall = Sensitivity = TPR = \frac{TP}{TP+FN}.$$

Data availability statement

The original contributions presented in the study are included in the article/Supplementary Material. Further inquiries can be directed to the corresponding authors.

Author contributions

YY and CL conceived and designed research. YF implemented the software. YF performed the research. YY and

CL drafted the manuscript and critically revised the manuscript. All authors read and approved the final manuscript.

Funding

This work was supported by the National Natural Science Foundation of China (31870240).

Conflict of interest

The authors declare that the research was conducted in the absence of any commercial or financial relationships that could be construed as a potential conflict of interest.

Publisher's note

All claims expressed in this article are solely those of the authors and do not necessarily represent those of their affiliated organizations, or those of the publisher, the editors and the reviewers. Any product that may be evaluated in this article, or claim that may be made by its manufacturer, is not guaranteed or endorsed by the publisher.

Supplementary material

The Supplementary Material for this article can be found online at: https://www.frontiersin.org/articles/10.3389/fcimb.2022.931072/full#supplementary-material

SUPPLEMENTARY FIGURE 1
They effectively compress data by contigs. Compare contigs with kmer in five various models. The X-axis is the sequence of the protein sequence, and the Y-axis is the number of kmer or contig. **(A)** The effective compression of the AA model (k=8). **(B)** The effective compression of the HY model (k=22). **(C)** The effective compression of the PO model (k=27). **(D)** The effective compression of the CH model (k=19). **(E)** The effective compression of the CHP model (k=15).

SUPPLEMENTARY FIGURE 2
The predicted probability distribution of positive and negative pairs. **(A)** The predicted probability distribution of Gor-Ara. **(B)** The predicted probability distribution Psy-Ara. **(C)** The predicted probability distribution Hpa-Ara. **(D)** The predicted probability distribution of All-Ara. AA contig index model, the number of species was 503 and the kmer parameter setting was 6. The horizontal axis "Probability" is the output by random forest predicted result. The vertical axis "Percentage" is the proportion of the number of negative and positive sample pairs in the corresponding interval.

SUPPLEMENTARY FIGURE 3
The taxonomy of 503 species used to construct the phylogenetic profile.

SUPPLEMENTARY FIGURE 4
The performance of the combine and concatenate method. The auPRC of Gor-Ara, Psy-Ara, and Hpa-Ara by 10-fold-cross-validation are shown in **(A)**, **(B)**, **(C)**, and **(D)**, respectively.

SUPPLEMENTARY FIGURE 5
The performance of different ML methods. The auPRC of Gor-Ara, Psy-Ara, Hpa-Ara and All-Ara by 10-fold-cross-validation are shown in **(A)**, **(B)**, **(C)**, and **(D)**, respectively.

SUPPLEMENTARY TABLE 1
The classification of amino acids and five built phylogenetic profile models.

SUPPLEMENTARY TABLE 2
The influence of prediction performance by different species.

SUPPLEMENTARY TABLE 3
The list of 503 species for building the phylogenetic profile.

SUPPLEMENTARY TABLE 4
The influence of performance by different kmer lengths.

SUPPLEMENTARY TABLE 5
The performance of concatenating different phylogenetic profile feature models with the structure-based method.

SUPPLEMENTARY TABLE 6
The species of bacteria and virus and positive pairs.

SUPPLEMENTARY TABLE 7
Predictions of human-virus PHI pairs.

SUPPLEMENTARY TABLE 8
Predictions of human-bacteria PHI pairs.

References

Ako-Adjei, D., Fu, W., Wallin, C., Katz, K. S., Song, G., Darji, D., et al. (2015). HIV-1, human interaction database: current status and new features. *Nucleic Acids Res.* 43, D566–D570. doi: 10.1093/nar/gku1126

Ammari, M. G., Gresham, C. R., McCarthy, F. M., and Nanduri, B. (2016). HPIDB 2.0: a curated database for host-pathogen interactions. *Database (Oxford)* 2016. doi: 10.1093/database/baw103

Bernardes-de-Assis, J., Storari, M., Zala, M., Wang, W. X., Jiang, D. H., Li, S. D., et al. (2009). Genetic structure of populations of the rice-infecting pathogen rhizoctonia solani AG-1 IA from China. *Phytopathology* 99, 1090–1099. doi: 10.1094/PHYTO-99-9-1090

Brass, A. L., Dykxhoorn, D. M., Benita, Y., Yan, N., Engelman, A., Xavier, R. J., et al. (2008). Identification of host proteins required for HIV infection through a functional genomic screen. *Science* 319, 921–926. doi: 10.1126/science.1152725

Calderone, A., Licata, L., and Cesareni, G. (2015). VirusMentha: a new resource for virus-host protein interactions. *Nucleic Acids Res.* 43, D588–D592. doi: 10.1093/nar/gku830

Chen, T., Yu, W.-H., Izard, J., Baranova, O. V., Lakshmanan, A., and Dewhirst, F. E. (2010). The human oral microbiome database: a web accessible resource for investigating oral microbe taxonomic and genomic information. *Database* 2010, baq013. doi: 10.1093/database/baq013

Consortium U (2014). Activities at the universal protein resource (UniProt). *Nucleic Acids Res.* 42, D191–D198. doi: 10.1093/nar/gkt1140

Date, S. V., and Marcotte, E. M. (2003). Discovery of uncharacterized cellular systems by genome-wide analysis of functional linkages. *Nat. Biotechnol.* 21, 1055–1062. doi: 10.1038/nbt861

Dosztanyi, Z., Csizmok, V., Tompa, P., and Simon, I. (2005). IUPred: web server for the prediction of intrinsically unstructured regions of proteins based on

estimated energy content. *Bioinformatics* 21, 3433–3434. doi: 10.1093/bioinformatics/bti541

Dyer, M. D., Murali, T. M., and Sobral, B. W. (2007). Computational prediction of host-pathogen protein-protein interactions. *Bioinformatics* 23, i159–i166. doi: 10.1093/bioinformatics/btm208

Dyer, M. D., Murali, T. M., and Sobral, B. W. (2011). Supervised learning and prediction of physical interactions between human and HIV proteins. *Infection. Genet. Evol.* 11, 917–923. doi: 10.1016/j.meegid.2011.02.022

Eisen, J. A., and Wu, M. (2002). Phylogenetic analysis and gene functional predictions: phylogenomics in action. *Theor. Popul. Biol.* 61, 481–487. doi: 10.1006/tpbi.2002.1594

Emamjomeh, A., Goliaei, B., Zahiri, J., and Ebrahimpour, R. (2014). Predicting protein-protein interactions between human and hepatitis c virus *via* an ensemble learning method. *Mol. Biosyst.* 10, 3147–3154. doi: 10.1039/C4MB00410H

Evans, P., Dampier, W., Ungar, L., and Tozeren, A. (2009). Prediction of HIV-1 virus-host protein interactions using virus and host sequence motifs. *BMC Med. Genomics* 2, 27. doi: 10.1186/1755-8794-2-27

Gregory, S. G. (2005). Contig assembly. *Encycl. Life Sci.* 1-4. doi: 10.1038/npg.els.0005365

Guirimand, T., Delmotte, S., and Navratil, V. (2015). VirHostNet 2.0: surfing on the web of virus/host molecular interactions data. *Nucleic Acids Res.* 43, D583–D587. doi: 10.1093/nar/gku1121

Guo, Y., Yu, L., Wen, Z., and Li, M. (2008). Using support vector machine combined with auto covariance to predict protein-protein interactions from protein sequences. *Nucleic Acids Res.* 36, 3025–3030. doi: 10.1093/nar/gkn159

Hong, Y., Jeong, H., Park, K., Lee, S., Shim, J. Y., Kim, H., et al. (2021). STING facilitates nuclear import of herpesvirus genome during infection. *Proc. Natl. Acad. Sci. U.S.A.* 118(33), e2108631118. doi: 10.1073/pnas.2108631118

Hoskins, J., Lovell, S., and Blundell, T. L. (2006). An algorithm for predicting protein-protein interaction sites: Abnormally exposed amino acid residues and secondary structure elements. *Protein Sci.* 15, 1017–1029. doi: 10.1110/ps.051589106

Hsu, W. L., Oldfield, C., Meng, J., Huang, F., Xue, B., Uversky, V. N., et al. (2012). Intrinsic protein disorder and protein-protein interactions. *Pac. Symp. Biocomput.*, 116–127. doi: 10.1142/9789814366496_0012

Ito, T., Chiba, T., Ozawa, R., Yoshida, M., Hattori, M., and Sakaki, Y. (2001). A comprehensive two-hybrid analysis to explore the yeast protein interactome. *Proc. Natl. Acad. Sci.* 98, 4569–4574. doi: 10.1073/pnas.061034498

Jiang, Z. (2008). Protein function predictions based on the phylogenetic profile method. *Crit. Rev. Biotechnol.* 28, 233–238. doi: 10.1080/07388550802512633

Kanehisa, M., and Goto, S. (2000). KEGG: kyoto encyclopedia of genes and genomes. *Nucleic Acids Res.* 28, 27–30. doi: 10.1093/nar/28.1.27

Kerrien, S., Aranda, B., Breuza, L., Bridge, A., Broackes-Carter, F., Chen, C., et al. (2012). The IntAct molecular interaction database in 2012. *Nucleic Acids Res.* 40, D841–D846. doi: 10.1093/nar/gkr1088

Krishnadev, O., and Srinivasan, N. (2011). Prediction of protein-protein interactions between human host and a pathogen and its application to three pathogenic bacteria. *Int. J. Biol. Macromol.* 48, 613–619. doi: 10.1016/j.ijbiomac.2011.01.030

Lian, X., Yang, S., Li, H., Fu, C., and Zhang, Z. (2019). Machine-Learning-Based predictor of human-bacteria protein-protein interactions by incorporating comprehensive host-network properties. *J. Proteome Res.* 18, 2195–2205. doi: 10.1021/acs.jproteome.9b00074

Li, Y., Calvo, S. E., Gutman, R., Liu, J. S., and Mootha, V. K. (2014). Expansion of biological pathways based on evolutionary inference. *Cell* 158, 213–225. doi: 10.1016/j.cell.2014.05.034

McDermott, J. E., Diamond, D. L., Corley, C., Rasmussen, A. L., Katze, M. G., and Waters, K. M. (2012). Topological analysis of protein co-abundance networks identifies novel host targets important for HCV infection and pathogenesis. *BMC Syst. Biol.* 6, 28. doi: 10.1186/1752-0509-6-28

Meng, F., Uversky, V. N., and Kurgan, L. (2017). Comprehensive review of methods for prediction of intrinsic disorder and its molecular functions. *Cell Mol. Life Sci.* 74, 3069–3090. doi: 10.1007/s00018-017-2555-4

Mukhtar, M. S., Carvunis, A. R., Dreze, M., Epple, P., Steinbrenner, J., Moore, J., et al. (2011). Independently evolved virulence effectors converge onto hubs in a plant immune system network. *Science* 333, 596–601. doi: 10.1126/science.1203659

Pedregosa, F., Varoquaux, G., Gramfort, A., Michel, V., Thirion, B., Grisel, O., et al. (2011). Scikit-learn: Machine learning in Python. *J. Mach. Learn. Res.* 12, 2825–2830.

Pellegrini, M., Marcotte, E. M., Thompson, M. J., Eisenberg, D., and Yeates, T. O. (1999). Assigning protein functions by comparative genome analysis: Protein phylogenetic profiles. *P. Natl. Acad. Sci. U.S.A.* 96, 4285–4288. doi: 10.1073/pnas.96.8.4285

Qi, Y., Tastan, O., Carbonell, J. G., Klein-Seetharaman, J., and Weston, J. (2010). Semi-supervised multi-task learning for predicting interactions between HIV-1 and human proteins. *Bioinformatics* 26, i645–i652. doi: 10.1093/bioinformatics/btq394

Rosa, N., Campos, B., Esteves, A. C., Duarte, A. S., Correia, M. J., Silva, R. M., et al. (2020). Tracking the functional meaning of the human oral-microbiome protein-protein interactions. *Adv. Protein Chem. Struct. Biol.* 121, 199–235. doi: 10.1016/bs.apcsb.2019.11.014

Savary, S., Ficke, A., Aubertot, J. N., and Hollier, C. (2012). Crop losses due to diseases and their implications for global food production losses and food security. *Food Secur.* 4, 519–537. doi: 10.1007/s12571-012-0200-5

Scheiner, S., Kar, T., and Pattanayak, J. (2002). Comparison of various types of hydrogen bonds involving aromatic amino acids. *J. Am. Chem. Soc* 124, 13257–13264. doi: 10.1021/ja027200q

Shen, J., Zhang, J., Luo, X., Zhu, W., Yu, K., Chen, K., et al. (2007). Predicting protein-protein interactions based only on sequences information. *Proc. Natl. Acad. Sci. U. S. A.* 104, 4337–4341. doi: 10.1073/pnas.0607879104

Stark, C., Breitkreutz, B. J., Reguly, T., Boucher, L., Breitkreutz, A., and Tyers, M. (2006). BioGRID: a general repository for interaction datasets. *Nucleic Acids Res.* 34, D535–D539. doi: 10.1093/nar/gkj109

Uetz, P., Giot, L., Cagney, G., Mansfield, T. A., Judson, R. S., Knight, J. R., et al. (2000). A comprehensive analysis of protein-protein interactions in saccharomyces cerevisiae. *Nature* 403, 623–627. doi: 10.1038/35001009

Urban, M., Cuzick, A., Rutherford, K., Irvine, A., Pedro, H., Pant, R., et al. (2017). PHI-base: a new interface and further additions for the multi-species pathogen-host interactions database. *Nucleic Acids Res.* 45, D604–D610. doi: 10.1093/nar/gkw1089

Wessling, R., Epple, P., Altmann, S., He, Y., Yang, L., Henz, S. R., et al. (2014). Convergent targeting of a common host protein-network by pathogen effectors from three kingdoms of life. *Cell Host Microbe* 16, 364–375. doi: 10.1016/j.chom.2014.08.004

Wuchty, S. (2011). Computational prediction of host-parasite protein interactions between p. falciparum and h. sapiens. *PloS One* 6(11), e26960. doi: 10.1371/journal.pone.0026960

Wu, J., Kasif, S., and DeLisi, C. (2003). Identification of functional links between genes using phylogenetic profiles. *Bioinformatics* 19, 1524–1530. doi: 10.1093/bioinformatics/btg187

Yang, S., Li, H., He, H., Zhou, Y., and Zhang, Z. (2019). Critical assessment and performance improvement of plant-pathogen protein-protein interaction prediction methods. *Brief Bioinform.* 20, 274–287. doi: 10.1093/bib/bbx123

Yang, X., Yang, S., Li, Q., Wuchty, S., and Zhang, Z. (2020). Prediction of human-virus protein-protein interactions through a sequence embedding-based machine learning method. *Comput. Struct. Biotechnol. J.* 18, 153–161. doi: 10.1016/j.csbj.2019.12.005

Yan, R., Xu, D., Yang, J., Walker, S., and Zhang, Y. (2013). A comparative assessment and analysis of 20 representative sequence alignment methods for protein structure prediction. *Sci. Rep.* 3, 2619. doi: 10.1038/srep02619

Zhou, Y., Zhou, Y. S., He, F., Song, J., and Zhang, Z. (2012). Can simple codon pair usage predict protein-protein interaction? *Mol. Biosyst.* 8, 1396–1404. doi: 10.1039/c2mb05427b

Frontiers in
Cellular and Infection Microbiology

Investigates how microorganisms interact with their hosts Explores bacteria, fungi, parasites, viruses, endosymbionts, prions and all microbial pathogens as well as the microbiota and its effect on health and disease in various hosts.

Discover the latest Research Topics

See more →

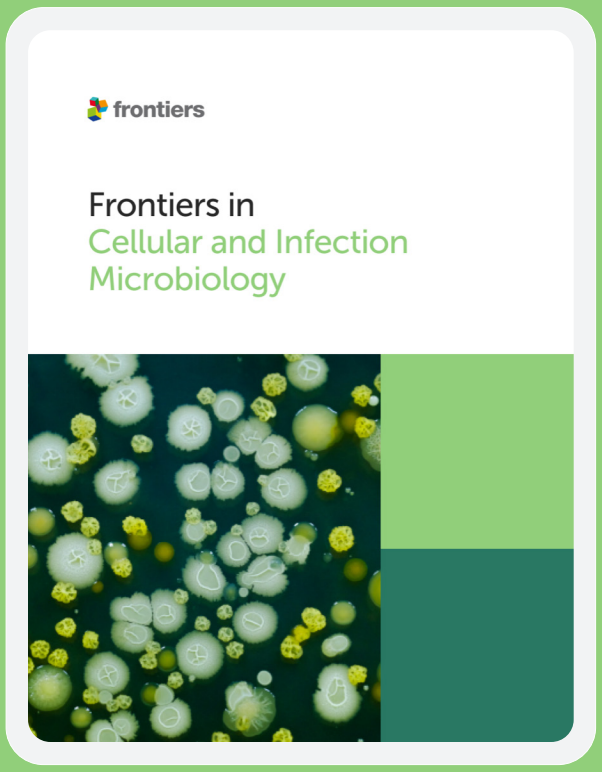

Frontiers

Avenue du Tribunal-Fédéral 34
1005 Lausanne, Switzerland
frontiersin.org

Contact us

+41 (0)21 510 17 00
frontiersin.org/about/contact